2

DOT/FAA/PM-87/10

Program Engineering
and Maintenance Service
Washington, D.C. 20591

Pressuremeter Moduli for Airport Pavement Design and Evaluation

J.-L. Briaud
P. J. Cosentino
T. A. Terry

Civil Engineering Department
and Texas Transportation Institute
Texas A & M University System
College Station, Texas 77843

August 1987

Final Report

This document is available to the public through the National Technical Information Service, Springfield, Virginia 22161.

U.S. Department of Transportation
Federal Aviation Administration

NOTICE

This document is disseminated under the sponsorship of the Department of Transportation in the interest of information exchange. The United States Government assumes no liability for its contents or use thereof.

Technical Report Documentation Page

1. Report No. DOT/FAA/PM-87/10	2. Government Accession No. A188338	3. Recipient's Catalog No.
4. Title and Subtitle PRESSUREMETER MODULI FOR AIRPORT PAVEMENT DESIGN AND EVALUATION		5. Report Date August 1987
		6. Performing Organization Code
7. Author(s) J.-L. Briaud, P. J. Cosentino, T. A. Terry		8. Performing Organization Report No. RF 7035
9. Performing Organization Name and Address Civil Engineering Dept. and Texas Transportation Institute, Texas A&M University, College Station, TX 77843		10. Work Unit No. (TRAIS)
		11. Contract or Grant No.
12. Sponsoring Agency Name and Address U.S. Department of Transportation, Federal Aviation Administration, 800 Independence Avenue, S.W. Washington, D.C. 20591		13. Type of Report and Period Covered Final Report
		14. Sponsoring Agency Code APM-740

15. Supplementary Notes Texas A&M University was a subcontractor to Pailen-Johnson Associates where Claude Johnson was the contact person. At the Federal Aviation Administration, Hisao Tomita was the contact person.

16. Abstract The pavement pressuremeter is a new tool which is used to obtain the moduli of the base course and the subgrade soil. These moduli are necessary in the design, evaluation, and repair of airport pavements. The test consists of opening a 1.35 inch diameter, 5 feet deep hole in the pavement and lowering a 9 inch long cylindrical probe at the testing depth. The probe is inflated radially and a stress strain curve is recorded in situ. No drilling rig is necessary.

Current practice makes use of the cyclic triaxial test to obtain the moduli. The pavement pressuremeter has major advantages over the cyclic triaxial test: it is much less expensive, much less time consuming, almost nondestructive and yields comparable moduli. This was shown at three airports, one on sand, two on stiff clay. The pavement pressuremeter tests were performed and the moduli were calculated. Samples were obtained (with great difficulty in the sand) and cyclic triaxial tests were performed to get the moduli. Falling weight deflectometer tests were also performed and provided measured deflections. These deflections were predicted while using the pavement pressuremeter moduli and then the cyclic triaxial tests moduli. Comparison of predicted and measured deflections showed that the pressuremeter predicted as well if not better the deflections in clay and in sand.

This study shows that the pavement pressuremeter is a tool which can be used advantageously for the prediction of pavement deflections and is ready to be used progressively for the design of new pavements, the extension of existing pavements, the evaluation of existing pavements and the design of pavement overlays.

17. Key Words Airport, ~~Pavement~~, Moduli, Pressuremeter, Cyclic Triaxial Test, Falling Weight Deflectometer, Sand, Clay.	18. Distribution Statement Document is available to the public through the National Technical Information Service, Springfield, Virginia 22961.

19. Security Classif. (of this report)	20. Security Classif. (of this page)	21. No. of Pages	22. Price
Unclassified	Unclassified	137	

Form DOT F 1700.7 (8-72) Reproduction of completed page authorized

ACKNOWLEDGMENTS

This study was performed by Texas A&M University as a subcontractor to Pailen-Johnson Associates (PJA). PJA was sponsored by the Federal Aviation Administration. Mr. Claude Johnson of Pailen-Johnson Associates and Mr. Hisao Tomita of the Federal Aviation Administration are thanked for their support throughout the project.

At Texas A&M University Mr. Larry Tucker and Dr. William Sprinsky helped with the computer programming required. Dr. Robert Lytton offered very valuable advice throughout the course of the study. Mr. Mark Howard and Dr. Derek Morris helped in the performance of the cyclic triaxial tests. The authors are also indebted to all those who have made the field testing possible including the airport managers, personnel and Eres Inc.

EXECUTIVE SUMMARY

A relatively new tool, the pavement pressuremeter, was used at three airports in order to evaluate its usefulness in pavement design. The pavement pressuremeter test consists of hand drilling a 1.35 in. (3.43 cm) diameter hole through the pavement down to a depth of say 5 ft (1.52 m), then inserting in the open hole a 1.3 in. (3.30 cm) diameter, 9 in. (22.86 cm) long cylinder; once at the testing depth the cylinder is inflated with water; the pressure against the soil and the relative increase in radius of the cylinder are recorded; this allows to obtain an in situ stress-strain curve since the pressure is the radial stress at the cavity wall and the relative increase in radius is by definition the hoop strain at the cavity wall. By running the tests at various depths in the borehole, a series of stress-strain curves can be recorded in the base course, subbase and subgrade.

From these in situ stress-strain curves, resilient moduli can be measured by performing unload-reload loops during the inflation of the cylinder. Moduli vary with the strain level, the stress level, the number of load cycles and the rate of loading or creep. Models were selected to describe these variations; they are:

Strain level model:

$$1/E = a + b\varepsilon \tag{1}$$

Stress level model:

$$E = K_2 \left(\frac{\theta}{P_a}\right)^{n} \tag{2}$$

Number of cycles model:

$$E_N = E_1 N^{-n_{cyc}} \tag{3}$$

Duration of load model:

$$E_t = E_{t=t_o} \left(\frac{t}{t_o}\right)^{-n_{crp}} \tag{4}$$

During this study, pressuremeter testing procedures were developed to obtain the parameters necessary in the above models (a, b, K_2, n, n_{cyc} and n_{crp}) on the basis of 32 tests in sand, and 32 tests in clay. The strain parameters a and b are obtained from a pressuremeter test where unload-reload loops are performed over various ranges of the hoop strain. The parameters K_2 and n are obtained from a pressuremeter test where unload-reload loops are performed at various stress levels. The cyclic parameter (n_{cyc}) is obtained from a pressuremeter test where 10 unload-reload cycles are performed between two stress levels. The creep or rate effect parameter (n_{crp}) is obtained from a pressuremeter test curve where the radial stress is kept constant for five minutes. The parameters a, b, K_2, n, n_{cyc} and n_{crp} obtained with the pavement pressuremeter in this study compared favorably with values published in the literature. A pavement pressuremeter test procedure was developed where in a single test all of the above parameters can be obtained.

Of the three airports where testing took place, two had clay subgrades and one had a sand subgrade. A total of 34 pavement pressuremeter (PPMT) tests were performed in the base courses and subgrades of the three airports. Also 17 cyclic triaxial (CT) tests were performed on samples recovered from the three airport subgrades. In order to establish a ground truth, a total 92 locations at the 3 airports were tested with the Falling Weight Deflectometer (FWD). The pavement pressuremeter (PPMT) results were compared with the results of cyclic triaxial (CT) tests and falling weight deflectometer (FWD) tests. The comparison consisted of predicting the FWD deflection using the proper PPMT moduli and then using the CT procedure established by the Waterways Experiment Station (WES). For the PPMT it was found that the best predictions are obtained when the strain level model is used for clay subgrades and the stress level model is used for sand. The predicted deflections by the proposed PPMT method were within $\pm$ 25% of the measured deflections. The approach proposed by WES on the use of CT moduli to predict deflections makes the same distinction between clay and sand. Indeed moduli are based on the deviator stress level for clays (the deviator stress relates directly to the strain level) and on the mean confining stress for sands. The deflections of the FWD were predicted using the properly selected triaxial test moduli. The predicted deflections by the established CT method were as good as the PPMT predictions for the clay but not as good for the sand. This is due in part to the great difficulty experienced in retrieving undisturbed samples of sand.

A comparison of moduli was also made. The moduli which predicted best the measured FWD deflections were selected for comparison purposes. The PPMT moduli from the strain level model for the clays and the stress level model for the sand were compared with the CT moduli from the deviator stress approach for the clays and the mean confining stress approach for the sand. The plot shows a much larger variation than the comparison of deflections. Moduli were also backfigured from the FWD deflection results. In this case only one average FWD modulus is backfigured for the entire subgrade, instead of several moduli versus depth for the CT and PPMT tests. The plot comparing PPMT and FWD moduli shows a somewhat better correlation than the plot comparing CT and FWD moduli.

A comparison of the advantages and drawbacks of the three different pieces of equipment and corresponding design approaches is presented. Overall this study shows that the pressuremeter is an economical and avantageous alternative to the cyclic triaxial test. Indeed the PPMT is less costly, much less damaging to the pavement, and simpler to use than the cyclic triaxial test and predicts the deflections of the FWD as well if not better than the cyclic triaxial test. The pavement pressuremeter is particularly useful in sand subgrades where it is easier to drill a 1.35 inch (3.43 cm) diameter hole than it is to recover an undisturbed sand sample.

It is recommended that the pavement pressuremeter be used instead of the cyclic triaxial test.

PRESSUREMETER MODULI FOR AIRPORT PAVEMENT DESIGN

AND EVALUATION

		Page
1.	INTRODUCTION	1
2.	OBJECTIVE	3
3.	SCOPE	5
4.	DESCRIPTION OF THE PAVEMENT PRESSUREMETER EQUIPMENT AND BACKGROUND	7
	4.1 The Pavement Pressuremeter	7
	4.2 Cost, Advantages and Disadvantages of the Pavement Pressuremeter	11
	4.3 Pavement Pressuremeter Design Method as Proposed in 1979	11
5.	MODULI FROM THE PAVEMENT PRESSUREMETER TEST	19
	5.1 Modulus as a Function of Stress, Strain, Creep and Cycles	19
	5.2 Obtaining Moduli from Pavement Pressuremeter Tests	26
	5.3 Influence of the Probe Insertion Technique	31
6.	PAVEMENT PRESSUREMETER TESTING PROCEDURE AND TEST DATA	41
	6.1 Pavement Pressuremeter Testing Procedure	41
	6.2 Pavement Pressuremeter Test Data Reduction	43
	6.2.1 Membrane Resistance Correction	43
	6.2.2 System Compressibility Correction	43
	6.2.3 Hydrostatic Pressure Correction	48
	6.2.4 Correction for Initial Gage Pressure	48
	6.2.5 Modulus Calculations	49
	6.2.6 Limit Pressure Estimation	49
	6.2.7 Strain Calculations	49
	6.3 Pavement Pressuremeter Test Results	50
7.	FIELD EXPERIMENTS	53
	7.1 Airport Sites, Soil, and Test Programs	53
	7.1.1 Easterwood Airport	53
	7.1.2 San Antonio International Airport	59
	7.1.3 Possum Kingdom Airport	59

7.2 Pavement Pressuremeter Test Results 67

7.2.1 Easterwood Airport PPMT Test Results 70
7.2.2 San Antonio International Airport PPMT Test Results 70
7.2.3 Possum Kingdom PPMT Test Results 70

7.3 Cyclic Triaxial Test Results 70

7.3.1 Cyclic Triaxial Test Equipment and Procedure . . 70
7.3.2 Cyclic Triaxial Test Results for the Three Airports 79

7.4 Falling Weight Deflectometer Test Results 82

7.4.1 Falling Weight Deflectometer Equipment and Procedure 82
7.4.2 Falling Weight Deflectometer Test Results . . . 85

8. COMPARISON OF MEASURED FWD DEFLECTIONS WITH PREDICTED FWD DEFLECTIONS USING PPMT MODULI AND CT MODULI 89

8.1 The Finite Element Program ILLIPAVE 89
8.2 Predicted FWD Deflections Based on the PPMT Moduli . . 89
8.3 Predicted FWD Deflections Based on the CT Tests and on the WES Approach 95

9. COMPARISON OF MODULI 115

9.1 Moduli Comparison between PPMT, CT and FWD Tests . . . 115
9.2 Comparison with CBR Moduli and Plate Moduli 115

10. SUMMARY, CONCLUSIONS AND RECOMMENDATIONS 121

10.1 Summary 121
10.2 Conclusions 121
10.3 Recommendations 124

REFERENCES 127

APPENDIX A - Pavement Pressuremeter Test Curves 131

APPENDIX B - Pavement Pressuremeter Test Parameters 149

APPENDIX C - AIRPRESS Microcomputer Program User's Manual 165

APPENDIX D - Cyclic Triaxial Test Results 193

APPENDIX E - Falling Weight Deflectometer Test Results 207

APPENDIX F - Theoretical Derivation of the Average Strain and Average Stress in the Soil Mass During a Pavement Pressuremeter Unload-Reload Cycle 235

1. INTRODUCTION

Due to the costs and the uncertainties associated with current evaluation methods for airport pavements, the Federal Aviation Administration (FAA) sponsored research on the use of the pavement pressuremeter (PPMT) to evaluate airport pavement moduli (Briaud 1979). The pressuremeter is an in situ soil testing device capable of giving an in situ stress-strain curve which yields soil parameters useful in design. The pressuremeter moduli are to be compared to moduli obtained from current state-of-the-art tests, namely the cyclic triaxial (CT) test (Barker and Brabston 1975) and the Falling Weight Deflectometer (FWD) test (Smith and Lytton 1983). The advantage of being able to use the PPMT for design and evaluation of airport pavements is that it is much less complicated and much less time consuming than the cyclic triaxial test and that it allows a direct layer-by-layer evaluation of the pavement unlike the Falling Weight Deflectometer. The question addressed in this research is "Can the pavement pressuremeter yield the necessary moduli for pavement design and evaluation?" This question is answered by comparing moduli and deflections for the PPMT, CT and FWD.

2. OBJECTIVE

The objective of this research is to investigate whether or not the pavement pressuremeter can provide a simple and rapid in situ test method for determining moduli of elasticity values for pavement layers as accurate as those obtained by the current cyclic triaxial test method. This project is not to develop a new and comprehensive design method for airport pavements, however the complete design process will be kept in mind throughout the study. This ensures that the results will properly fit current procedures and allow full use of the pavement pressuremeter for the design of new runways, the extension of existing runways, the evaluation of existing pavements, and the design of pavement overlays.

3. SCOPE

The project will include the following tasks:

1. Improve the PPMT equipment from its 1979 model (Briaud 1979).
2. Study the influence of the insertion technique used to place the probe at the desired depth, and recommend the best technique.
3. Select three airports in Texas.
4. Obtain laboratory samples and conduct PPMT and FWD tests at the 3 airports.
5. Perform the cyclic triaxial tests.
6. Reduce in situ tests and laboratory tests data.
7. Predict the FWD deflections using the finite element method with the PPMT moduli and then with the CT moduli. Compare the measured FWD deflections with the predicted deflections.
8. Compare the moduli from the PPMT, the CT and the FWD.

4. DESCRIPTION OF THE PAVEMENT PRESSUREMETER EQUIPMENT AND BACKGROUND

4.1 The Pavement Pressuremeter

The pavement pressuremeter was developed in 1976 (Briaud 1979). The PPMT device (Figure 1) consists of a control unit, a tubing and a probe which is lowered in a prebored 1.35 inch (3.43 cm) diameter borehole. Once at the testing depth the 9 inch (22.9 cm) long, 1.3 inch (3.3 cm) diameter cylindrical probe covered with a flexible membrane, is inflated with water by turning the manual actuator; this creates a pressure against the walls of the borehole. During a test, the pressure in the probe is recorded on a pressure gage and the increase in volume of the probe ΔV is recorded on the displacement indicator. Several tests are performed at chosen depths in the borehole. The basic idea of the PPMT test is to obtain a series of in situ stress-strain curves in the subgrade and the base layers (Figure 2). This is possible because the pressure against the wall of the hole is the radial stress σ_{rr} and the relative increase in radius of the cavity $\Delta R_c/R_c$ is by definition the hoop strain ($\varepsilon_{\theta\theta}$) in the soil at the borehole wall. During a test, the expanding probe first fills the gap between the probe membrane and the hole (portion OA in Figure 2). This determines the initial radius of the cavity R_c, shown in Figure 2. Then the soil deforms linearly (portion AB in Figure 2). A soil modulus E_o, is obtained from the slope of AB in Figure 2 (Baguelin et al. 1978). At point B, the soil starts yielding and at point D, a limit pressure p_l is reached.

Prior to this project the hole was made by driving a 1.37 inch (3.5 cm) diameter E rod to a depth of 5 ft (1.52 m) below the ground or pavement surface (Briaud and Shields 1979a). This E rod was then withdrawn and the 1.35 inch (3.43 cm) diameter probe was lowered into the open hole to the first testing depth immediately below the surface course. After completing the first test, a second test was performed one foot below the first one. The remaining PPMT tests were performed at one foot intervals to a depth of 5 ft (1.52 m).

For each test the probe was inflated while recording p and ΔV (Figure 3). At the end of the straight part of the curve (Figure 3) the pressure was decreased to zero and then the probe was reinflated. A reload modulus E_r was obtained from the slope of the reload portion of the curve. This modulus was calculated by assuming that the pressuremeter expands as an infinitely long cylinder in a homogeneous linear elastic space (Baguelin et al. 1978) using:

$$E_r = 2\ (1 + \nu)\left(\frac{\Delta p}{\Delta V}\right) V_m \qquad (1)$$

where: ν = Poisson's Ratio, $\Delta p/\Delta V$ = slope of the reload portion of the cyclic loop, V_m = volume of the probe midway through the cycle.

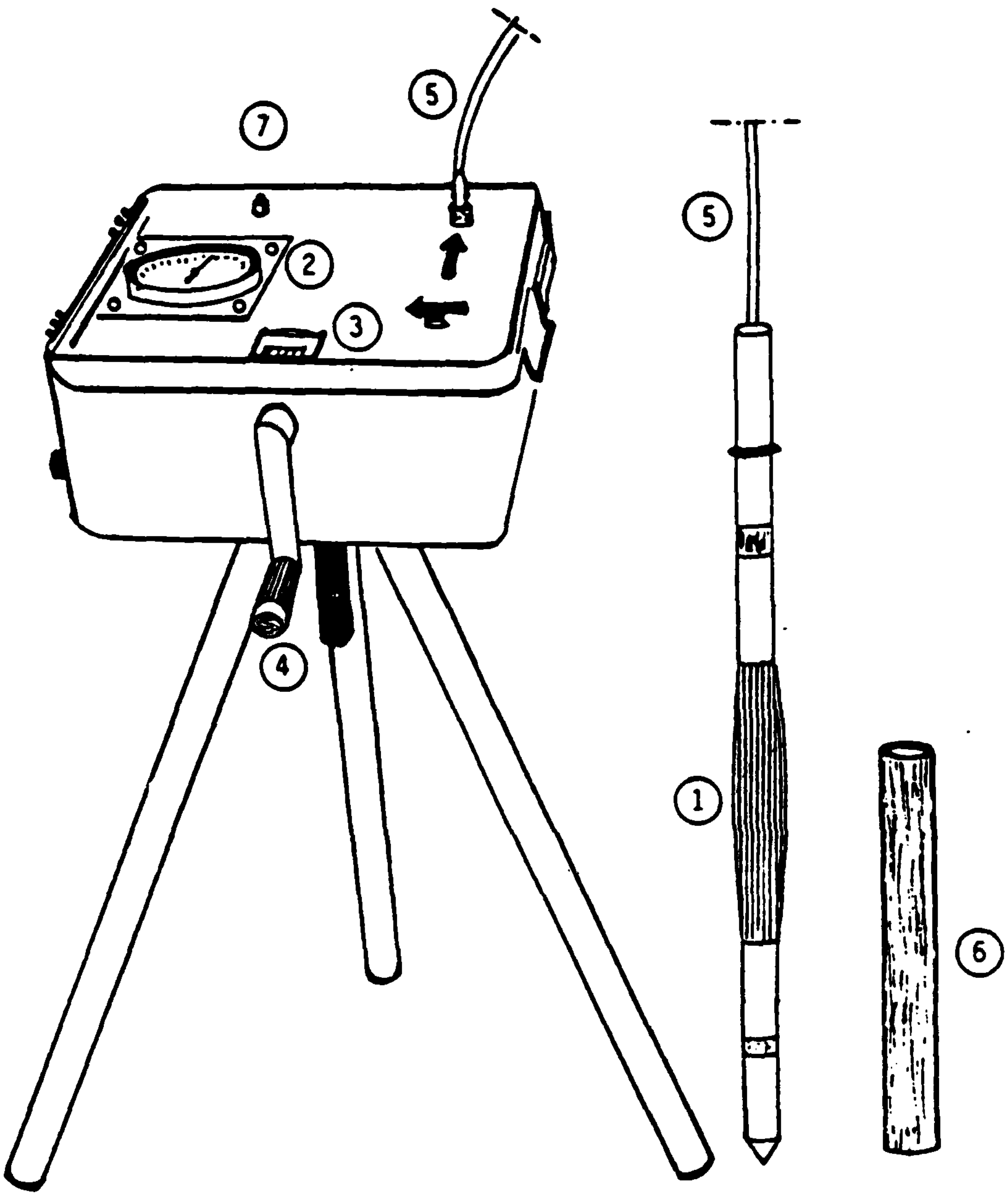

Fig. 1 Schematic of the latest Pavement Pressuremeter 1. Probe 2. Pressure gauge, 3. Displacement indicator, 4. Manual actuator, 5. Tubing, 6. Steel pipe for volume calibration, 7. Connection to water reservior.

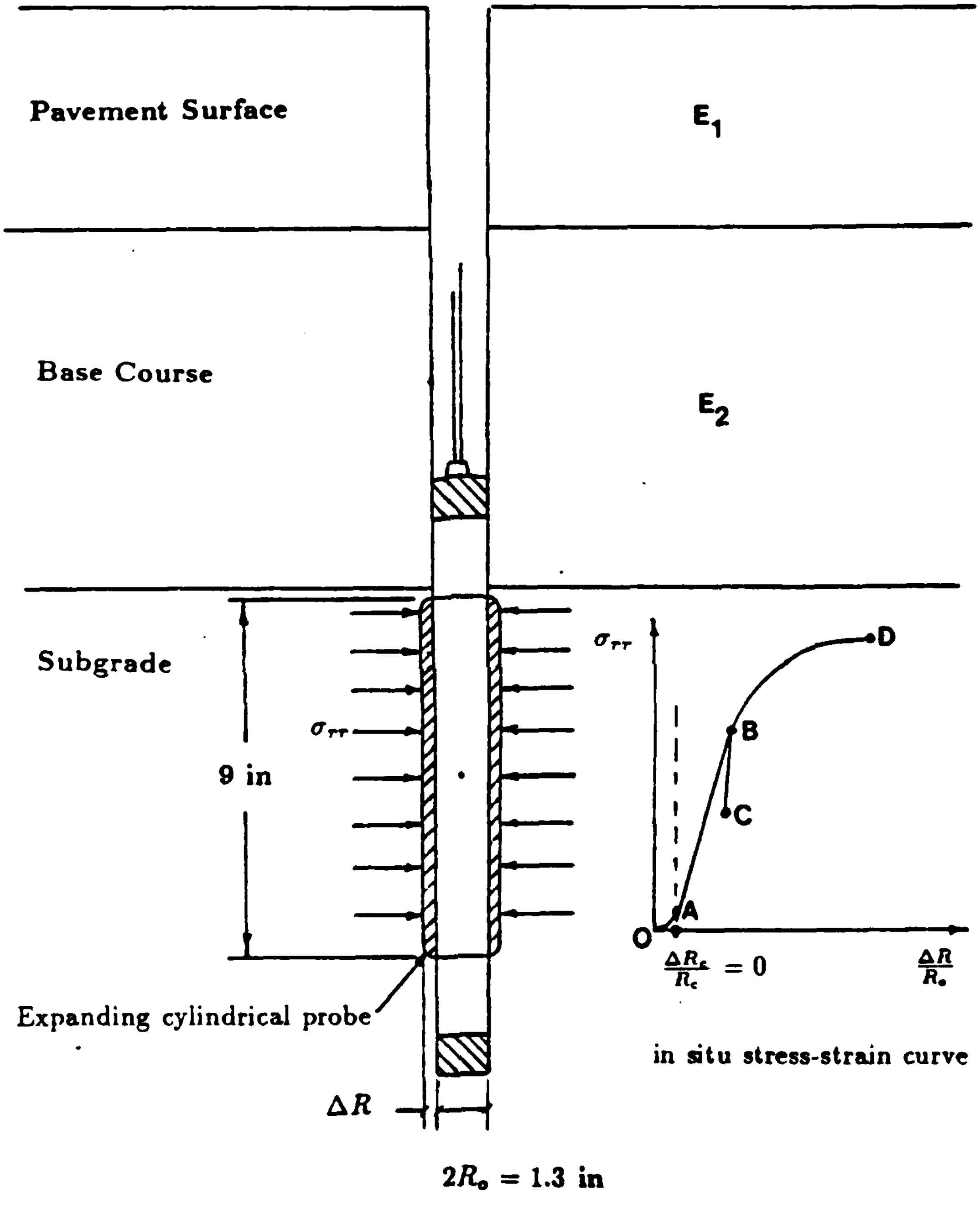

Fig. 2 Typical Pavement Pressuremeter Test and Pavement Cross Section

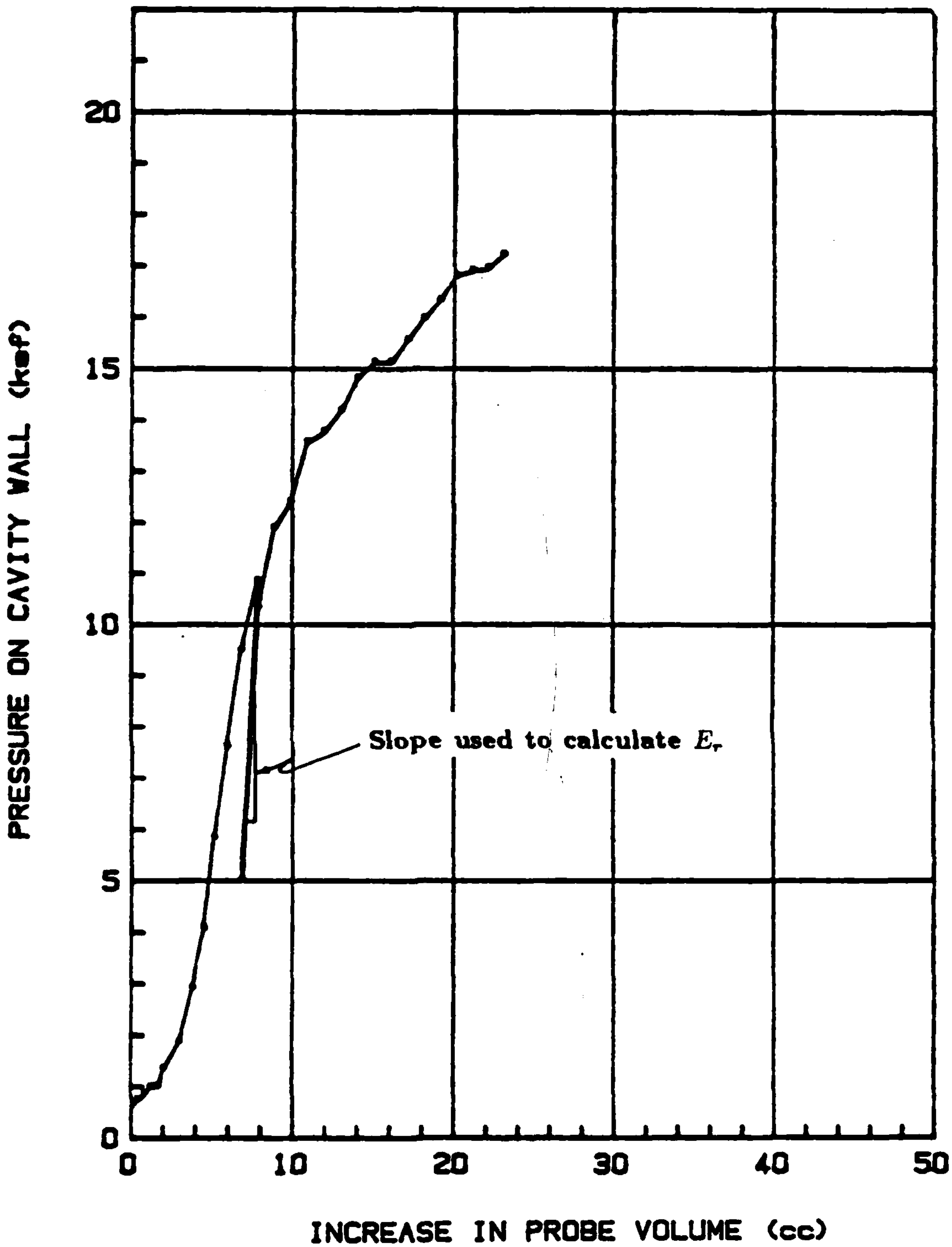

Fig. 3 Typical Pressure vs Volume Pressuremeter Curve

4.2 Cost, Advantages and Disadvantages of the Pavement Pressuremeter

The pavement pressuremeter equipment shown on Figure 1 costs approximately $4000 (1986). The control unit comes in a small suitcase; the probe and tubing come separately. At the airport site the pavement surface is drilled with a hand held concrete drill which costs about $1000 (1986). Once the 1.5 inch hole is opened through the surface course, a 1.35 inch diameter hand auger is used to hand drill a hole 4 or 5 ft deep. This auger is made of a 1.35 inch diameter, 6 inch long wood bit screwed into rods and connected to a handle. The auger costs less than $100. Note that no drilling rig is necessary so that for less than $6000 one can be fully equipped to perform pavement pressuremeter tests.

By comparison, for the cyclic triaxial test, a drill rig is necessary to retrieve samples. A drill rig costs about $150,000 to buy and $1500/day to rent with a crew. The cyclic triaxial test equipment is expensive; the major components are the pump, the controller and wave generator, the triaxial cell, the cell pressure system, the transducers and LVDTs, the data acquisition system, the strip chart or X-Y plotter. The cost is estimated to be about $50,000. By comparison also the Falling Weight Deflectometer cost about $100,000 to buy or $1000/day to rent plus mobilization and demobilization.

The pavement pressuremeter test lasts about 10 minutes. After including time for drilling the hole and moving from station to station, 20 to 30 tests can be performed in an 8 hour day. By comparison, in addition to the sampling time with the drill rig at the airport, it takes about 1 day to run 1 cyclic triaxial test. By comparison also it takes about 3 minutes to run a Falling Weight Deflectometer test with 4 load levels; about 130 to 150 tests can be performed in an 8 hour day. The FWD is therefore faster than the PPMT and should be used anytime a large pavement area needs to be surveyed. The FWD however does not give the moduli profile versus depth like the PPMT does. The PPMT should be used in the areas where the FWD points out that a problem exists. The FWD is not used for the design of new pavements or extension of existing pavements; the PPMT can easily be used in those cases.

Other comparisons between the PPMT, CT and FWD are summarized in Table 1. One point of interest is that FWD results can be used to back-calculate a subgrade modulus if the pavement thickness is known accurately. This information is often obtained from construction drawings; there can be large discrepancies between drawings and reality. For example PPMT tests revealed 24 inches of concrete plus asphalt at the airport in San Antonio when the drawings indicated 12 inches; at the airport in College Station 1 inch of base course was found whereas 6 to 8 inches was shown on the drawings. These discrepancies can lead to drastic errors in the backcalculated FWD moduli.

4.3 Pavement Pressuremeter Design Method as Proposed in 1979

The airport pavement pressuremeter design procedure was developed

Variable	Falling Weight Deflectometer	Pressuremeter Test	Cyclic Triaxial Test
Price of Equipment	$100,000	$6,000	$80,000
Cost of Test	low	medium	high
Equipment Durability	medium	high	medium
Complexity of Use of Equipment	medium	medium	very complex
Time Required for Test	3 minutes	20 minutes	480 minutes
Time Required to Evacuate Runway for Emergency	Immediately	2 minutes	15 minutes (evacuate drill rig)
Data Acquired	Surface Deflections Wave Propagation	Stress/Strain Curve In Situ	Stress/Strain Curve in Laboratory
Horizontal Stresses at Rest	No	Yes	Difficult
Data Reduction	Complicated	Complicated	Complicated
Data Reduced to	Layer Moduli (if layer thicknesses accurately known) as a Function of Load Level & Cycles from Repeated Tests	Layer Moduli as Function of Stress, Strain, Cycles and Rate of Loading	Layer Moduli as Function of Stress, Strain, Cycles and Rate of Loading
Load Rating of Pavements	Light Pavements Only	Yes	Yes
Check Pavement Thickness	No	Yes	Yes
Recover Sample	No	Disturbed (Useful for Identification, Water Content . .)	Undisturbed
Design of New Pavements or Extension of Existing Pavement	Yes	Yes	Yes
Evaluation of Existing Pavement	Yes	Yes	Yes
Overlay Design	Yes	Yes	Yes

Table 1

Comparison of the Falling Weight Deflectometer, Pressuremeter and Cyclic Triaxial Tests for Pavement Design and Evaluation in Canada (Briaud 1979). It is based on the principles used in the Canadian design procedure and described in the Transport Canada manual AK-68-12 (Transport Canada 1976). This Canadian design is based on results of an NDT test called the McLeod plate test (McLeod 1947). This plate test consists of applying a load (S), on a 30 inch (76.2 cm) diameter plate, such that if the load is repeated 10 times a 0.5 in (12.5 mm) deflection of the surface will occur at the 10th repetition. If the test is performed on the pavement surface the load (S) is called the pavement bearing strength (S_p) and if the test is performed on the subgrade, the load is called the subgrade bearing strength (S_s).

The subgrade bearing strength is the basic design parameter for airports in Canada. In general, S_s is not measured directly but is deduced from the measurement of S_p. A relationship between S_s and S_p has been established (McLeod 1947):

$$S_s = S_p \times 10^{-(\frac{t}{165})} \tag{2}$$

where t is the equivalent granular thickness of the pavement in centimeters calculated by using equivalency factors based on equivalent granular thicknesses of each material. For example, 1 cm of base course equals 2 cm of equivalent granular thickness. The equivalency factor can be determined as follows (Briaud et al. 1982). If two different base course materials A and B are available to build a pavement, the use of each material will result in a different base course thicknesses, H_A and H_B. If A is the reference base course, the ratio H_B/H_A is the equivalency factor of base course B with respect to A. The equivalency factor is determined from Odemark's approximate equation (1949):

$$\frac{H_b}{H_a} = \left(\frac{E_a}{E_b}\right)^{0.33} \tag{3}$$

where E_A and E_B are the moduli of each material measured with the pressuremeter.

The following procedure, based on a chart approach, can be used to design new flexible airfield pavements. It is based on the pavement pressuremeter test results (Briaud and Shields 1979b) and on the fact that a good correlation was found between the average pavement pressuremeter modulus and the pavement bearing strength (Figure 4).

1. Pavement pressuremeter tests are performed in the subgrade at regular intervals along the proposed pavement section. The test holes are spaced about 300 ft (100 m) apart and at each hole location a series of tests are performed at 1 foot (0.3 m) intervals to a depth of 5 ft (1.5 m).
2. The reload modulus (E_r), (Figure 3 and Eq. 1) is calculated for each test, and a profile of E_r versus depth is prepared.

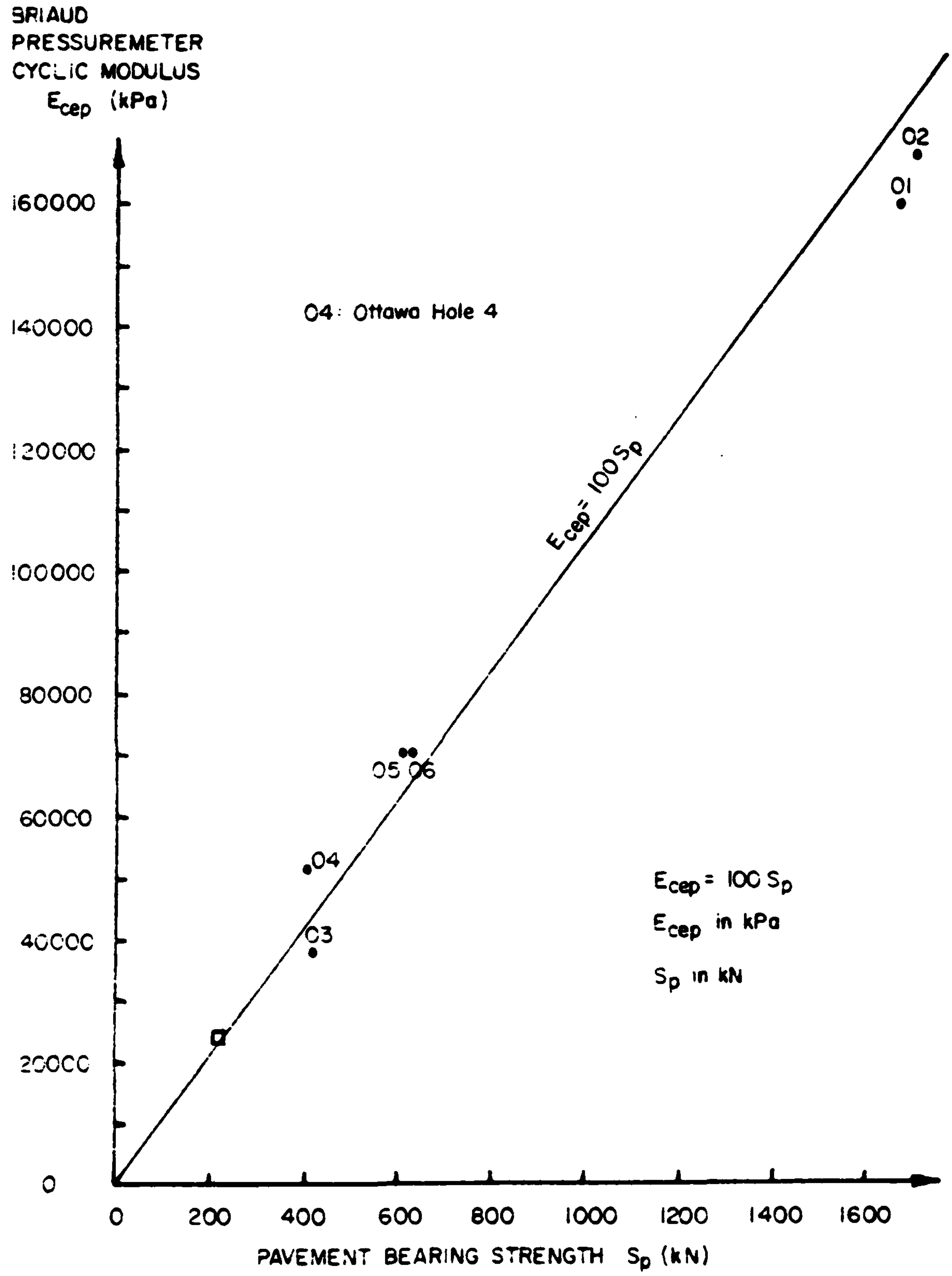

Fig. 4 - Pavement Equivalent Briaud Pressuremeter Cyclic Modulus versus Pavement Bearing Strength (Multilayer Elastic Analysis).

3. The subgrade average pressuremeter reload modulus (E_{res}) is determined for each test-hole location. In order to do this, a subgrade bearing strength (S_s) has to be assumed in order to calculate the settlement of the rigid plate (s) using a multilayer elastic theory. An S_s value of 20,000 lbs (100 kN) is recommended. Note that this assumption has no influence on the magnitude of E_{res}. The value of E_{res} is easily determined if a Finite Element Method program is available. If it is desired to find E_{res} by hand the following approximate equation is used.

$$\frac{1}{E_{res}} = 0.1[(22.1/E_1) + (33.5/E_2) + (24.6/E_3) + (14.8/E_4) + (5/E_5)] \qquad (4)$$

where E_1 is the reload modulus obtained at the shallowest test in the subgrade, and E_2, E_3, E_4 and E_5 are the reload moduli corresponding to the next four test depths (1 foot increments). This formula was obtained by considering a single average strain distribution below the plate (Briaud et al. 1982).

4. The E_{res} values are multiplied by the applicable spring reduction factor, and the lower quartile factor E_{res} value is determined. The spring reduction factor takes into account the loss of subgrade strength during the thawing of the frozen ground in the spring of the year. This value is equal to one for climates with no spring thaw. A statistical analysis leads to the lower quartile E_{res}, which is considered to be the design in situ E_{res} value.
5. The aircraft load rating of the design plane is obtained (Briaud and Shields 1979b). The in situ E_{res} and the design chart of Figure 5 are used to determine the required equivalent granular thickness (t_1).
6. If base course material is available from different borrow sections, it may be desirable to prepare pavement test sections with the different base course materials and to test them with the pressuremeter.

For the evaluation and design of overlays on existing pavements, the following procedure applies:

1. Pavement pressuremeter tests are performed in the subgrade at regular intervals along the proposed pavement section. The test holes are spaced about 300 ft (100 m) apart and at each hole location a series of tests are performed at 1 ft (0.3 m) intervals to a depth of 5 ft (1.5 m).
2. The reload modulus (E_r)(Eq. 1), is calculated for each test, and a profile of E_r versus depth is prepared.
3. Only the results from the tests in the subgrade are considered for use in the design, but tests in the base and the subbase are of considerable value, since they allow the engineer to assess the competence of the layers of the pavement.

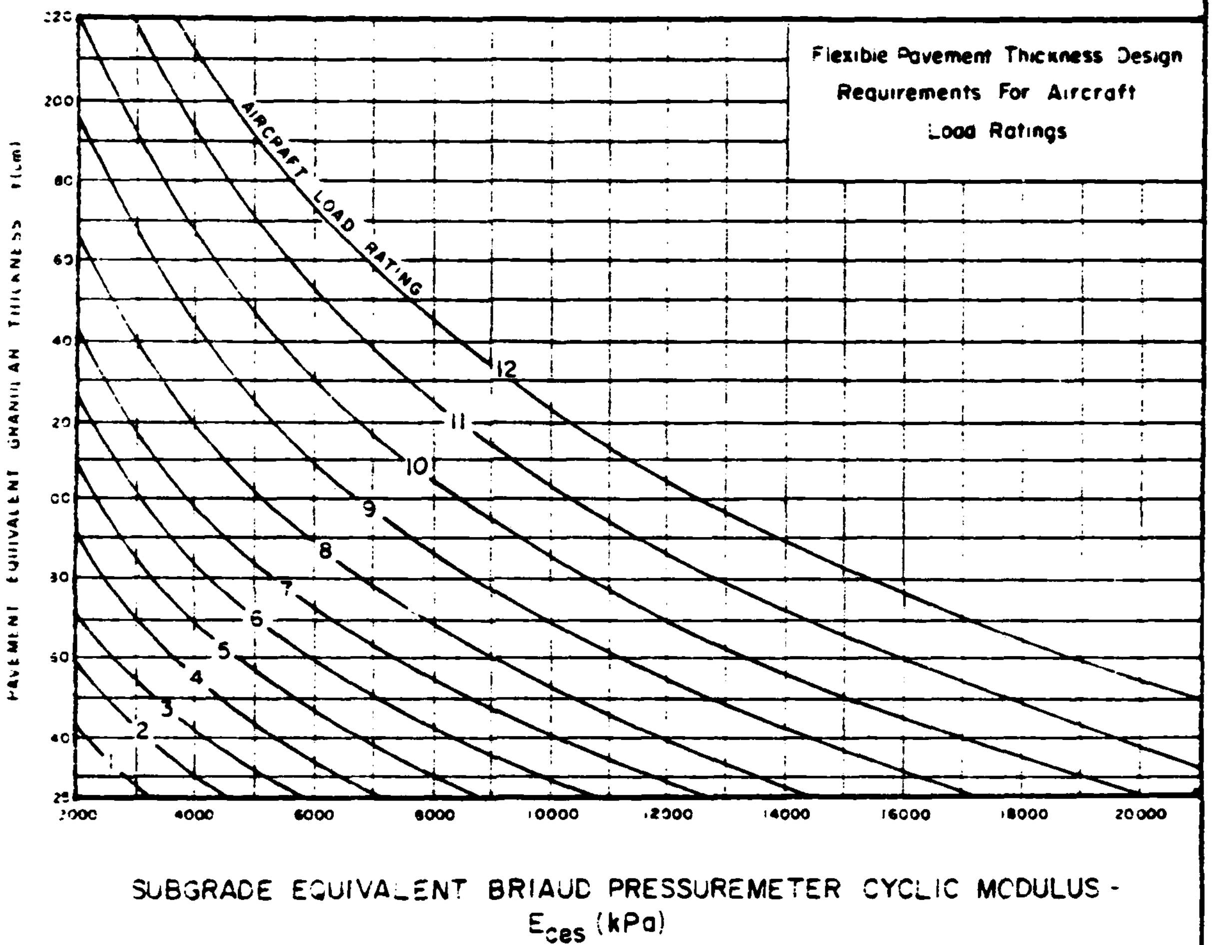

Fig. 5 - Thickness Design Chart Based on the Briaud Pressuremeter Test for Airfield Flexible Pavement.

4. Follow step 4 of the pressuremeter new pavement design procedure.
5. Follow step 5 of the pressuremeter new pavement design procedure.
6. This required thickness (t_1) is compared to the equivalent granular thickness of the existing pavement (t_2). An overlay is necessary if t_1 is greater than t_2 and is calculated using:

$$t_{overlay} = \frac{(t_1 - t_2)}{\text{equivalency factor}} \tag{5}$$

where the equivalency factor is determined as previously described.

As part of the study by Briaud (1979) a second approach was taken for solving the problem of pavement design and evaluation. This approach was based on the use of multilayer elastic theory. In this case the pavement/subgrade system is considered to be a multilayered elastic continuum. Each layer is characterized by a modulus of elasticity (E), and a Poisson's ratio (ν). Two strains are considered to be critical for engineering purposes, the maximum horizontal tensile strain (ε_h) at the lower face of the asphalt layer, and the maximum vertical compressive strain (ε_v) at the top of the subgrade. The design asphalt and pavement thicknesses required, ensure that the magnitude of ε_h and ε_v are within acceptable limits.

For the multilayer elastic approach, moduli and Poisson's ratio values were assigned to the asphalt, while pressuremeter reload moduli (E_r) were used as elastic moduli for the base, subbase and subgrade layers. The computer program BISAR (Bitumen-Structures-Analysis-in-Roads) (Claessen et al. 1977) was used to calculate ε_h, ε_v and the maximum pavement deflection (s) under a single aircraft gear loading for the design aircraft. The results from BISAR indicated that the predicted horizontal and vertical strains were too high (i.e. too close to the limiting strains). It was concluded that the use of E_r in multilayer elastic design was not compatible with the use of the established limiting strain criteria (Claessen et al. 1977). The E_r values were too small, resulting in calculated strains which were too large. The reason is that the modulus E_r was calculated over an average of 4% volumetric strain. It has been shown (Kondner 1963) that E_r values calculated over smaller volumetric strains are much higher. The basic conclusions of this portion of the research by Briaud (1979) was to continue investigating the determination of E_r values over much smaller strain levels.

Briaud et al. (1982) studied the effects on the PPMT modulus of various strain levels and various stress levels and showed that it was possible to obtain much higher moduli at much lower strains.

Another segment of the research conducted by Briaud et al. (1982), was the use of the PPMT soil limit pressure (p_L), for determining the ultimate capacity of a pavement. In this manner the limit pressure could be used to determine the maximum load that could be carried by the pavement.

5. MODULI FROM THE PAVEMENT PRESSUREMETER TEST

5.1 Modulus as a Function of Stress, Strain, Creep and Cycles

Soil moduli are measures of the deformation properties of a soil. The soil modulus is influenced by many factors. For a given soil the major influencing factors are:

a.) the strain level at which the modulus is measured,
b.) the stress level at which the modulus is measured,
c.) the rate of loading, and
d.) the number of load repetitions.

The influence of the **strain level** on the soil modulus was studied by Kondner (1963). He approached the problem by considering stress-strain curves resulting from typical triaxial tests conducted on soil samples (Figure 6). Kondner then fit a hyperbola to those stress strain curves:

$$\frac{\varepsilon}{\sigma} = a + b\varepsilon \tag{6}$$

where a and b are as shown on Figure 6. Figure 7 is a plot of the straight line form of Eq. 6 with ε/σ replaced by 1/E. In order to find a and b for a given soil, the data points of the stress strain curve are plotted in a graph such as the one of Figure 7 and a best fit linear regression is used to find the intercept a and the slope b.

The influence of the mean **stress level** on the modulus was studied by Janbu (1963). With the exception of the quick failure of saturated soils (i.e. unconsolidated undrained tests, it was found that both the tangent modulus E_t and the compressive strength q_u of soils vary with the confining stress σ_3 (Figure 8). Janbu's (1963) experimental studies have shown that the relationship between the initial tangent modulus and confining pressure may be expressed as (Duncan and Chang 1970):

$$E_i = K_2 \left(\frac{\sigma_3}{p_a}\right)^n \tag{7}$$

where: E_i is the initial tangent modulus, σ_3 is the minor principal stress, p_a is the atmospheric pressure, K_2 is a modulus number, and n is the exponent determining the rate of variation of E_i with σ_3. The values of the parameters K_2 and n may be determined from the results of a series of triaxial tests by plotting log E_i versus log σ_3 and fitting a straight line to the data (Figure 9). Later this model was modified by writing $E = K_1\theta^n$ and then normalized:

$$E = K_1 \theta^n \tag{8}$$

and then $$E = K_2 \left(\frac{\theta}{p_a}\right)^n \tag{9}$$

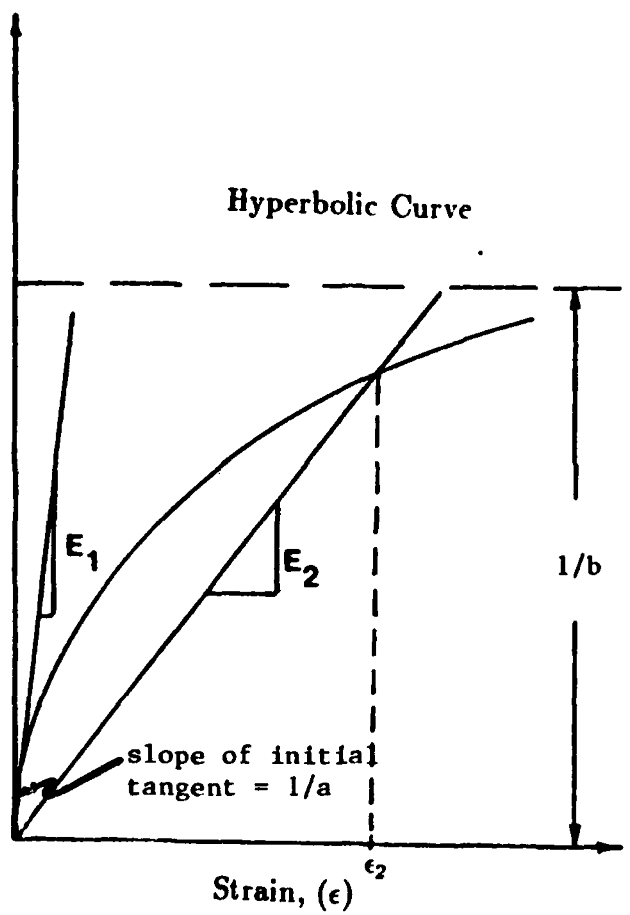

Fig. 6 Typical Stress-Strain Curve (constant σ_3)

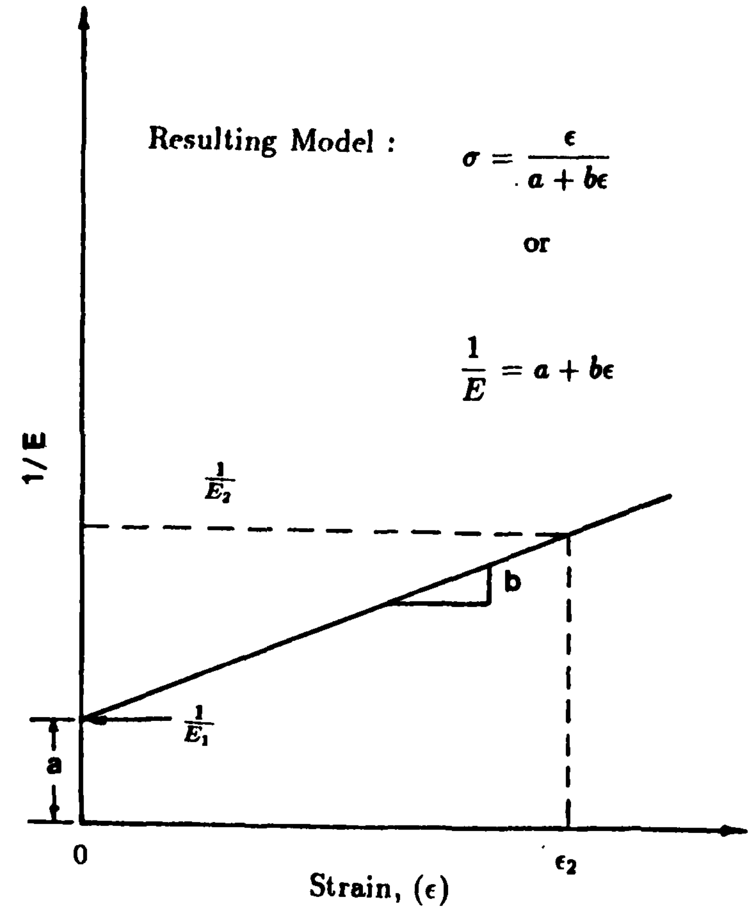

Fig. 7 Resulting Strain Level Plot

where θ is the mean normal stress and p_a is the atmospheric pressure. In this study, the last model was selected (Figure 8 and 9 and Eq. 9).

The effect of **Rate of Loading or Creep** on the secant modulus was studied by Riggins (1981). The physical reason for the rate-dependent responses of clays is not simple (Lacasse 1979, Mitchell 1976, Pike 1981, and Whitman 1970). Three elements in clays contribute to rate dependency of the engineering properties: the pore water, the particle contacts and the water/soil-skeleton interaction (Briaud and Garland 1985). The free water in the pores is a viscous fluid. In fact water alone is much more viscous than clays since it is a Newtonian fluid (i.e. the viscosity is constant throughout the range of applied stresses). At higher water contents increasing the load rate leads to a higher modulus for clays. The particle contacts also exhibit viscous behavior. These contacts are formed by penetration of the particle with its adsorbed water layer into the adsorbed water layer of the adjacent particles. The viscosity of the adsorbed water is larger than the viscosity of the free water (Low 1947). Thus the thicker the adsorbed water layer the more viscous the clay. The water/soil-skeleton interaction varies with shearing rate. At slow rates, the particles in the soil-skeleton have time to deform along the path of least resistnce. At high rates, the particles in the soil skeleton do not have time to find that path and the soil dilates more than at slow rates; this leads to lower excess pore pressures. Riggins (1981) developed a model which related the increase in undrained shear strength S_u to the time of failure t as:

$$\frac{S_{u1}}{S_{u2}} = \left(\frac{t_2}{t_1}\right)^{n_{crp}} \qquad (10)$$

where: S_{u1} and S_{u2} are the undrained shear strengths measured at times to failure t_1 and t_2, respectively, and n_{crp} is the viscous exponent.

Based on the results of 152 undrained laboratory tests on clay found in in the literature, the range of n_{crp} falls between 0.02 and 0.10 with an average of 0.061 (Briaud and Garland 1985). Eq. 9 can be adapted to predict the variation of the secant modulus at any load level with time (Figure 10). This model shows that the faster a soil is loaded the higher the modulus will be (Figure 11). In terms of the secant modulus Eq. 9 becomes:

$$\frac{E_{st}}{E_{s0}} = \left(\frac{t_t}{t_0}\right)^{-n_{crp}} \qquad (11)$$

where: E_{st} and E_{s0} are secant moduli measured in times $t = t_o$ and $t = t$ after the start of the creep portion of the test, respectively, and n_{crp} is the viscous exponent which indicates a higher viscosity (i.e. higher modulus) as values approach zero.

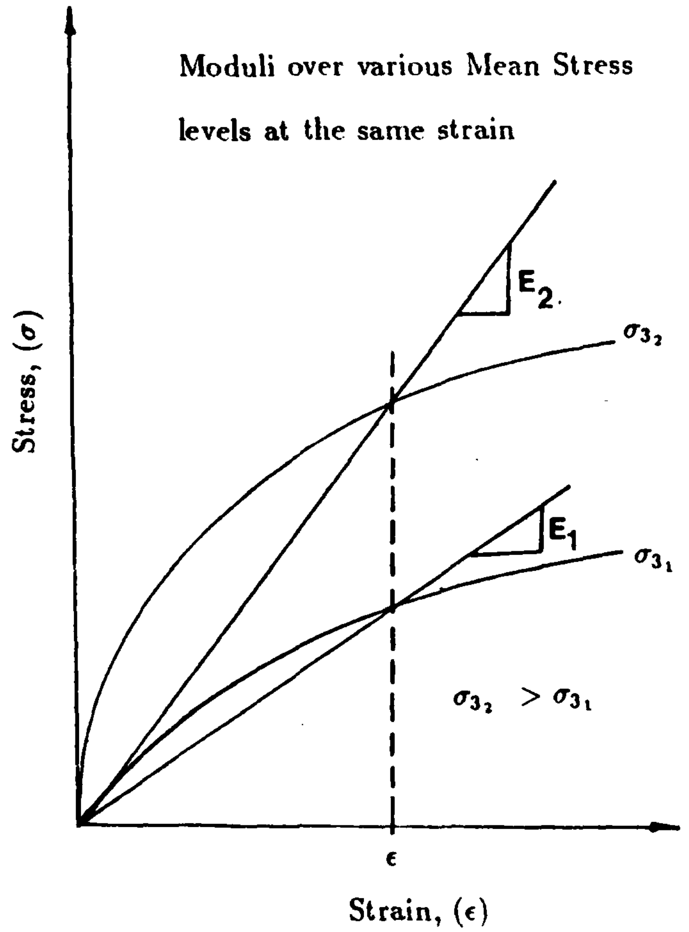

Fig. 8 Typical Stress-Strain Curve (variable σ_3)

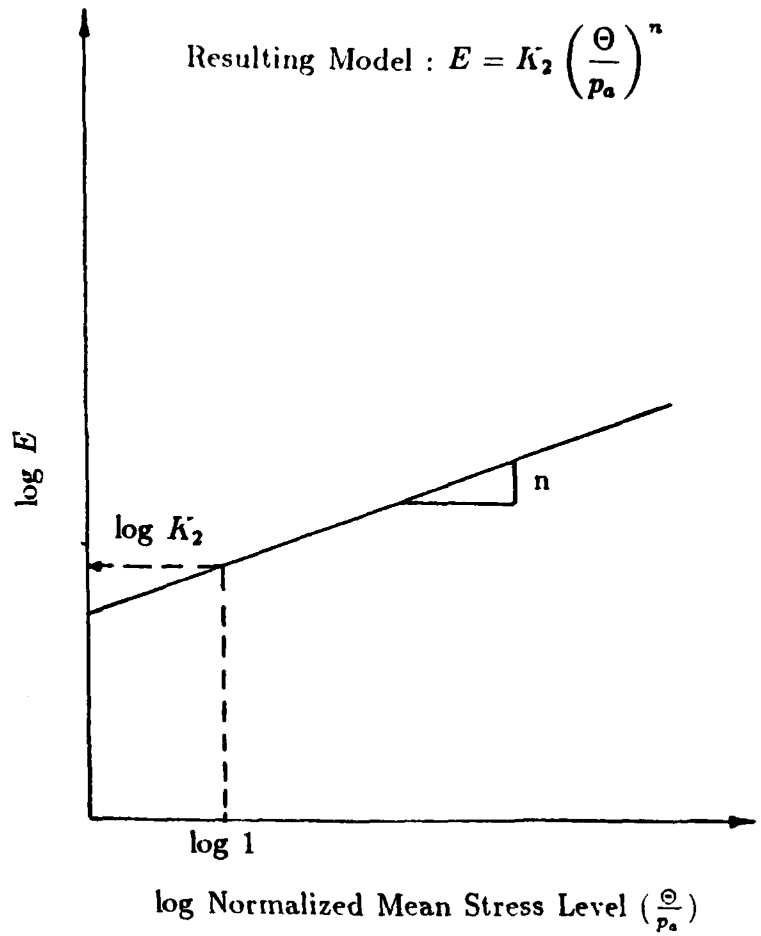

Fig. 9 Resulting Stress Level Plot

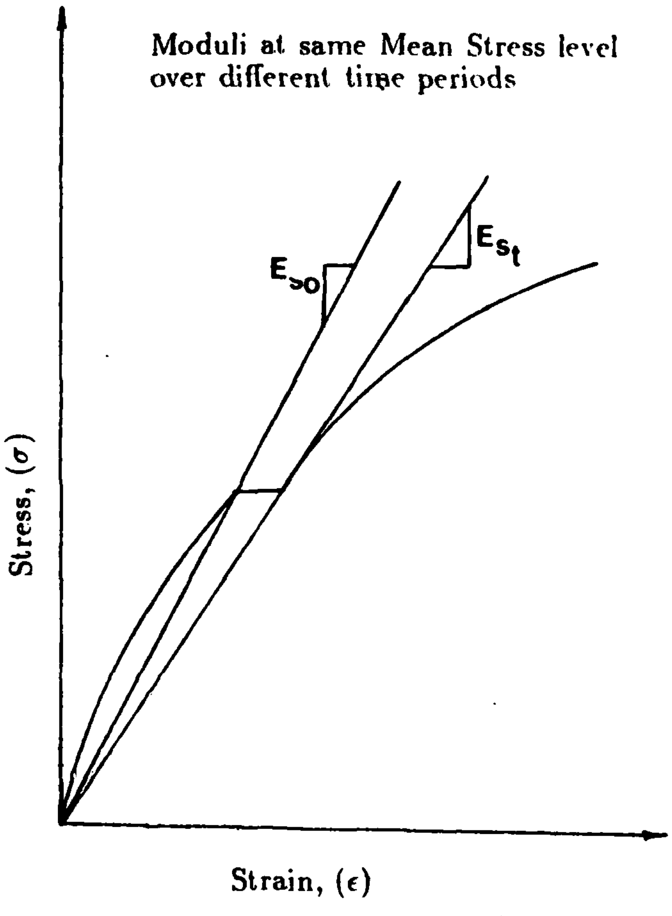

Fig. 10 Typical Stress-Strain Curve with Creep

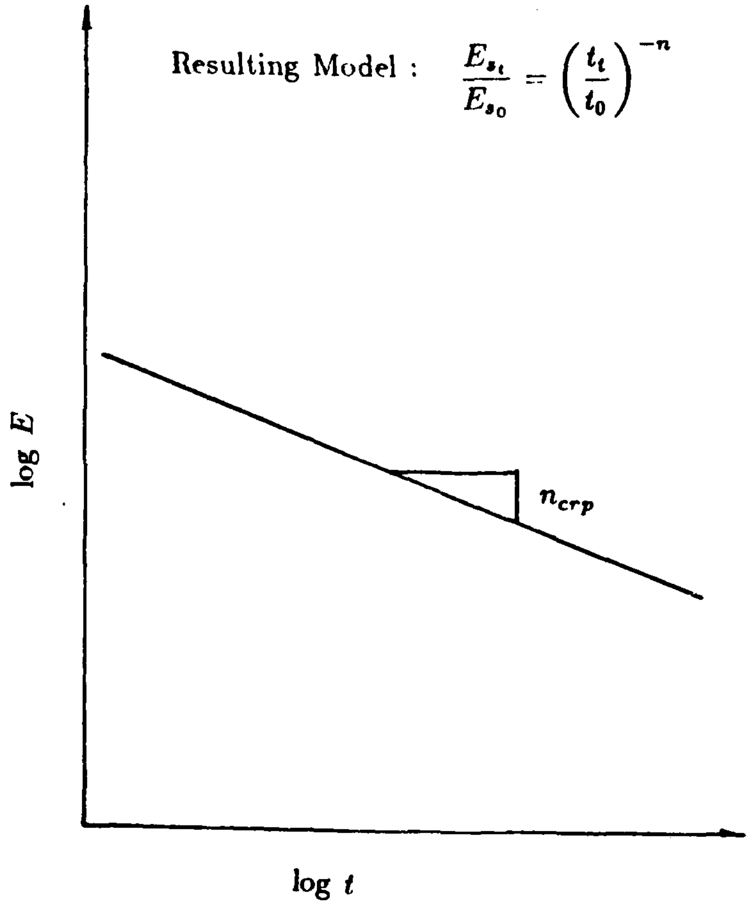

Fig. 11 Resulting Creep Test Plot

The slope of the log E versus log t plot (Figure 11) is the viscous exponent n_{crp}.

The effect of **repetitive loading** on the modulus (Figure 12) is significant. Idriss et al. (1978) developed an inverse power law model for the effects of earthquake loadings on the modulus. The degradation of the modulus due to cyclic loading for soft clays was determined by looking at two typical cyclic tests on soft clays (Idriss et al. 1978). One test was strain controlled and the other test was stress controlled. Both indicated that the shear modulus G_s decreased with increasing number of cycles. These two tests along with a series of cyclic triaxial tests found in the literature revealed the following:

a) The slope of the hysteresis loop is steeper for smaller strains
b) The total energy loss W increases with increasing strains.
c) As the number of cycles increases (Figure 12) the secant modulus E_s decreases.

The ratio E_{sn}/E_{s1} (Figure 12, 13) is a measure of the degradation of the soil stiffness and is defined as the degradation index δ. The data of Idriss et al. (1978) showed that a plot of log E_{sn}/E_{s1} versus log N was a straight line with a slope of -n. This implies that E_{sn}/E_{s1} could be related to the number of cycles N by a power law of the form:

$$\frac{E_{sn}}{E_{s1}} = N^{-n} \tag{12}$$

in which n, the slope, is defined as a degradation parameter. Values of n were found to range from 0.05 to 0.25 for soft clays. Idriss et al. found that n increased with the cyclic strain level applied to the specimen, that n was essentially independent of the initial confining pressure, and that n appeared to be a reasonably unique function of the cyclic strain over a fairly wide range of initial water contents and confining pressures.

Equation 12 was written for the secant modulus E_s, the cyclic modulus E_c, and the resilient modulus M_r (Figure 12, 13). For the secant modulus the equation becomes:

$$\frac{E_{sn}}{E_{s1}} = N^{-n_{sec}} \tag{13}$$

For the cyclic modulus (slope of the reload part of the cycle) and for the resilient modulus (slope of the unload part of the cycle) the Idriss model becomes:

$$\frac{E_{cn}}{E_{c1}} = N^{-n_{cyc}} \tag{14}$$

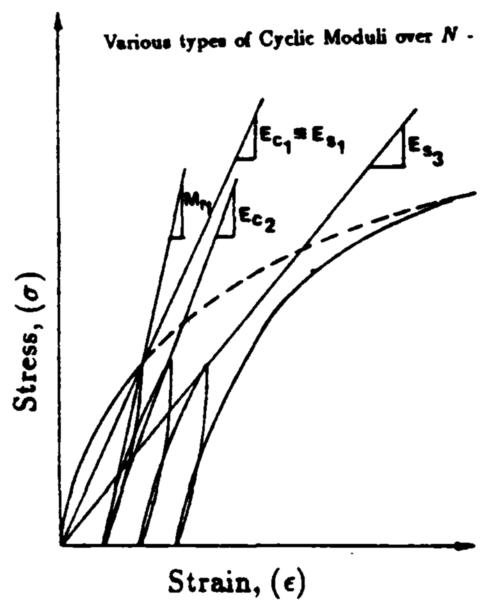

Fig. 12
Typical Stress-Strain Curve
with Cycles

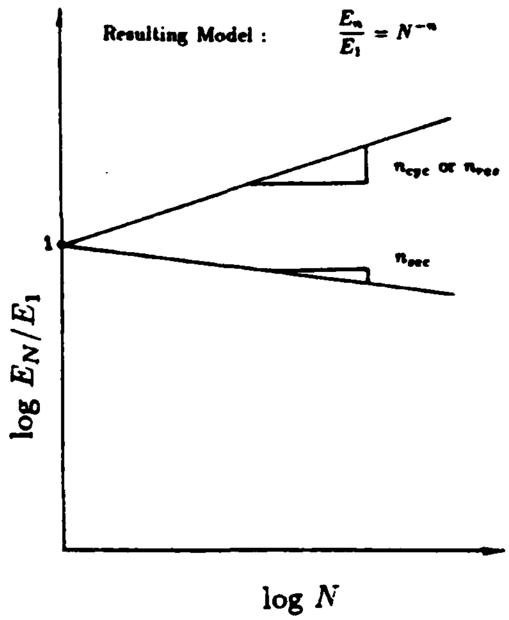

Fig. 13
Resulting Cyclic Model Plots

$$\frac{M_{rn}}{M_{r1}} = N^{-n_{res}} \qquad (15)$$

where: E_{cn} and E_{c1} are the cyclic moduli of the n^{th} and 1st cycle respectively. M_{rn} and M_{r1} are the resilient moduli of the n^{th} and 1st cycle respectively, and n_{cyc} and n_{res} are the cyclic exponents for the cyclic and resilient moduli, respectively.

A plot of log E_{sn}/E_{s1} versus log N yields the cyclic exponent n_{sec} as the slope of the line (Figure 13). Similar plots for the cyclic and resilient moduli yield n_{cyc} and n_{res}, respectively.

5.2 Obtaining Moduli from Pavement Pressuremeter Tests

It is possible to run the pavement pressuremeter test so that many of the loadings encountered at airports can be simulated. Each portion of the airport pavement is subjected to different loading conditions. The runway is subjected to two dynamic loads, the impact load during landing plus the cyclic loading from high speed passage of the aircraft. The taxiway is subjected to dynamic loads resulting from aircraft speeds of about 20 mph (32 kmh). The apron or parking area is subjected to dynamic loads which results from speeds of about 5 mph (8 kmh) plus static loads which occur during parking of the aircraft. To simulate the effect on the modulus due to various size aircraft, the stress level and strain level at which the modulus is obtained in a pressuremeter test can be controlled. To simulate the effects on the modulus from load repetitions encountered on the runways and taxiways it is possible to conduct a number of unload-reload cycles at any time during the PPMT test. To simulate the effects on the modulus from various rates and creep loads it is possible to maintain a constant stress during the PPMT test over any length of time. The models described in section 5.1 were adapted to the PPMT test and are described below.

The first model considered is the **strain model** (Eq. 6). The parameters to be obtained are a and b. This can be done by measuring moduli (E) for various values of the strain. In the pressuremeter test, moduli values are obtained from the slope of unload-reload loops (Figure 14). The relative increase in cavity radius is $\Delta R_c/R_c$ (Figure 14). By definition the hoop strain $\varepsilon_{\theta\theta}$ in the soil at the cavity wall is:

$$\varepsilon_{\theta\theta} = \frac{u}{R_c} \qquad (16)$$

where u is the radial replacement. Since the radial displacement (u) is the increase in cavity radius ΔR_c, the strain can be written as:

$$\varepsilon_{\theta\theta} = \frac{\Delta R_c}{R_c} \qquad (17)$$

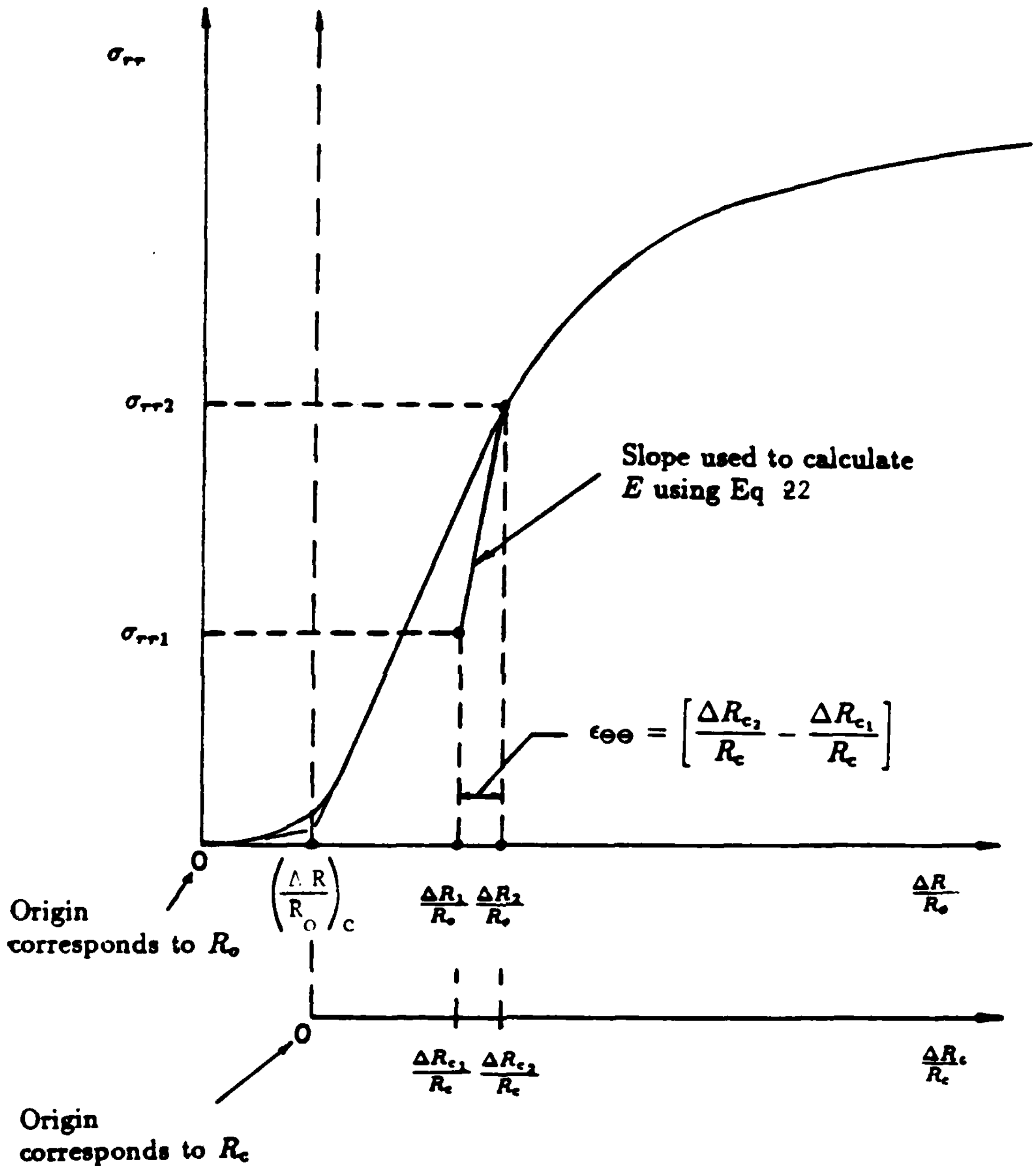

Fig 14

Definition Sketch for Establishing the Radius of the Cavity for PPMT Tests

The incremental hoop strain for an unload reload loop is (Figure 14):

$$\varepsilon_{\theta\theta} = \frac{\Delta R_{c1}}{R_c} - \frac{\Delta R_{c2}}{R_c} \tag{18}$$

The initial radius of the cavity R_{co} is calculated from (Figure 14):

$$R_{co} = R_o + \left(\frac{\Delta R}{R_o}\right)_c \times R_o \tag{19}$$

where R_o is the radius of the deflated probe, and $(\Delta R/R_o)_c$ is obtained as shown on Figure 14. The current radius of the cavity R_c is:

$$R_c = R_o + \left(\frac{\Delta R}{R_o}\right) \times R_o \tag{20}$$

Then the increase in cavity radius is:

$$\Delta R_c = R_c - R_{co} \tag{21}$$

Using the above equation it is therefore possible to calculate the hoop strain at any point during the test by using the pressuremeter curve (Figure 14). Note that in elasticity, the hoop strain $\varepsilon_{\theta\theta}$ is equal to the radial strain ε_{rr} (Baguelin et al. 1978).

By performing unload-reload loops over several strain ranges (Figure 18a), several values of E corresponding to several values of $\varepsilon_{\theta\theta}$ can be obtained by (Briaud et al. 1986):

$$E = (1+\nu)\left[\left(1+\frac{\Delta R_1}{R_o}\right)^2 + \left(1+\frac{\Delta R_2}{R_o}\right)^2\right]\left[\frac{\sigma_{rr2} - \sigma_{rr1}}{(1+\frac{\Delta R_2}{R_o})^2 - (1+\frac{\Delta R_1}{R_o})^2}\right] \tag{22}$$

where ΔR_1 and ΔR_2 are the increases in probe radii at the beginning and end of the unload-reload loop (Figure 14), σ_{rr2} and σ_{rr1} are the radial stresses at the cavity wall, at the top and bottom of the unload-reload loop, respectively (Figure 14), ν is Poisson's ratio (assumed to be 0.33 in all cases), and R_o is the initial radius of the probe.

The strain $\varepsilon_{\theta\theta}$, is the hoop strain at the wall of the soil cavity. The modulus $E_{\varepsilon\theta\theta}$ (or E in Eq. 22) is the average modulus measured in the soil mass. Therefore, $\varepsilon_{\theta\theta}$ does not correspond directly to $E_{\varepsilon\theta\theta}$ and must be corrected to represent the average $\varepsilon_{\theta\theta}$ in the soil mass, ($\bar{\varepsilon}_{\theta\theta}$). This can be done approximately from the following equation (see Appendix F for derivation):

$$\bar{\varepsilon}_{\theta\theta} = 0.32\ \varepsilon_{\theta\theta} \tag{23}$$

Then each loop yields one set of $\bar{\varepsilon}_{\theta\theta}$ and $E_{\bar{\varepsilon}\theta\theta}$. A plot of $1/E_{\bar{\varepsilon}\theta\theta}$ versus $\bar{\varepsilon}_{\theta\theta}$ then gives, by regression, the values of a and b for the strain model (Figure 16).

The second model is the **stress model** (Eq. 9). The parameters to be obtained are K_2 and n. This can be done by measuring E for various values of the stress level. In the pressuremeter test, moduli values are obtained from the slope of unload-reload loops. By performing those unload-reload loops at several stress levels, but over the same strain range (Figure 17) several values of E corresponding to several values of θ can be obtained. The mean normal stress (θ), is the average of the average radial stress ($\bar{\sigma}_{rr}$) within the soil mass plus the average hoop stress within the soil mass ($\bar{\sigma}_{rr}$) plus the average vertical stress within the soil mass (σ_{zz}). This mean normal stress is expressed as:

$$\theta = \frac{1}{3}\left(\bar{\sigma}_{rr} + \bar{\sigma}_{\theta\theta} + \bar{\sigma}_{zz}\right) \tag{24}$$

The radial stress (σ_{rr}) exists at the cavity wall and is the one measured during the PPMT test. The mean horizontal stress within the plastic zone of the soil mass is (Appendix F):

$$\sigma_m = \frac{\bar{\sigma}_{rr} + \bar{\sigma}_{\theta\theta}}{2} = 0.40\ \sigma_{rr} \tag{25}$$

The average vertical stress $\bar{\sigma}_{zz}$ is taken as:

$$\bar{\sigma}_{zz} = \gamma \times h \tag{26}$$

where γ is the total unit weight of the soil, h is the depth at which $\bar{\sigma}_{zz}$ is calculated.

Therefore, the mean normal stress is found from Eq. 24 to 26 as:

$$\theta = \frac{1}{3}\left(0.8\ \sigma_{rr} + \gamma h\right) \tag{27}$$

where σ_{rr} is the radial stress measured by the pressuremeter at mid-height through the loop of the unload-reload cycle. The corresponding modulus (Eq. 22) is obtained from the unload-reload loop as in the case

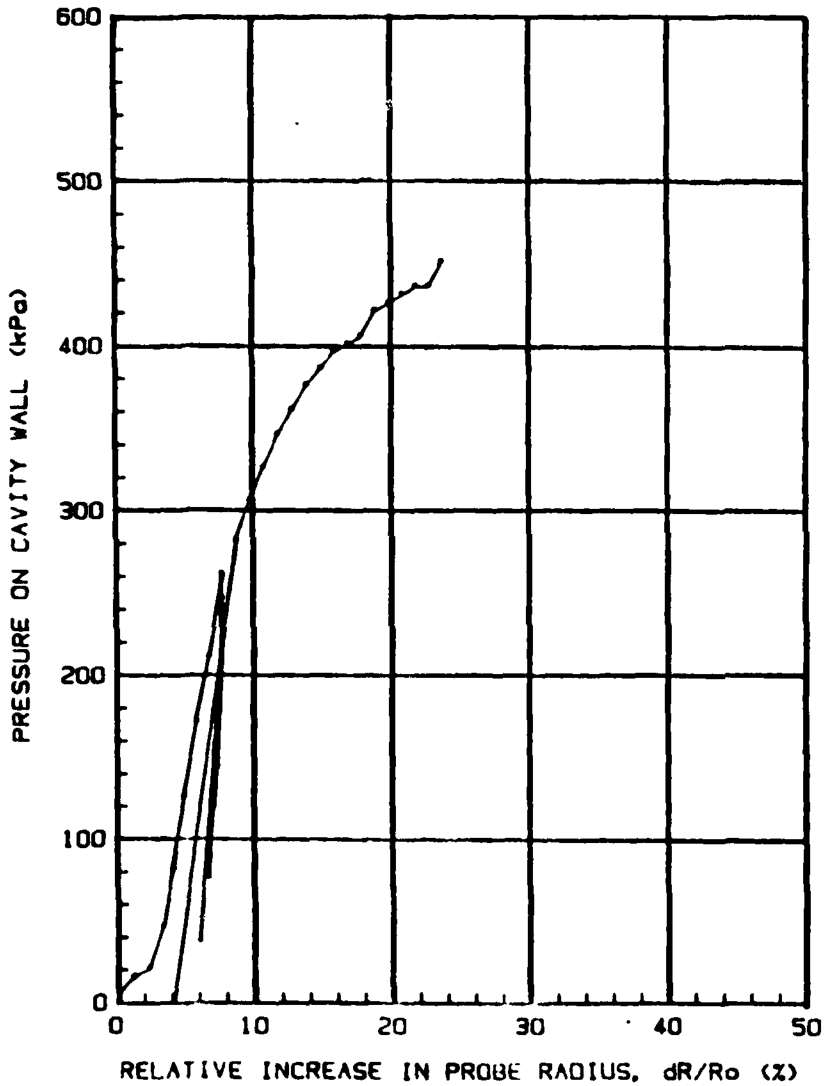

Fig. 15 Typical PPMT Strain Level Plot

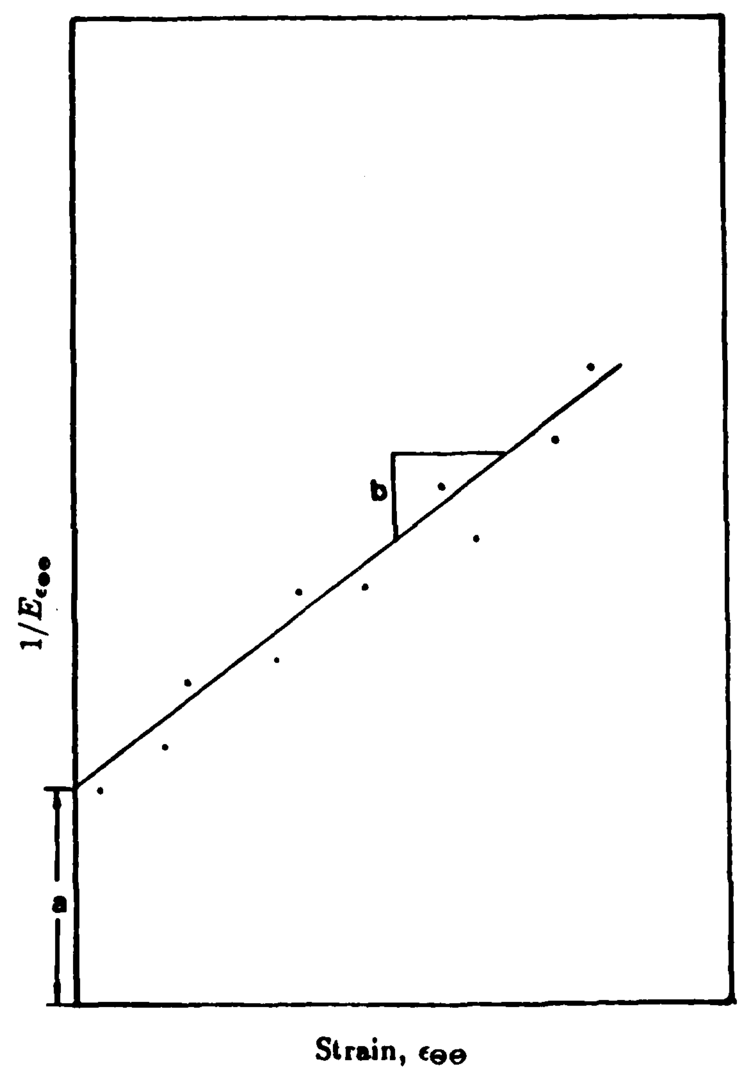

Fig. 16 Resulting PPMT Strain Model Plot

of the strain model. Then each loop yields a set of E_θ and θ values. A plot of log E_θ versus log θ/p_a (p_a is the atmospheric pressure) gives, by regression, the values of K_2 and n for the stress model (Figure 18). The stresses used in Eq. 27 are total stresses. They are also effective stresses if the soil is unsaturated, which was the case in this study and is most often the case for airports, or if the soil drains fast enough. For saturated silts and clays, a pore pressure measurement on the pressuremeter membrane and an assumption of the distribution of excess pore pressures in the soil mass would enable proper use of Janbu's model. For airport pavements on saturated silts and clays however the aircraft loading condition represents an undrained behavior of the soil.

The third model is the **creep or rate of loading model** (Eq. 11). The parameter to be obtained is the viscous exponent n_{crp}. This can be done by maintaining a constant pressure in the pressuremeter while recording the increase in volume of the cavity. The secant modulus E_{s_t} is calculated from the slope S_{s_t} corresponding to an elapsed time t (Figures 19 & 20). The elapsed time t is measured from the beginning of the pressure step. The secant modulus E_s is calculated using Eq. 22). A plot of log E_{s_t}/E_{s_o} versus log t/t_o then gives, by regression, the value of n_{crp} (Figure 21). The secant modulus E_{s_o} is the reference modulus calculated from the slope S_{s_o} corresponding to an elapsed time of 1 minute after the beginning of the pressure step (t_o). This time of 1 minute was chosen because research has indicated that the variation of E_{s1} prior to 1 minute can be erratic (Briaud et al. 1986). Note that the time dependent behavior modeled here, is the result of creep only for the case of unsaturated soils and corresponds to the superposition of consolidation and creep in the case of saturated soils.

The fourth model is the **cyclic model** proposed by Idriss et al. (1978)(Eqs. 13 to 15). The parameters to be obtained are n_{sec}, n_{cyc}, n_{res}. These parameters can be obtained by measuring E_{sn}, E_{cn} and M_{rn} over several cycles (Figure 22). The secant modulus E_{sn} is calculated from the slope S_{sn}, joining the origin which is adjusted to the radius of the cavity to the top of the N^{th} cycle (Figure 23). The cyclic modulus E_{cn} is calculated from the slope S_{cn} of the loading portion of the N^{th} unload-reload loop (Figure 23). The resilient modulus M_{rn} is calculated from the slope S_{cn} of the unloading portion of the N^{th} unload-reload loop (Figure 23). All moduli values are calculated using Eq. 21. A plot of log E_{sn}/E_{s1} versus log N allows to obtain n_{sec} by regression (Figure 24). A plot of log E_{cn}/E_{c1} versus log N allows to obtain n_{cyc} by regression (Figure 25). A plot of log M_{rn}/M_{r1} versus log N allows to obtain n_{res} by regression (Figure 26).

5.3 Influence of the Probe Insertion Technique

The pavement pressuremeter probe can be inserted into the base and

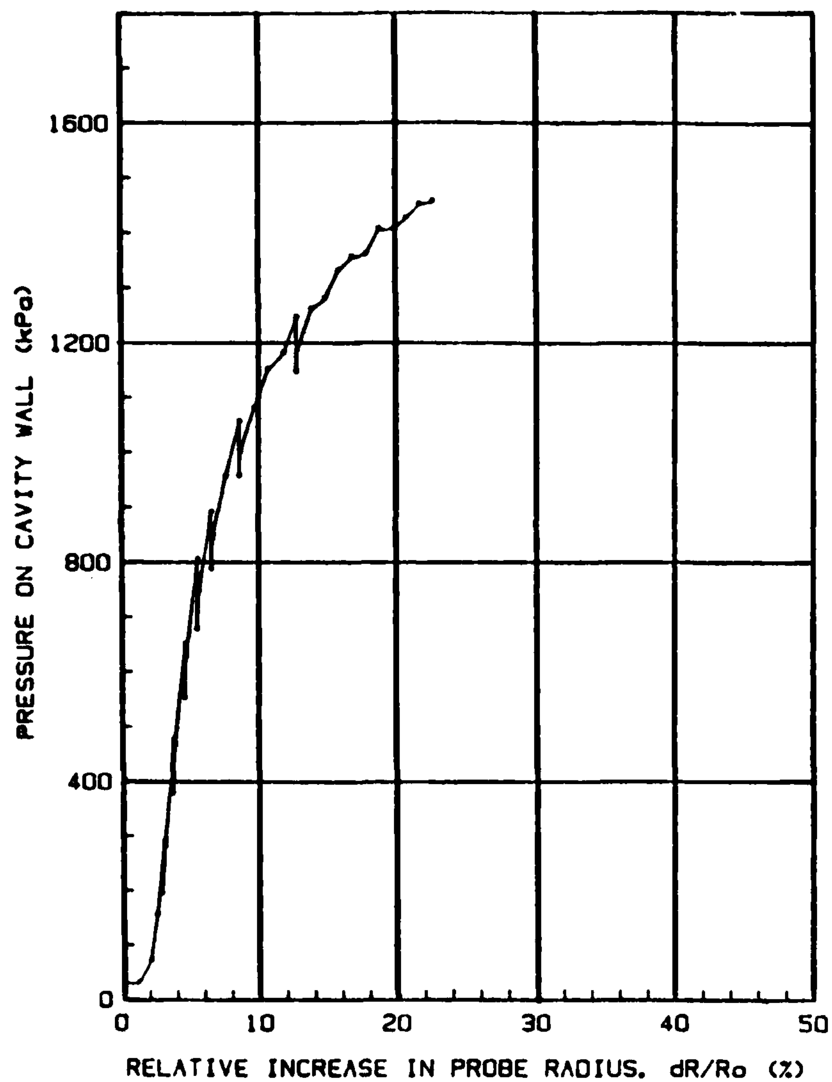

Fig. 17 Typical PPMT Stress Level Plot

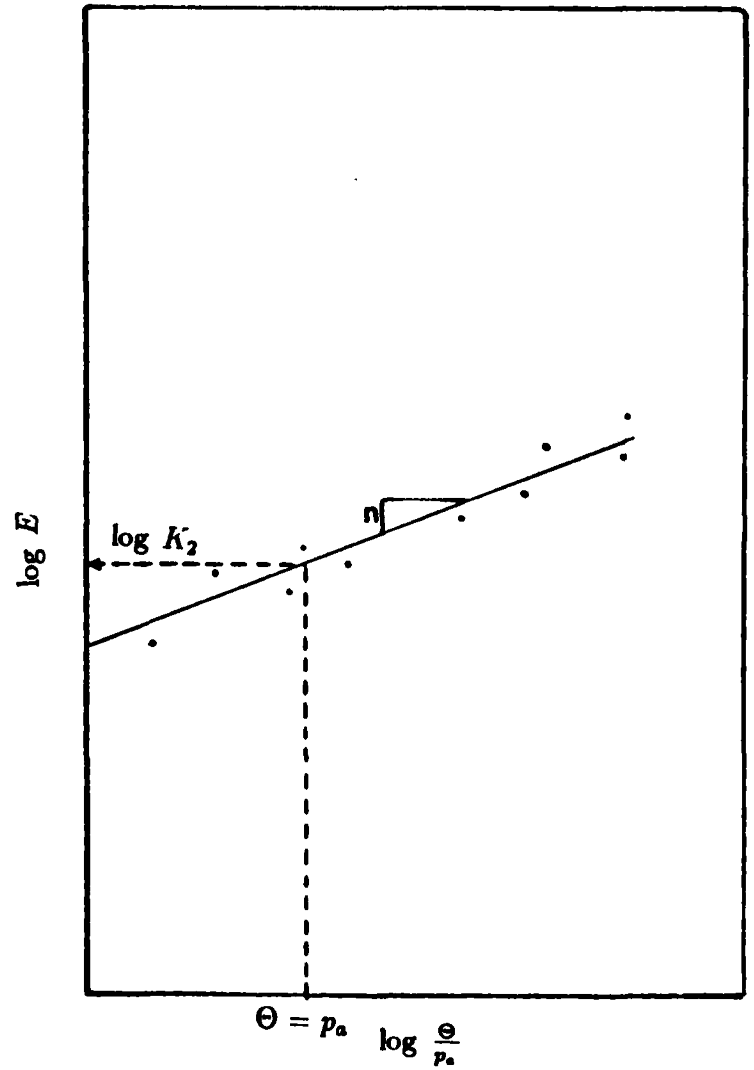

Fig. 18 Resulting PPMT Stress Model Plot

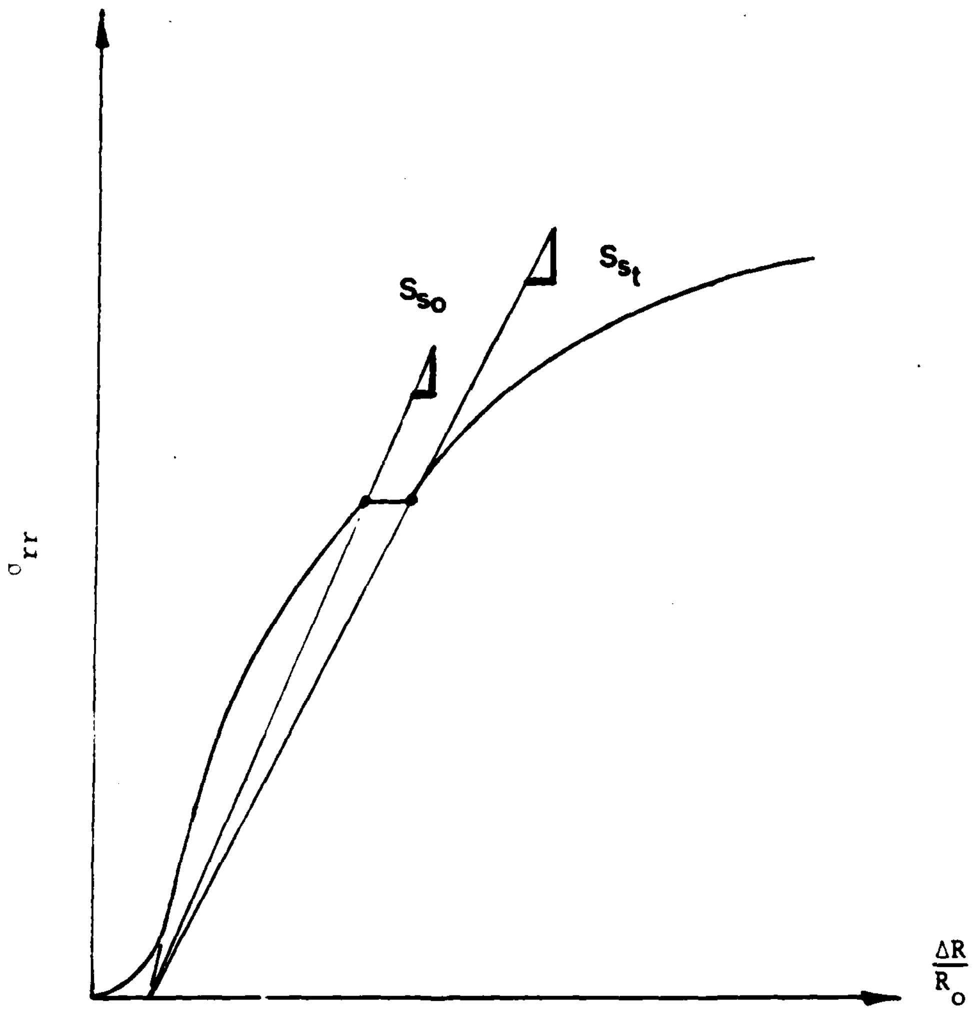

Fig. 19 Typical PPMT Creep Plot Depicting Definitions

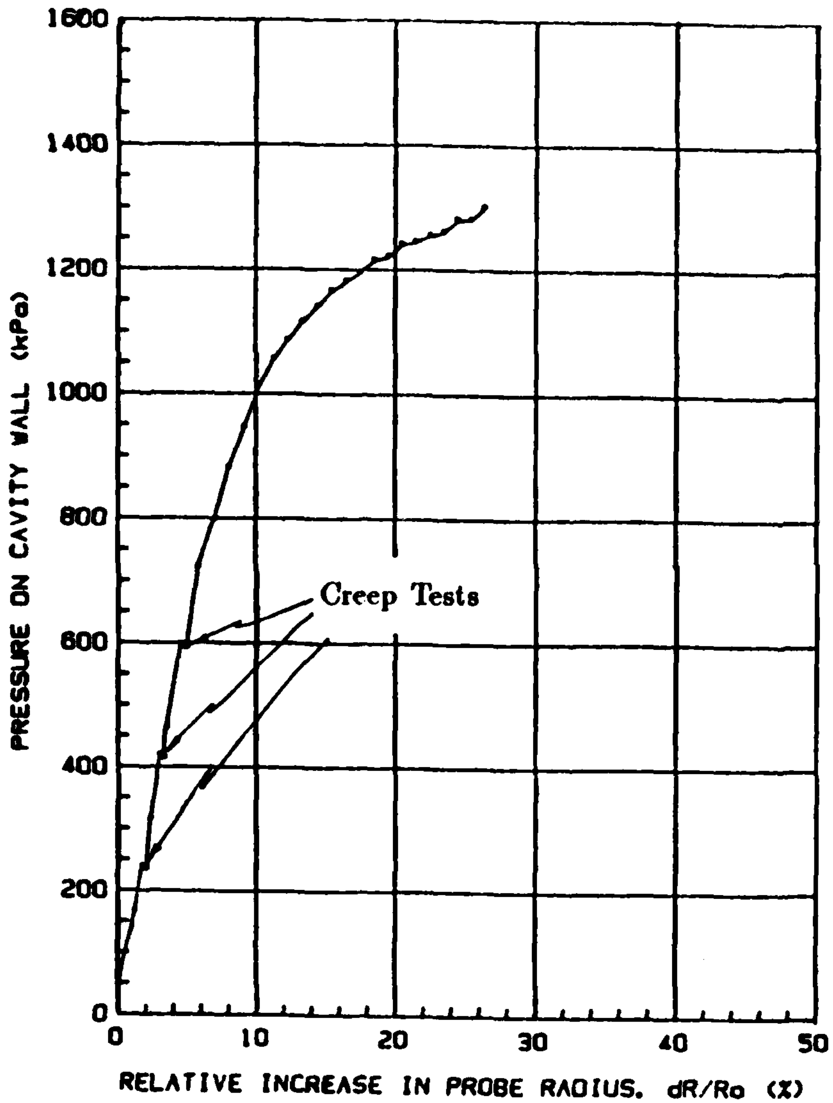

Fig. 20 Typical PPMT Creep Plot

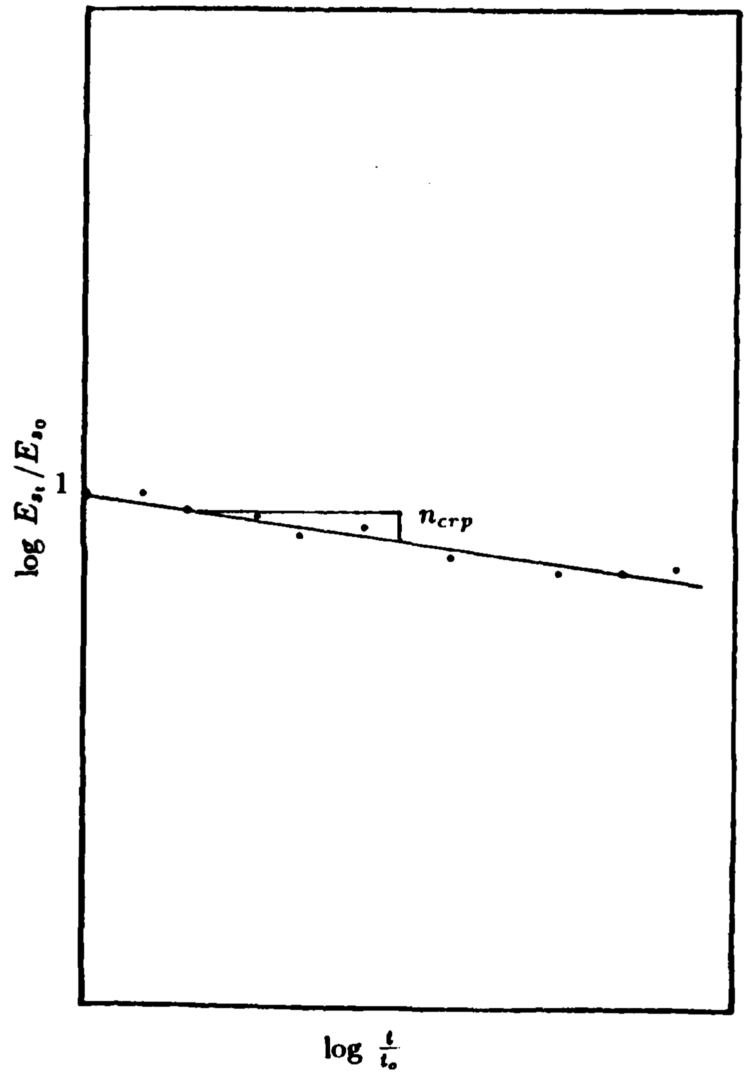

Fig. 21 Resulting PPMT Creep Model Plot

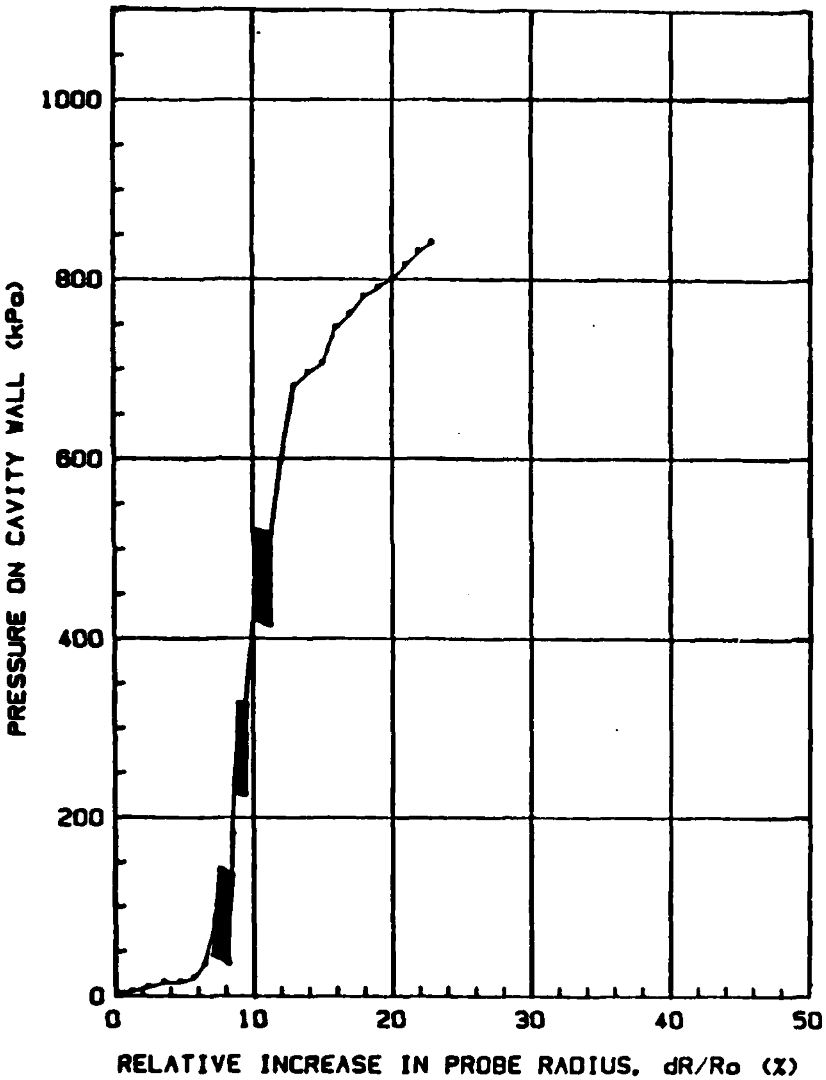

Fig. 22 Typical PPMT Cyclic Plot

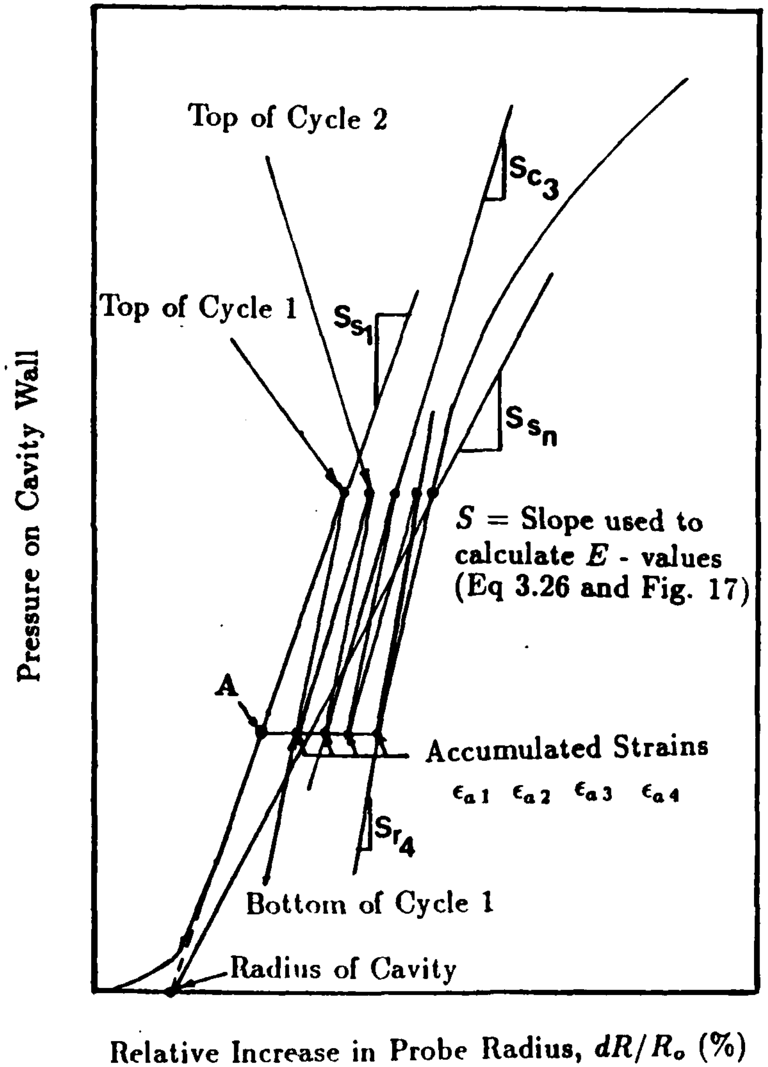

Fig. 23 Typical PPMT Cyclic Plot Depicting Definitions

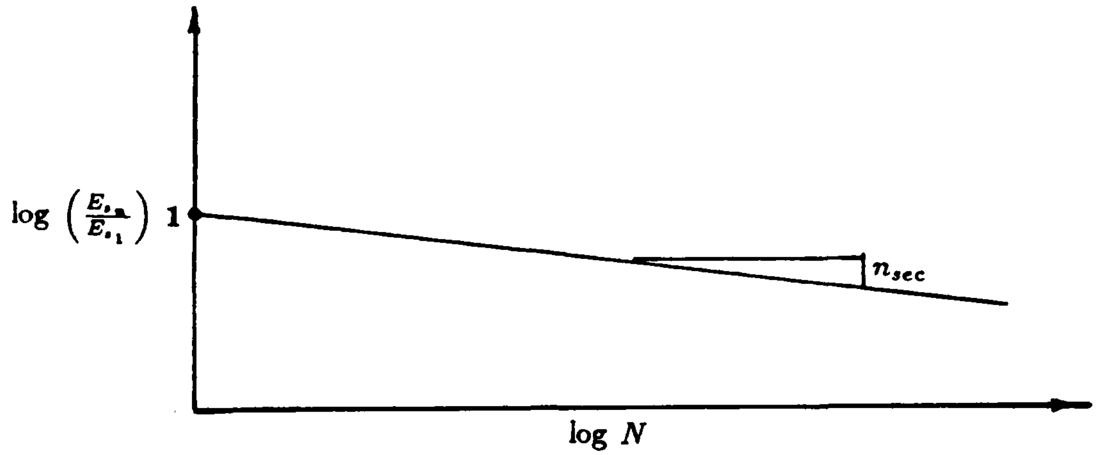

Fig. 24 Log-Log Plot of $\left(\frac{E_{s_n}}{E_{s_1}}\right)$ vs N

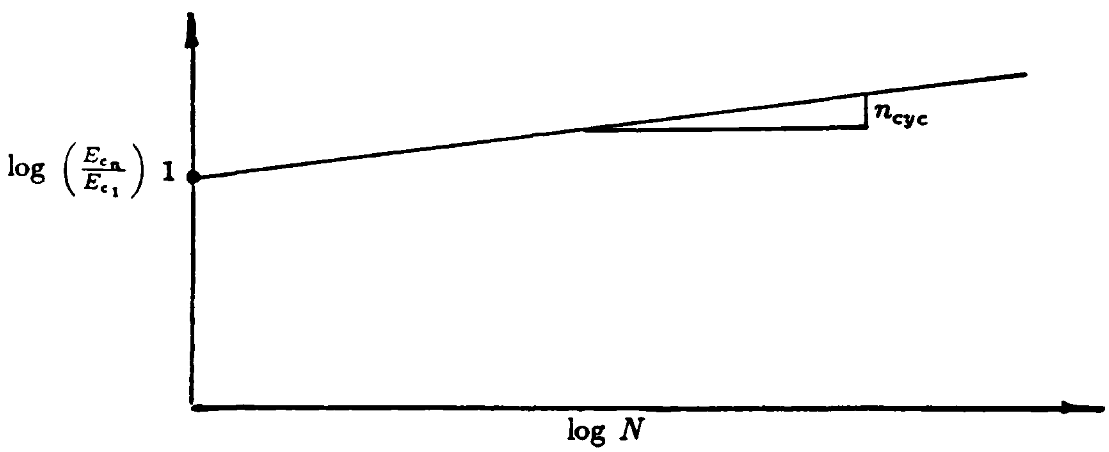

Fig. 25 Log-Log Plot of $\left(\frac{E_{c_n}}{E_{c_1}}\right)$ vs N

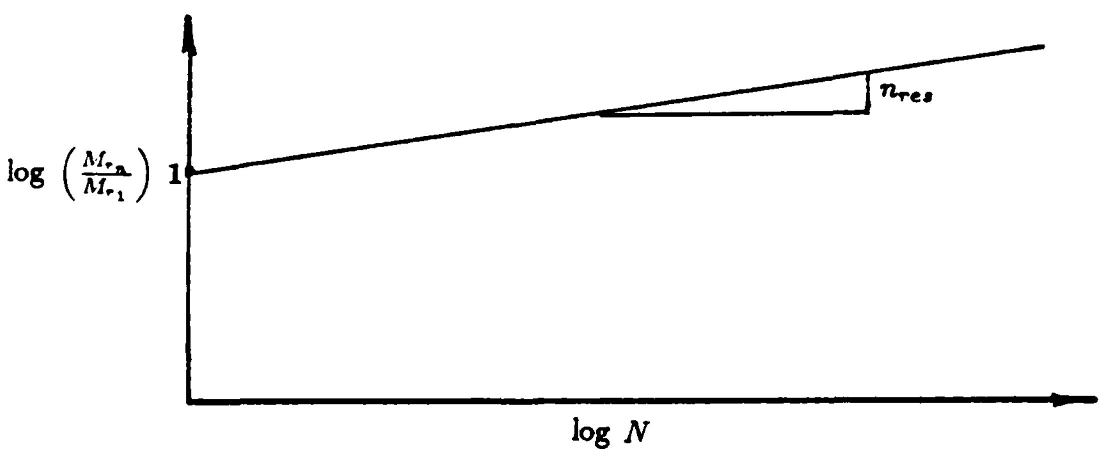

Fig. 26 Log-Log Plot of $\left(\frac{M_{r_n}}{M_{r_1}}\right)$ vs N

subgrade layers by two methods. The first method is to auger a 1.35 in. (3.4 cm) diameter hole, withdraw the auger and lower the probe down to the bottom of the hole. The second method is to drive the probe to the desired test depth with a hammer. Driving is convenient in certain granular soils which may cave into the augered hole. In a separate part of this study a series of tests were performed to compare the results obtained with the driven technique to those obtained with the augering technique (Briaud, et al. 1986). This series of tests was also performed to establish the methods required to obtain the moduli models from the pressuremeter tests. These tests were performed in a clay deposit and repeated in a sand deposit. Figures 27 to 30 show examples of the differences in pressuremeter curves obtained. For the driven pressuremeter test the deflated volume of the probe has an influence on the shape of the resulting curve and on the parameters calculated from the curve. Indeed this zero volume can be such that the inflatable part of the probe has a diameter smaller, equal or larger than the diameter of the steel cone point which precedes the membrane during the driving process (Figure 1). In this study the zero volume was determined by placing the 1.27 in. (3.27 cm) diameter probe inside a 1.30 in. (3.30 cm) diameter (ID) thick wall steel tube and inflating the probe to 100 psi of pressure. Upon deflation the zero volume was determined as the volume of the probe when it was first possible to slide the probe out of the steel tube by hand.

The results of that part of the study led to the following conclusions:

1. The augering technique yields PPMT results which are more consistent and is preferred in all cases.
2. If augering is not possible as is the case of caving of the hole then driving is permitted but the parameters must be transformed into augering parameters by using the relationships presented in Table 2.

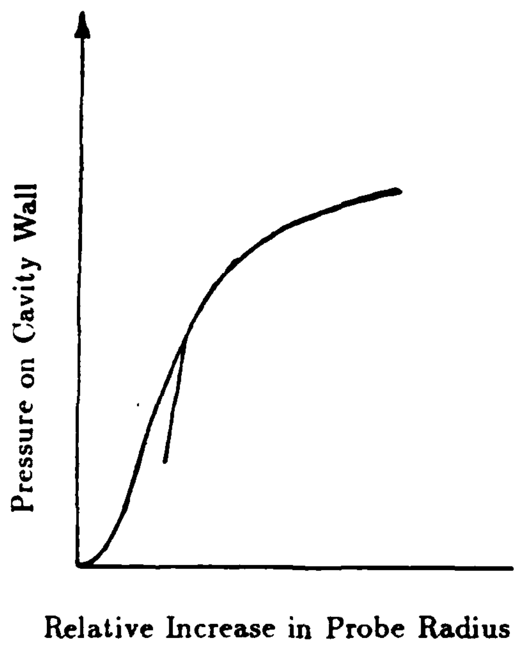

Fig. 27

Typical Augered PPMT Test on Clay

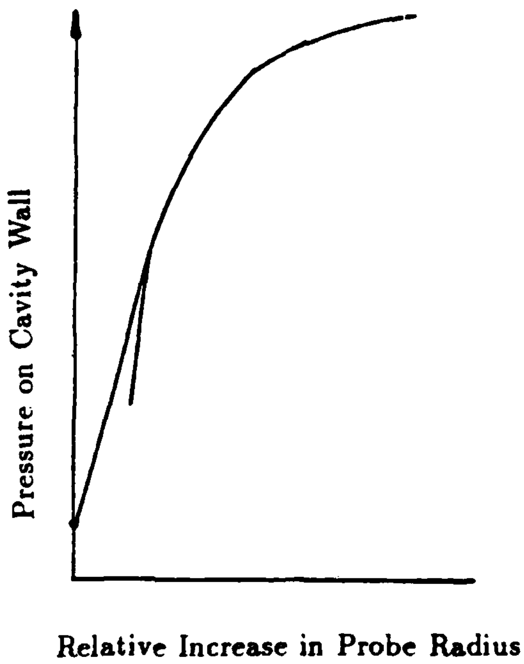

Fig. 28

Typical Driven PPMT Test on Clay

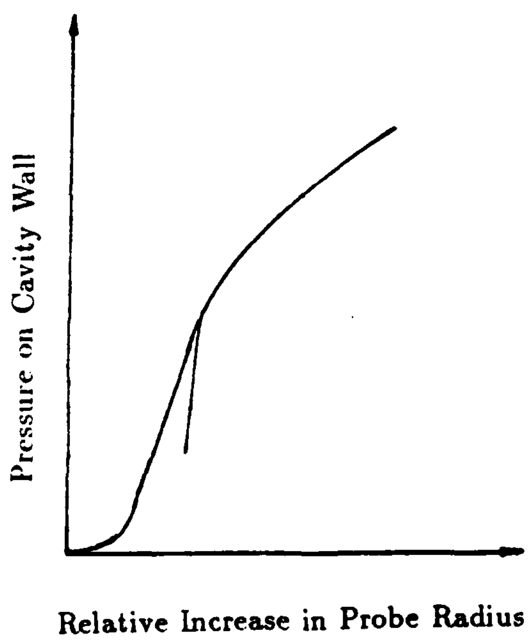

Fig. 29

Typical Augered PPMT Test on Sand

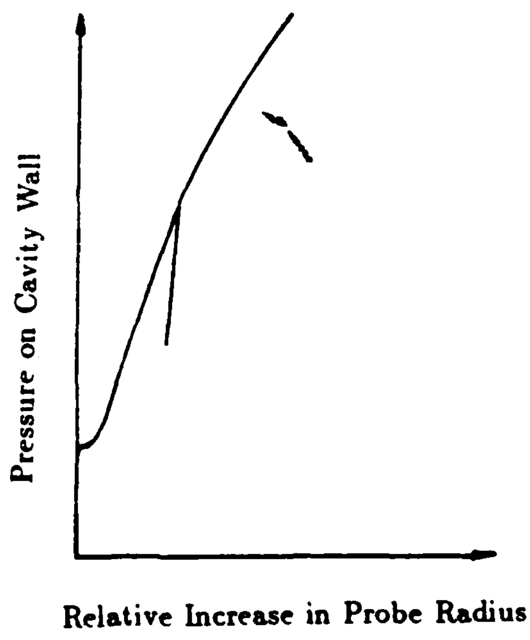

Fig. 30

Typical Driven PPMT Test on Sand

PPMT Test Model	Parameter	Sand	Clay
		Driven x M = Prebored	Driven x M = Prebored
STANDARD	E_o (kPa)	Driven x 0.403 = Prebored	Driven x 0.971 = Prebored
	E_r (kPa)	Driven x 0.397 = Prebored	Driven x 0.794 = Prebored
	p_L (kPa)	Driven x 0.560 = Prebored	Driven x 0.855 = Prebored
STRAIN	$a \times 10^{-5}\,(\text{kPa})^{-1}$	Driven x 1.690 = Prebored	Driven x 1.500 = Prebored
	$b \times 10^{-5}\,(\text{kPa})^{-1}$	Driven x 5.130 = Prebored	Driven x 1.050 = Prebored
STRESS	K_2	Driven x 0.980 = Prebored	Driven x 1.270 = Prebored
	n	Driven x 0.847 = Prebored	Driven x 2.390 = Prebored
CREEP	n_{crp}	Driven x 1.040 = Prebored	Driven x 1.280 = Prebored
CYCLIC Power Law	n_{sec}	Driven x 0.838 = Prebored	Driven x 1.100 = Prebored
	n_{cyc}	Driven x 0.901 = Prebored	Driven x 0.476 = Prebored

Table 2

PPMT Parameter Summary: Conversion Multipliers from Driven to Preboring
(1 tsf = 95.8 kPa)

6. PAVEMENT PRESSUREMETER TESTING PROCEDURE AND TEST DATA

6.1 Pavement Pressuremeter (PPMT) Testing Procedure

The procedures described in Section 5.2 require one type of PPMT test for each of the 4 modulus models. This is not convenient for airport pavement as it would take too much time. Instead a test procedure had to be developed so that in one pressuremeter test all four moduli models could be established; strain level model, stress level model, repetitive load model, rate of loading model.

The proposed PPMT test procedure, followed in this study (Figure 31) consisted of the following step by step procedure:

1. Saturate the probe, check it for leaks, determine the zero volume and expand it 3 times to work the rubber membrane (Roctest 1985).
2. Conduct a membrane resistance calibration to quantify the resistance expected from the membrane during expansion (Figure 31). This is done by expanding the probe in the air while recording the pressure and the volume.
3. Conduct a system compressibility calibration to measure the expected compressibility of the system during expansion (Figure 31). This is done by sliding the probe into a tight fitting steel tube, then expanding it while recording the pressure and the volume.
4. Core a 1.5 in. (3.7 cm) diameter hole through the pavement surface and hand auger a 1.35 in. (3.4 cm) diameter hole down to the first testing depth. The 1.35 in. (3.4 cm) diameter hand auger is made of a bit shaped like those used for wood cutting. Only if hand augering is not possible should the probe be driven.
5. Place the center of the expandable part of the probe at the desired test depth.
6. Conduct the pavement pressuremeter test by inflating the probe with water in equal volume increments lasting 15 seconds each. It is recommended that the volume increments be 5 cm^3. The field curve is obtained by recording the pressures and the volumes at the end of each 15 second increment as the volume is increased. Ten cycles are performed near the end of the elastic or straight line portion of the raw field curve, where the pressure is p (Figure 31). The end of the straight line portion of the curve is determined during the test by recording the increase in volume ΔV and the corresponding increase in pressure Δp. The end of the straight line is found when the ratio $\Delta p/\Delta V$ starts to decrease. Cycles are carried out between p and 1/2 p (Figure 31). Each unloading step or reloading step lasts 15 seconds. Once the cycles are completed, two or three 5 cm^3 volume increments are applied, and then a 5 minute creep test is conducted with pressure readings taken every 15 seconds (Figure 31). Following the creep test, the expansion of the probe is completed to about 1.25 times its original volume (for the PPMT used this requires inputing 120 cc (7.3 ci) of water) or until the limit of the pressure gauge is reached. At this point the probe is deflated using the following decrements, each lasting 15 seconds:

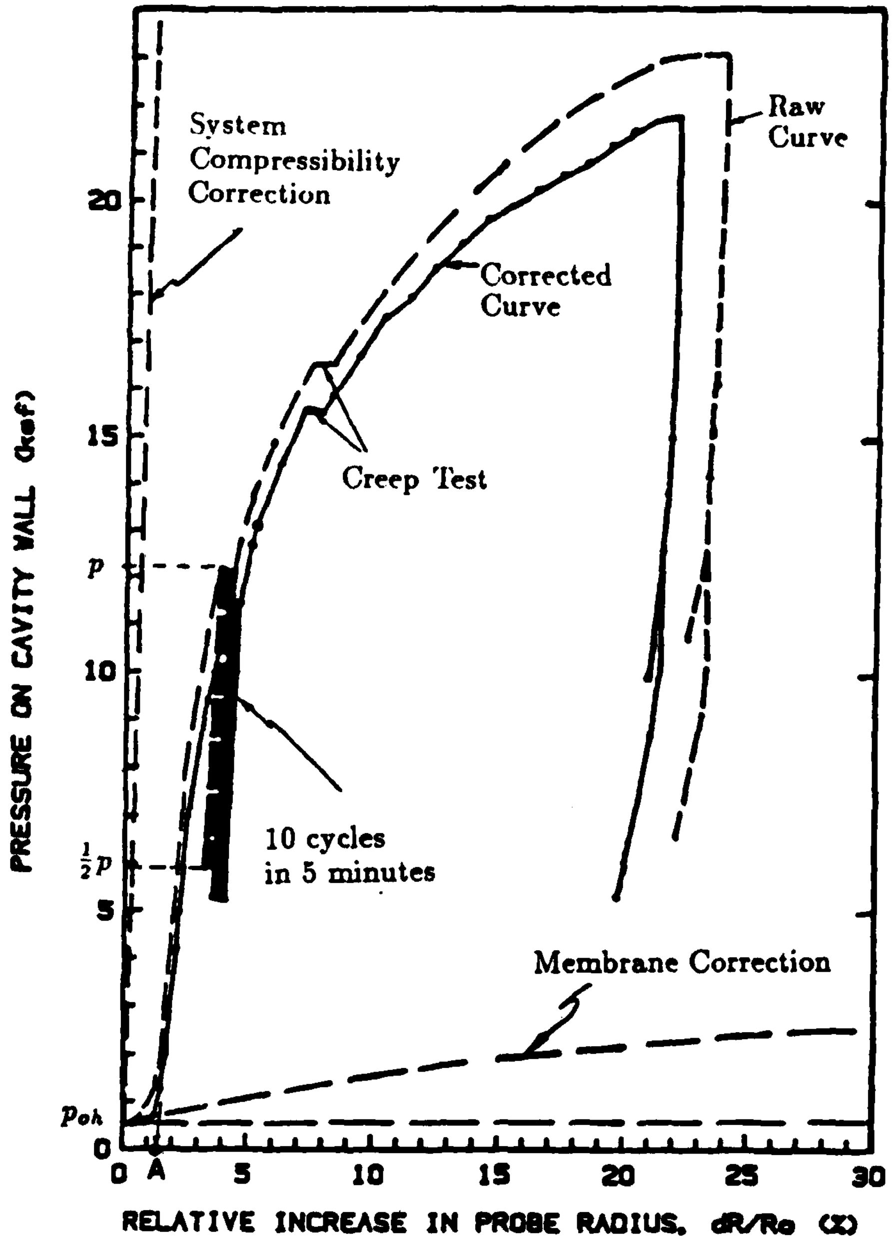

Fig. 31 Conceptual Airport Pressuremeter Test Curve

0.5, 1.0, 2.0, 5.0 and 10 cc (.03, .06, .12, .3 and .6 ci) down to one-half the maximum pressure (Figure 31). Once this point is reached, the probe is inflated by injecting 0.5 cc (.03 ci) and then deflated by withdrawing 0.5 cc (.03 ci) to complete the test (Figure 31).

7. Deflate the probe and remove it from the augered hole. Advance the hole with the hand auger to the next testing depth. Place the probe at the next test depth and carry out a new test. The tests are usually run every foot starting immediately below the surface course to a depth of 5 feet.

6.2 Pavement Pressuremeter Test Data Reduction

Once the raw pressuremeter data is recorded the pressures and volumes must be corrected to compensate for four items: membrane stiffness, system compressibility, hydraulic head between the measuring unit and the probe and initial pressure in the system before insertion of the probe into the borehole.

6.2.1 Membrane Resistance Correction

This correction takes into account the resistance due to the rubber membrane and the protective metal sheeting. The membrane resistance may be obtained by placing the probe at the height of the pressure gage on the control unit and inflating the probe in the air with water, using equal volume increments each lasting 15 seconds, to full expansion. A typical membrane resistance curve is shown in Figure 31. This pressure must be subtracted from the raw pressure on the pressuremeter curve since it is not part of the soil resistance. A special problem occurs due to the cyclic loading during the actual PPMT test. The cyclic loading causes different effects on the membrane correction than the monotonic loading. Figure 32 shows a typical membrane correction curve with cycles. In the case of cyclic tests an average membrane resistance curve is used as shown on Figure 32.

6.2.2 System Compressibility Correction

The system compressibility includes expansion of the tubing, compressibility of the probe and of the inflating fluid. This calibration is performed by pressuri·ing the probe inside a thick walled casing up to the limit of the gage pressure. Depending upon the size of the steel casing, the resulting curve may require adjustment for the probe having to seat itself against the casing wall. This adjustment is depicted in Figure 33. As in the case of the membrane calibration, cyclic loading causes different effects on the system compressibility than monotonic loading. This effect is shown in Figure 34. To decrease the error associated with ignoring these differences, an average curve may be input for the system compressibility (Figure 34). After this curve is chosen the resulting adjusted curve is the volume calibration curve shown in Figure 31. It is assumed that the steel casing does not expand under the pressures imposed by the pressuremeter and therefore that the

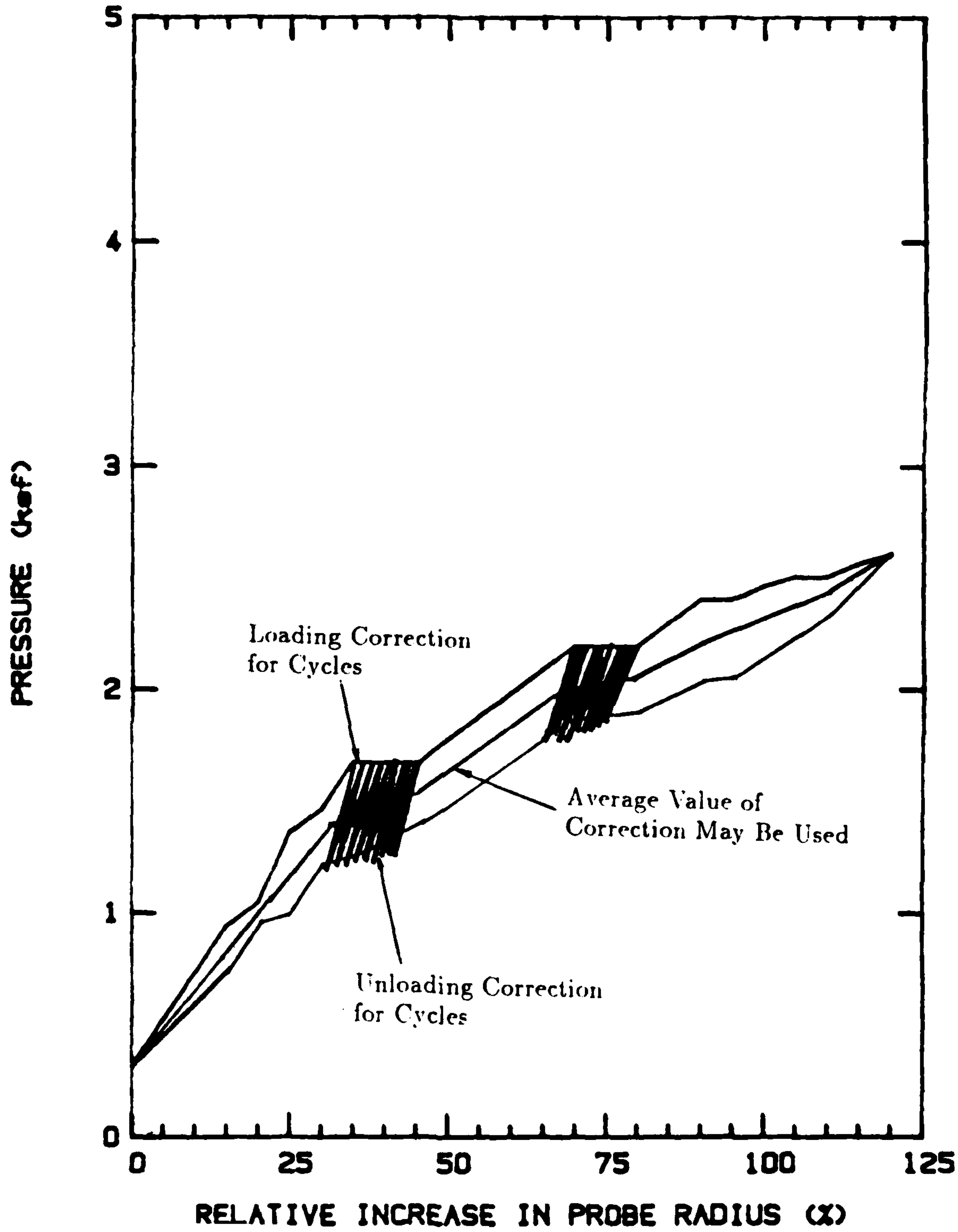

Fig. 32 Typical Membrane Correction Curve

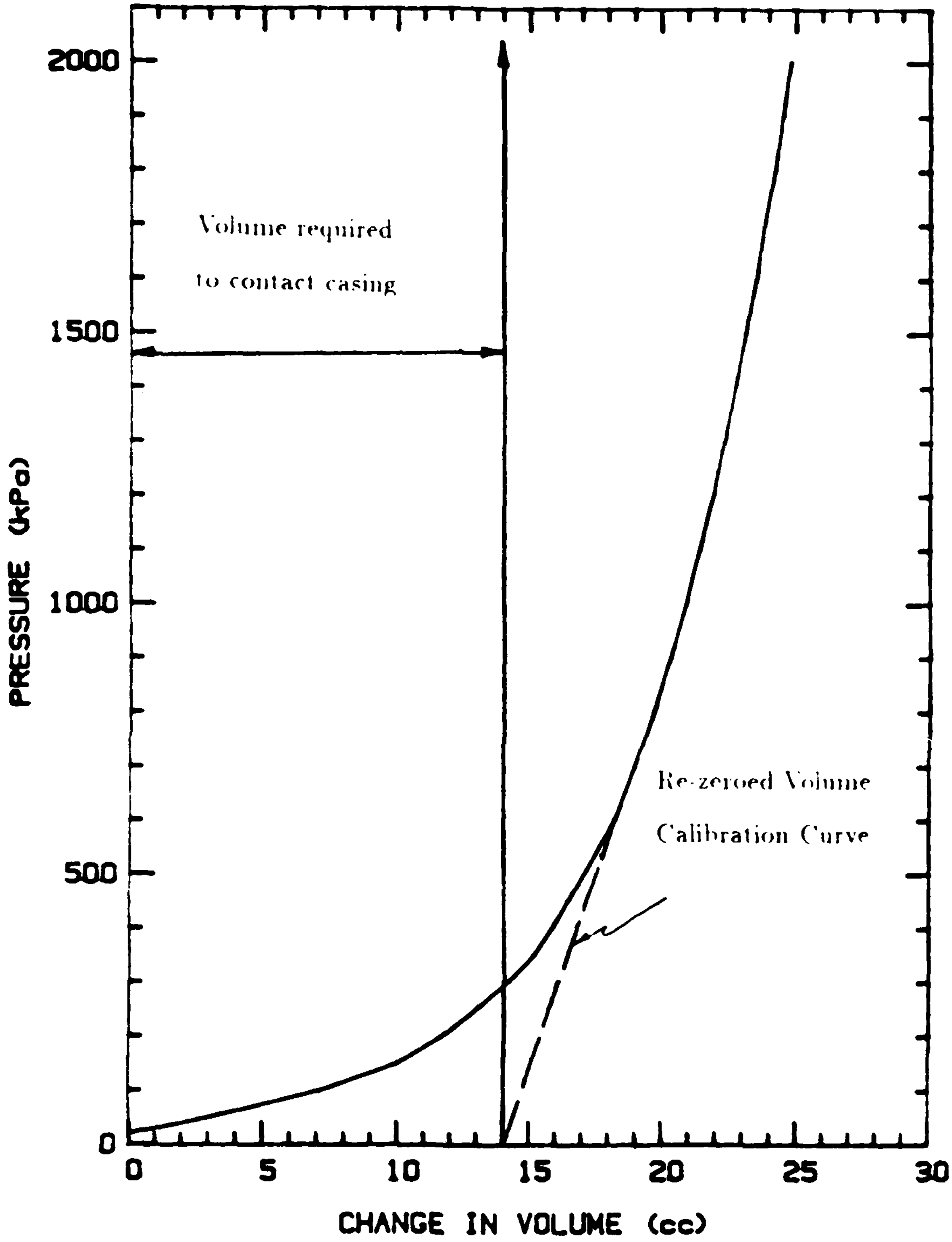

Fig. 33 Correcting Volume Calibration Curve for Size of Casing

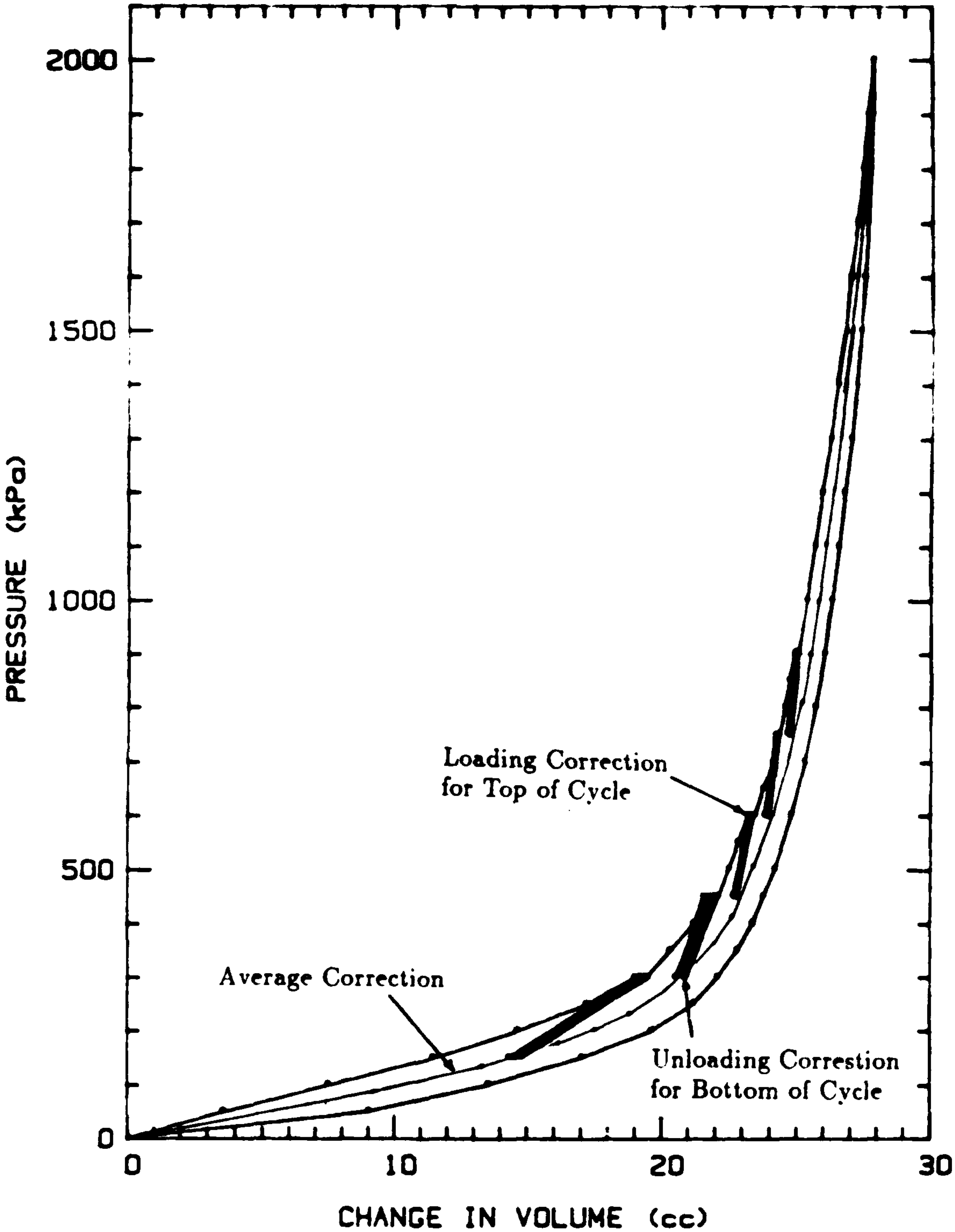

Fig. 34 Cyclic Effects on the Volume Calibration

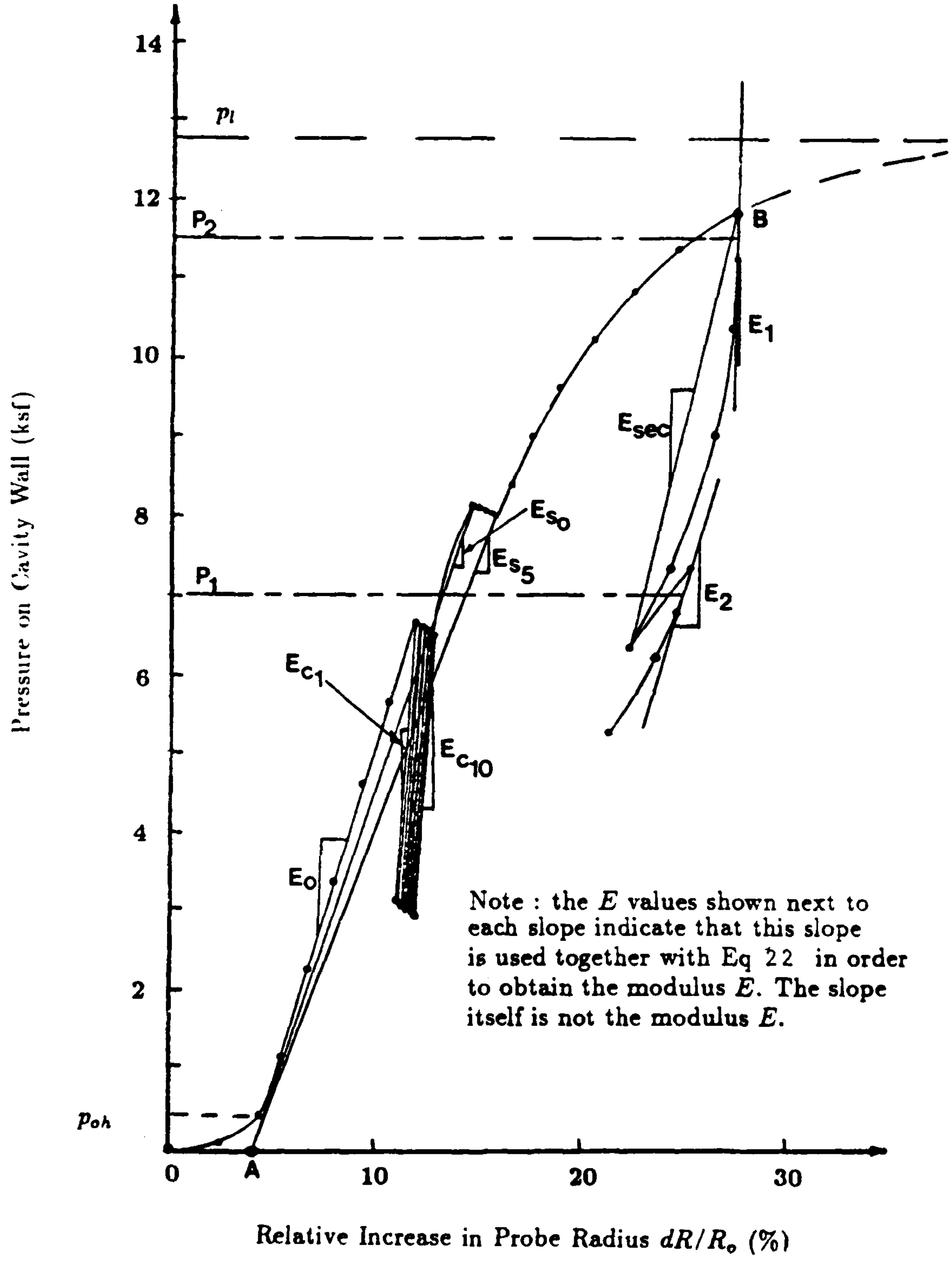

Fig. 35 Definitions for Airport PPMT Test

volume increase read in this calibration does not correspond to any expansion of the probe. Therefore, this additional volume must be subtracted from the raw volume on pressuremeter curve.

6.2.3 Hydrostatic Pressure Correction

The raw pressuremeter curve must also be corrected for the hydrostatic pressure developed inside the probe by the height of the column of fluid between the control unit and the probe at the test depth. This pressure is exerted on the probe but is not registered by the pressure gage, and is therefore added to the raw pressuremeter curve.

6.2.4 Correction for Initial Gage Pressure

The pressure gage does not always read zero when the probe is at the gage height (i.e. top of control unit) and at atmospheric pressure. This initial gage pressure may be due to such things as gage error, temperature changes, or inflation of the membrane to reach an initial volume (V_0). This error may be corrected by zeroing the pressure gage prior to each test, but this is not always practical. This pressure is subtracted from the raw pressure on the pressuremeter curve so that re-zeroing of the pressure gage is not necessary before each test.

The complete correction process is accomplished for each point on the raw pressuremeter curve as follows:

$$P_{corr} = P_r - P_c + P_h - P_i \tag{28}$$

$$V_{corr} = V_r - V_c \tag{29}$$

where P_{corr} is the corrected pressure exerted on the soil, P_r is the raw pressure read on the gage during the test, P_c is the pressure correction due to membrane stiffness, P_h is the hydrostatic pressure correction = H x γ, H is the distance from the pressure gage to the center of the probe and γ is the unit weight of the inflating fluid, P_i is the initial pressure reading when the probe is at gage height, V_{corr} is the corrected volume increase of the probe, V_r is the raw volume increase read during the test and V_c is the volume due to system compressibility.

The correction process is performed automatically by the program AIRPRESS written for this purpose. This is a microcomputer program which is described in Appendix C. Once the data is corrected, the corrected curve is plotted as pressure on the cavity wall, P_{corr}, versus relative increase in probe radius, dR/R_0, in percent. These axes are preferred to the P_{corr} versus V_{corr} axes because the results for all types of pressuremeters to be normalized and therefore compared.

6.2.5 Modulus Calculations

The modulus is calculated between two points on the pressuremeter curve (Figure 14):

$$E = (1+\nu)\left[\left(1+\frac{\Delta R_1}{R_o}\right)^2 + \left(1+\frac{\Delta R_2}{R_o}\right)^2\right]\left[\frac{\sigma_{rr2} - \sigma_{rr1}}{\left(1+\frac{\Delta R_2}{R_o}\right)^2 - \left(1+\frac{\Delta R_1}{R_o}\right)^2}\right] \qquad (30)$$

where ΔR_1 and ΔR_2 are the increases in probe radii for the points considered, R_o is the initial radius of the probe, and σ_{rr1} and σ_{rr2} are the pressures against the cavity wall for the two points considered (Figure 14). Using this equation moduli can be calculated between any two points on the pressuremeter curve (Figure 35).

6.2.6 Limit Pressure Estimation

The limit pressure p_L is defined as the pressure at an inflation equal to twice the initial cavity volume. This pressure may be estimated by extrapolating the corrected pressure versus dR/R_o curve. As an example for the PPMT, the initial volume of the probe is about 200 cc (12.2 in^3). This corresponds to an initial radius R_o of 1.675 cm (0.66 in.). If the initial volume is doubled, the 400 cc (24.4 $in.^3$) volume would lead to a value of 41.4% for dR/R_o. Therefore to estimate p_L, the P versus dR/R_o curve would have to be extrapolated to dR/R_o of 41.4% and the corresponding pressure would be the limit pressure. Often the initial cavity volume is larger than the initial volume of the probe. If it takes 20 cm^3 for the probe to come in contact with the borehole wall then the initial cavity volume is 220 cm^3; twice this volume is 440 cm^3 or 240 cm^3 of water injected into the probe. Referring to Figure 14, the limit pressure p_L always corresponds to a value of dR/R_o equal to:

$$p_L = p \text{ at } \frac{\Delta R}{R_o} = 0.41 + 1.41\left(\frac{\Delta R}{R_o}\right)_c \qquad (31)$$

6.2.7 Strain Calculations

Calculations of the hoop strains are performed as detailed in section 5.2. The hoop strain at the wall of the cavity can be calculated at any point along the pressuremeter p versus $\Delta R/R_o$ curve by:

$$\varepsilon_{\theta\theta} = \frac{\Delta R/R_o - \left(\Delta R/R_o\right)_c}{1 + \left(\Delta R/R_o\right)_c} \qquad (32)$$

where $(\Delta R/R_o)_c$ is the relative increase in probe radius which corresponds to the initial size of the cavity.

6.3 Pavement Pressuremeter Test Results

The PPMT tests are reduced such that the following base course, subbase and subgrade parameters and properties are obtained. Refer to Figures 35 to 37 for definitions and for examples of PPMT test plots.

1. p_{oh} - the at rest horizontal pressure obtained by visually inspecting the initial portion of the curve to obtain the point of maximum curvature.
2. E_o - obtained from the slope of the initial straight line portion of the curve by using the theory of elasticity and Eq. 21.
3. p_L - the limit pressure of the soil obtained by extrapolating the p versus $\Delta R/R_o$ plot to twice the initial cavity volume (section 6.2.6).
4. E_r - obtained from the slope of the unload portion of the first cycle by using the theory of elasticity and Eq. 22.
5. n_{sec} - the secant exponent for the model $E_{sn}/E_{c1} = N^{-n_{sec}}$ as detailed in section 5.2.
6. n_{cyc} - the cyclic exponent for the model $E_{cn}/E_{c1} = N^{-n_{cyc}}$ as detailed in section 5.2.
7. n_{res} - the resilient exponent for the model $M_{rn}/M_{r1} = N^{-n_{res}}$ as detailed in section 5.2.
8. n_{crp} - the creep exponent for the model $E_{st}/E_{so} = (t_t/t_o)^n$ as detailed in section 5.2.
9. K_2 - the modulus constant for the stress model $E = K_2 (\frac{\sigma}{p_a})^n$ as detailed in section 5.2.
10. n - the stress level exponent for the model $E = K_2 (\frac{\sigma}{p_a})^n$ as detailed in section 5.2.
11. a - the strain level intercept for the model $1/E = a + b\varepsilon$ as detailed in section 5.2.
12. b - the slope of the strain level model $1/E = a + b\varepsilon$ as detailed in section 5.2.

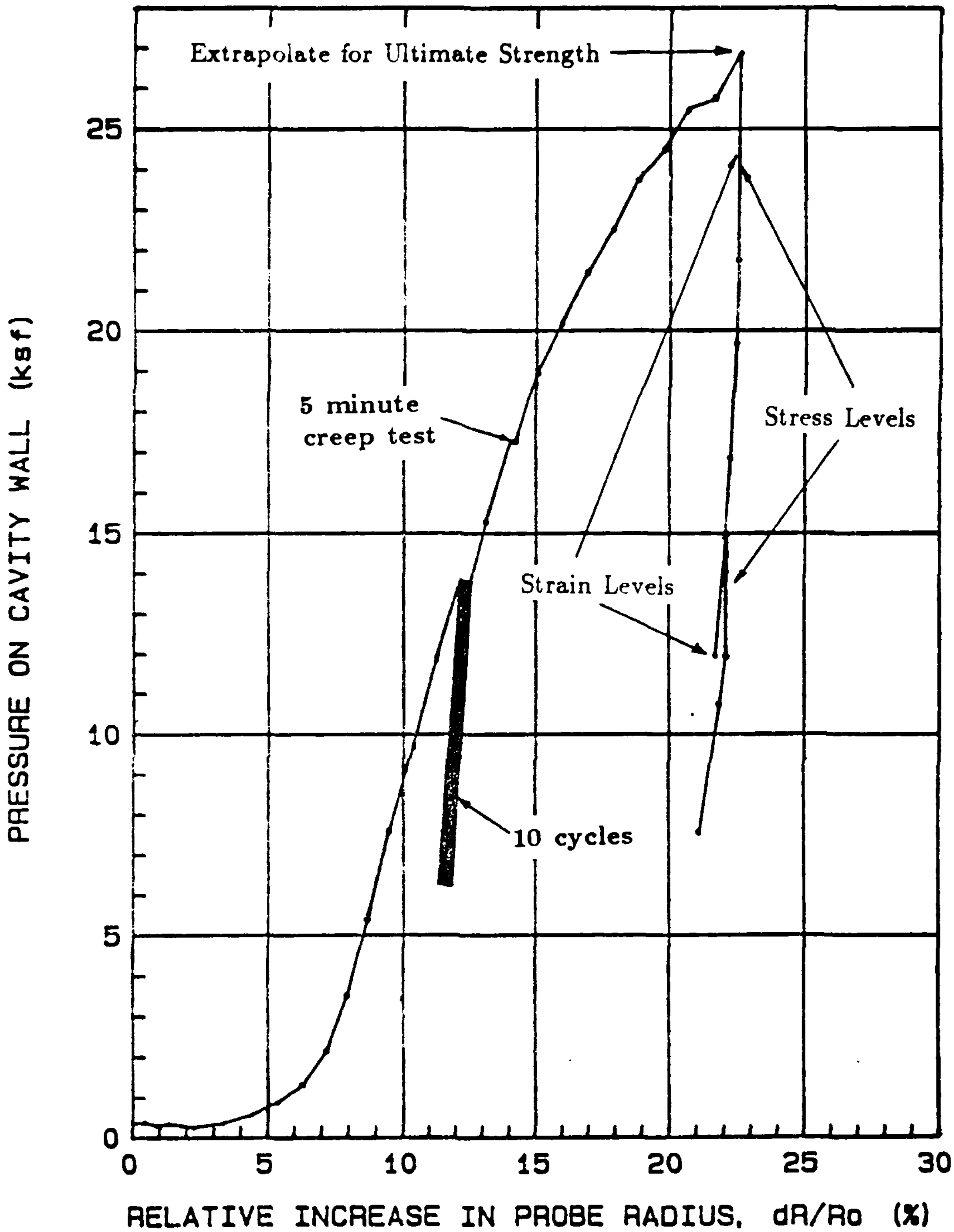

POSSUM KINGDOM AIRPORT (PK-2) 13"-DEPTH STANDARD AIRPORT TEST

Fig. 36 Typical Airport Pressuremeter Results on Sands

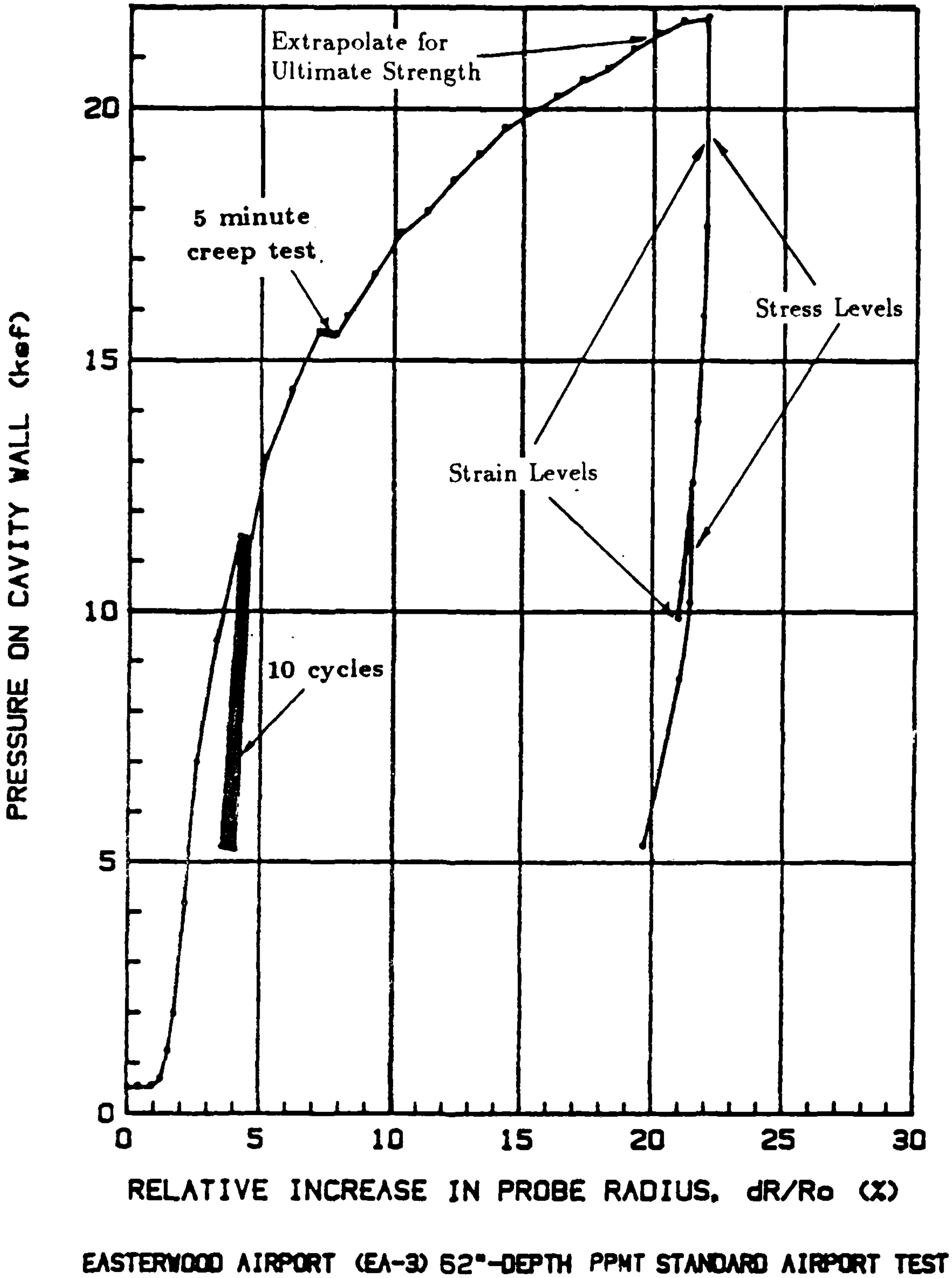

Fig. 37 Typical Airport Pressuremeter Results on Clays

7. FIELD EXPERIMENTS

7.1 Airport Sites, Soil, and Test Program

The airport locations, the type of pavements and the subgrade soil conditions encountered are presented in this section. The airports chosen were selected on the basis of their relative size, type of subgrade soil, climate, and accessibility from Texas A&M University. The airports chosen were Easterwood airport in College Station and San Antonio International airport which have clay subgrades and Possum Kingdom airport which has a sand subgrade. Figure 38 shows the general location of the three airports.

The field testing program included three different types of tests which were conducted in two phases. Phase one consisted of performing pressuremeter tests (PPMT) at one foot intervals starting at the top of the base course and collecting shelby tube samples with a drill rig for the cyclic triaxial (CT) test. Phase two consisted of performing Falling Weight Deflectometer (FWD) tests in the vicinity of the PPMT tests and the sampling hole. The PPMT tests and the sample collection were conducted from December 3 to December 19, 1985. The FWD tests were conducted from March 25 to March 26, 1986.

7.1.1 Easterwood Airport

Easterwood airport is located in College Station, Texas, and is part of Texas A&M University; it is the main airport for the Bryan/College Station area (Figure 39). It consists of three runways in the standard triangular configuration popularized during World War II. The testing area is located on an apron near the terminal. The pavement where the testing was conducted consisted of 6 inches of concrete over 8 inches of sand and gravel over a stiff to hard gray high plasticity clay (USCS classification CH)(Figure 40). The clay has the following average properties to a depth of 10 feet: total unit weight γ_t = 124 pcf, water content ω_c = 16.3%, plastic limit PL = 19%, liquid limit LL = 53% and undrained shear strength from pocket penetrometer S_u = 3240 psf. Figure 40 shows the pavement and subgrade profile with relevant soil parameters.

The location of the field tests is shown in Figure 41. Phase one began on December 3 and was completed on December 19, 1985. Weather conditions during the testing varied from about 45 to 55°F (7.2 to 12.8°C). The concrete pavement was cored by SMI, Incorporated, of Bryan, Texas. Thirteen PPMT tests were conducted in three test borings with depths as shown in Figure 42. SMI also collected eight undisturbed shelby tube samples to a depth of 10 feet (3.05 m). Phase two was conducted on March 25, 1986. It consisted of FWD testing and two demonstration PPMT tests performed in a fourth test boring. The FWD tests were conducted by Eres Consultants, Inc., from Champaign, Illinois. The temperature ranged from 50 to 65°F (10 to 18°C) under clear skies. FWD tests were performed on 10 slabs (Figure 41). For 9 slabs, 4 different weights were dropped. For 1 slab the highest weight was dropped 24 times in a row.

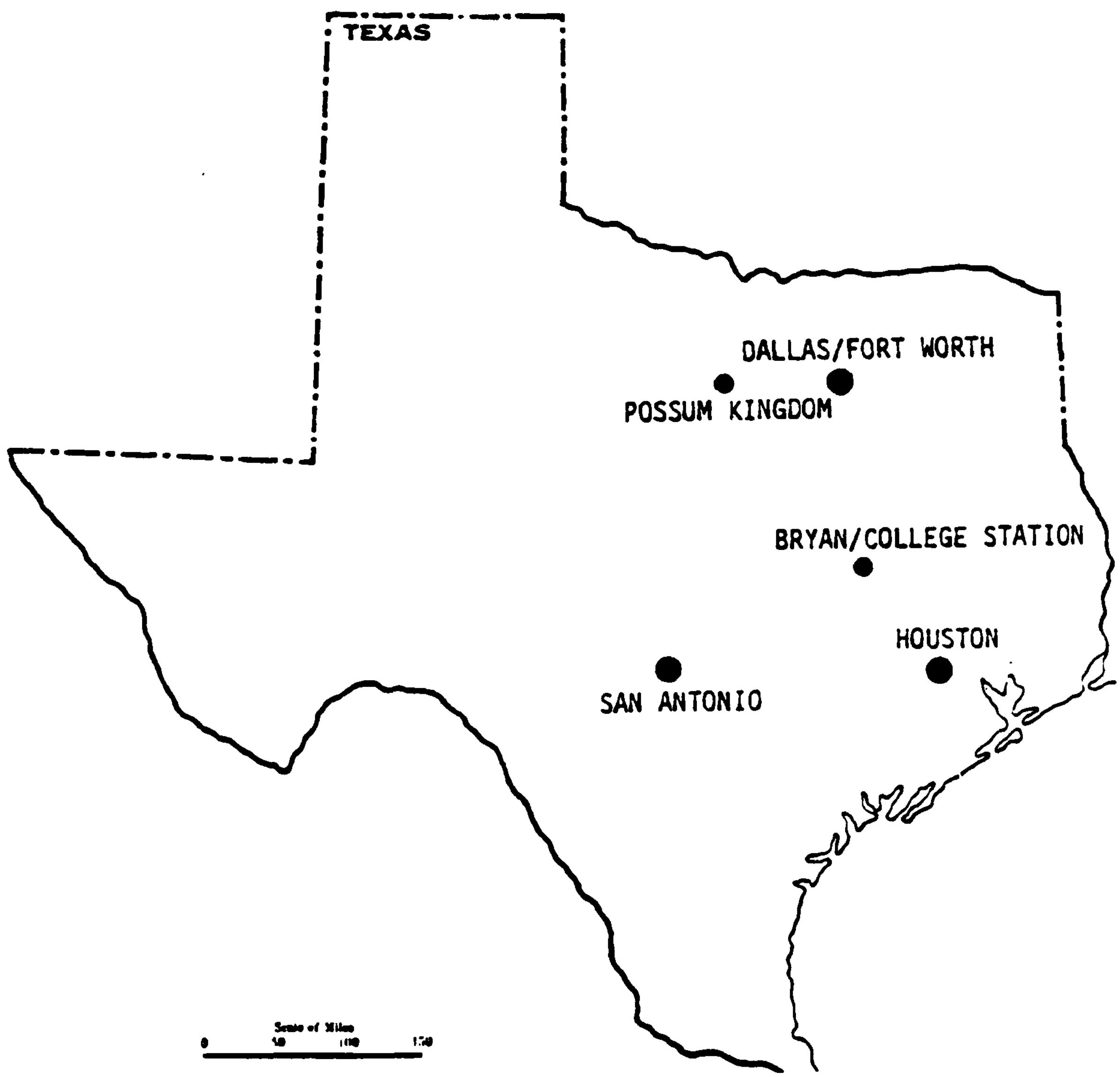

Fig. 38 General Airport Locations

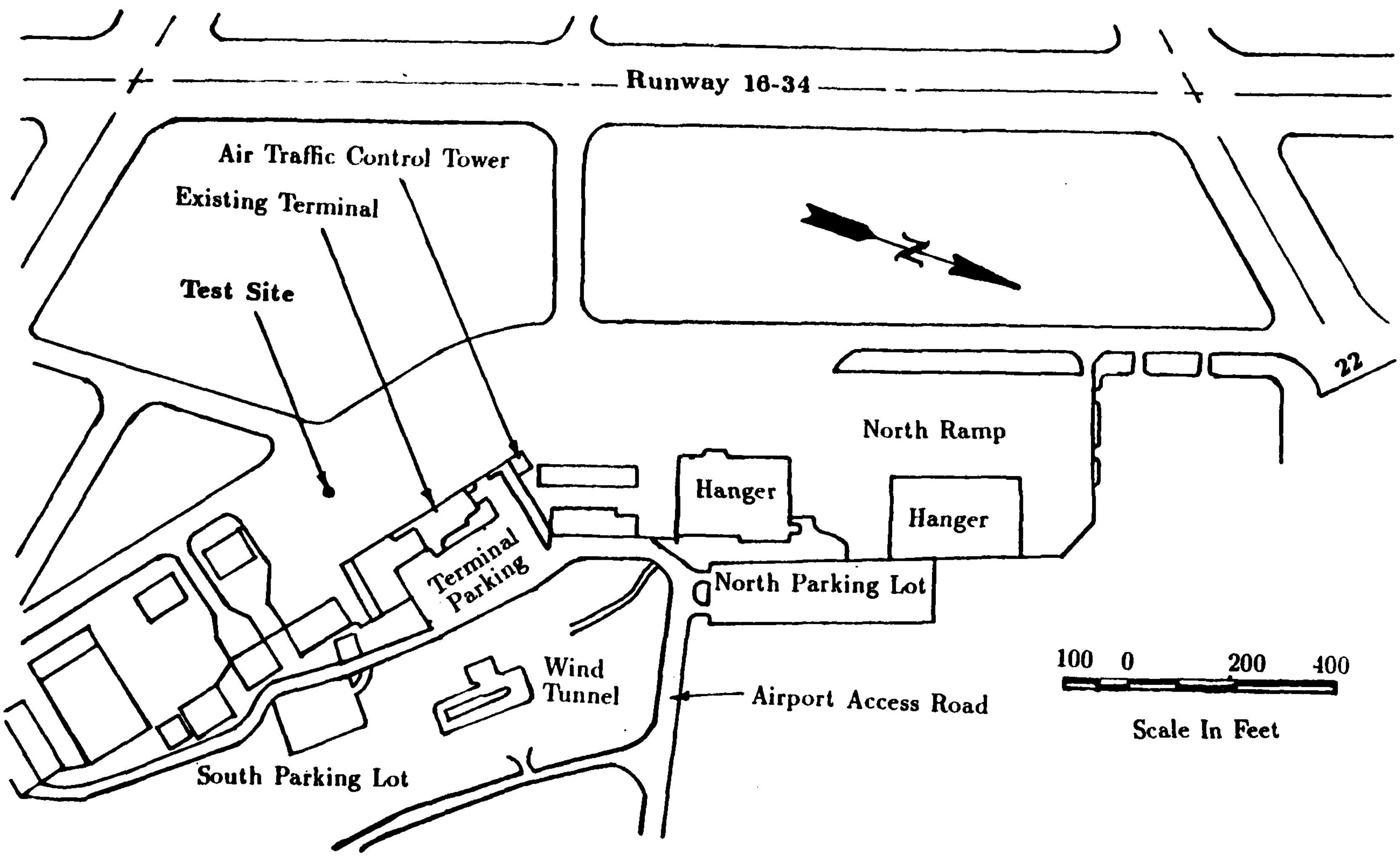

Fig. 39 Easterwood Airport, Terminal Area Plan

Description	Total Unit Weight (γ_t) (pcf)	Water Content ω_c (%)	Liquid Limit LL (%)	Plastic Limit PL (%)	Undrained Shear Strength S_u (psf)
0 to 6 in. Concrete	145	*	*	*	*
6 to 10 in. Granular Base 1/2 in. Max Part. Size	130	*	*	*	*
10 in. to 2.5 ft. Stiff, Tan & Gray **CLAY (CH)**	118.0	12.4	53	19	1850
2.5 to 4.0 ft. **CLAY,** Trace of Sand	127.0	17.8	*	*	4000
4.0 to 6.0 ft. Hard, Gray **CLAY,** Trace of Gravel Trace of Carbon	131.5	14.1	53	19	4000
> 6.0 ft. Hard, Tan & Gray, Silty **CLAY** Little Fine Sand	124.0	17.0	53	19	3500

1. LL determined from One Point Liquid Limit Procedure ASTM D4318.
2. S_u = Pocket Penetrometer Reading.
3. * $\Rightarrow$ Not Applicable

Fig. 40 Easterwood Airport Profile with Soil Parameters

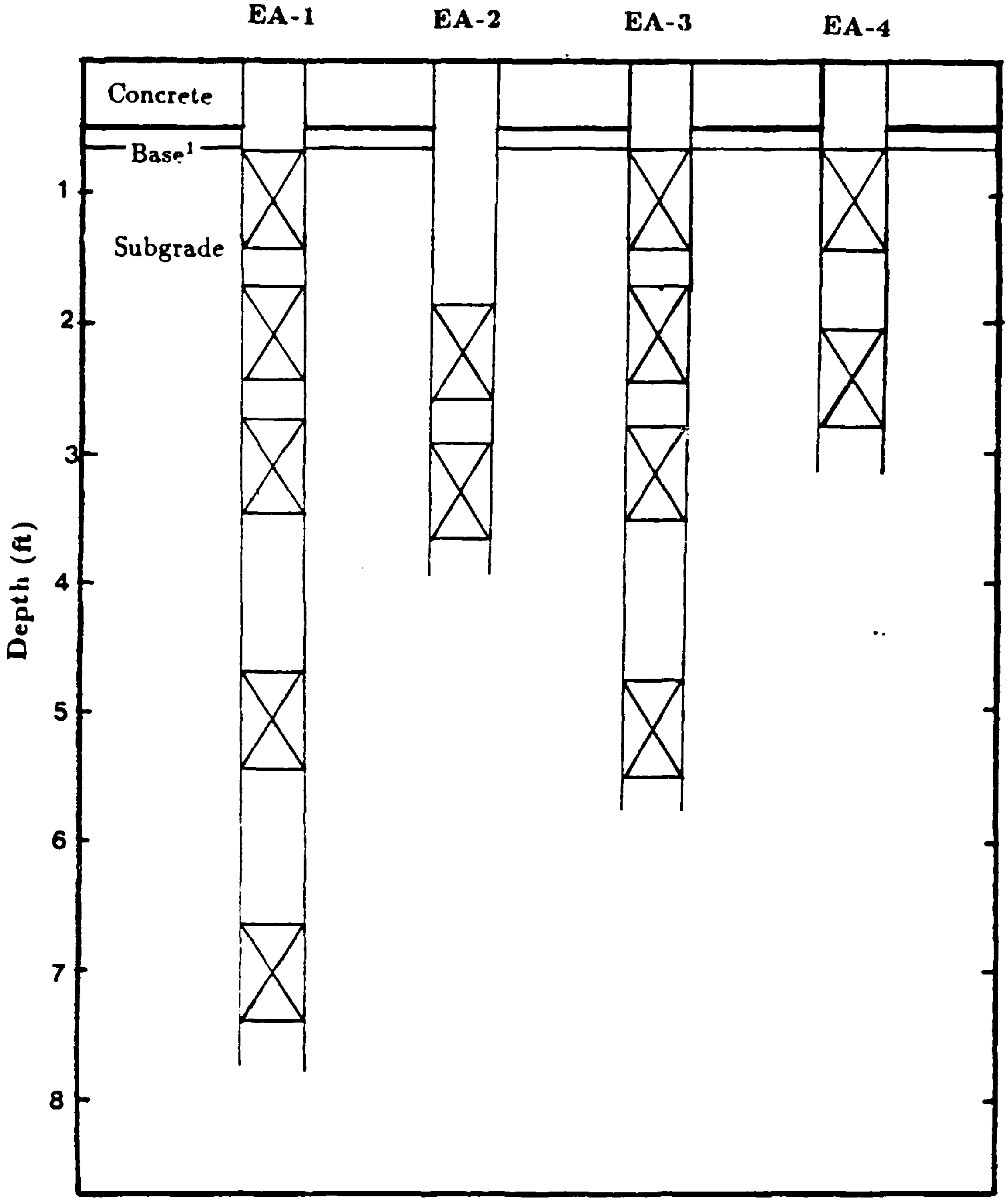

1. Granular Base reported to be 10" from Construction Drawings.
Note: The PPMT test in EA-2 directly below the Granular Base could not be conducted due to problems from augering of the hole.

Fig. 41 Easterwood Airport PPMT Testing Profile

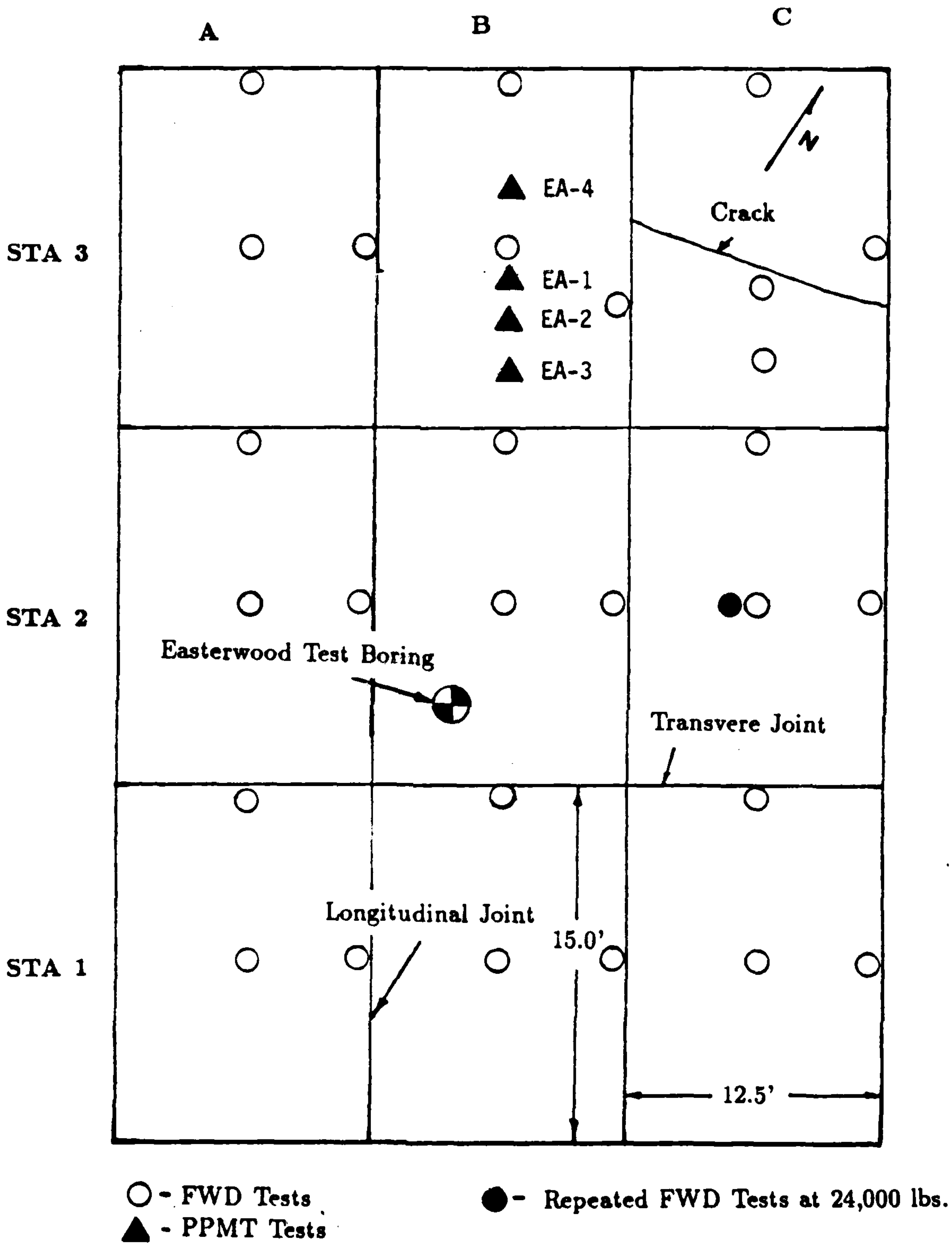

Fig. 42 Easterwood Airport Field Testing Grid

7.1.2 San Antonio International Airport

San Antonio International airport is located on the northeast side of San Antonio, north of the intersection of U.S. 281 and Interstate 410 (Figure 38). The airport is the 24th largest in the U.S. There are two terminals and two main runways. The runways are in an L shape as depicted on Figure 43.

The airport tests were conducted on the air cargo apron at the parking location of the UPS overnight delivery plane west of Terminal 2 (Figure 43). The pavement tested consisted of 16 in. (40.6 cm) of concrete overlying 6 in. (15.2 cm) of asphalt. The subgrade is a stiff to very stiff gray clay (USCS classification CH), which is overlain by a thin (2 in.; 5.1 cm) granular base. A profile of the pavement system is shown on Figure 44. The clay has the following average properties to a depth of 10 feet: total unit weight γ_t = 126.2 pcf, water content ω_c = 15.9%, plastic limit PL = 23%, liquid limit LL = 43% and undrained shear strength from pocket penetrometer S_u = 3750 psf.

A plan location of the field tests is shown in Figure 45. Contracts were let to Holes of San Antonio, for coring the concrete and to Raba-Kistner Consultants Inc., of San Antonio for obtaining undisturbed shelby tube samples for the cyclic triaxial testing. So as not to interfere with the normal operations on the air cargo apron, tests had to be conducted between 9:00 p.m. and 6:00 a.m. The temperature during both phases of the testing varied from about 35 to 45°F (1.7 to 7.2°C). Holes of San Antonio was asked to drill one 10 in. (25.4 cm) diameter hole through the 22 in. thick surface course for the sampling operation of Raba-Kistner and four 2 in. (5.1 cm) diameter holes for the PPMT testing. Raba-Kistner used a 9 in. (22.8 cm) diameter hollow stem auger to obtain 9 shelby tube samples (3 in. diameter) for the CT tests. Eleven PPMT tests were conducted in 4 test borings (Figure 46). Eres conducted FWD tests similar to those at Easterwood (Figure 45). The FWD tests were conducted in two parts. Part one consisted of testing 12 slabs by dropping 4 different weights each time. Part two consisted of repeating the highest load between 32 and 48 times at 3 different locations.

7.1.3 Possum Kingdom Airport

Possum Kingdom airport is a small general aviation airport located in the resort community of Possum Kingdom, Texas about 60 miles (97 kM) west of Dallas/Fort Wort (Figure 38). The airport consists of a single runway, two small taxiways and an apron area (Figure 47). The asphalt pavement consists of 2 inches of asphalt over about 4 in. (10 cm) of gravel and approximately 10 ft (3.7 m) of compacted sand (Figure 48).

The airport tests were conducted on the southernmost taxiway (Figure 47). A plan location of the field tests is shown in Figure 49. The temperature varied from 35 to 45°F (2 to 7°C) with overcast morning skies and clear afternoon skies. Southwestern Laboratories from Dallas was contracted to try to obtain undisturbed shelby tube samples of the sand subgrade. Ten shelby tube samples were attempted in one foot

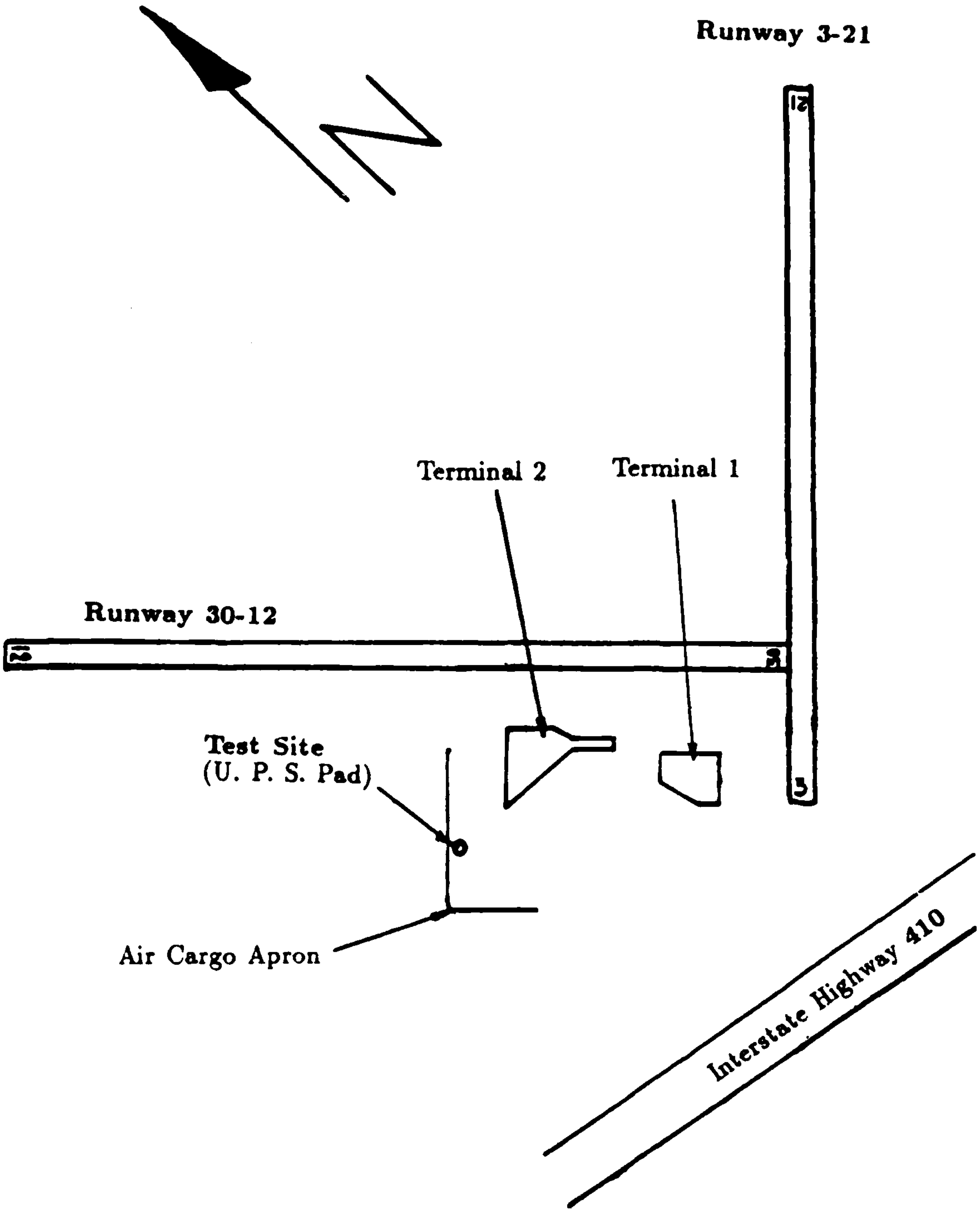

Fig. 43 San Antonio International Airport

Description	Total Unit Weight (γ_t) (pcf)	Water Content ω_c (%)	Liquid Limit LL (%)	Plastic Limit PL (%)	Undrained Shear Strength S_u (psf)
0 to 1.33' Concrete	145	*	*	*	*
1.33 to 2.0' Asphalt Concrete	140	*	*	*	*
2.0 to 4.0' Stiff, Gray **CLAY (CL)**	122.0	19.0	43	23	2500
> 4.0' Very Stiff, Tan & Gray **CLAY**, Trace of Organics	127.0	17.8	43	23	4000

1. LL determined from One Point Liquid Limit Procedure ASTM D4318.
2. S_u = Pocket Penetrometer Reading.
3. * ⇒ Not Applicable

Fig. 44 San Antonio International Airport Profile with Soil Parameters

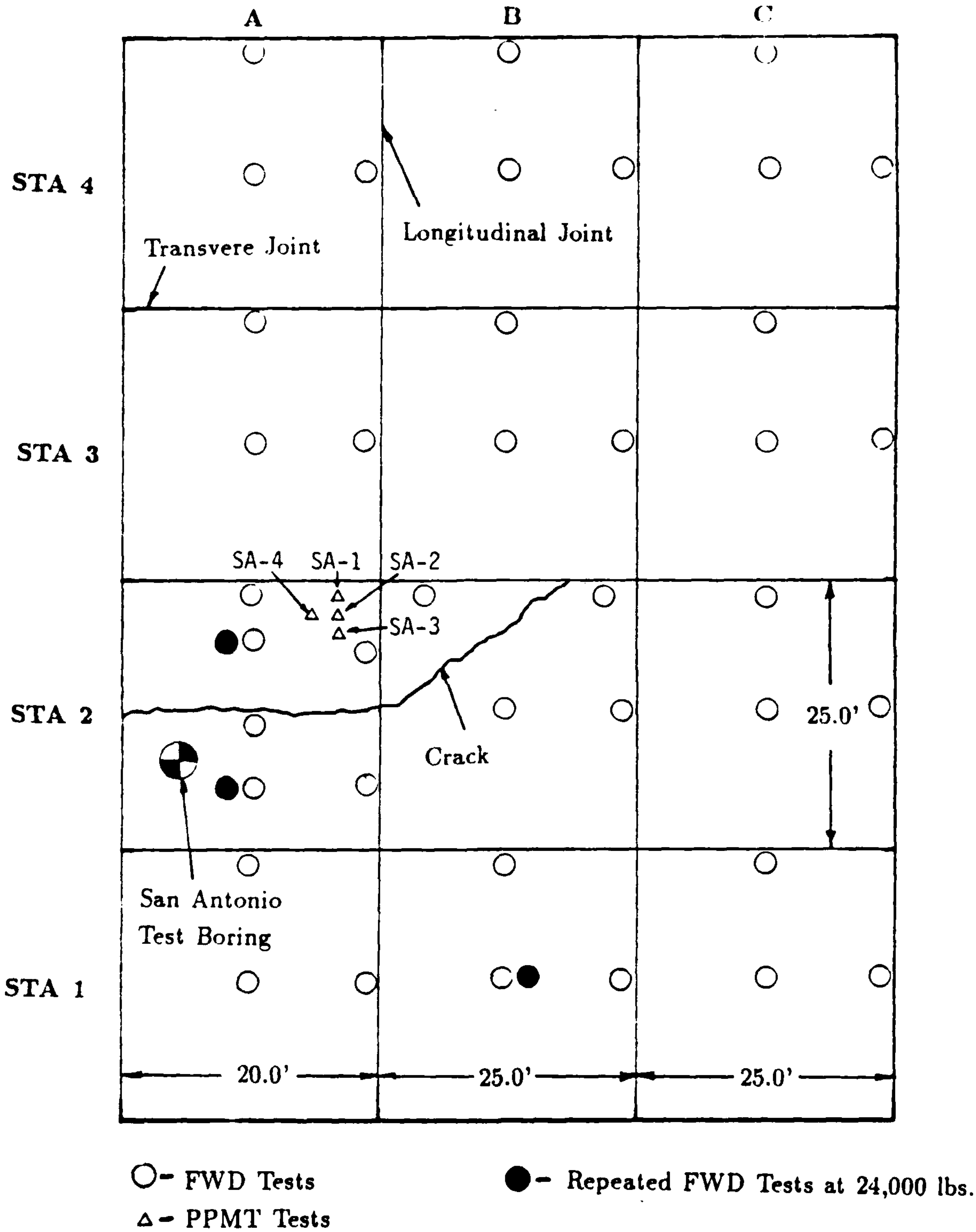

Fig. 45 San Antonio International Airport Field Testing Grid

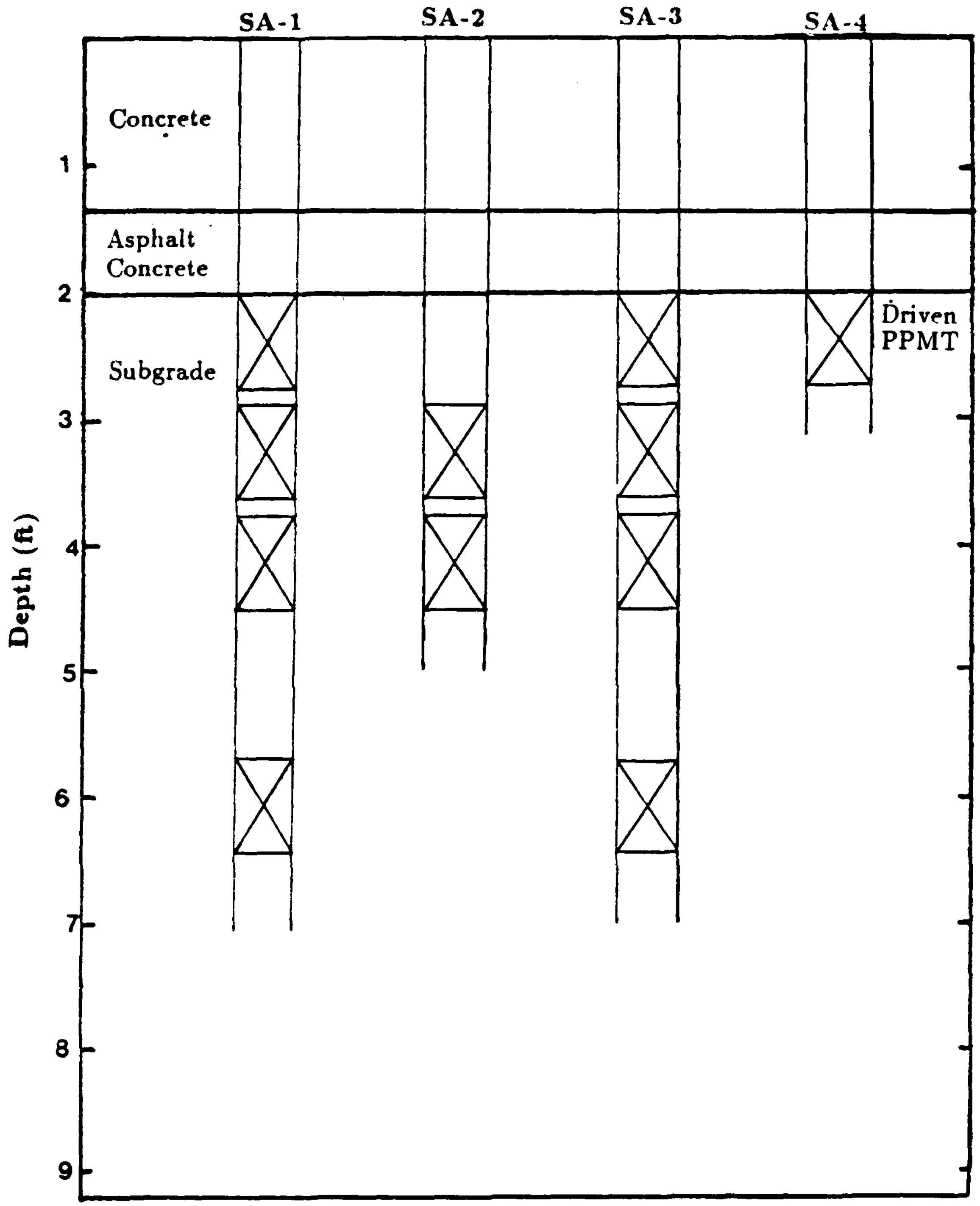

Note: The PPMT test in SA-2 directly below the Granular Base could not be conducted due to problems from augering of the hole.

Fig. 46 San Antonio International Airport PPMT Testing Profile

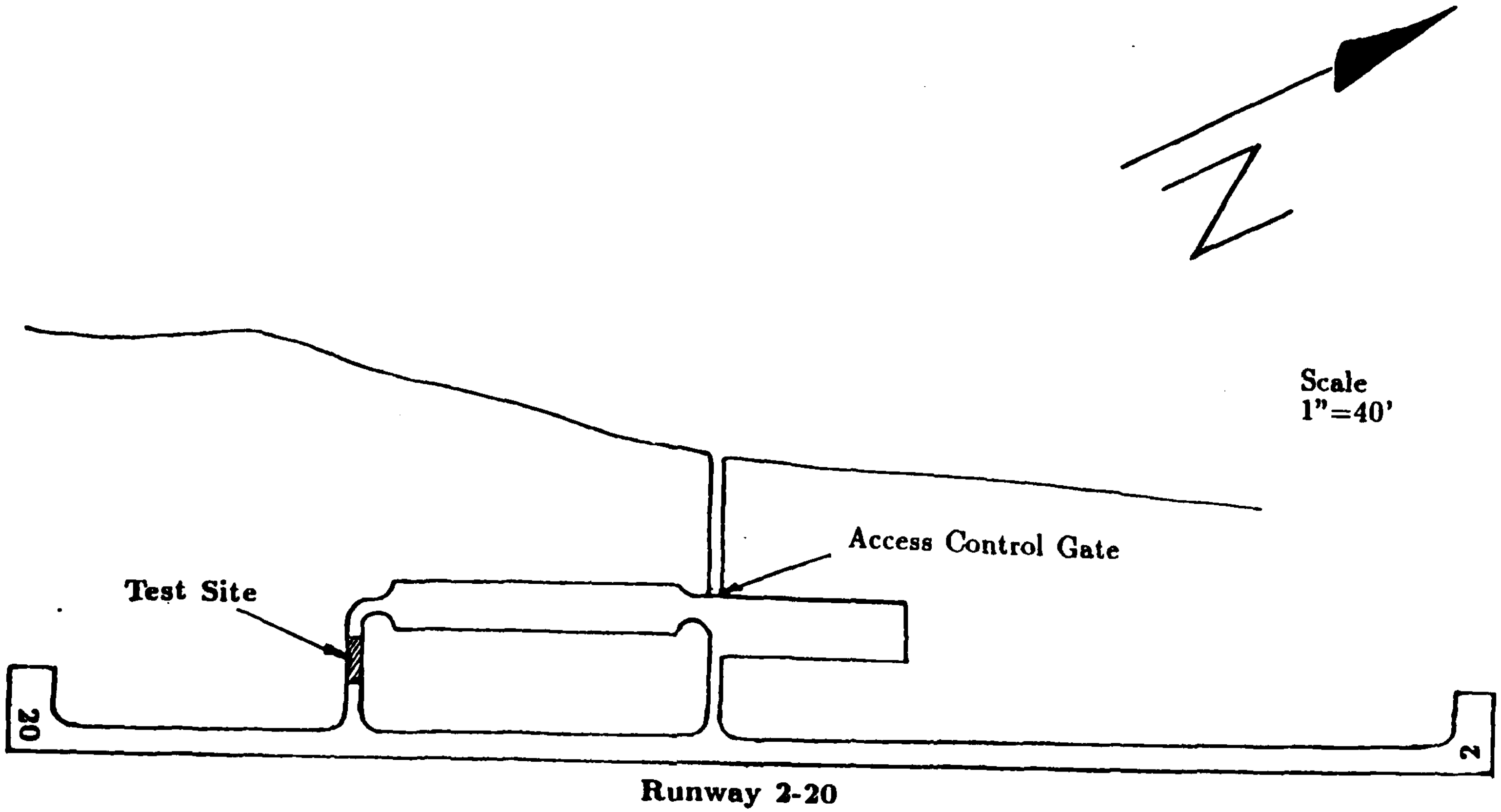

Fig. 47 Possum Kingdom Airport

Description	Total Unit Weight (γ_t) (pcf)	Water Content ω_c (%)
0 to 2" Asphalt Concrete	145	*
2 to 4" Granular Base	130	*
4" to 4.0' Brown **SAND (SC)**	110.0	4.0
> 4.0' Gray **SAND**, Trace Gravel (FILL)	125.0	9.8
5' Becomes Clayey Sand	*	*

* ⇒ Not Applicable

Fig. 48 Possum Kingdom Airport Profile with Soil Properties

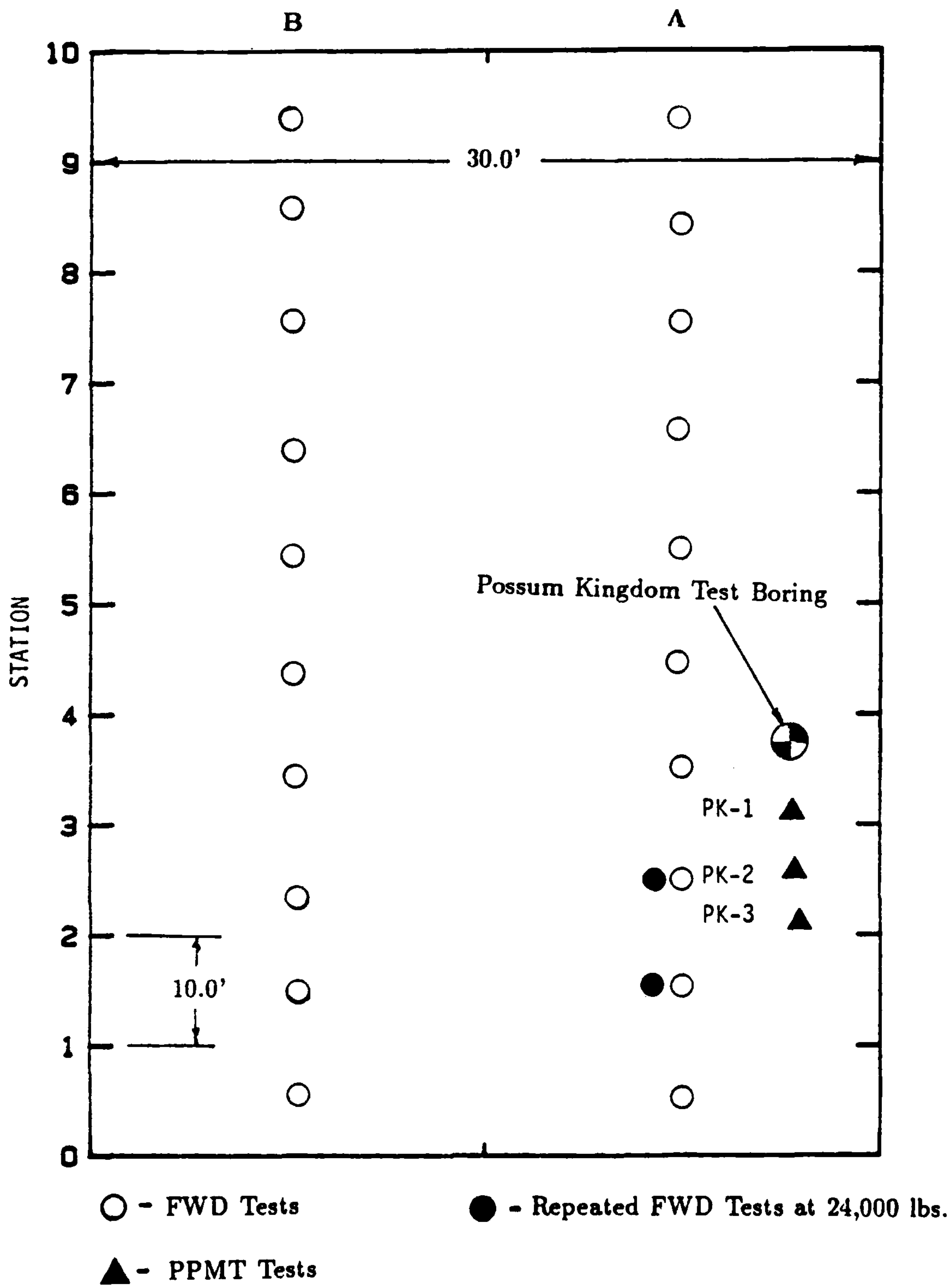

Fig. 49 Possum Kingdom Airport Field Testing Grid

intervals. Only four samples contained enough material for CT tests and classification tests. A sieve analysis was performed on the sand (Figure 50) and led to the USCS classification of SC. The average water content (.) was 10% and the average total unit weight (γ_t) was 114 pcf. In addition 8 PPMT tests were conducted (Figure 51). Based on the limit pressures (p_L) from the pressuremeter the sand was dense with an estimated Standard Penetration Test (SPT) blow count of 50 blows per foot.

Eres Incorporated conducted the FWD tests (Figure 49). The tests were conducted on March 26, 1986. Weather conditions during the FWD test varied from about 40 to 55°F (4 to 10°C) with clear skies. The FWD testing program was conducted in two parts. Part one consisted of performing FWD tests at 20 locations by dropping three weights each time. Part two consisted of performing repeated FWD tests at 2 locations by dropping one weight 24 times at each location (Figure 49).

7.2 Pavement Pressuremeter (PPMT) Test Results

The PPMT tests are reduced such that the following base course, subbase and subgrade parameters and properties are obtained. Refer to Figures 14 to 30 and Figure 35 for definitions and for examples of PPMT test plots.

1. p_{oh} - the at rest horizontal pressure obtained by visually inspecting the initial portion of the curve to obtain the point of maximum curvature.
2. E_o - obtained from the slope of the initial straight line portion of the curve by using the theory of elasticity and equation 22.
3. p_L - the limit pressure of the soil obtained by extrapolating the p versus $\Delta R/R_o$ plot to twice the initial cavity volume ($2V_c$).
4. E_r - obtained from the slope of the unload portion of the first cycle by using the theory of elasticity and equation 22.
5. n_{sec} - the secant exponent for the model $E_{sn}/E_{s1} = N^{-n_{sec}}$ as detailed in section 5.2 (Figures 12, 13).
6. n_{cyc} - the cyclic exponent for the model $E_{cn}/E_{c1} = N^{-n_{cyc}}$ as detailed in section 5.2 (Figures 12, 13).
7. n_{res} - the resilient exponent for the model $M_{rn}/M_{r1} = N^{-n_{res}}$ as detailed in section 5.2 (Figures 12, 13).
8. n_{crp} - the creep exponent for the model $E_{st}/E_{so} = (t_t/t_o)^{-n_{crp}}$ as detailed in section 5.2 (Figures 10, 11).
9. K - the modulus constant for the stress model $E = K_2(\theta/p_a)^n$ as detailed in section 5.2 (Figures 8, 9).
10. n - the stress level exponent for the model $E = K_2(\theta/p_a)^n$ as detailed in section 5.2 (Figures 8, 9).
11. a - the strain level intercept for the model $1/E = a+b\varepsilon$ as detailed in section 5.2 (Figures 6, 7).
12. b - the slope of the strain level model $1/E = a+b\varepsilon$ as detailed in section 5.2 (Figures 6, 7).

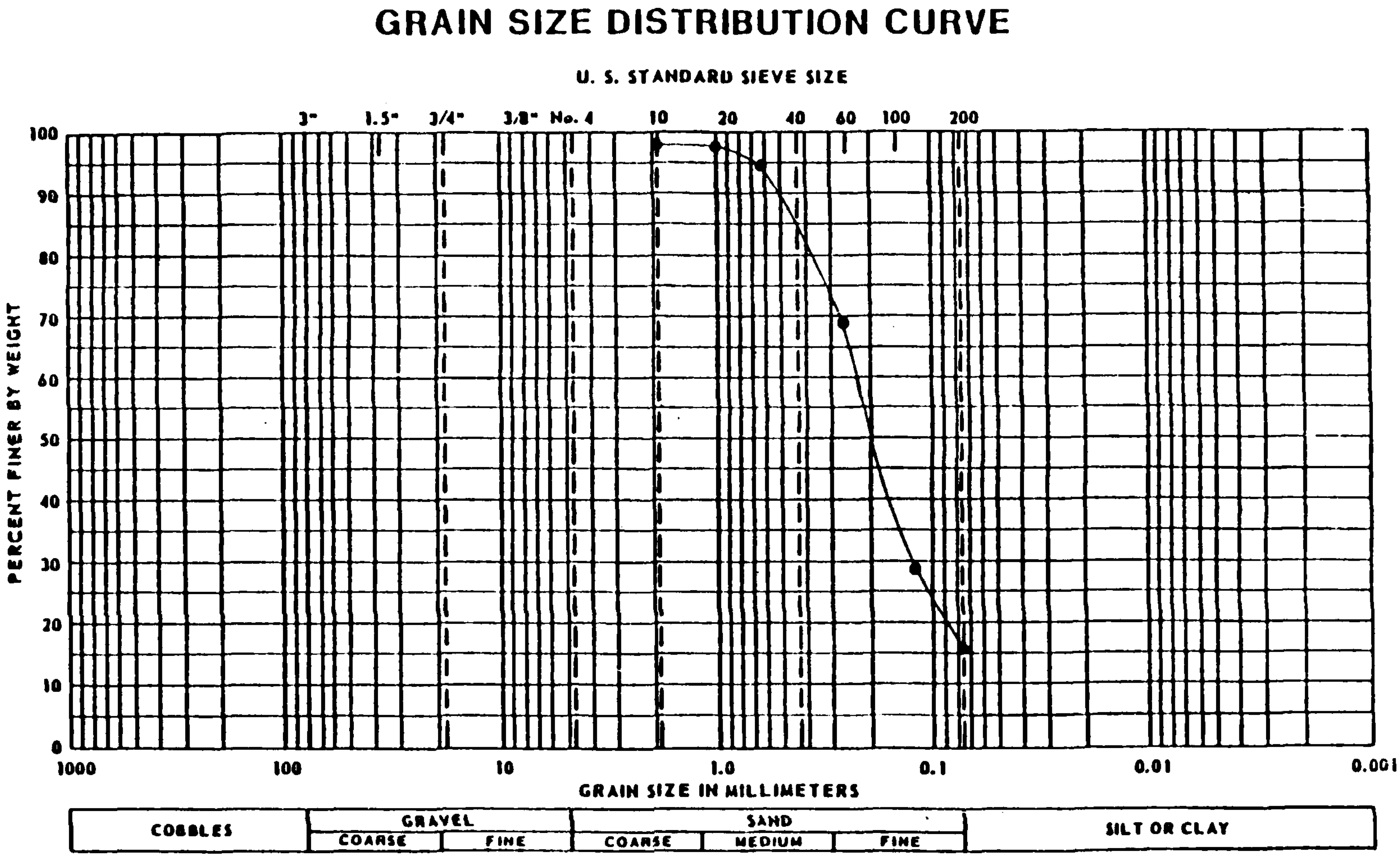

Fig. 50 Possum Kingdom Airport Subgrade Grain Size Analysis

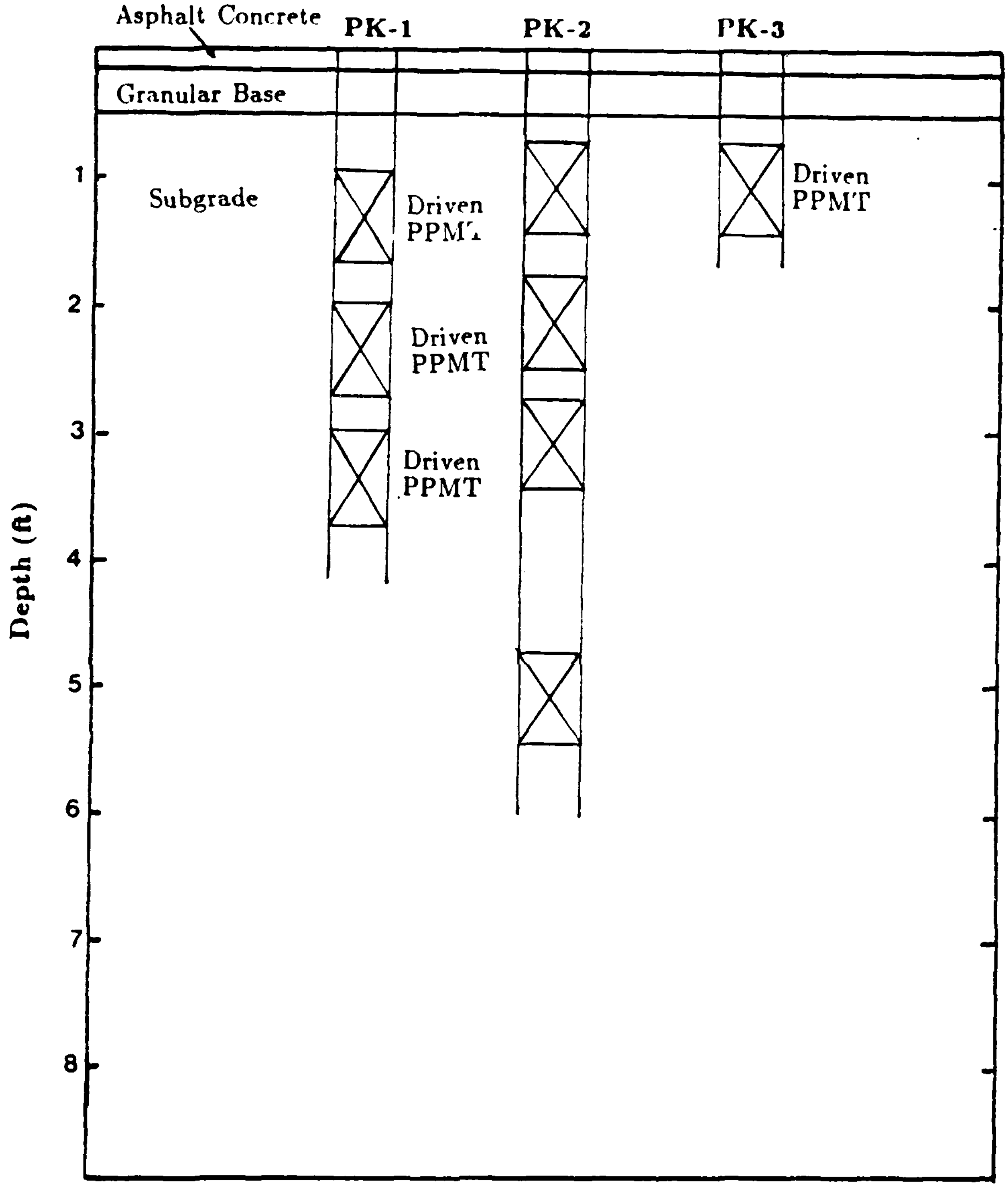

Fig. 51 Possum Kingdom Airport PPMT Testing Profile

7.2.1 Easterwood Airport PPMT Test Results

The results of the 13 PPMT tests conducted in the 4 test borings are given in Table 3. All of the reduced pavement pressuremeter curves and the PPMT parameter profiles are presented in Appendix A and B. All of the tests at Easterwood were conducted in prebored holes in the clay subgrade.

The testing procedure described in section 5.1 was followed for the Easterwood PPMT tests except for one aspect. The procedure required that once the maximum pressure on the cavity wall was reached (Point B, Figure 40), the first volume decrement should be 0.5 cc (0.03 ci). The procedure used for most of the Easterwood tests was to unload 1 cc (0.06 ci) (denoted by an [*] on Table 3).

Additional PPMT tests (test boring 4) were conducted on March 25, 1985 as a demonstration for the clients who sponsored the project. The PPMT test procedure was varied during these tests in order to conduct a more complete demonstration.

7.2.2 San Antonio International Airport PPMT Test Results

The results of the 11 PPMT tests conducted in the 4 test borings are given in Table 4. All of the reduced pavement pressuremeter curves and the PPMT parameter profiles are presented in Appendix A and B. For one test the probe was driven into the subgrade while the remaining tests were conducted in prebored holes in the subgrade. For the driven PPMT test, the slope used for calculating E_0 was the slope given by the first few data points (Appendix A). For all calculations the origin of the pressuremeter curve (point A on Figure 35) was taken as the intersection of the horizontal axis (dR/R_0) and the extrapolation of the slope used for the E_0 calculation.

7.2.3 Possum Kingdom Airport PPMT Test Results

A summary of the 8 PPMT tests in the 3 test borings is given in Table 5. All of the reduced pavement pressuremeter curves and the PPMT parameter profiles are presented in Appendix A and B. Four tests were conducted by driving the probe into place and four tests were conducted in prebored holes in the sand subgrade. Driving was used first because it was thought that the hole would collapse if hand augering was used. Later it was discovered that hand augering was possible.

7.3 Cyclic Triaxial (CT) Test Results

7.3.1 Cyclic Triaxial Test Equipment and Procedure

The cyclic triaxial test (Barker and Brabston 1975) is a laboratory test performed on cylindrical soil samples placed in a cell. The samples are either undisturbed or remolded depending on the soil type and the sampling equipment used. The objective of the test is to determine a resilient modulus, M_r by performing unload-reload cycles. The

Test Boring	Depth (in)	E_o (ksf)	E_r (ksf)	p_{oh} (ksf)	p_l (ksf)	n_{sec}	n_{cyc}	n_{res}	n_{crp}	K_2 (ksf)	n	a $(ksf)^{-1}$	b $(ksf)^{-1}$
1	13	73	283	0.5	4.5	***	***	***	***	***	***	***	***
	25	89	293	0.9	8.5	***	***	***	***	***	***	***	***
	37	174	398	1.3	13.0	***	***	***	***	***	***	***	***
	61	378	707	1.9	17.5	***	***	***	***	***	***	***	***
	85*	315	705	1.4	18.0	0.03	0.11	0.12	0.02	1300	0.78	2.6×10^{-4}	1.3×10^{-3}
2	27*	159	547	0.5	9.0	0.02	-0.04	0.10	0.02	***	***	5.6×10^{-4}	3.4×10^{-3}
	39	246	419	1.8	10.0	***	***	***	***	***	***	***	***
3	13*	41	160	0.3	4.5	0.02	-0.06	0.18	0.03	950	0.69	1.1×10^{-4}	4.8×10^{-3}
	26*	214	450	1.0	9.5	0.03	0.04	0.08	0.03	985	0.78	6.0×10^{-4}	2.4×10^{-3}
	38*	190	492	0.8	13.0	0.04	0.11	0.11	0.02	992	1.02	3.5×10^{-4}	1.9×10^{-4}
	62	920	1155	0.8	27.0	0.05	0.12	0.10	0.03	1805	1.02	1.0×10^{-4}	1.1×10^{-3}
4	13**	144	393	0.5	10.0	0.04	0.08	***	0.02	2400	1.0	2.5×10^{-5}	3.0×10^{-3}
	29**	164	520	1.7	10.5	0.04	0.05	***	0.05	1700	2.25	1.0×10^{-4}	2.5×10^{-3}

*** - 1.0 cc volume change used to determine *a* and *b*.**

**** - 0.2 cc volume change used to determine *a* and *b*.**

***** - these parameters were not found since Standard PPMT tests were conducted (Figure 11).**

Table 5
Easterwood Airport PPMT Summary

Test Boring	Depth (in)	E_o (ksf)	E_r (ksf)	p_{oh} (ksf)	p_l (ksf)	n_{sec}	n_{cyc}	n_{res}	n_{crp}	K_2 (ksf)	n	a $(ksf)^{-1}$	b $(ksf)^{-1}$
1	26	98	469	0.7	16	**	**	**	**	**	**	2.2×10^{-4}	2.0×10^{-3}
	39	110	345	1.8	9	**	**	**	**	**	**	**	**
	50	302	682	0.5	12	**	**	**	**	**	**	2.3×10^{-4}	2.3×10^{-3}
	74	434	1351	1.0	28	**	**	**	**	**	**	1.5×10^{-4}	8.5×10^{-4}
2	39	75	346	1.3	9	0.08	-0.03	0.08	0.01	1000	0.47	7.3×10^{-4}	2.0×10^{-3}
	50	327	419	1.8	10	0.05	0.06	0.09	0.04	1067	0.62	6.2×10^{-4}	2.2×10^{-3}
3	26	47	171	0.9	10	0.06	-0.05	0.10	0.01	1240	0.46	7.9×10^{-4}	4.7×10^{-3}
	39	202	424	1.3	10	0.04	0.05	0.22	0.02	1530	1.15	3.4×10^{-4}	2.4×10^{-3}
	50	210	434	0.8	10	0.04	0.02	0.10	0.02	1295	0.51	5.0×10^{-4}	2.2×10^{-3}
	74	469	1048	0.7	25	0.05	0.11	0.12	0.03	1855	0.64	2.0×10^{-4}	1.0×10^{-3}
4	26*	557	1509	5.0	55	0.05	0.24	0.06	0.03	645	0.80	4.0×10^{-5}	5.6×10^{-4}

*** - Driven PPMT Test**

**** - these parameters werre not found since Standard PPMT tests were conducted (Figure 11).**

Table 4
San Antonio International Airport PPMT Summary

Test Boring	Depth (in)	E_o (ksf)	E_r (ksf)	p_{oh} (ksf)	p_l (ksf)	n_{sec}	n_{cyc}	n_{res}	n_{crp}	K_2 (ksf)	n	a $(ksf)^{1}$	b $(ksf)^{1}$
1	16*	994	3681	1.8	42	**	**	**	**	**	**	**	**
	28*	892	3545	1.5	60	0.04	0.13	0.09	0.008	240	1.86	5.5×10^{5}	5.2×10^{4}
	40*	1448	5721	2.9	80	0.04	0.10	0.06	0.006	605	1.42	5.5×10^{5}	5.5×10^{4}
2	13	380	1310	1.2	38	0.02	0.06	0.08	0.008	2180	0.89	8.5×10^{5}	8.5×10^{4}
	25	367	2057	1.9	55	0.02	0.15	0.11	0.006	2113	0.96	6.5×10^{5}	7.8×10^{4}
	37	528	2788	1.3	60	0.03	0.10	0.10	0.004	1700	1.09	4.5×10^{5}	5.8×10^{4}
	61	168	8710	0.8	19	0.03	0.11	0.12	0.011	2955	0.54	1.3×10^{4}	1.3×10^{3}
3	13*	933	3700	10.5	40	0.05	0.09	0.06	0.020	3060	0.75	6.0×10^{5}	4.6×10^{4}

* - Driven PPMT Tests

** - these parameters were not found since Standard PPMT tests were conducted (Figure 11).

Table 5
Possum Kingdom Airport PPMT Summary

resilient modulus is defined as the slope of the unload portion of the cycles on a plot of deviator stress (σ_d) versus axial strain (ϵ_r).

In order to run cyclic triaxial tests for the evaluation of an existing airport pavement, field samples of the materials supporting the pavement must be obtained. The field samples are normally obtained in either an undisturbed state, using shelby tub samplers, or a disturbed state, by any conventional soil sampling technique. This normally involves drilling a hole through the existing pavement to the subgrade and obtaining the samples in the subgrade. If disturbed samples are recovered in the field they are reconstructed to their evaluated in place density and water content in the laboratory. To begin the laboratory testing the sample is placed in the cyclic triaxial cell (Figures 52 & 53). The confining pressure σ_3 is applied. The vertical axial load is increased thereby increasing the deviator stress σ_d. Then 200 unload-reload cycles are applied. At the same time the vertical strain ϵ_v is measured using a Linear Variable Differential Transducer (LVDT) which records the change in length of the sample during each cycle (i.e. between points A and B on Figure 52). The LVDT is held in place by 2 spring loaded clamps which are shown on Figure 52 and detailed in Figure 53.

For cohesive soils σ_3 is maintained constant throughout the test. The deviator stress σ_d is first increased to a chosen value and 200 cycles between 0 stress and σ_d are applied while recording ϵ_v. Then σ_d is increased to a second value and another 200 cycles are applied. This sequence continues until failure is reached (Figure 54).

For cohesionless soils, the procedure for cohesive soils is repeated for each chosen value of σ_3 (Figure 55). The reason for varying σ_3 in cohesionless soils is that M_r is sensitive to the mean normal stress , while for cohesive soils M_r depends mainly on σ_d (Barker and Brabston 1975).

It is important to point out that many more problems were encountered during the cyclic triaxial testing program than in either the PPMT or FWD testing programs. The complicated nature of the CT equipment and procedures led to problems with the electrical and hydraulic equipment as well as with the sample preparation. Some of the typical electrical problems were:

a) shorts in the Linear Variable Differential Transducers (LVDT),
b) shorts in the continuous feed two pen plotter used to record the loads and the displacements, and
c) complicated electrical input of the square wave loading at the start of each test.

Some of the typical hydraulic problems were:

a) variable pressures in the hydraulic line, causing the zero load point to drift, and
b) leakage of the hydraulic fluid due to worn connections.

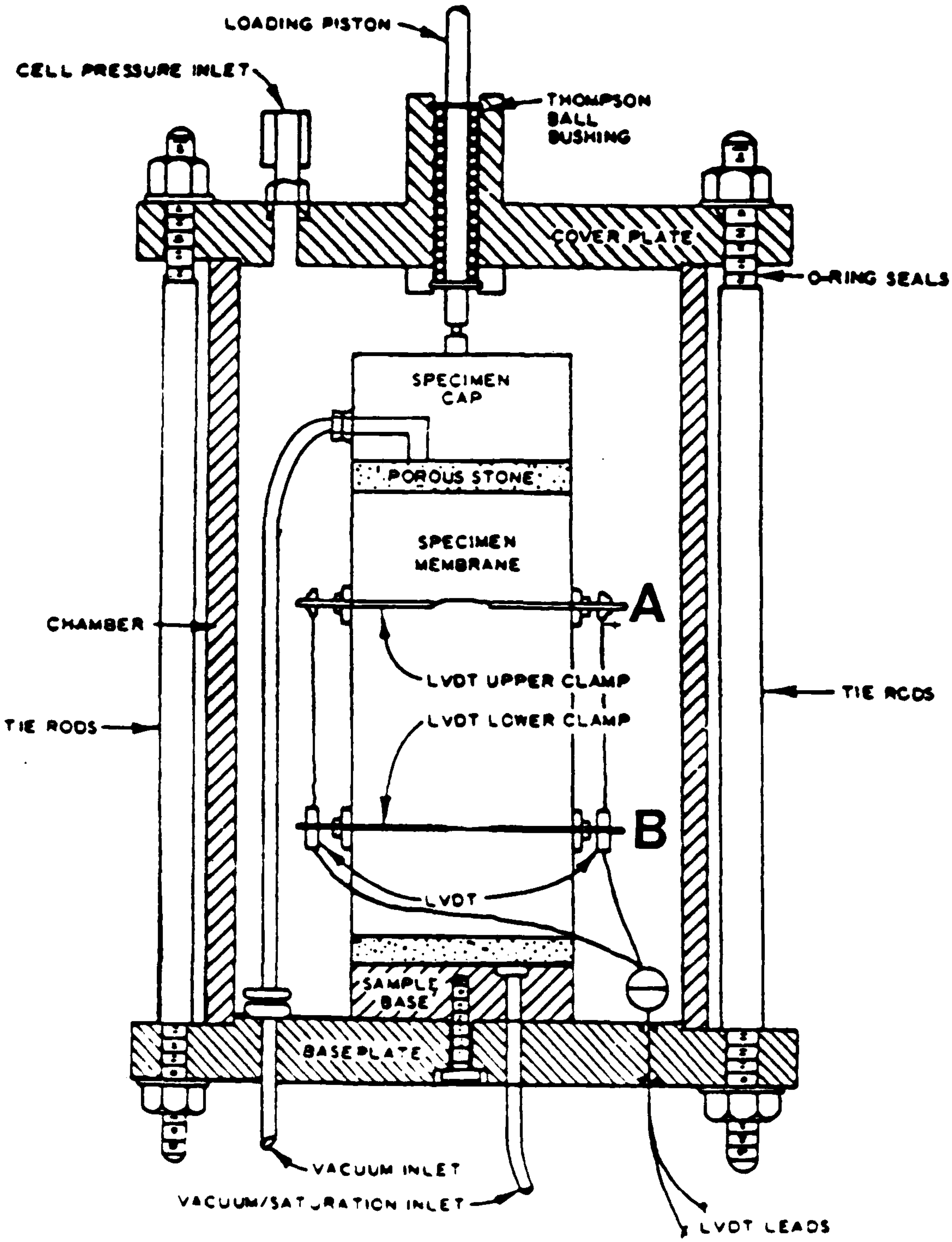

Fig. 52 Cyclic Triaxial (CT) Cell (from Barker and Brabston 1975)

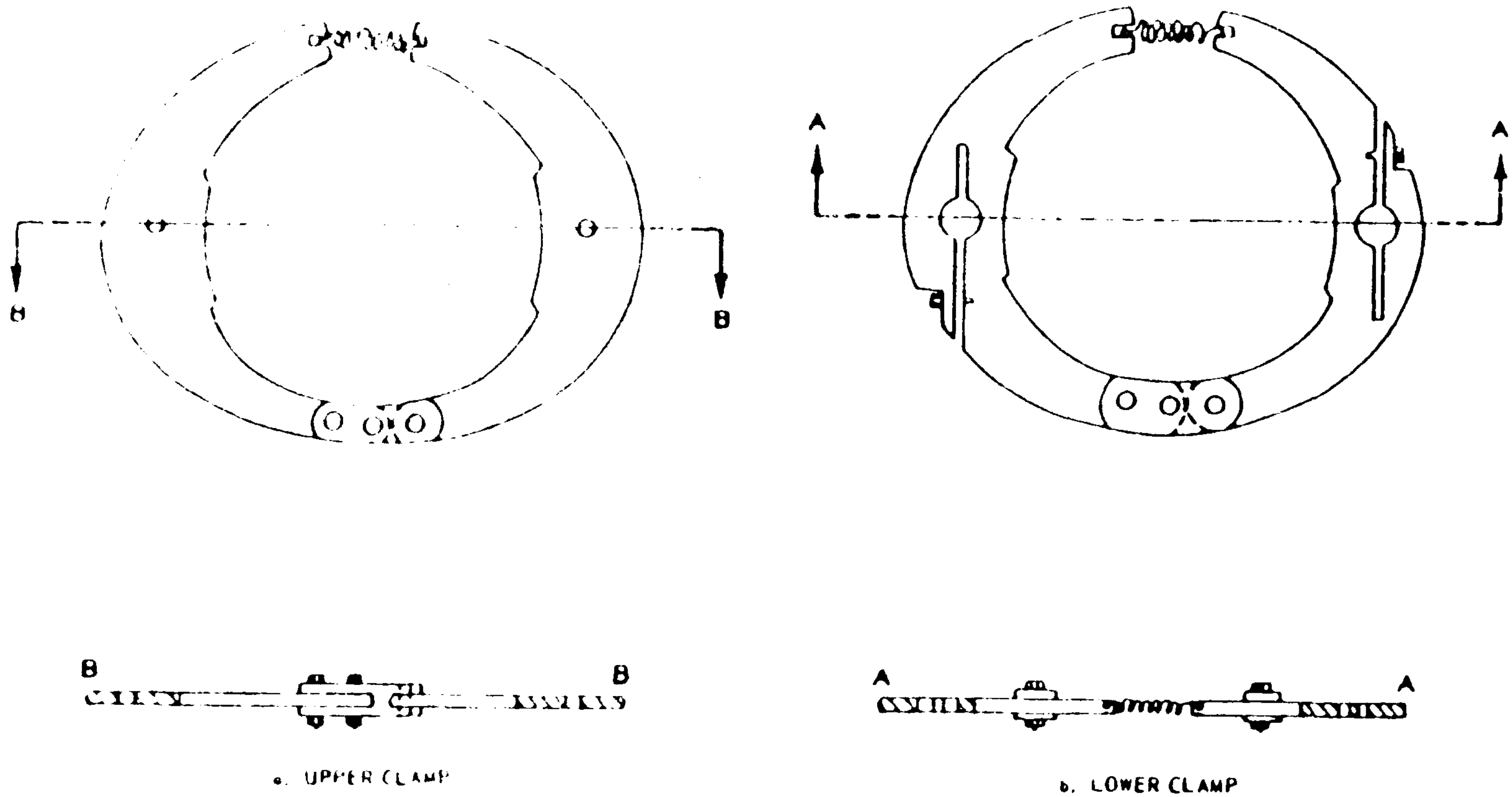

Fig. 53 Cyclic Triaxial Clamps (from Barker and Brabston 1975)

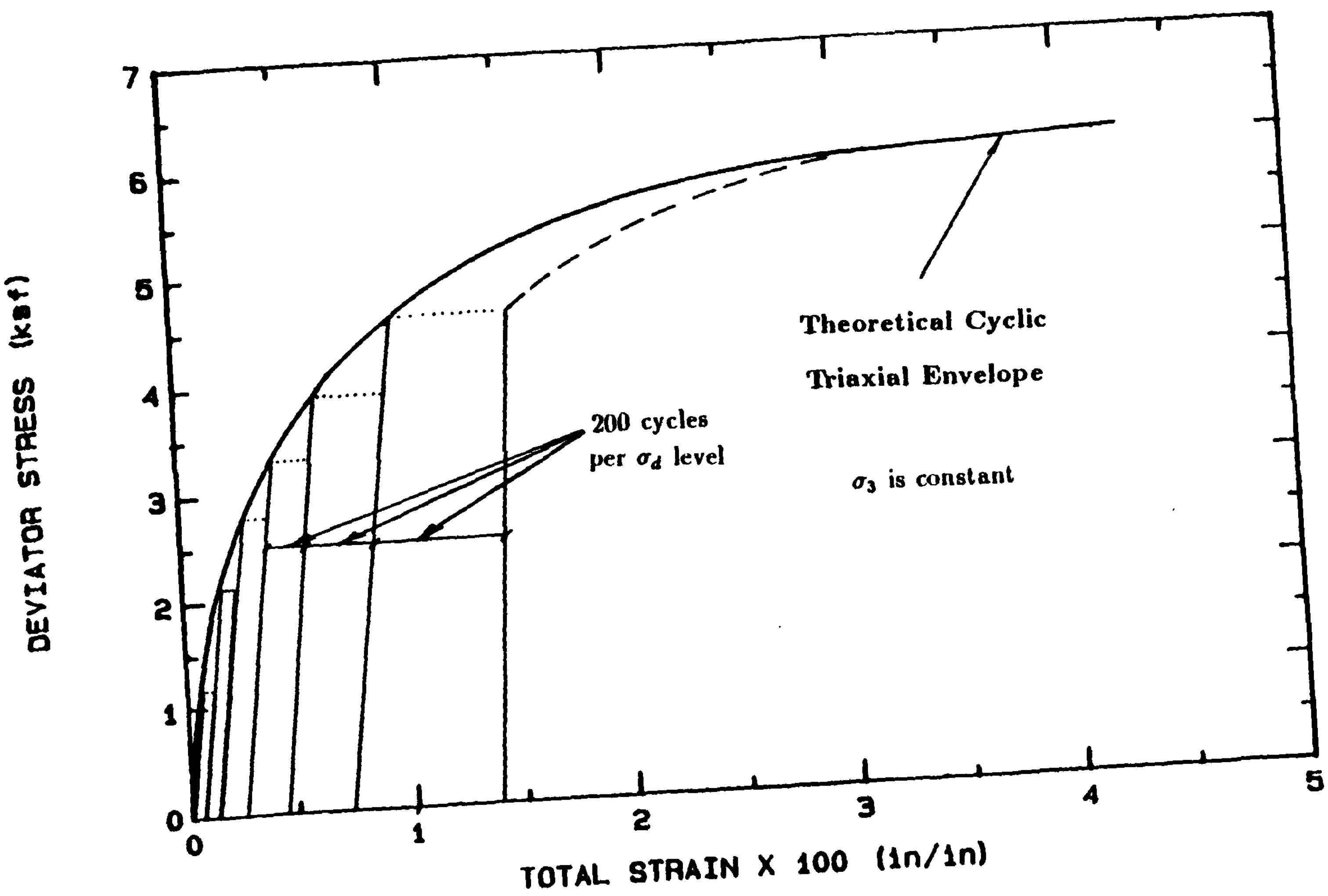

Fig. 54 Typical CT Test Results for Cohesive Soils

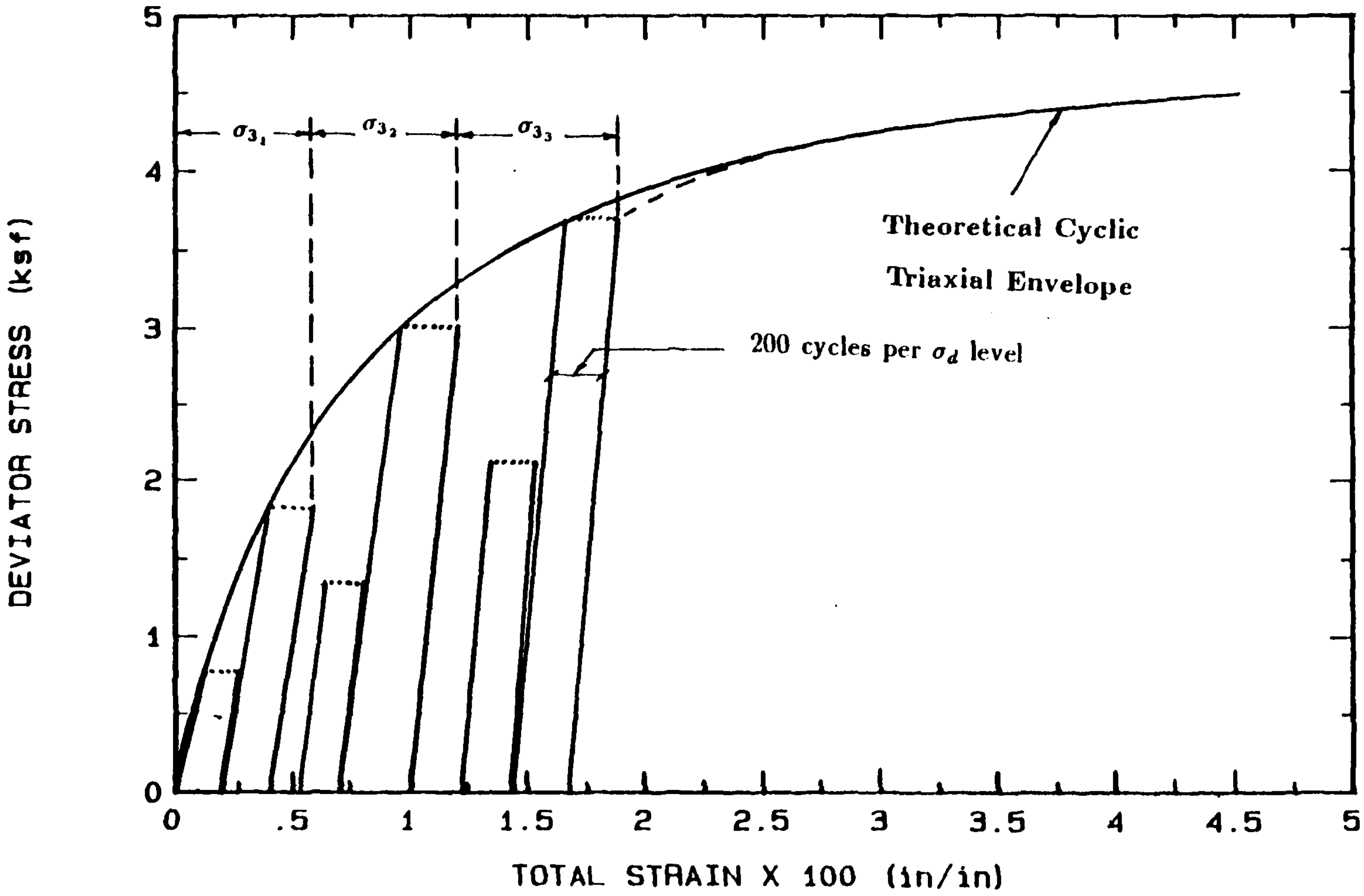

Fig. 55 Typical CT Test Results for Cohesionless Soils

The problems with sample preparation varied somewhat with the type of sample. For the clay the most common problems were:

a) proper extrusion and trimming of the specimen,
b) movement of the LVDT clamps as the triaxial cell was lowered onto the base plate. This occurred due to the limited clearance between the inside of the cell and the edge of the LVDT clamps, and
c) improper alignment of the loading pistons and specimens cap.

For the sand samples the most common problems included b and c for the clay samples plus the following:

a) Remolding the sample to its in situ state was extremely difficult and time consuming.
b) Attaching the vacuum to the sample in order to place the LVDT and LVDT clamps onto the sample resulted in further disturbance of the remolded sample.
c) At the lower deviator stresses the amount of movement of the LVDT was so small that the continuous feed two pen plotter would not indicate any movement.

7.3.2 Cyclic Triaxial (CT) Test Results for the Three Airports

Each sample was 2.8 in. (7.1 cm) in diameter and 6 in. (15.2 cm) in length. Two hundred load repetitions were applied at each deviator stress ($_d$) level.

Figure 56 is a conceptual plot of a cyclic triaxial test. The CT parameters obtained during this study are listed below (Figure 56).

1. E_{s_i} - secant modulus obtained from the slope of the line joining the origin of the stress-strain curve to the top of the i^{th} cycle.
2. E_{c_i} - cyclic modulus obtained from the loading part of the unload-reload loop of the i^{th} cycle.
3. M_{c_i} - resilient modulus obtained from the unloading part of the unload-reload loop of the i^{th} cycle.
4. The exponents n_{sec}, n_{cyc} and n_{res} for the corresponding Idriss cyclic moduli models are found using the same procedure as for the PPMT tests.

For Easterwood airport, 6 CT tests were conducted on the shelby tube samples taken from the test boring. The results are presented in Table 6. Even though 10 shelby tube samples were taken from the test boring, results from only 6 tests are presented, since insufficient sample recovery and the equipment problems stated above prevented testing of all 10 samples. All of the cyclic triaxial curves and parameter profiles are presented in Appendix D.

For San Antonio International airport, 7 CT tests were conducted on the shelby tube samples taken from the test boring. The results are presented in Table 6. Even though 10 shelby tube samples were taken

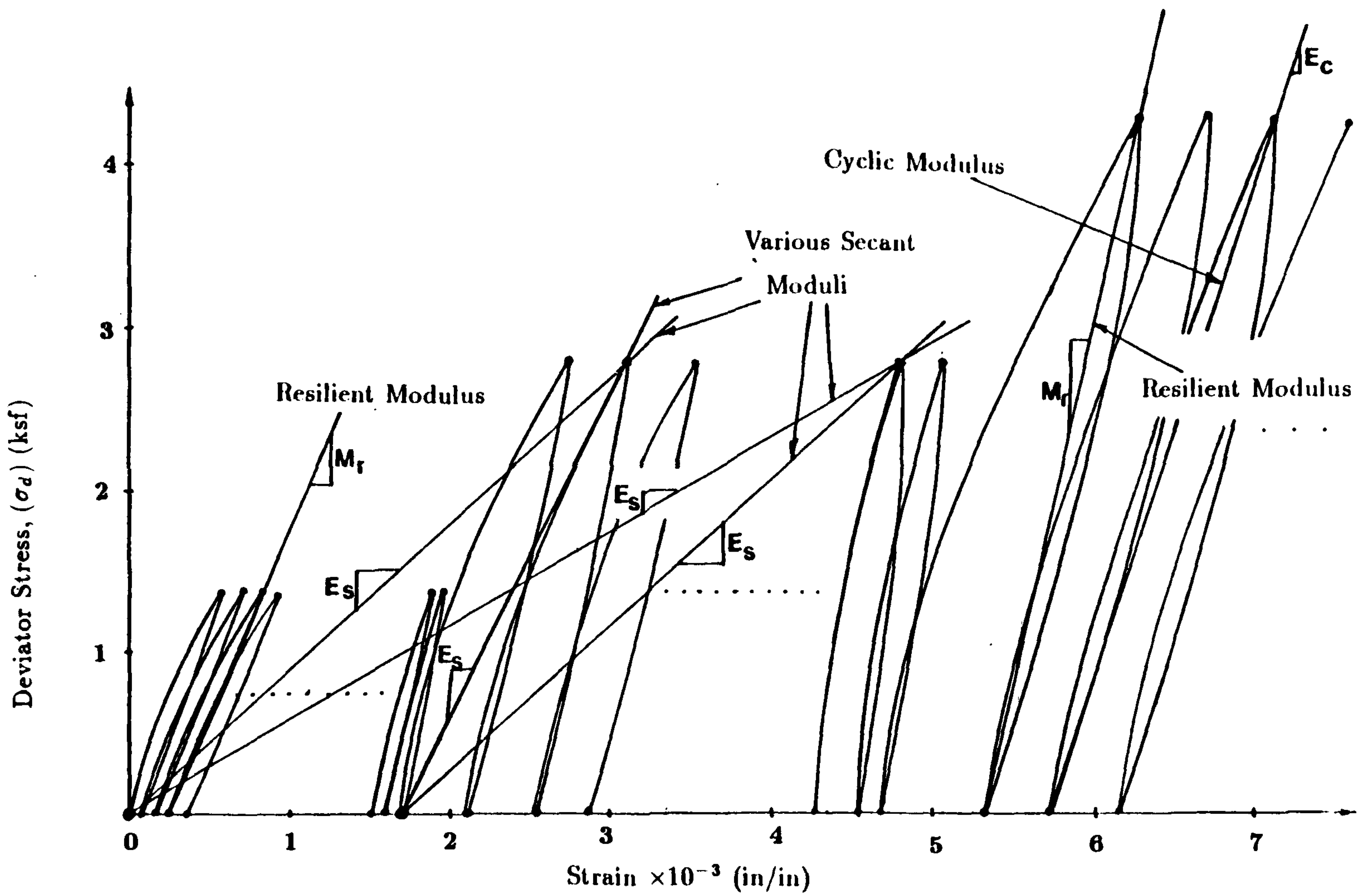

Fig. 56 Definitions for Airport CT Test

Airport	Depth (ft)	E_o [1] (ksf)	M_r [2] (ksf)	σ_3 [3] (ksf)	σ_d [4] (ksf)	σ_{ult} [5] (ksf)	n_{sec} [6]	n_{cyc} [6]	n_{res} [6]
Easterwood	1	408	382	0.14	0.86-2.45	2.54	0.01	0.02	0.004
	2	419	421	0.28	0.86-2.88	2.88	0.06	0.02	0.02
	3	326	647	0.48	0.86-3.74	3.74	0.11	0.05	0.06
	7	852	852	1.01	2.01-4.70	4.70	0.13	0.03	0.06
	8	7107	1495	1.15	1.87-4.00	4.00	0.51	0.11	0.12
	9	957	957	1.30	1.38-3.65	3.65	0.18	0.18	0.02
San Antonio	2	967	1111	0.29	0.43-5.20	5.20	0.07	0.07	0.01
	3	1048	1029	0.43	0.86-6.70	6.70	0.03	0.02	0.008
	4	1625	1548	0.58	2.10-9.98	9.98	0.03	0.04	0.01
	5	1550	1243	0.72	3.60-8.30	8.30	0.05	0.02	0.01
	7	298	298	1.01	2.20-14.80	14.80	0.04	0.02	0.02
	8	3098	3098	1.15	2.20-6.30	6.30	0.04	0.03	0.02
	10	1787	1716	1.44	2.20-11.60	11.60	0.04	0.01	0.01
Possum Kingdom	0.5	30100	60252	1.1-2.9	2.20-3.60	5.47**	0.06	0.007	0.02
	1	9561	16289	0.7-2.9	0.72-4.40	5.47**	0.02	0.05	0.06
	5	14958	14530	0.7-4.3	1.44-4.30	5.47**	0.002	0.04	0.04
	6	21390	21390	1.1-4.3	1.20-2.80	5.47**	0.008	0.02	0.08

* - detailed plots in Appendix D

** - estimated from average ϕ values of all four tests on sands.

1. E_o is the initial modulus from first deviator stress level of test.
2. M_r is the first resilient modulus from first deviator stress level of test.
3. Confining Stress during test.
4. Deviator stress range during test.
5. Ultimate Deviator Stress applied to sample during test.
6. Average exponents calculated by averaging the values for each deviator stress

Table 6
Airport CT Testing Summary *

from the test boring, results from only 7 tests are presented, since insufficient sample recovery and the equipment problems stated above prevented testing of all 10 samples. All of the cyclic triaxial curves and parameter profiles are presented in Appendix D.

For Possum Kingdom airport, 4 CT tests were conducted on the shelby tube samples taken from the test boring. The results are presented in Table 6. Even though 10 shelby tube samples were taken from the test boring, results from only 4 tests are presented, since insufficient sample recovery prevented testing of all 10 samples. All of the cyclic triaxial curves and parameter profiles are presented in Appendix D.

7.4 Falling Weight Deflectometer (FWD) Test Results

7.4.1 Falling Weight Deflectometer Equipment and Procedure

The Falling Weight Deflectometer (Smith and Lytton 1983) is a non-destructive (NDT) pavement evaluation device delivering an impulse force to the pavement which may be varied to simulate different vehicle loads. The trailer mounted Dynatest Model FWD system, used in this research is shown in Figure 57. The FWD trailer and loading plate on which the weight drops exert a small load on the pavement. This load varies from 3 to 18% of the dynamic load. During a test a weight is lifted to a given height on a guide system and then dropped to simulate a single wheel loading on the pavement (Smith and Lytton 1985). By varying the mass of the falling weight and/or the drop height, the impulse force exerted on the pavement can be varied. The duration of the impulse force is about 0.2 seconds. This impulse force generates a deflection basin as shown in Figure 58. The geophones used to measure the deflections are spaced at known distances from the load.

A dynamic force ranging from 1500 to 24,000 lbs (6.7 to 106.8 kN) can be developed by varying the drop heights and weights. The system is equipped with four mass levels weighing 110, 220, 440 and 660 lbs (.5, 1.0, 2.0 and 2.9 kN). By varying the drop heights the following force ranges can be achieved for the four mass levels:

1. 1500 to 4000 lbs (7 to 18 kN) with the 110 lbs (0.5 kN) load
2. 3000 to 8000 lbs (13 to 35 kN) with the 220 lb (1.0 kN) load
3. 5500 to 16,000 lbs (25 to 70 kN) with the 440 lb (2.0 kN) load
4. 8000 to 24,000 lbs (35 to 105 kN) with the 660 lb (2.9 kN) load

The weights are raised hydraulically and released by an electronic signal. The weights drop onto a rubber buffer system to provide a load pulse in approximately a half-sine wave form. This rubber buffer system is an 11.8 in. (300 mm) diameter loading plate. The impulse load is measured using a strain gage load transducer (load cell) in the center of the loading plate.

The deflections are measured by seven velocity transducers mounted on a bar and lowered on the pavement surface automatically with the loading plate. Their locations are shown on Figures 58 and 59. One of

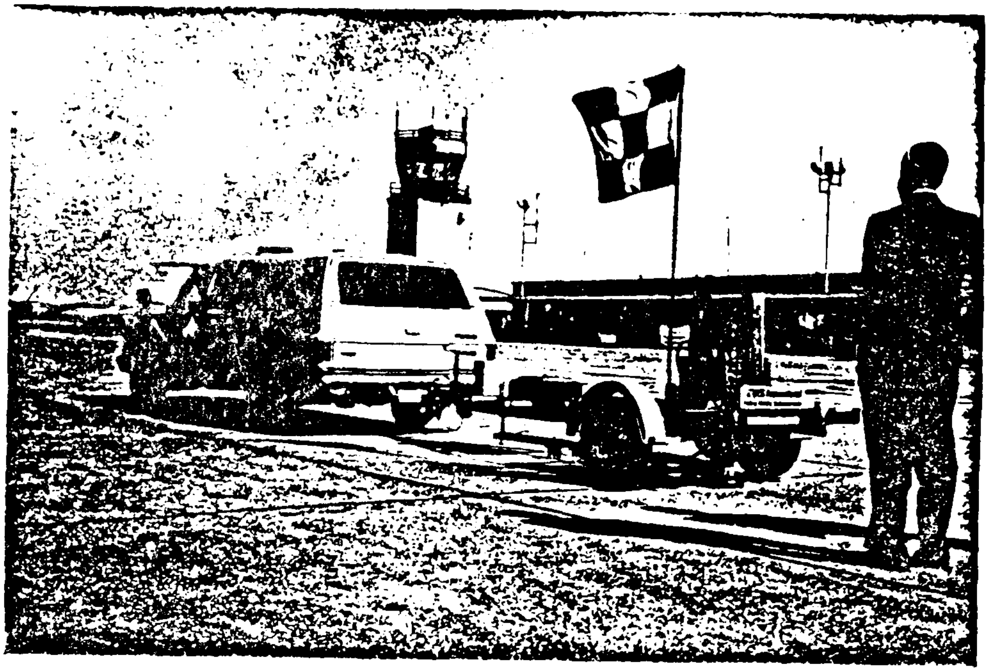

Fig. 57 Falling Weight Deflectometer (FWD))

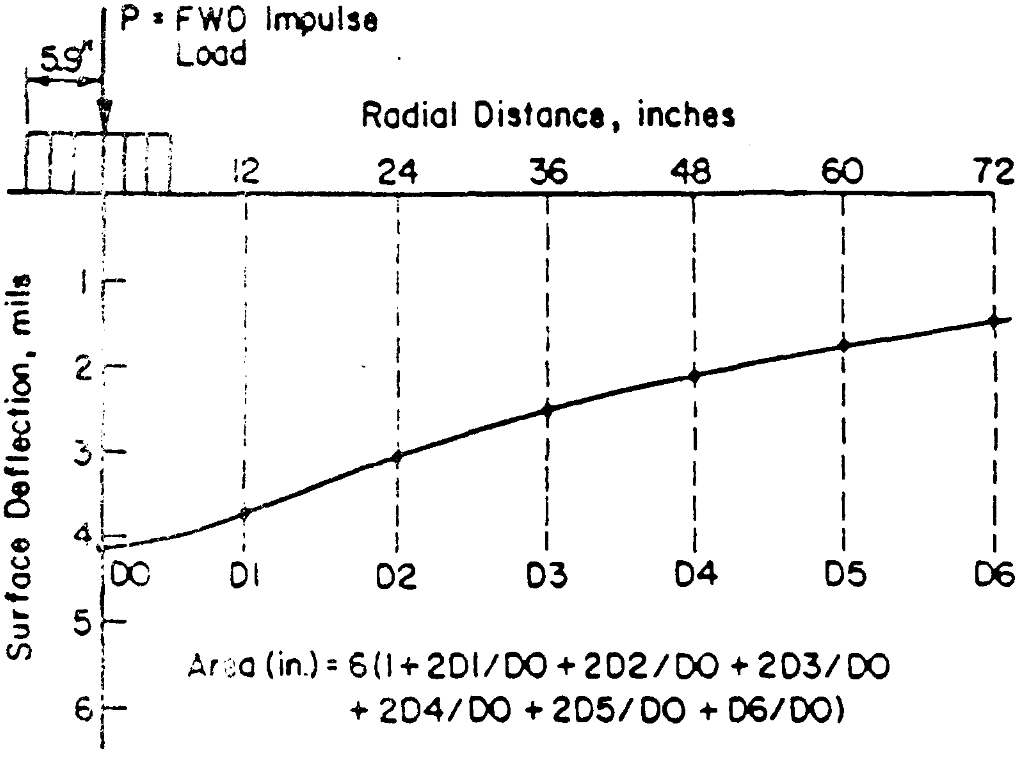

Fig. 58 Resulting FWD Deflection Basin

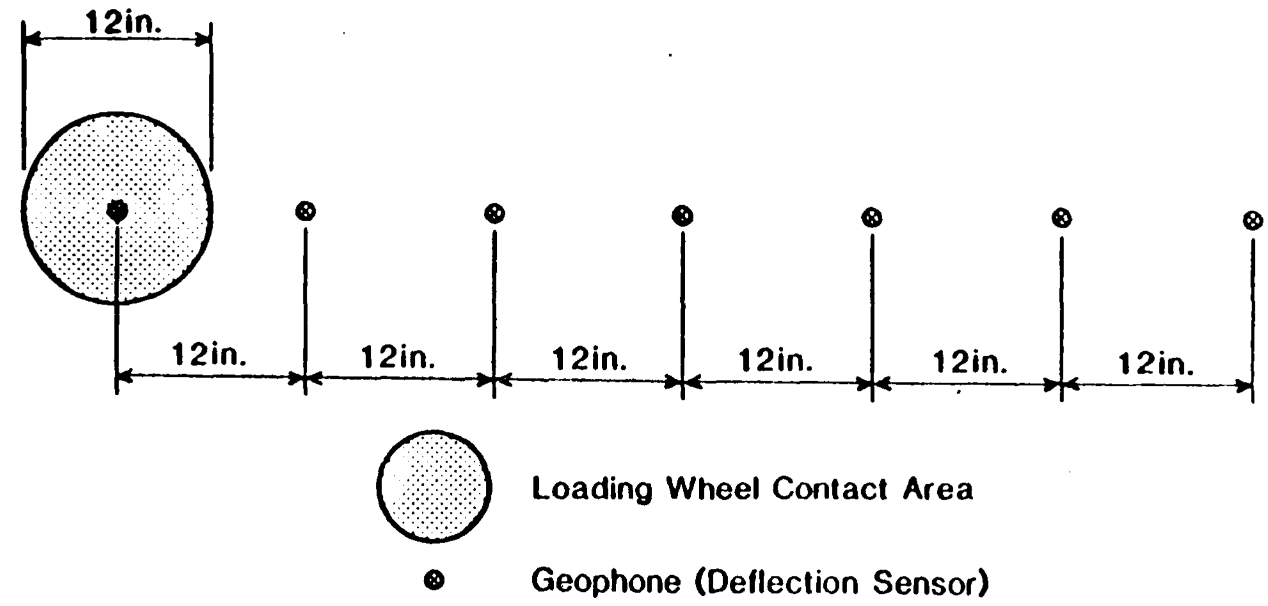

Fig. 59 Typical Location of Loading Plate and Geophones for FWD (from Smith and Lytton 1983)

(1 in = 25.4 mm)

the seven transducers is located at the center of the loading plate.

The information from the geophones and the load cell is recorded by a Hewlett Packard Model 85 (HP-85) computer. Records of the loads and deflections at each test location are stored on a paper tape and magnetic cassette. The display, the printed results and the stored data can be either in metric or English units. A typical set of results is shown in Table 7.

The normal operation sequence for a field test is to move the device to the test location and hydraulically lower the loading plate and transducers onto the pavement. A normal test sequence is then completed by using four drop heights of a chosen weight. The HP-85 equipment records and stores the data. The loading plate and sensors are then hydraulically lifted and the device is ready to move to the next location. Testing at one pavement location takes about 2 minutes.

7.4.2 Falling Weight Deflectometer Test Results

The FWD tests were reduced by Eres, Inc. in order to back-calculate the modulus of the subgrade. This was done by assuming a surface course thickness and modulus, then back-calculating a modulus which would best match the deflection basin measured with the FWD. These subgrade/ base course moduli are presented in Table 8. Note that the airport testing grids presented in Figures 41, 45 & 49 are used as references for the locations of the moduli. In addition the Dynamic Stiffness Modulus (DSM) was calculated for each FWD location. The DSM is a measure of the overall stiffness of the pavement with higher values representing stiffer pavement systems. The DSM is defined as:

$$\frac{Q_{max} - Q_{min}}{DO_{max} - DO_{min}} \tag{33}$$

where: Q_{max} is the maximum load during testing in pounds, Q_{min} is the minimum load during testing in pounds, DO_{max} is the deflection associated with the maximum load during testing in mils (10^{-3} inches), and DO_{min} is the deflection associated with the minimum load during testing in mils (10^{-3} inches).

The detailed FWD results are in Appendix E.

Station	Load (lbs)	DO	D1	D2	D3	D4	D5	D6	AREA[1] (mils^2)	DSM[2] (lbs/mil)
1CLGJT[3]	9000	4.6	2.4	2.1	1.8	1.5	1.3	1.1	47.8	
	13000	7.3	3.8	3.3	2.8	2.4	2.1	1.8	47.8	
	17000	9.5	5.0	4.3	3.7	3.1	2.7	2.3	47.8	
	23000	13.2	6.9	5.9	5.0	4.2	3.6	3.1	47.8	1628

Deflections D0 to D6 are in mils.
1. AREA = Area of deflection basin found by Trapezoidal rule (Appendix E).
2. DSM = Dynamic Stiffness Modulus = [Max Load - Min Load (lbs)] divided by [DO at Max Load - DO at Min Load]
3. 1CLGJT ⇒ FWD test location: Station 1C, Longitudinal Joint

Table 7

Typical FWD Deflections

Normalized Deflection Data

Station	Easterwood[1] Moduli (ksi)	San Antonio[1] Moduli (ksi)	Possum Kingdom Moduli (ksi)
1A	16.3	30.5	12.6
2A	15.5	34.4	12.1
2A2[2]	—	29.3	—
3A	13.5	33.0	11.8
4A	—	33.3	11.6
5A	—	—	12.3
6A	—	—	12.5
7A	—	—	13.4
8A	—	—	12.8
9A	—	—	12.7
10A	—	—	12.5
1B	23.3	26.0	12.6
2B	16.6	32.7	11.9
3B	14.8	30.7	12.7
4B	—	28.1	12.8
5B	—	—	12.7
6B	—	—	12.9
7B	—	—	12.9
8B	—	—	12.3
9B	—	—	12.3
10B	—	—	11.9
1C	16.5	34.3	—
2C	16.5	27.7	—
3C	14.9	29.8	—
4C	—	28.9	—

1. Average Moduli are presented for the center of the slabs.
2. Slab 2A at San Antonio had transverse crack allowing for FWD tests on both sides.

Table 8.
Airport FWD Moduli Summary

8. COMPARISON OF MEASURED FWD DEFLECTIONS WITH PREDICTED FWD DEFLECTIONS USING PPMT MODULI AND CT MODULI

The comparison consisted of comparing measured FWD deflections with the predicted deflections obtained by using PPMT or CT moduli as input into the finite element computer program ILLIPAVE (Barenberg 1972).

8.1 The Finite Element Program ILLIPAVE

ILLIPAVE models the pavement as a three-dimensional continuum. It is possible to break the pavement system into numerous layers, with the stipulation that the number of elements and nodes be limited to 400 and 500 respectively. The individual layers can then be modeled using one of the four approaches which follow:

1. materials with a modulus varying as a function of the minor principal stress, σ_3,
2. materials with a modulus varying as a function of the deviator stress, σ_d,
3. materials with a linear stress-strain curve (i.e. constant E), and
4. materials with a modulus varying as a function of the first stress invariant, $\Theta_T = (\sigma_1 + \sigma_2 + \sigma_3)$.

The program outputs material properties, gravity stresses, the finite element mesh with identified materials within the mesh, the deflections of each node, the stresses in each element and the moduli associated with each element.

8.2 Predicted FWD Deflections Based on the PPMT Moduli

The first analysis was based on the strain level approach. Since the strains developed in the subgrade by the aircraft loading are very small, the PPMT moduli corresponding to zero strain were first used as input. These moduli are the values of 1/a from Tables 3, 4 and 5 and are shown in Table 9. The resulting predictions are shown in Figure 60. The results for Easterwood airport indicate that the FWD deflections were 35 to 56 percent more than the predicted zero strain level deflections. The results for the San Antonio airport indicate that the FWD deflections were 27 to 32 percent less than the predicted zero strain level deflections. The results for the Possum Kingdom airport indicate that the FWD deflections were about 3.25 times larger than the predicted zero strain level deflections. A summary of the ILLIPAVE output is shown in Tables 10, 11 and 12.

In order to compensate for the fact that the subgrade strain is not zero, the strains were adjusted. The strain level in the subgrade due to each FWD loading was calculated by taking the FWD deflection and dividing it by the assumed depth of influence of the loading. This depth of influence was taken as two times the diameter of the loaded

Airport Site	Depth to Center of Layer (in)	Strain Level Modulus (psi)	Mean Radial Stress[1] σ_r (psi)	Hoop Strain[1] $\epsilon_{\Theta\Theta}$ (%)	Mean Total Stress[1] Θ^2_{ave} (psi)
Easterwood	AC	3,000,000	NA[3]	NA[3]	NA[3]
	15	10,500	15.5	0	10.7
	30	19,860	24.8	0	25.9
	108	69,450	50.0	0	35.9
San Antonio International	C	3,000,000	NA[3]	NA[3]	NA[3]
	AC	400,000	NA[3]	NA[3]	NA[3]
	48	14,200	26.8	0	19.1
	126	40,850	59.8	0	43.0
Possum Kingdom	AC	400,000	NA[3]	NA[3]	NA[3]
	Base	200,000	NA[3]	NA[3]	NA[3]
	18	102,780	80.6	0	54.1
	45	208,300	124.8	0	84.2
	120	53,400	44.0	0	32.1

1. Mean values in the soil during pressuremeter test at time of PPMT modulus measurement
2. $\Theta_{ave} = 1/3(0.8\sigma_r + \sigma_z)$ where : $\sigma_r = 0.4\sigma_{r_{max}}$
3. NA = Not Applicable

Note : AC is Asphalt Concrete, C is Concrete and Base is Base Course.

Table 9.
PPMT Moduli Summary for the 0 % *Strain Approach* ILLIPAVE Input

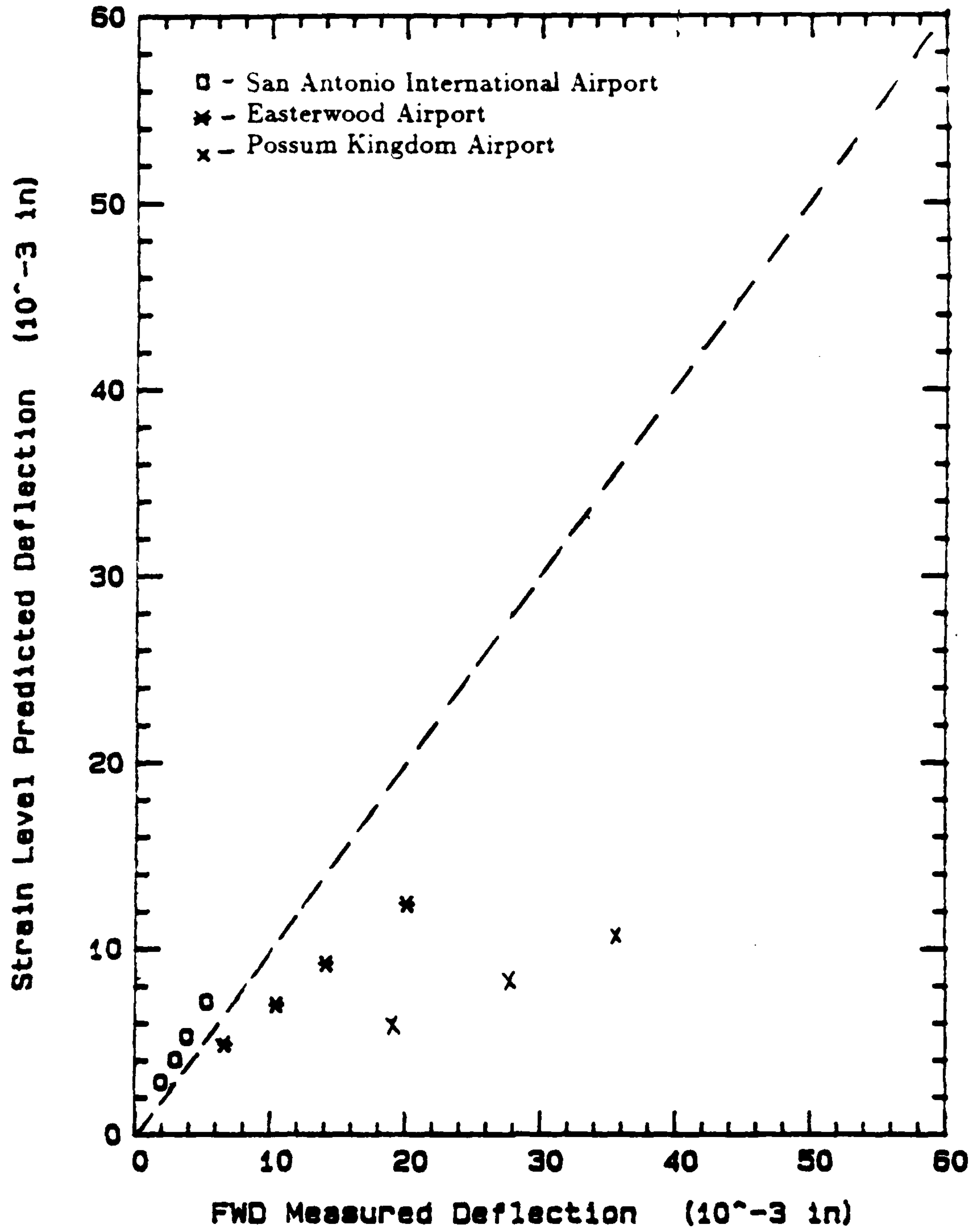

Fig. 60 PPMT J % Strain Level Model Predicted vs FWD Deflections

Depth to Center of Layer (in)	FWD Load (lbs)	Strain[1] Level Modulus (psi)	Mean Radial[2] Stress σ_r (psi)	Vert.[2] Strain ϵ_v (%)	Mean Total[2] Stress Θ^3_{ave} (psi)	Predicted Deflection (in)	Measured Deflection (in)
15	9,000	10,500	4.5	0.0170	3.4	0.0049	0.0066
30		19,860	6.5	0.0069	5.1		
108		69,450	18.4	0.0006	14.8		
15	13,000	10,500	5.6	0.0240	4.1	0.0070	0.0104
30		19,860	7.2	0.0089	5.5		
108		69,450	18.8	0.0008	15.1		
15	17,000	10,500	6.7	0.0230	4.8	0.0092	0.0141
30		19,860	8.0	0.0120	6.0		
108		69,450	19.3	0.0011	15.4		
15	23,000	10,500	8.2	0.0430	5.8	0.0124	0.0201
30		19,860	9.0	0.0160	6.8		
108		69,450	19.9	0.0015	15.8		

1. Values calculated from PPMT Tests.
2. Values calculated by ILLIPAVE.
3. $\Theta_{ave} = 1/3(\sigma_r + \sigma_z + \sigma_\Theta)$ with σ_r, σ_z and σ_Θ as calculated by ILLIPAVE

Table 10.
Easterwood Airport
ILLIPAVE Moduli Output for PPMT 0 % *Strain Approach*

Depth to Center of Layer (in)	FWD Load (lbs)	Strain[1] Level Modulus (psi)	Mean Radial[2] Stess σ_r (psi)	Vert.[2] Strain ϵ_v (%)	Mean Total[2] Stress Θ^3_{ave} (psi)	Predicted Deflection (in)	Measured Deflection (in)
15	9,000	14,200	3.9	0.0037	3.8	0.00281	0.00190
30		40,850	12.8	0.0009	11.7		
15	13,000	14,200	4.3	0.0053	4.1	0.00405	0.00295
30		40,850	13.3	0.0014	12.0		
15	17,000	14,200	4.8	0.0069	4.4	0.00530	0.00380
30		40,850	13.7	0.0018	12.3		
15	23,000	14,200	5.4	0.0094	4.8	0.00717	0.00525
30		40,850	14.3	0.0024	12.7		

1. Values calculated from PPMT tests.
2. Values calculated by ILLIPAVE.
3. $\Theta_{ave} = 1/3(\sigma_r + \sigma_z + \sigma_\Theta)$ where : σ_r, σ_z and σ_Θ are as calculated by ILLI-PAVE

Table 11.
San Antonio International Airport
ILLIPAVE Moduli Output for PPMT 0 % *Strain Approach*

Depth to Center of Layer (in)	FWD Load (lbs)	Strain[1] Level Modulus (psi)	Mean Radial[2] Stress σ_r (psi)	Vert.[2] Strain ϵ_v (%)	Mean Total[2] Stress Θ^3_{oct} (psi)	Predicted Deflection (in)	Measured Deflection (in)
18	9,000	102,780	5.3	0.0084	3.9	0.00574	0.01847
45		208,300	3.6	0.0008	3.4		
120		53,400	5.9	0.0008	6.7		
18	13,000	102,780	8.3	0.0120	5.9	0.00830	0.02756
45		208,300	3.8	0.0012	3.5		
120		53,400	6.2	0.0012	6.9		
18	17,000	102,780	10.4	0.0160	7.3	0.01085	0.03560
45		208,300	4.0	0.0015	3.7		
120		53,400	6.7	0.0015	7.2		

1. Values calculated from PPMT tests.
2. Values calculated by ILLIPAVE.
3. $\Theta_{oct} = 1/3(\sigma_r + \sigma_z + \sigma_\Theta)$ with σ_r, σ_z and σ_Θ as calculated by ILLIPAVE

Table 12.
Possum Kingdom Airport
ILLIPAVE Moduli Output for PPMT 0 % *Strain Approach*

pavement area; for the FWD this depth is 24 inches. This strain was used with the PPMT strain level model (i.e. $1/E = a + b\epsilon$) to obtain a new set of moduli values for the layers located within the assumed zone of influence. The resulting predictions are shown on Figure 61. The results for Easterwood airport indicate that the FWD deflections are between 31 and 47 percent higher than the revised strain level predictions. The results for San Antonio airport do not change since the pavement is 24 inches thick and the stresses are assumed to dissipate over that depth. However, the results are still not satisfactory for the sand subgrade (Figure 61) since the FWD deflections are about twice as large as the revised strain level deflections. A summary of the ILLIPAVE input and output is shown in Tables 13, 14 and 15. The results of this approach indicate a slightly better correlation than the zero strain level approach (Figure 61).

The second analysis was based on the stress level approach. The model is $E = K_2(\Theta/p_a)^n$. The values of K_2 and n obtained from the PPMT tests were input for each layer (Table 16). The ILLIPAVE program generated the modulus values E based on the calculations of the mean principal stress Θ. The resulting predictions are shown on Figure 62. The results for Easterwood airport indicate that the FWD deflections are 2 to 44 percent higher than the predicted stress level deflections. The results from San Antonio airport indicate that the FWD deflections ranged from 52 to 58 percent less than the predicted stress level deflections. The results from Possum Kingdom airport indicate that the FWD deflections ranged from 0.93 to 1.28 times the predicted stress level deflections. A summary of the ILLIPAVE output for the three airports is shown in Tables 17, 18 and 19. The deflections shown on Figure 62 indicate that the stress level model gives acceptable results for both the clay and the sand subgrade.

The third analysis was based on the use of the modulus obtained from the unloading part of the first cycle during the PPMT test (Table 20). The resilient modulus has classically been referred to as E_r when associated with the pressuremeter, but was denoted as M_{r1} in order to indicate its relationship to the resilient modulus from the CT test. Recall that the resilient modulus is defined as the slope of the unloading portion of the loop. The results of this apporach are shown on Figure 63. They indicate that the use of M_{r1} gives acceptable results for the sand subgrade, but unacceptable results for the clay subgrades. The results for Easterwood airport indicate that the FWD deflection ranged from 62 to 67 percent less than the predicted M_{r1} deflections. The results for San Antonio airport indicate that the FWD deflections were about 84 percent less than the predicted M deflections. The results from the Possum Kingdom airport indicate that the FWD deflections were about 5 percent less than the predicted M_{r1} deflections.

8.3 Predicted FWD Deflections Based on CT Tests and on the WES Approach

The WES procedure for predicting the CT design modulus was used to obtain M_r values for input into ILLIPAVE (Barker and Brabston 1975).

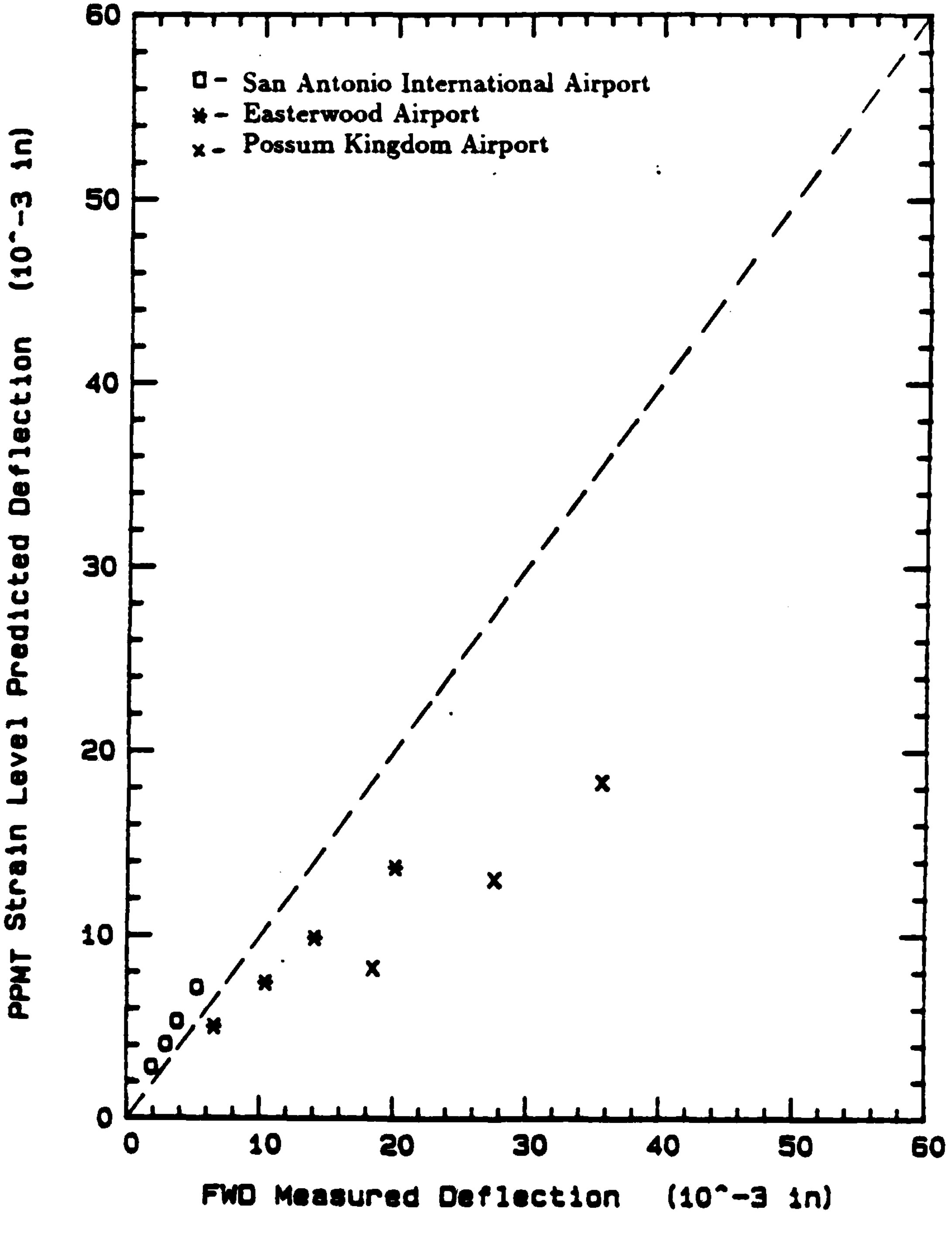

Fig. 61 PPMT Revised Strain Level Model Predicted vs FWD Deflections

Depth to Center of Layer (in)	FWD Load (lbs)	Strain[1] Level Modulus (psi)	Mean Radial[1] Stress σ_r (psi)	Vert.[1] Strain ϵ_v (%)	Mean Radial[2] Stress σ_r (psi)	Vert.[2] Strain ϵ_v (%)	Mean Total[2] Stress Θ^3_{ave} (psi)	Predicted Deflection (in)	Measured Deflection (in)
15	9,000	9,050	20.4	0.0275	3.3	0.0178	3.4	0.0050	0.0066
30		19,860	24.8	0.0000	5.6	0.0059	5.0		
108		69,450	50.0	0.0000	18.0	0.0006	15.0		
15	13,000	8,380	19.4	0.0433	3.7	0.0266	4.0	0.0074	0.0104
30		19,860	24.8	0.0000	5.9	0.0083	5.6		
108		69,450	50.0	0.0000	18.2	0.0008	15.1		
15	17,000	7,810	18.8	0.0588	4.2	0.0360	4.6	0.0098	0.0141
30		19,860	24.8	0.0000	6.2	0.0107	5.9		
108		69,450	50.0	0.0000	18.4	0.0011	15.4		
15	23,000	7,040	17.7	0.0838	4.8	0.0511	5.5	0.0137	0.0201
30		19,860	24.8	0.0000	6.7	0.0140	6.6		
108		69,450	50.0	0.0000	18.8	0.0014	15.8		

1. Values calculated from PPMT tests over a depth of $2B = 24$ inches; where B = diameter of FWD Loading Plate.
2. Values calculated by ILLIPAVE.
3. $\Theta_{ave} = 1/3(\sigma_r + \sigma_z + \sigma_\Theta)$ with σ_r, σ_z and σ_Θ as calculated by ILLIPAVE.

Table 13.
Easterwood Airport
Input and Output for PPMT *Revised Strain Approach* used with ILLIPAVE

Depth to Center of Layer (in)	FWD Load (lbs)	Strain[1] Level Modulus (psi)	Mean Radial[1] Stress σ_r (psi)	Vert.[1] Strain ϵ_v (%)	Mean Radial[2] Stress σ_r (psi)	Vert.[2] Strain ϵ_v (%)	Mean Total[2] Stress Θ^3_{ave} (psi)	Predicted Deflection (in)	Measured Deflection (in)
15	9,000	14,200	26.8	0.0079	3.9	0.0037	3.8	0.00281	0.00190
30		40,850	59.8	0.0000	12.8	0.0009	11.7		
15	13,000	14,200	26.8	0.0123	4.3	0.0053	4.1	0.00405	0.00295
30		40,850	59.8	0.0000	13.3	0.0014	12.0		
15	17,000	14,200	26.8	0.0158	4.8	0.0069	4.4	0.00530	0.00380
30		40,850	59.8	0.0000	13.7	0.0018	12.3		
15	23,000	14,200	26.8	0.0219	5.4	0.0094	4.8	0.00717	0.00525
30		40,850	59.8	0.0000	14.3	0.0024	12.7		

1. Values calculated from PPMT tests over a depth of $2B = 24$ inches; where B = diameter of FWD Loading Plate.
2. Values calculated by ILLIPAVE.
3. $\Theta_{ave} = 1/3(\sigma_r + \sigma_z + \sigma_\Theta)$ with σ_r, σ_z and σ_Θ as calculated by ILLIPAVE.

Table 14.
San Antonio International Airport
Input and Output for PPMT *Revised Strain Approach* used with ILLIPAVE

Depth to Center of Layer (in)	FWD Load (lbs)	Strain[1] Level Modulus (psi)	Mean Radial[1] Stress σ_r (psi)	Vert.[1] Strain ϵ_v (%)	Mean Radial[2] Stress σ_r (psi)	Vert.[2] Strain ϵ_v (%)	Mean Total[2] Stress Θ^3_{ave} (psi)	Predicted Deflection (in)	Measured Deflection (in)
15	9,000	12,000	166.0	0.0770	1.1	0.0362	2.6	0.0081	0.01847
30		7,150	124.8	0.0000	3.1	0.0132	3.8		
108		10,400	44.0	0.0000	6.0	0.0041	6.7		
15	13,000	19,900	159.7	0.1148	0.6	0.0372	3.1	0.0130	0.02756
30		8,900	124.8	0.0000	3.5	0.0150	4.2		
108		11,700	44.0	0.0000	6.3	0.0053	6.9		
15	17,000	26,200	152.8	0.1483	0.7	0.0420	4.3	0.0183	0.03560
30		15,800	124.8	0.0000	3.6	0.0120	4.4		
108		15,000	44.0	0.0000	6.6	0.0054	7.3		

1. Values calculated from PPMT tests over a depth of $2B = 24$ inches; where B = diameter of FWD Loading Plate.
2. Values calculated by ILLIPAVE.
3. $\Theta_{ave} = 1/3(\sigma_r + \sigma_z + \sigma_\Theta)$ with σ_r, σ_z and σ_Θ as calculated by ILLIPAVE.

Table 15.
Possum Kingdom Airport
Input and Output for PPMT *Revised Strain Approach* used with ILLIPAVE

Airport Site	Depth to Center of Layer (in)	Stress[1] Level Modulus (psi)	Total Princ. Stress[2] Θ^3 (psi)	Hoop Strain[2] $\epsilon_{\Theta\Theta}$ (%)	K_1[4] (psi)	K_2[5]	n[7] (psi)
Easterwood	C	3,000,000	NA[7]	NA[7]	NA[7]	NA[7]	NA[7]
	15	4,820	6.7	0.12	865	9,720	0.90
	30	8,940	13.4	0.12	865	9,720	0.90
	108	19,410	24.0	0.12	1113	12,500	0.90
San Antonio International	C	3,000,000	NA[7]	NA[7]	NA[7]	NA[7]	NA[7]
	AC	400,000	NA[7]	NA[7]	NA[7]	NA[7]	NA[7]
	48	8,350	14.2	0.12	1993	8,510	0.54
	126	15,060	19.6	0.12	3020	12,880	0.54
Possum Kingdom	AC	400,000	NA[7]	NA[7]	NA[7]	NA[7]	NA[7]
	Base	200,000	NA[7]	NA[7]	NA[7]	NA[7]	NA[7]
	18	88,070	96.5	0.12	1000	13,890	0.98
	45	138,356	153.0	0.12	1000	13,890	0.98
	120	39,940	51.6	0.12	4940	20,520	0.53

1. PPMT Stress Level Modulus = $K_1\Theta^n$ values in table input into ILLIPAVE.
2. Mean values in the soil during pressuremeter test at time of PPMT modulus measurement.
3. $\Theta = (0.8\sigma_r + \sigma_z)$ where : $\sigma_r = 0.4\sigma_{r_{max}}$
4. Calculated using $E = K_2(\frac{\Theta}{p_a})^n$ (Equation 3.4).
5. Calculated using $E = K\Theta^n$ (Equation 3.3) .
6. Average PPMT test results for layers chosen for ILLIAPVE input.
7. NA = Not Applicable

Note : AC is Asphalt Concrete, C is Concrete and Base is Base Course.

Table 16.
PPMT Moduli Summary for the *Stress Approach* ILLIPAVE Input

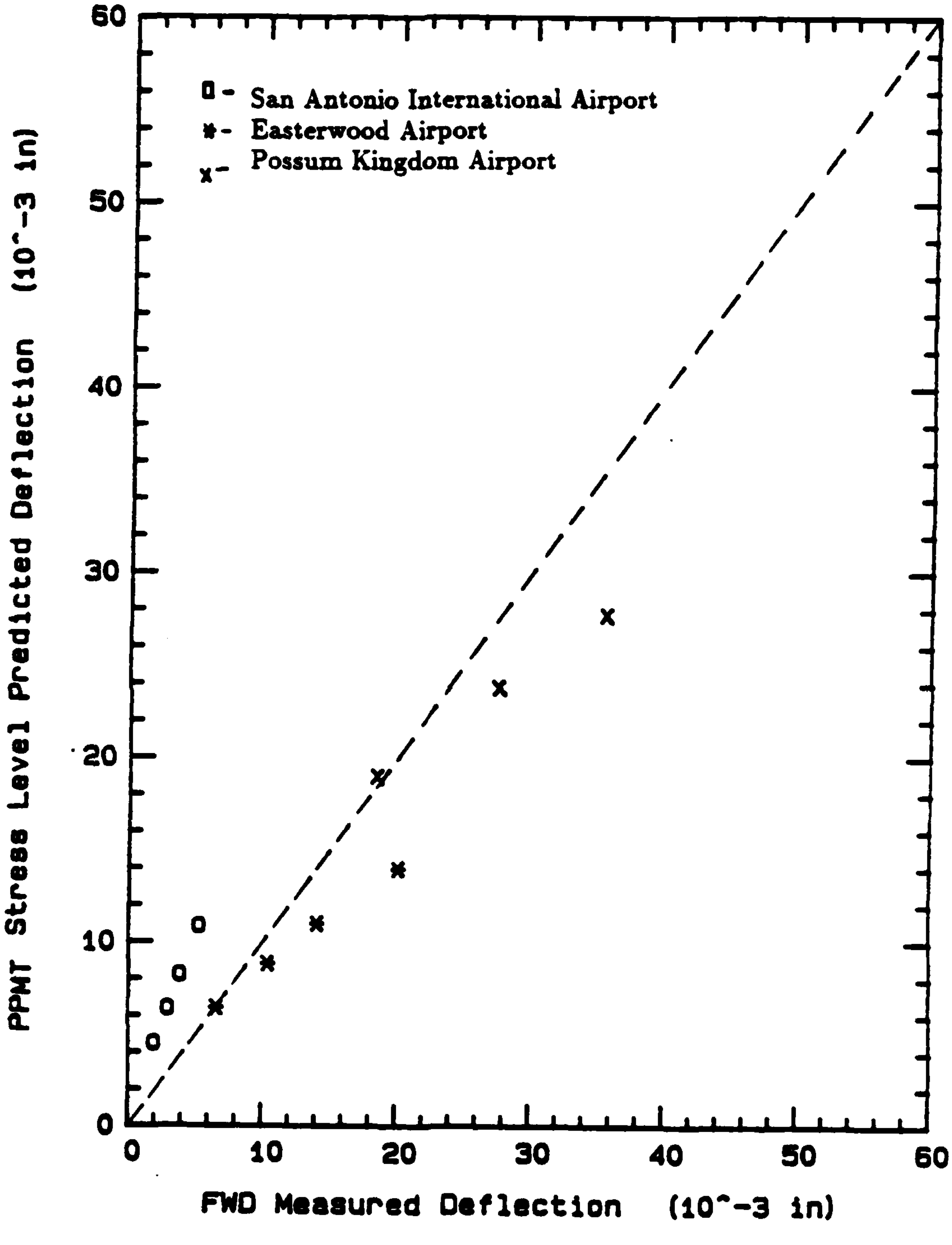

Fig 62 PPMT Stress Level Model $E = K(\frac{\Theta}{p_a})^n$ Predicted vs FWD Deflections

Depth to Center of Layer (in)	FWD Load (lbs)	Stress[1] Level Modulus (psi)	Radial[2] Stress σ_r (psi)	Vert.[2] Strain ϵ_v (%)	Mean Total[2] Stress Θ^3_{ave} (psi)	Predicted Deflection (in)	Measured Deflection (in)
15	9,000	31,500	2.8	0.0120	3.6	0.0064	0.0066
30		15,200	5.5	0.0110	5.1		
108		33,500	17.9	0.0071	14.8		
15	13,000	42,600	2.8	0.0162	4.5	0.0088	0.0104
30		18,200	5.6	0.0150	5.7		
108		33,800	18.2	0.0018	15.1		
15	17,000	53,400	2.7	0.0190	5.1	0.0109	0.0141
30		21,200	6.0	0.0180	6.3		
108		34,100	18.5	0.0024	15.4		
15	23,000	69,100	3.8	0.0220	7.0	0.0140	0.0201
30		25,600	6.1	0.0220	7.2		
108		34,800	18.8	0.0032	15.9		

1. Values calculated from PPMT tests.
2. Values calculated by ILLIPAVE.
3. $\Theta_{ave} = 1/3(\sigma_r + \sigma_z + \sigma_\Theta)$ with σ_r, σ_z and σ_Θ from ILLIPAVE.

Table 17.
Easterwood Airport
ILLIPAVE Moduli Output for PPMT *Stress Approach*

Depth to Center of Layer (in)	FWD Load (lbs)	Stress[1] Level Modulus (psi)	Radial[2] Stress σ_r (psi)	Vert.[2] Strain ϵ_v (%)	Mean Total[2] Stress Θ^3_{ave} (psi)	Predicted Deflection (in)	Measured Deflection (in)
48	9,000	9,520	4.1	0.0052	3.8	0.00452	0.00190
126		20,300	12.9	0.0019	11.7		
48	13,000	10,600	4.3	0.0069	4.1	0.00640	0.00295
126		20,400	13.1	0.0028	12.0		
48	17,000	10,600	4.5	0.0085	4.4	0.00824	0.00380
126		20,500	13.4	0.0036	12.3		
48	23,000	12,800	4.9	0.0107	4.9	0.01089	0.00525
126		20,700	13.7	0.0490	12.7		

1. Values calculated from PPMT tests.
2. Values calculated by ILLIPAVE.
3. $\Theta_{ave} = 1/3(\sigma_r + \sigma_z + \sigma_\Theta)$ with σ_r, σ_z and σ_Θ from ILLIPAVE.

Table 18.
San Antonio International Airport
ILLIPAVE Moduli Output for PPMT *Stress Approach*

Depth to Center of Layer (in)	FWD Load (lbs)	Stress[1] Level Modulus (psi)	Radial[2] Stress σ_r (psi)	Vert.[2] Strain ϵ_v (%)	Mean Total[2] Stress Θ^3_{ave} (psi)	Predicted Deflection (in)	Measured Deflection (in)
18	9,000	13,300	1.5	0.0447	3.4	0.01897	0.01847
45		10,700	3.6	0.0131	4.2		
120		87,100	6.1	0.0006	6.7		
18	13,000	17,500	1.3	0.0495	4.2	0.02380	0.02756
45		11,600	3.9	0.0179	4.8		
120		88,400	6.3	0.0008	6.9		
18	17,000	21,700	1.0	0.0547	5.0	0.02771	0.03560
45		12,400	4.3	0.0220	5.3		
120		89,700	6.5	0.0011	7.2		

1. Values calculated from PPMT tests.
2. Values calculated by ILLIPAVE.
3. $\Theta_{ave} = 1/3(\sigma_r + \sigma_z + \sigma_\Theta)$ with σ_r, σ_z and σ_Θ from ILLIPAVE.

Table 19.
Possum Kingdom Airport
ILLIPAVE Moduli Output for PPMT *Stress Approach*

Airport Site	Depth to Center of Layer (in)	Resilient Modulus M_r (psi)	Mean Radial[1] Stress σ_r (psi)	Hoop[1] Strain $\epsilon_{\Theta\Theta}$ %	Mean Total[1] Stress Θ^2_{ave} (psi)
Easterwood	AC	3,000,000	NA[3]	NA[3]	NA[3]
	15	1,910	3.3	1.0	2.6
	30	2,860	11.9	1.1	8.7
	108	5,130	19.4	1.0	15.6
San Antonio International	C	3,000,000	NA[3]	NA[3]	NA[3]
	AC	400,000	NA[3]	NA[3]	NA[3]
	48	2,815	13.3	1.2	10.1
	126	8,700	24.4	0.7	11.3
Possum Kingdom	AC	400,000	NA[3]	NA[3]	NA[3]
	Base	200,000	NA[3]	NA[3]	NA[3]
	18	19,155	46.4	0.7	31.2
	45	23,420	55.6	0.8	38.1
	120	6,515	16.9	0.7	14.0

1. Mean values in soil during pressuremeter test at time of PPMT modulus measurement.
2. $\Theta_{ave} = 1/3(0.8\sigma_r + \sigma_z)$ where : $\sigma_r = 0.4\sigma_{r_{max}}$
3. NA = Not Applicable

Note : AC is Asphalt Concrete, C is Concrete and Base is Base Course.

Table 20.
PPMT Moduli Summary for the *Resilient Modulus Approach* ILLIPAVE Input

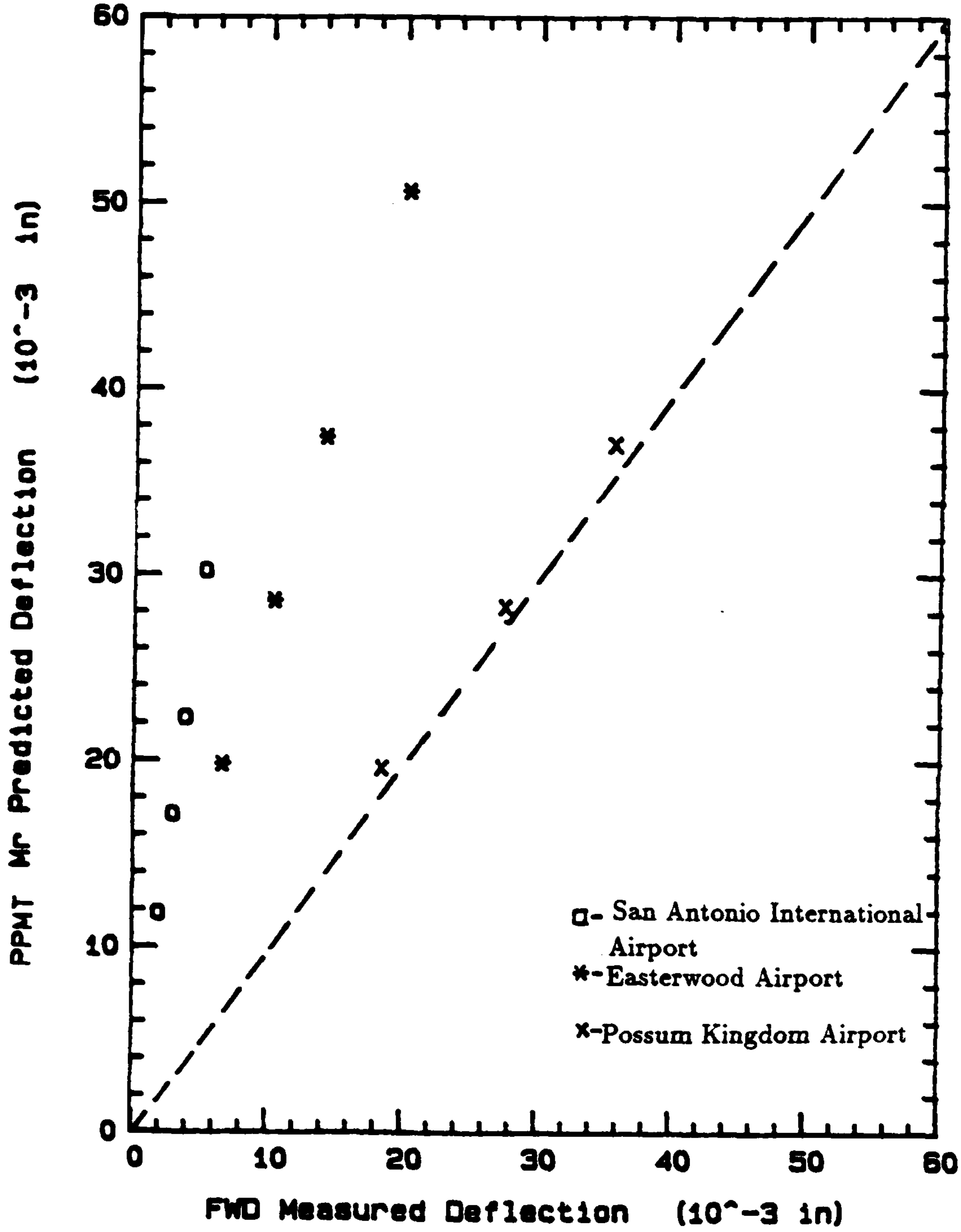

Fig 63 PPMT Deflection vs FWD Deflection From the First Unload Modulus, M_r

This procedure involves the following steps:

1. Upon completion of the CT test on a particular sample, resilient moduli values are tabulated for various number of cycles, deviator stresses σ_d and confining stresses σ_3.
2. The sum of the principal stresses (i.e. the first stress invariant Θ_T) is calculated.
3. Based on data collected from the airport operations the estimated number of annual departures is calculated.
4. For cohesive soils a plot of M_r versus σ_d is drawn (Figure 64) and for cohesionless soils a plot of log M_r versus log Θ_T is drawn (Figure 65).
5. For cohesive soils the following construction procedure is followed (Figure 64). Based on three estimated annual departure curves presented by Barker and Brabston (1975) the curve which most closely corresponds to the estimated annual departures is overlaid onto the M_r versus σ_d plot (Figure 64). The values of M_r found at the intersection of the two curves is the M_r used in design. For the airports used in this study these design M_r values are shown in Table 21. For cohesionless soils, a correction to Θ_T for overburden pressure is first made. Then the estimated annual departure curve is overlaid on to the plot of log M_r versus log Θ_T (Figure 65). The values of M_r found at the intersection of the two curves is the M_r used in design (Table 21).
6. The design M_r values are input into ILLIPAVE to predict deflections due to the FWD loads.

The ILLIPAVE outputs are summarized in Tables 22, 23 and 24. The resulting deflections are shown in Figure 66. They indicate that the predicted deflections are acceptably close to the measured deflections for the 2 clay subgrades, but not for the sand subgrade. The results for Easterwood airport indicate that the FWD deflections are 28 to 38 percent less than the predicted WES procedure deflections. The results from San Antonio airport indicate that the FWD deflections are about 50 percent less than the predicted WES procedure deflections. The results from Possum Kingdom airport indicate that the FWD deflections are about 4.85 times larger than the predicted WES procedure deflections.

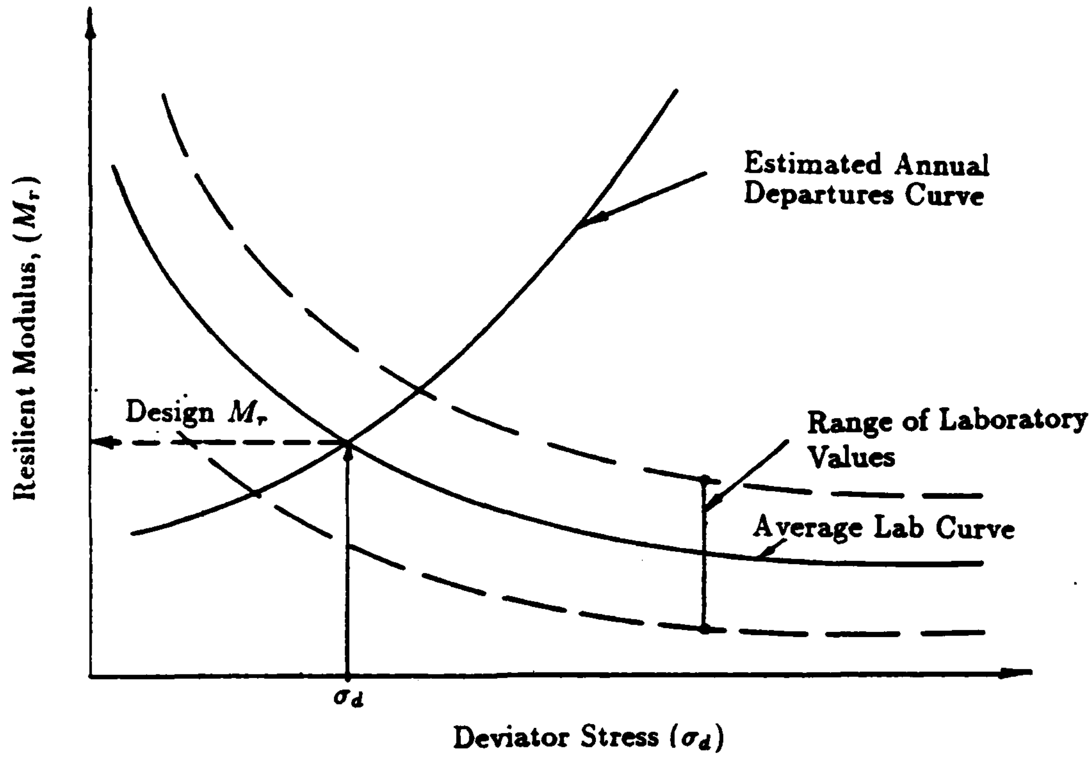

Fig. 64 Presentation of Results of CT Tests on Cohesive Soils

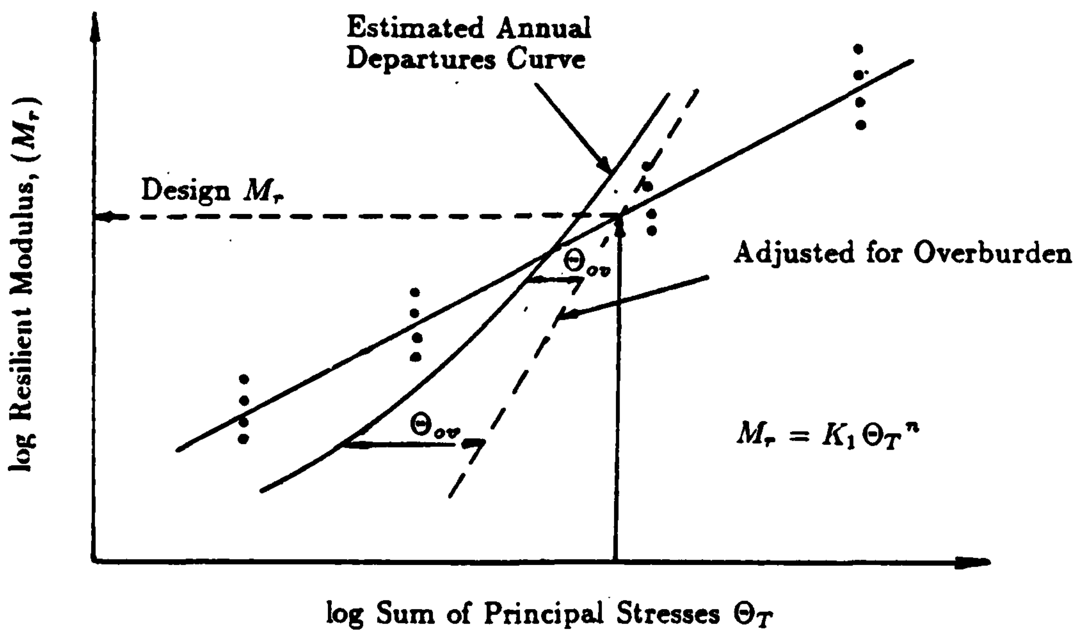

Fig. 65 Presentation of Results of CT Tests on Cohesionless Soils

Airport Site	Depth to Center of Layer (in)	Resilient[1] Modulus M_r (psi)	Principal[1] Stress σ_1 (psi)	Vert.[1] Strain ϵ_v %	Mean Total[1] Stress Θ^2_{ave} (psi)
Easterwood	C	3,000,000	NA[3]	NA[3]	NA[3]
	15	4,300	4.5	NA[3]	3.5
	30	7,000	8.6	NA[3]	4.9
	108	11,700	14.5	NA[3]	6.8
San Antonio International	C	3,000,000	NA[3]	NA[3]	NA[3]
	AC	400,000	NA[3]	NA[3]	NA[3]
	48	14,100	16.8	NA[3]	6.4
	126	20,000	22.0	NA[3]	12.0
Possum Kingdom	AC	400,000	NA[3]	NA[3]	NA[3]
	Base	200,000	NA[3]	NA[3]	NA[3]
	18	200,000	51.8	NA[3]	18.1
	45	200,000	23.5	NA[3]	9.9
	120	200,000	74.2	NA[3]	30.3

1. Design values determined using the WES approach for CT tests.
2. $\Theta_{ave} = 1/3(\sigma_1 + 2\sigma_3)$ where : σ_1 and σ_3 are from the CT tests.
3. NA = Not Applicable.

Note : AC is Asphalt Concrete, C is Concrete and Base is Base Course.

Table 21.
Summary of CT-WES Resilient Moduli for input.

Depth to Center of Layer (in)	FWD Load (lbs)	Resilient[1] Modulus M_r (psi)	Mean Radial[2] Stress σ_r (psi)	Vert.[2] Strain ϵ_v (%)	Mean Total[2] Stress Θ^3_{ave} (psi)	Predicted Deflection (in)	Measured Deflection (in)
15	9,000	4,300	3.0	0.0223	2.9	0.0106	0.066
30		7,000	5.5	0.0104	4.8		
108		11,700	18.0	0.0033	14.8		
15	13,000	4,300	3.4	0.0321	3.3	0.0153	0.0104
30		7,000	5.7	0.0150	5.1		
108		11,700	18.2	0.0048	15.2		
15	17,000	4,300	3.6	0.0420	3.8	0.0200	0.0141
30		7,000	6.0	0.0196	5.4		
108		11,700	18.5	0.0063	15.4		
15	23,000	4,300	4.1	0.0569	4.4	0.0271	0.0201
30		7,000	6.4	0.0266	6.0		
108		11,700	18.9	0.0086	15.9		

1. Input design values determined using the WES approach for CT tests.
2. Values calculated by ILLIPAVE.
3. $\Theta_{ave} = 1/3(\sigma_r + \sigma_z + \sigma_\Theta)$ with σ_r, σ_z and σ_Θ from ILLIPAVE

Table 22.
Easterwood Airport
ILLIPAVE Moduli Output for *WES Resilient Moduli*

Depth to Center of Layer (in)	FWD Load (lbs)	Resilient[1] Modulus M_r (psi)	Mean Radial[2] Stress σ_r (psi)	Vert.[2] Strain ϵ_v (%)	Mean Total[2] Stress Θ^3_{ave} (psi)	Predicted Deflection (in)	Measured Deflection (in)
48	9,000	14,100	4.1	0.0037	3.8	0.00387	0.00190
126		20,000	12.9	0.0019	11.7		
48	13,000	14,100	4.3	0.0053	4.1	0.00559	0.00295
126		20,000	13.1	0.0028	12.0		
48	17,000	14,100	4.5	0.0070	4.4	0.00732	0.00380
126		20,000	13.4	0.0036	12.3		
48	23,000	14,100	4.8	0.0939	4.8	0.00989	0.00525
126		20,000	13.7	0.0490	12.7		

1. Input design values determined using the WES approach for CT tests.
2. Values calculated by ILLIPAVE.
3. $\Theta_{ave} = 1/3(\sigma_r + \sigma_z + \sigma_\Theta)$ with σ_r, σ_z and σ_Θ from ILLIPAVE

Table 23.
San Antonio International Airport
ILLIPAVE Moduli Output for *WES Resilient Moduli*

Depth to Center of Layer (in)	FWD Load (lbs)	Resilient[1] Modulus M_r (psi)	Mean Radial[2] Stress σ_r (psi)	Vert.[2] Strain ϵ_v (%)	Mean Total[2] Stress Θ^3_{ave} (psi)	Predicted Deflection (in)	Measured Deflection (in)
18	9,000	200,000*	1.3	0.0208	3.4	0.00386	0.01847
45		200,000*	3.2	0.0041	3.8	(0.0121)	
120		200,000*	6.1	0.0015	6.7		
18	13,000	200,000*	1.4	0.0300	1.3	0.00558	0.02756
45		200,000*	3.4	0.0059	4.2	(0.0176)	
120		200,000*	6.3	0.0021	6.9		
18	17,000	200,000*	1.5	0.0392	1.4	0.00729	0.0356
45		200,000*	3.5	0.0078	4.5	(0.0229)	
120		200,000*	6.5	0.0028	7.3		

* The WES approach arbitrarily limits M_r to a maximum of 30,000* psi for cohesionless materials. The deflections in brackets come from using an M_r value equal to 30,000* psi.

1. Input design values determined using the WES approach for CT tests.
2. Values calculated by ILLIPAVE.
3. $\Theta_{ave} = 1/3(\sigma_r + \sigma_z + \sigma_\Theta)$ with σ_r, σ_z and σ_Θ from ILLIPAVE

Table 24.
Possum Kingdom Airport
ILLIPAVE Moduli Output for the WES *Resilient Modulus*

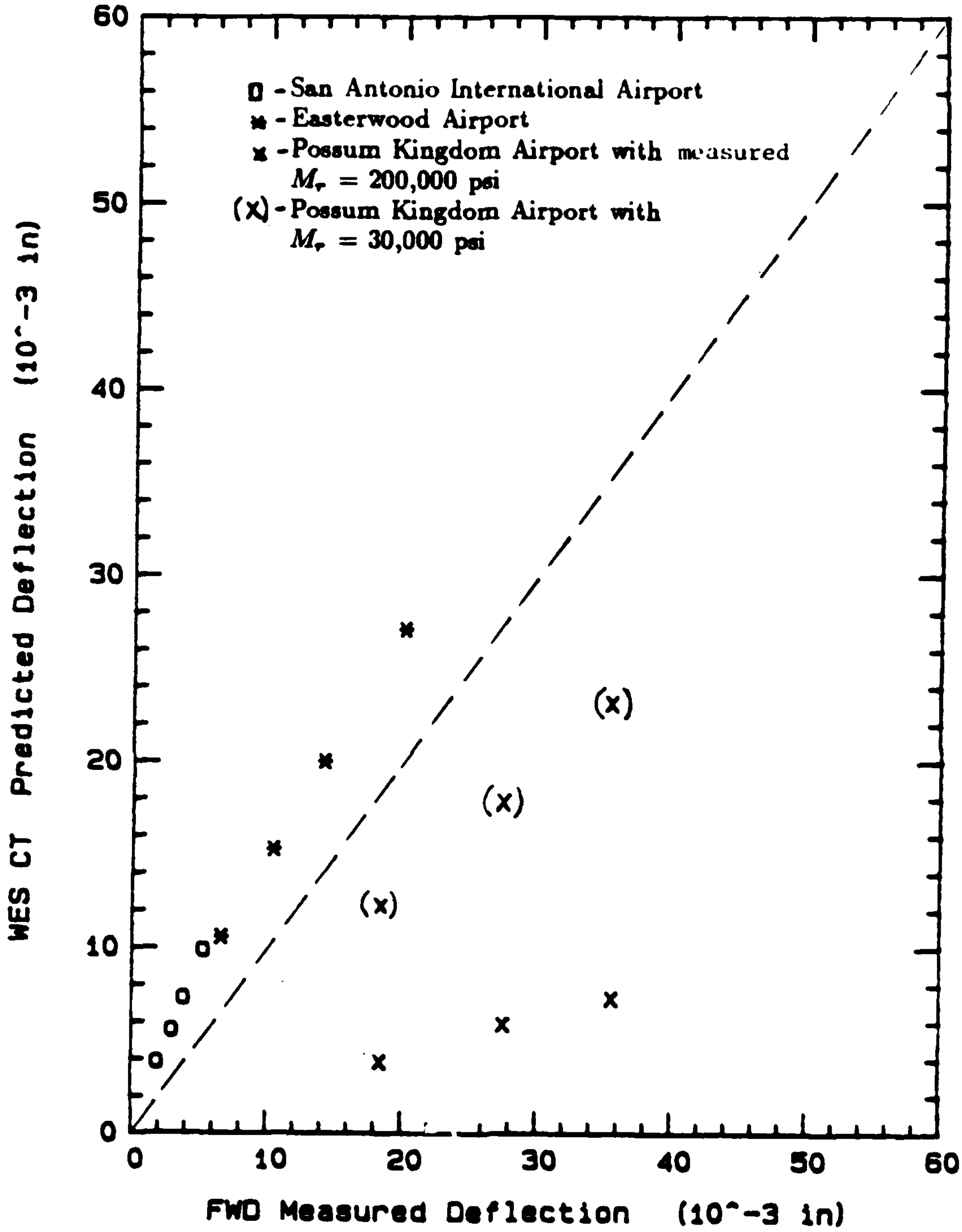

Fig. 66 CT Resilient Modulus from WES Procedure Predicted vs FWD Deflections

9. COMPARISON OF MODULI

9.1 Moduli Comparison Between PPMT, CT and FWD Tests

Moduli depend upon a number of variables including stress level and strain level. To make a useful comparison, moduli calculated over the same stress and strain levels must be compared. It was assumed that the more accurate the predicted deflections become, the closer the predicted stress and strain levels were to the actual stress and strain levels. As a result, the moduli for each PPMT and CT test which gave the closest predictions of the measured FWD deflections were selected for comparison purposes. The selected PPMT moduli were the revised strain level moduli in clay (Tables 13 and 14), and the stress level moduli in sand (Table 16). The selected CT test moduli were the ones obtained from the WES procedure (Table 21). The FWD test moduli backcalculated from the FWD tests, according to the ERES procedure described in section 7.4 (Table 8), were used in the comparisons.

These moduli are plotted in Figures 67, 68 and 69. Figure 67 is a plot of PPMT moduli versus CT moduli (Tables 13, 14, 16 and 21), where the results from the clay subgrades indicate that the PPMT moduli are equal to or larger than the CT moduli and the results from the sand subgrade indicate that the PPMT moduli are less than the CT moduli. Figure 68 is a plot of FWD moduli versus PPMT moduli (Tables 8 and 16), where the PPMT and FWD moduli for the clay subgrades indicate a relatively good correlation and the FWD moduli are greater than the PPMT moduli for the sand subgrade. Figure 69 is a plot of FWD moduli versus CT moduli (Tables 8 and 21), where the FWD moduli are larger than the CT moduli for the clay subgrade and the CT moduli are much larger than the FWD moduli for the sand subgrade.

9.2 Comparison with CBR Moduli and Plate Moduli

No CBR test or plate test was performed during this study. However an attempt was made at estimating moduli values that could have been obtained had those tests been run. This was done by using Table 7.4, p 236, of Yoder and Witczak (1975) which gives ranges of possible CBR and subgrade modulus k values on the basis of the classification of the soil in the USC system.

The subgrade modulus k is usually obtained from plate tests and is:

$$k = \frac{q}{s} \tag{34}$$

where q is the average pressure under the loaded area and s is the settlement. In elasticity the settlement s of a flexible plate (a tire

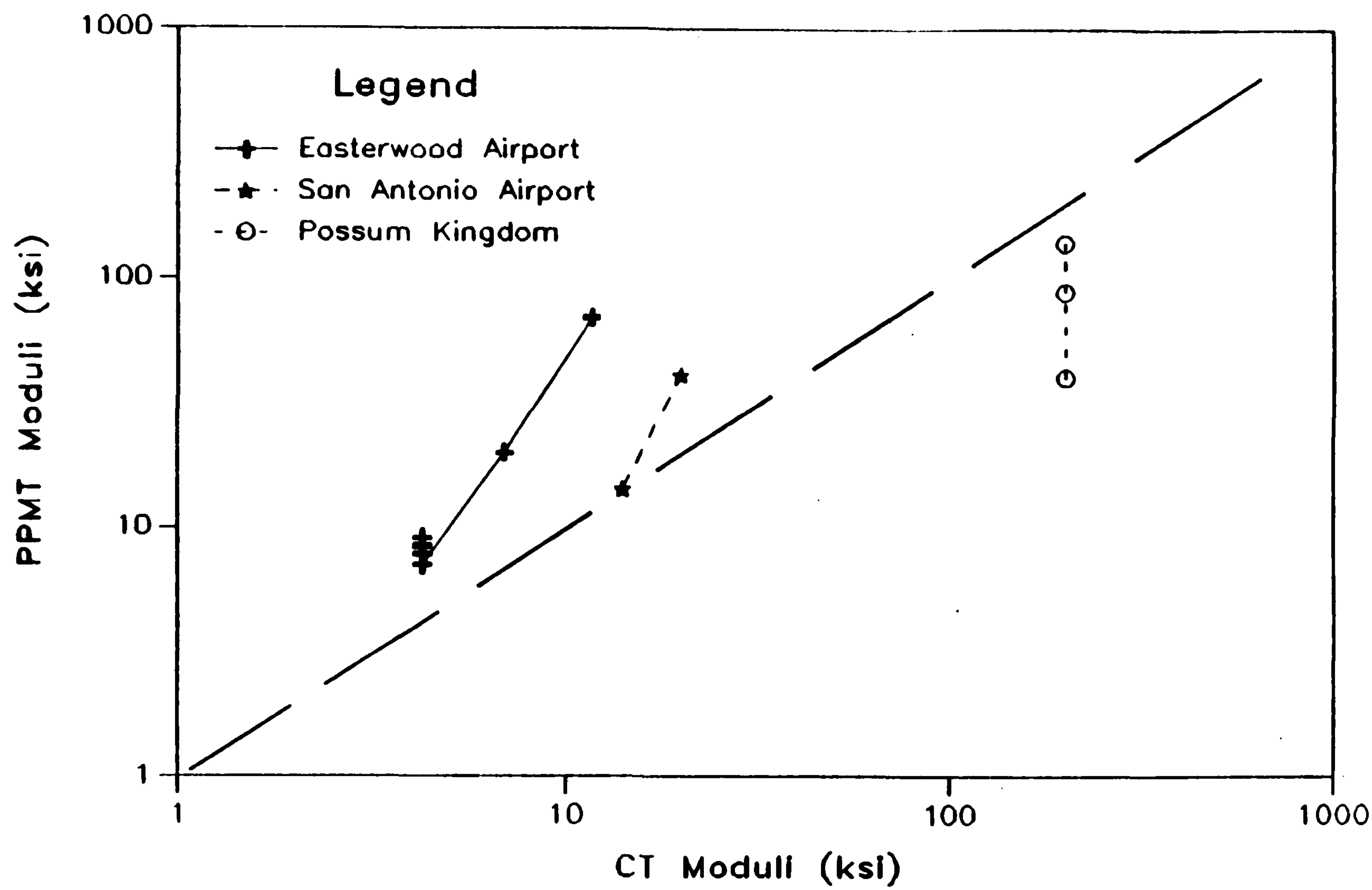

Fig. 67 PPMT Moduli vs CT Moduli

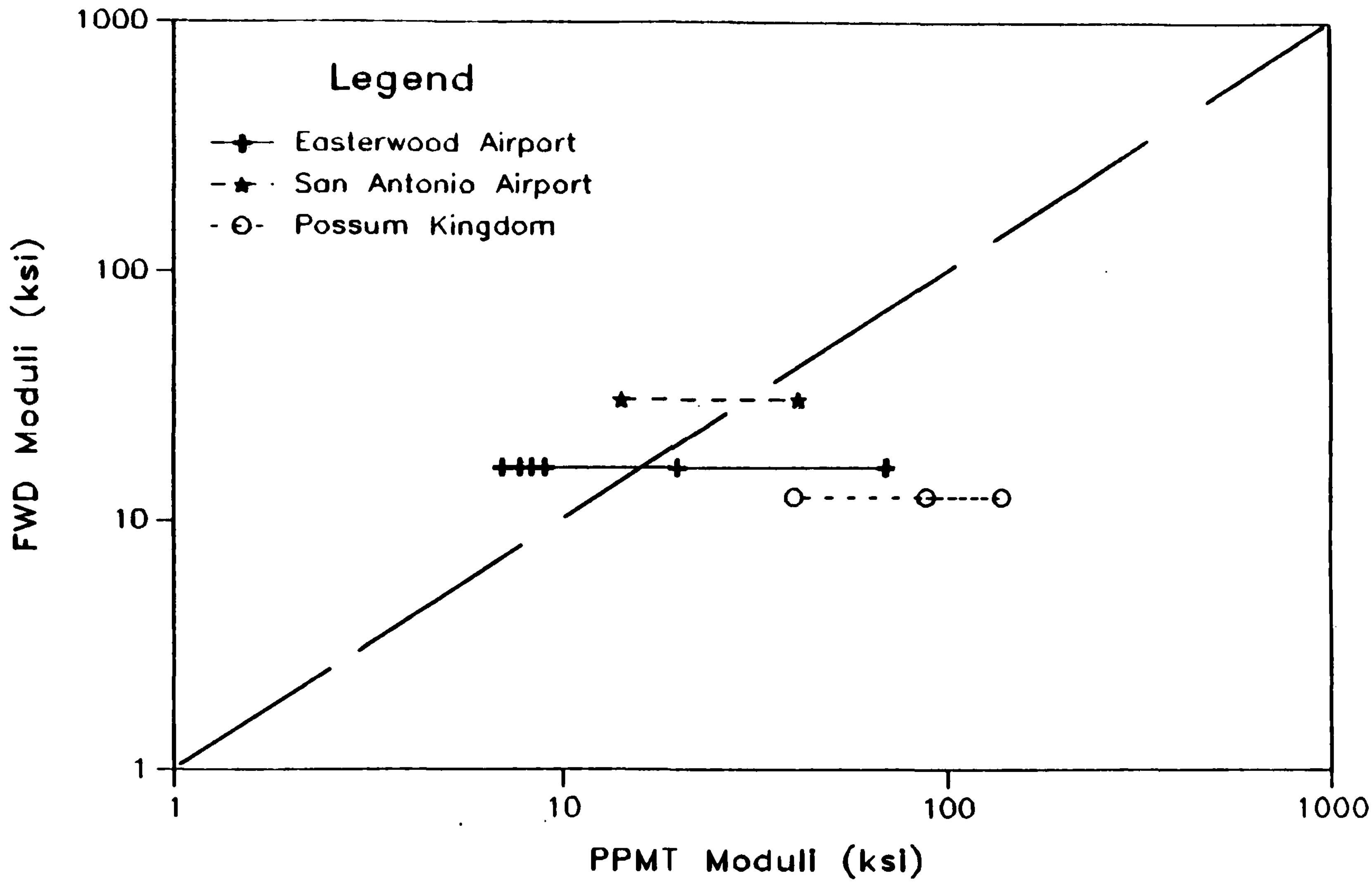

Fig. 68 PPMT Moduli vs FWD Moduli

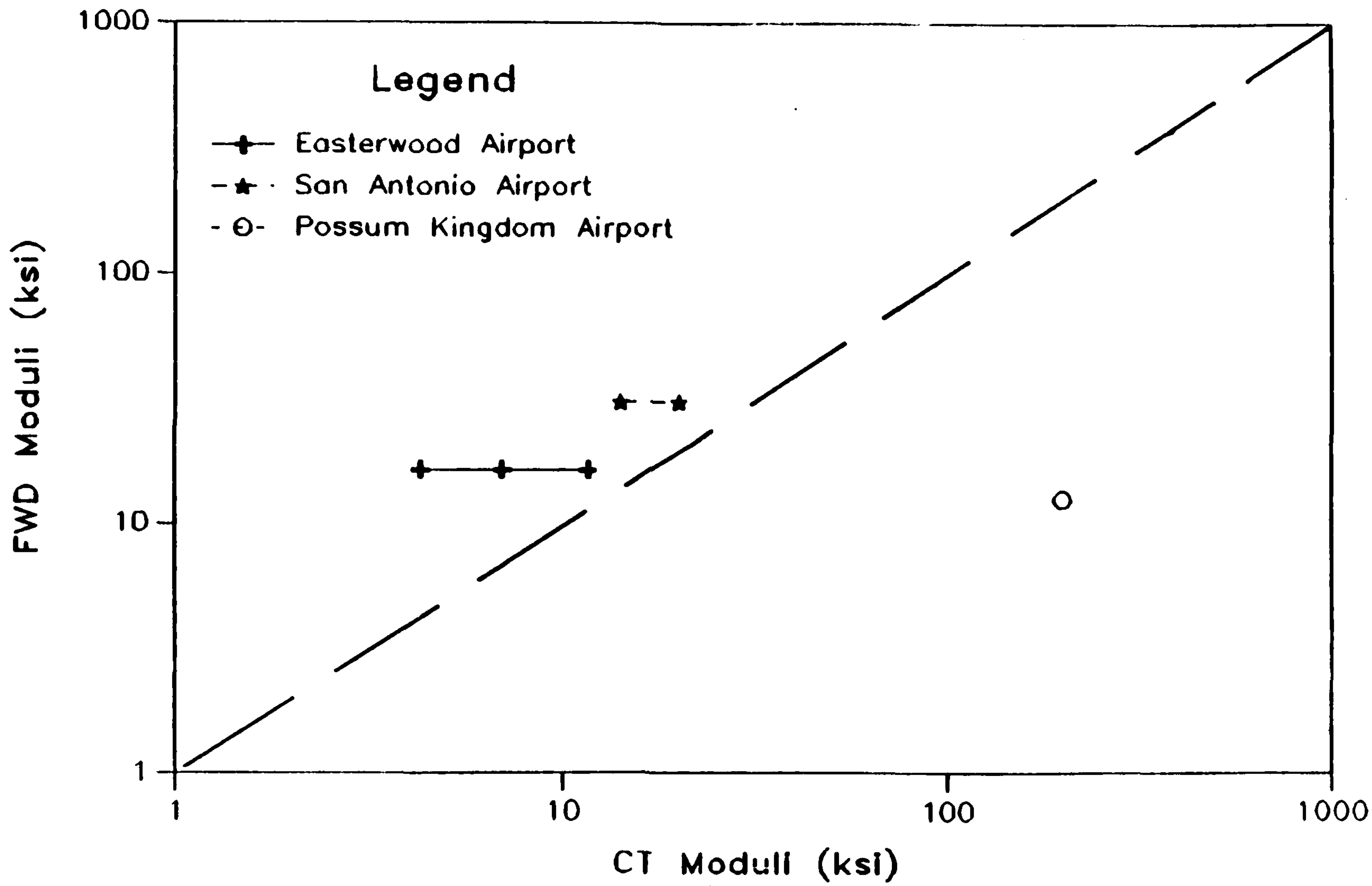

Fig. 69 FWD Moduli vs CT Moduli

is similar to a flexible plate) is given by:

$$s = (1-\nu^2)\ \frac{qD}{E} \tag{35}$$

where D is the plate diameter, E is Young's modulus and ν is Poisson's ratio. In order to obtain E from k a Poisson's ratio of 0.5 was assumed (undrained behavior) and a diameter of 1 foot was used to simulate a tire imprint:

$$E = kD\ (1-\nu^2) \tag{36}$$

The subgrade soils at Easterwood, San Antonio and Possum Kingdom airports were classified as CH, CL and SM respectively. For those classifications, Table 7.4, p 236 of Yoder and Witczak (1975) gave average k values of 75, 150, 250 pci (20, 41, 68 MN/m^3) respectively. These k values were used to generate the E values of Table 25.

The CBR is used to obtain moduli by simple correlations. The most commonly used correlation is:

$$E = 1500\ CBR \qquad \text{with E in psi} \tag{37}$$

Using the subgrade classifications, estimated mean CBR values were obtained from Table 7.4, p 236 of Yoder and Witczak (1975). These values were then used to obtain the moduli shown in Table 25.

As can be seen from Table 25, the moduli obtained from the estimated subgrade modulus k is consistently 5 to 20 times lower than the moduli measured in the field tests. The moduli obtained from the estimated CBR values is much closer to the measured moduli. The drawbacks of the field CBR and the plate test include destruction of the pavement and length of time involved.

Airport	Depth (in.)	PPMT[1] (psi)	CT[2] (psi)	FWD[3] (psi)	CBR[4] (psi)	Plate[5] Test (psi)
Easterwood	15	8070	4300	16433	6000	675
	30	19860	7000	16433	6000	675
	108	69450	11700	16433	6000	675
San Antonio	15	14200	-	30669	15000	1350
	30	40850	-	30669	15000	1350
	48	-	14100	30669	15000	1350
	126	-	20000	30669	15000	1350
Possum	15	88070	200000	12465	45000	2250
Kingdom	45	138356	200000	12465	45000	2250

[1] see Tables 13, 14 and 15 for details.

[2] see Table 21.

[3] Average values.Ranges can be found in Table 8.

[4] No CBR were performed in this study; the moduli values were obtained from 1500 CBR where CBR was taken from Table 7.4, p 236 of Yoder and Witczak (1975) knowing the soil classification.

[5] No Plate Tests were performed in this study; the moduli values were obtained from $E = kB(1- {}^{2})$ where k was taken from Table 7.4. p 236 of Yoder and Witczak (1975) knowing the soil classification.

Table 25

Comparison of Moduli

10. SUMMARY, CONCLUSIONS AND RECOMMENDATIONS

10.1 Summary

A relatively new tool, the pavement pressuremeter, was used at three airports in order to evaluate its usefulness in pavement design. The pavement pressuremeter test consists of hand drilling a 1.35 in. (3.43 cm) diameter hole through the pavement down to a depth of say 5 ft (1.52 m), then inserting in the open hole a 1.3 in. (3.30 cm) diameter, 9 in. (22.86 cm) long expandable cylinder; once in place the cylinder is inflated with water and the response of the soil surrounding the cylinder is monitored; the pressure against the soil and the relative increase in radius of the cylinder are recorded; this allows to obtain an in situ stress strain curve. By running the tests at various depths a series of stress-strain curves and therefore moduli can be obtained in the base course, subbase and subgrade. The pressuremeter results were compared to cyclic triaxial test results and Falling Weight Deflectometer test results. Of the three airports tested two of the airports had clay subgrades, one had a sand subgrade.

10.2 Conclusions

1. The effects on the modulus due to various stress levels, strain levels, creep and cycles can be obtained by performing unload-reload loops during the inflation of the cylinder. Soil moduli vary with the stress level, the strain level, the rate of loading or creep and the number of load cycles; the following models were selected to describe these variations;

Strain (Eq. 6)

$$1/E = a + b\varepsilon \tag{38}$$

Stress (Eq. 9)

$$E = K_2 \left(\frac{\theta}{p_a}\right)^{n} \tag{39}$$

Creep (Eq. 11)

$$E_1 = E_{t=t_o} \left(\frac{t}{t_o}\right)^{-n_{crp}} \tag{40}$$

Cycles (Eq. 13)

$$E_N = E_1 N^{-n_{cyc}} \tag{41}$$

2. During this study, pressuremeter testing procedures were developed

to obtain the parameters necessary to evaluate the above models (a, b, K_2, n, n_{crp}, n_{cyc}). The strain parameters a and b are obtained from a pressuremeter test where unload-reload loops are performed over various ranges of the hoop strain. The parameters K_2 and n are obtained from a pressuremeter test where unload-reload loops are performed at various stress levels. The creep or rate effect parameter n_{crp} is obtained from a pressuremeter test where the radial stress is held constant for five minutes. The cyclic parameter n_{cyc} is obtained from a pressuremeter test where 10 unload-reload cycles are performed between two stress levels. The parameters used to evaluate the modulus (a, b, K_2, n, n_{crp} and n_{cyc}) obtained with the pavement pressuremeter in this study compared favorably with values published in the literature. A pavement pressuremeter test was developed where in a single test all of the above parameters can be obtained. A manual describing how the data is reduced and a microcomputer program called AIRPRESS to reduce that data automatically, are presented in Appendix C.

3. The pavement pressuremeter results (PPMT) were compared with the results of cyclic triaxial (CT) tests and falling weight deflectometer (FWD) tests. For this study, 17 cyclic triaxial (CT) tests on samples recovered from the three airport subgrades were performed. At the same time, 32 pavement pressuremeter (PPMT) tests in the base courses and subgrades of the three airports were performed. In order to establish a ground truth, a total of 92 pavement locations were tested with the Falling Weight Deflectometer (FWD) at the three airports.
4. One comparison consisted of predicting the FWD deflection by inputing into the finite element program ILLIPAVE various moduli from the PPMT and CT results and comparing these deflections to the measured FWD deflections. The proper PPMT moduli were selected based on the four moduli models. The CT procedure established by the Waterways Experiment Station (WES) was used to select the proper resilient moduli. For the PPMT it was found that the best predictions are obtained when the strain level model is used for clay subgrades and the stress level model is used for sand subgrades (Figure 70). The predicted deflections by the proposed PPMT methods were within $\pm 35\%$ of the measured deflections (Figures 61 & 62). For the CT test the WES approach makes the distinction that moduli are based on the deviator stress level (σ_d) for clays (the deviator stress relates directly to the strain level) and on the confining stress (σ_3) for sands. The measured FWD deflections were predicted using the cyclic triaxial moduli selected by the WES procedure. The predicted deflections by the established CT method (Figure 66) were as good as the PPMT predictions (Figures 61 and 62) for the clay but not as good for the sand. This is due in part to the great difficulties experienced in retrieving the undisturbed sand samples and the problems associated with reconstructing the sand samples in the laboratory.
5. A comparison of moduli was also made. The moduli which predicted best the measured FWD deflections were selected for comparison purposes. The PPMT moduli from the strain level model for the clays and the stress level model for the sand were compared with the CT

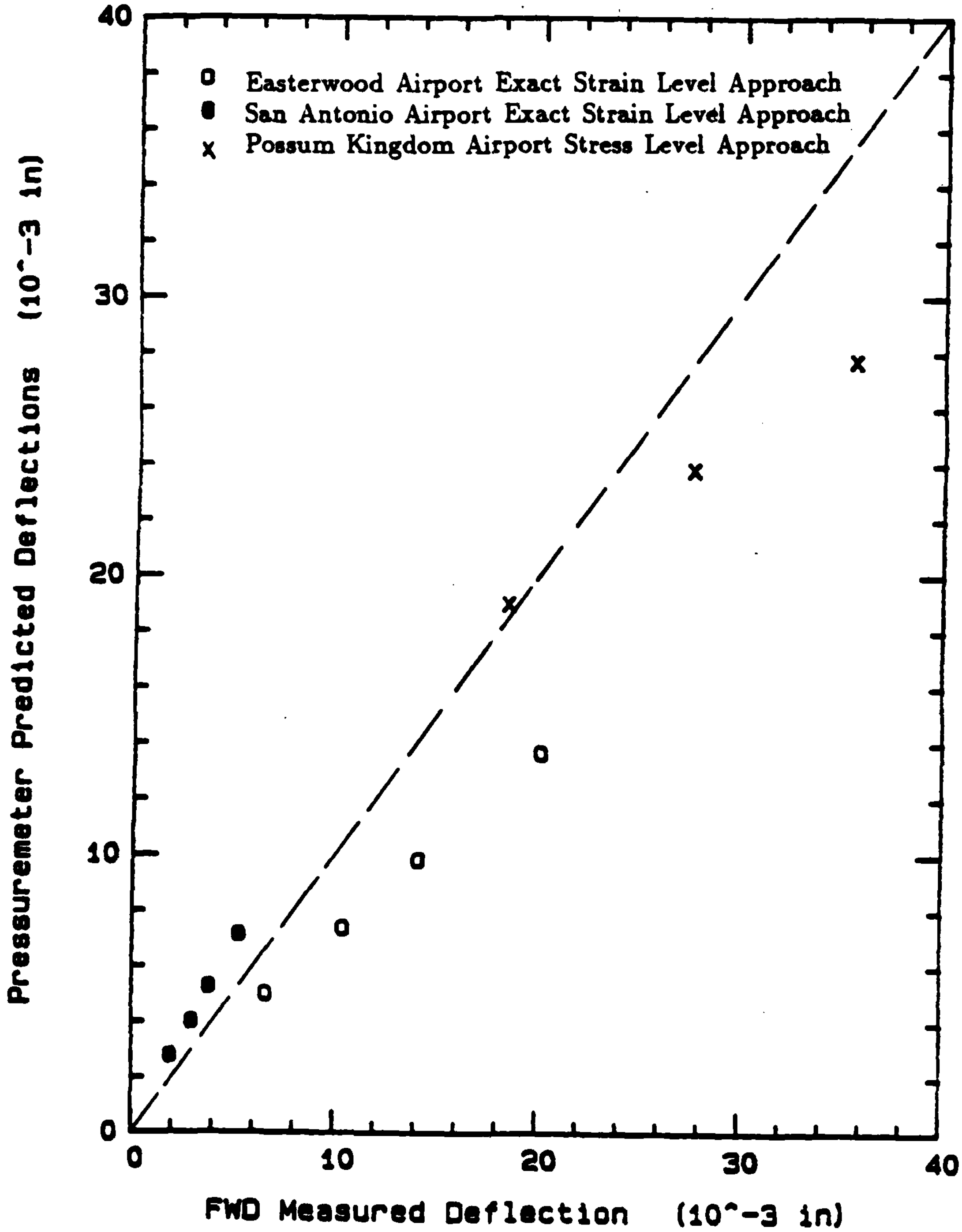

Fig. 70 PPMT Deflections vs FWD Deflections
Based on the Proposed Pressuremeter Approach for Each Subgrade

moduli from the deviator stress approach for the clays and the mean confining stress approach for the sand. The plot of PPMT moduli versus CT moduli (Figure 67) shows a much larger variation than the comparison of deflections. Moduli were also back-calculated from the FWD deflection results. In this case only one average FWD modulus is back-calculated for the entire subgrade, instead of several moduli versus depth for the CT and PPMT tests. The plot comparing PPMT and FWD moduli (Figure 68) shows a somewhat better correlation than the plot comparing CT and FWD moduli (Figure 69).

6. A comparison of the advantages and drawbacks of the three different pieces of equipment and corresponding design approaches is presented in Table 1. Overall this study shows that the pressuremeter is an economical and viable alternative to the cyclic triaxial test. Indeed the PPMT is less costly and simpler to use than the cyclic triaxial test and predicts the deflections of the FWD as well if not better than the cyclic triaxial test.

10.3 Recommendations

1. This study shows that the PPMT is a tool which can be used advantageously for the prediction of pavement deflections and is ready to be used progressively for the design of new pavement, the extension of existing pavements, the evaluation of existing pavements and the design of pavement overlays. However only three airports were tested and more data must be collected at other airports across the U. S. Comparison of predicted deflections with measured deflections under full size aircraft would be particularly useful and would allow to further improve the method.
2. Since the Falling Weight Deflectometer test is faster than the PPMT test, the FWD can be used to survey large areas in little time and help locate the zones of weakness. Within those zones the pavement pressuremeter can already:

   a. provide a profile of the moduli and moduli model parameters so that the proper modulus under any loading configuration can be obtained,
   b. provide information on rutting (moduli as a function of cycles) and creep (moduli as a function of rate or duration of loading),
   c. give, through the coring process, an exact thickness of the layers involved,
   d. provide small cores of the surface course for moduli and strength determination, and
   e. provide disturbed samples of the base course, subbase and subgrade for index properties determination (water content, grain size, liquid, plastic and shrinkage limit, classification).

3. The pavement pressuremeter also has some other potential uses provided further research takes place;

   a. it could be used to measure the effect of moisture variation on the modulus values. This would be done by running the pavement pressuremeter test during each season of the year at various airports.

b. it could give a measure of the high horizontal stress locked in the pavement due to compaction and repeated loading; these horizontal residual stresses are considered to be very important and may control future behavior of the pavement,
c. it could give a means of load rating light pavements through the use of the pressuremeter limit pressure, and
d. it could be used to test the asphalt or the concrete, thereby eliminating the need for testing concrete specimens.

4. There is a need also to:

   a. develop a complete manual for the use of the pavement pressuremeter equipment,
   b. develop a detailed manual for the use of the data reduction microcomputer program, and
   c. organize one or more seminars to present the results of this study and describe the usefulness of the pavement pressuremeter.

5. From a more general standpoint, there is a need to perform a sensitivity analysis to document the effect of modulus variation in various design and evaluation methods.

REFERENCES

Baguelin, F., Jezequel, J.F., & Shields, D.H. 1978, "The Pressuremeter and Foundation Engineering," Trans. Tech. Publ., Clausthal, Germany.

Barenberg, E., 1972, "ILLIPAVE: A Finite Element Analysis of Pavement Stresses," Civil Engineering Department, University of Illinois at Urbana-Champaign, Champaign-Urbana, Ill.

Barker, W.R. & Brabston, W.N., 1975, "Development of a Structural Design Procedure for Flexible Airport Pavements," FAA-RD-74-199, Federal Aviation Administration, Washington, D.C.

Briaud, J.-L., 1979, "The Pressuremeter: Application to Pavement Design," Ph.D. Dissertation, Department of Civil Engineering, University of Ottawa, Ontario, Canada.

Briaud, J.-L. & Garland, E., 1985, "Loading Rate Method for Pile Response in Clay," Jour. of Geotechnical Engineering, ASCE, Vol. III, No. 3, pp. 319-335.

Briaud, J.-L., Lytton, R.L. & Hung, J.T., 1982, "Using a Pressuremeter for Pavement Design and Evaluation," Int. Sym. on the Bearing Capacity of Roads and Airfields, Civil Aviation Admin., Oslo, The Norwegian Institute of Tech., Trondheim, Norway.

Briaud, J.-L. & Shields, D.H., 1979a, "A Special Pressure Meter and Pressure Meter Test for Pavement Evaluation and Design," ASTM Geotechnical Testing Journal, Vol. 2, No. 3, pp. 143-151.

Briaud, J.-L. & Shields, D.H., 1979b, "Use of the Pressuremeter Test to Predict Modulus and Strength of Pavement Layers," Tran. Res. Rec. 810 Layered Pavement Systems, TRB 810, pp. 33-42.

Briaud, J.-L., Terry, T.A., Cosentino, P.J., Tucker, L.M. & Lytton, R.L., 1986, "Influence of Stress, Strain, Creep and Cycles on Moduli from Preboring and Driven Pressuremeters," Research Report 7035-1 to the Federal Aviation Administration, Department of Civil Engineering, Texas A&M University, College Station, Texas.

Claessen, A.E.M., Edwards, J.M., Sommer, P. & Uge, P., 1977, "Asphalt Pavements Design: The Shell Method," Proc. 4th Int. Conf. on the Structural Design of Asphalt Pavements, Vol. 1, pp 39-74, Univ. of Michigan, Ann Arbor, Michigan.

Duncan, J.M. & Chang, C.-Y., 1970, "Nonlinear Analysis of Stress and Strain in Soils," Jour. of Soil Mech. and Found. Division, ASCE, Vol. 96, No. SM5, pp 1629-1653.

Idriss, I.M., Dobry, R. & Sings, R.D., 1978, "Non-linear Behavior of Soft Clays During Cyclic Loading," Jour. of Geotech. Engineering Division, ASCE, Vol. 104, No. GT12, pp 1427-1448.

Janbu, Nilmar, 1963, "Soil Compressibility as Determined by Oedometer and Triaxial Tests," European Conf. on Soil Mech. and Found. Eng., ASCE, Weisbaden, Germany, Vol. 1, pp 123-156.

Kondner, R.L., 1963, "Hyperbolic Stress-Strain Response: Cohesive Soils," J. of Soil Mech. and Fdn. Eng., ASCE, 89, No. SM1, Proc. Paper 3429, pp 115-143.

Lacasse, S., 1979, "Safety of Gravity Platform: Effect of Load Duration on Undrained Behavior of Clay and Sand - Literature Survey," Internal Report 40007-1, Norwegian Geotechnical Institute, Norway.

Low, P.F., 1976, "Physical Chemistry of Clay Water Interaction," Advances in Agronomy, Vol. 13, Academic Press, New York, N.Y., pp 269-327.

McLeod, N.W., 1947, "Airport Runway Evaluation in Canada," International Rep. Trans. Canada, Ottawa, Ontario, Canada.

Mitchell, J.K., 1976, "Fundamentals of Soil Behavior," John Wiley & Sons, Inc., New York, N.Y.

Odemark, N., 1949, "Undersoking Av Elasticitetsegenskaperna Hos Olika Jordarter Samt Teom for Berakning Av Bellaggningar Enligt Elasticitetstreorin," Statens Vaginstsitut Report, Meddelande 77, Stockholm.

Pike, R., 1981, "A Preliminary Study of Rate of Loading Effects on Axial Pile Capacities," Report to the Union Oil Co. of Calif., Science and Technology Div., California.

Riggins, M., 1981, "Viscoelastic Characteristics of Marine Sediment in Large Scale Simple Shear," Ph.D. Dissertation, Department of Civil Engineering, Texas A&M University.

Roctest, Inc., 1985, "The TEXAM Pressuremeter Instruction Manual," Roctest, Inc., Plattsburgh, N.Y.

Smith, R.E. & Lytton, R.L., 1983, "Synthesis Study of Non- destructive Testing Devices for Use in Overlay Thickness Design of Flexible Pavements," Rep. No. FHWA/RD-83/097, Eres Inc., Champaign-Urbana, Ill.

Smith, R.E. & Lytton, R.L., 1985, "Operating Characteristics of and User Satisfaction with Commercially Available NDT Equipment," 64th Annual TRB, Washington, D.C.

Transport Canada, 1976, "Pavement Design and Rehabilitation," Manual AK 68-12, Ottawa, Ontario, Canada.

Whitman, R.V., 1970, "The Response of Soils to Dynamic Loadings," Rep.

26, Final Report, U.S. Army Engineers, Waterways Experiment Station, Vicksburg, Miss.

Yoder, E.J. & Witczak, M.W., 1975 "Principles of Pavement Design," Second Edition, John Wiley & Sons, Inc..

APPENDIX A

Pavement Pressuremeter Test Curves

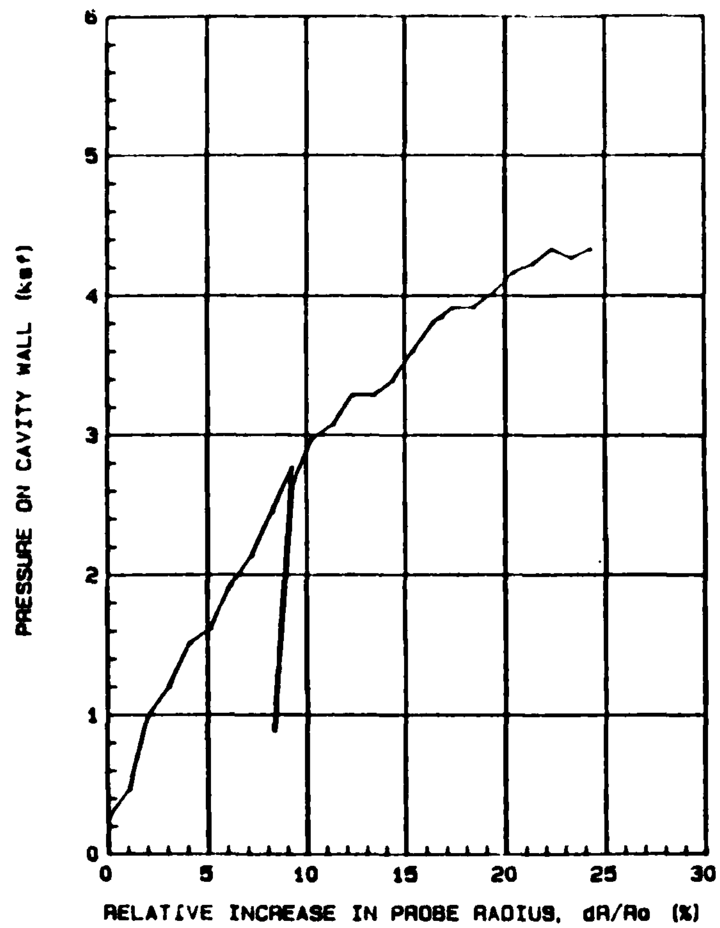

EASTERWOOD AIRPORT STANDARD (EA-1) PPMT TEST 9.5" - 18" DEPTH

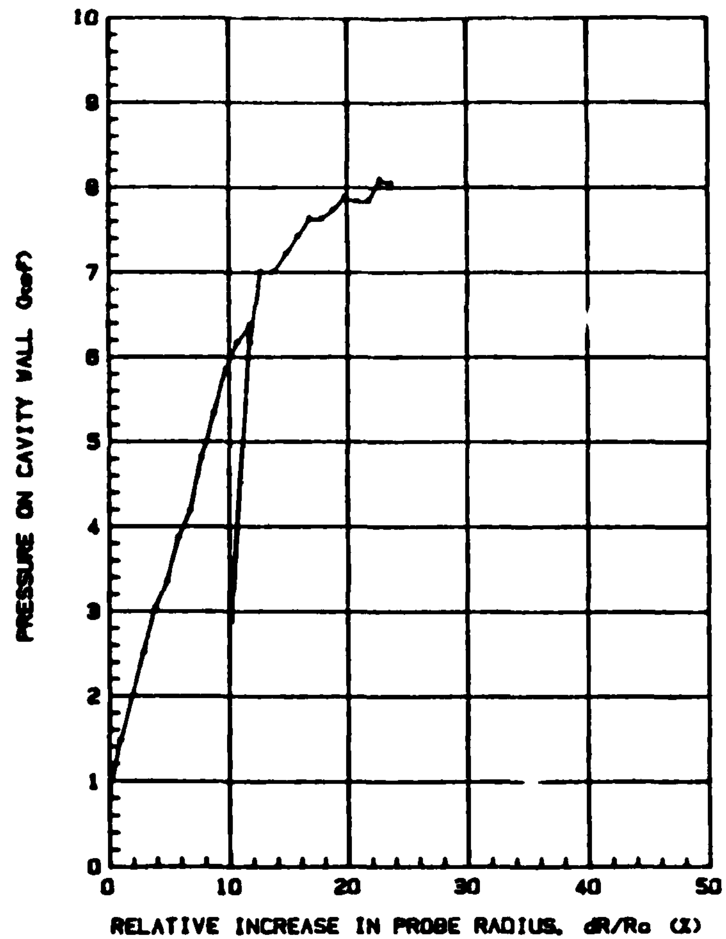

EASTERWOOD AIRPORT (EA-1) 25"-DEPTH STANDARD TEST

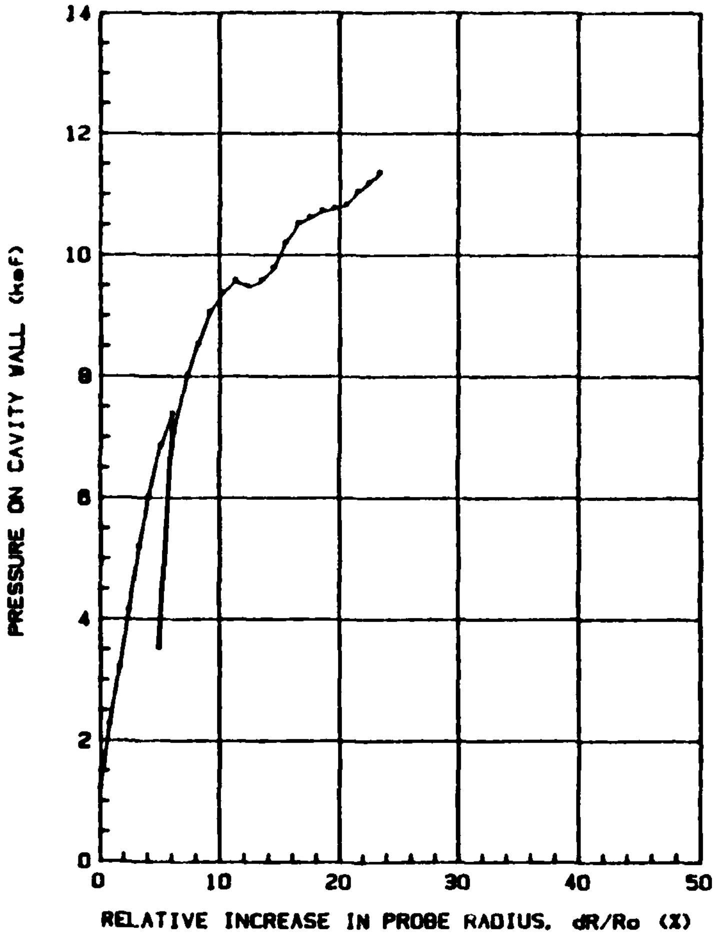

EASTERWOOD AIRPORT (EA-1) 37"-DEPTH STANDARD TEST

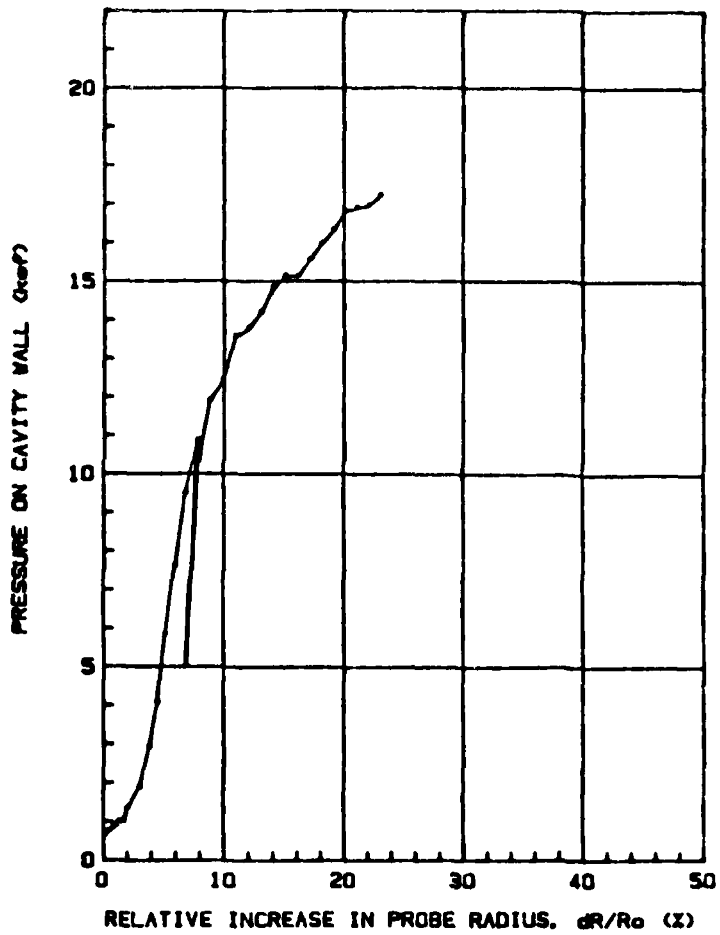

EASTERWOOD AIRPORT (EA-1) 61"-DEPTH STANDARD TEST

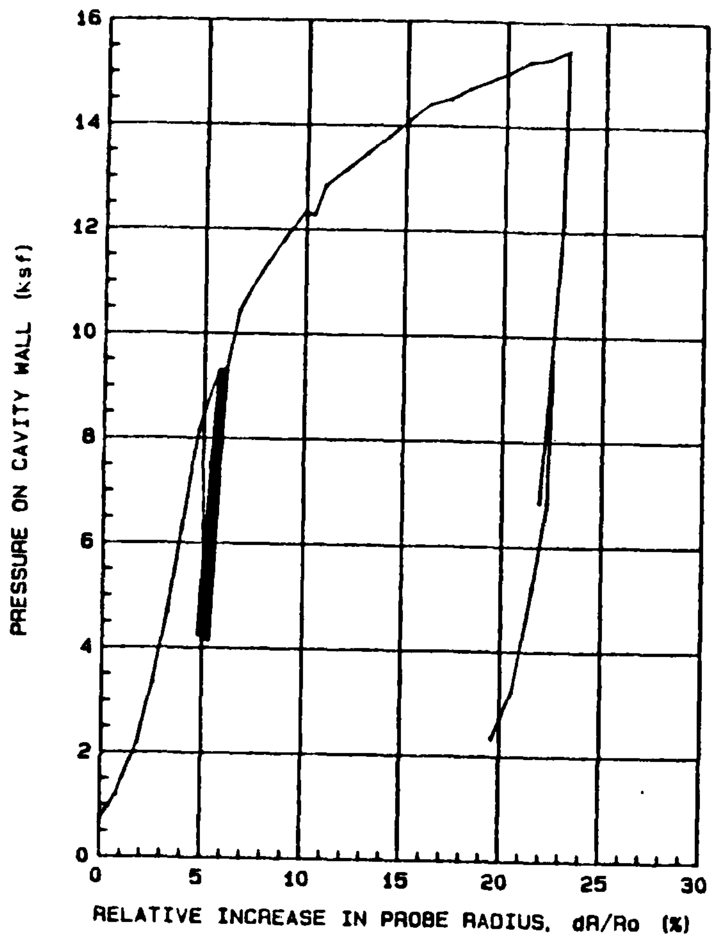

EASTERWOOD AIRPORT (EA-1) 85"-DEPTH PPMT STANDARD AIRPORT TEST

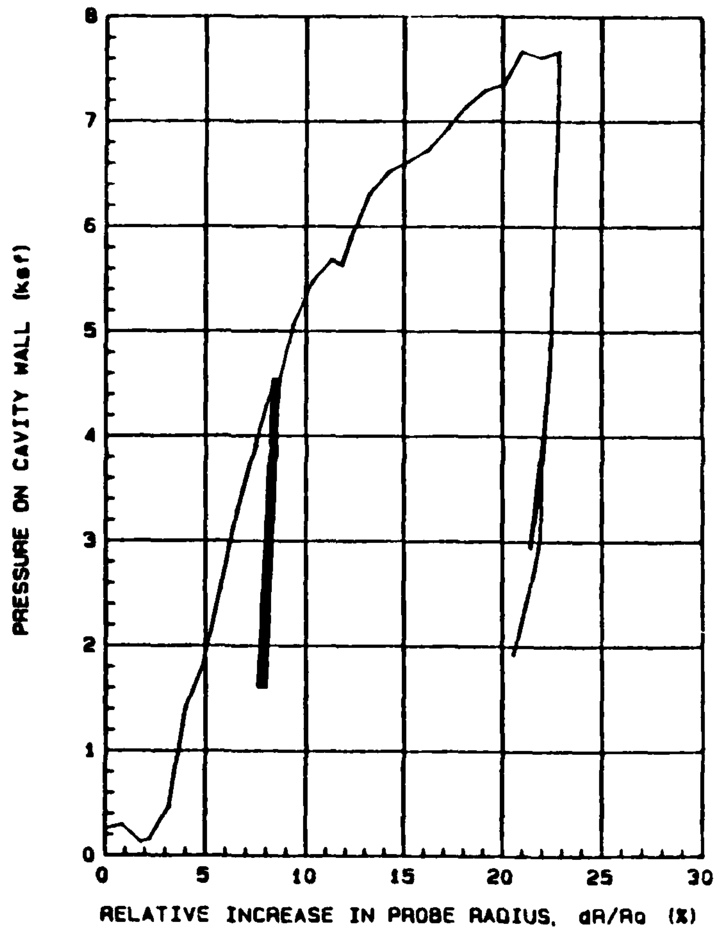

EASTERWOOD AIRPORT (EA-2) 27"-DEPTH PPMT STANDARD AIRPORT TEST

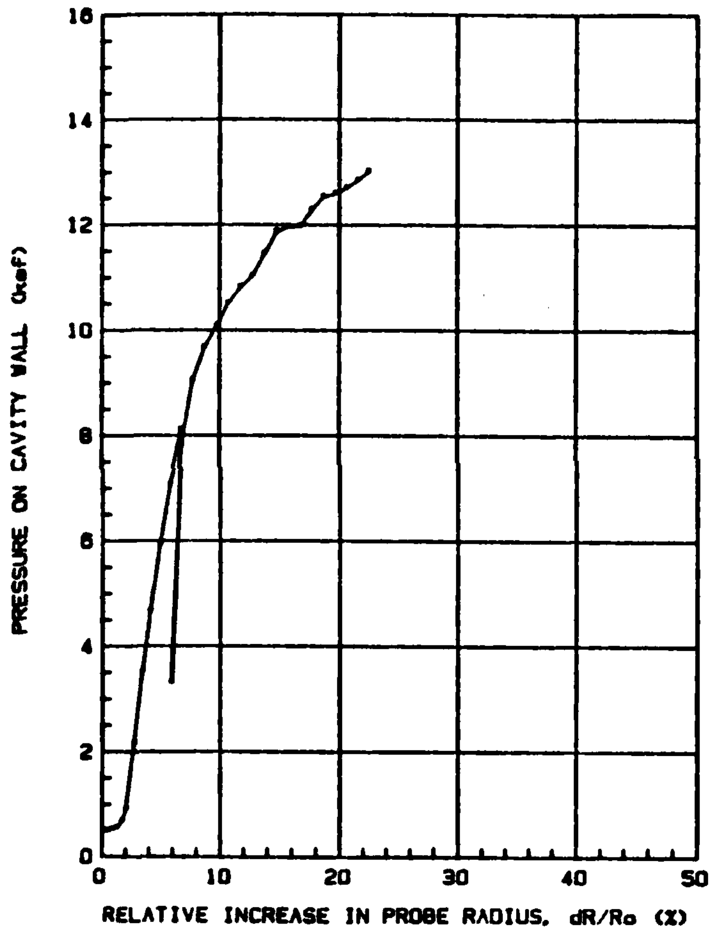

EASTERWOOD AIRPORT (EA-2) 39"-DEPTH STANDARD TEST

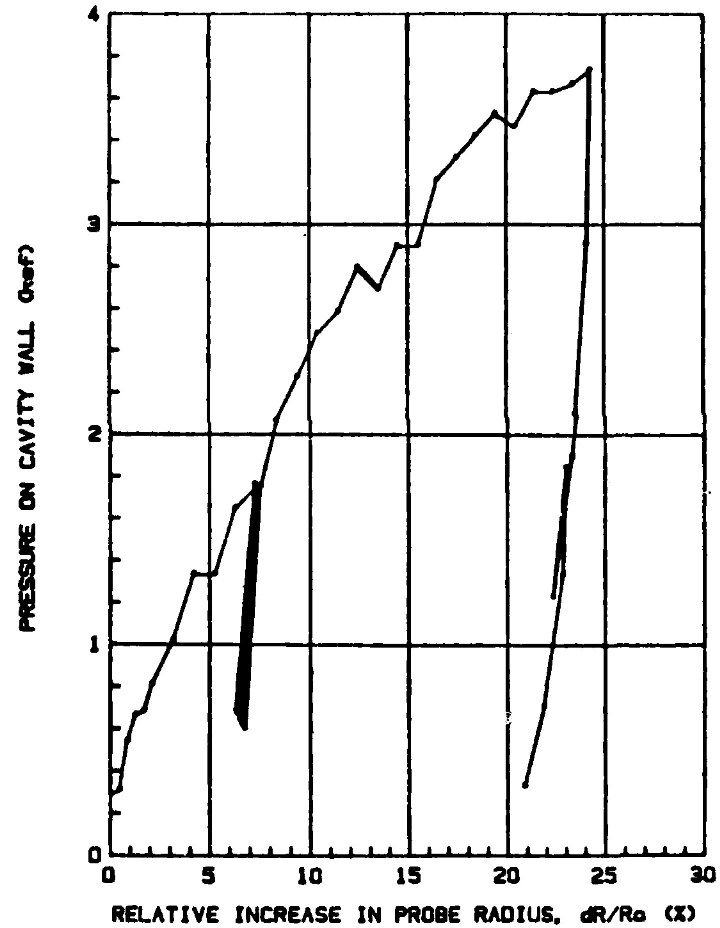

EASTERWOOD AIRPORT (EA-3) 13"-DEPTH PPMT STANDARD AIRPORT TEST

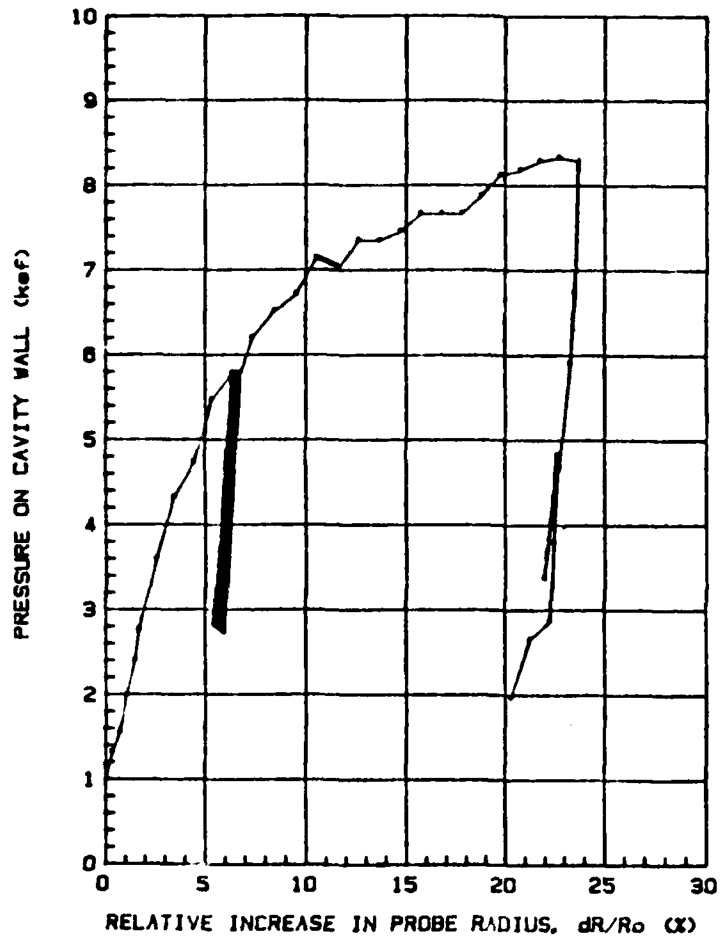

EASTERWOOD AIRPORT (EA-3) 20"-DEPTH PPMT STANDARD AIRPORT TEST

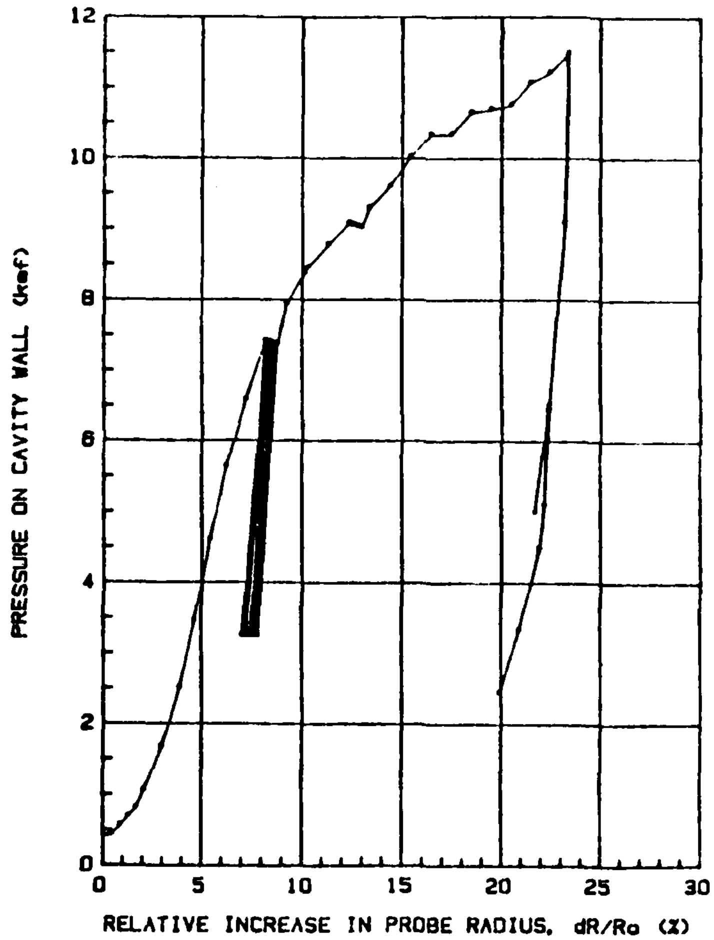

EASTERWOOD AIRPORT (EA-3) 38"-DEPTH PPMT STANDARD AIRPORT TEST

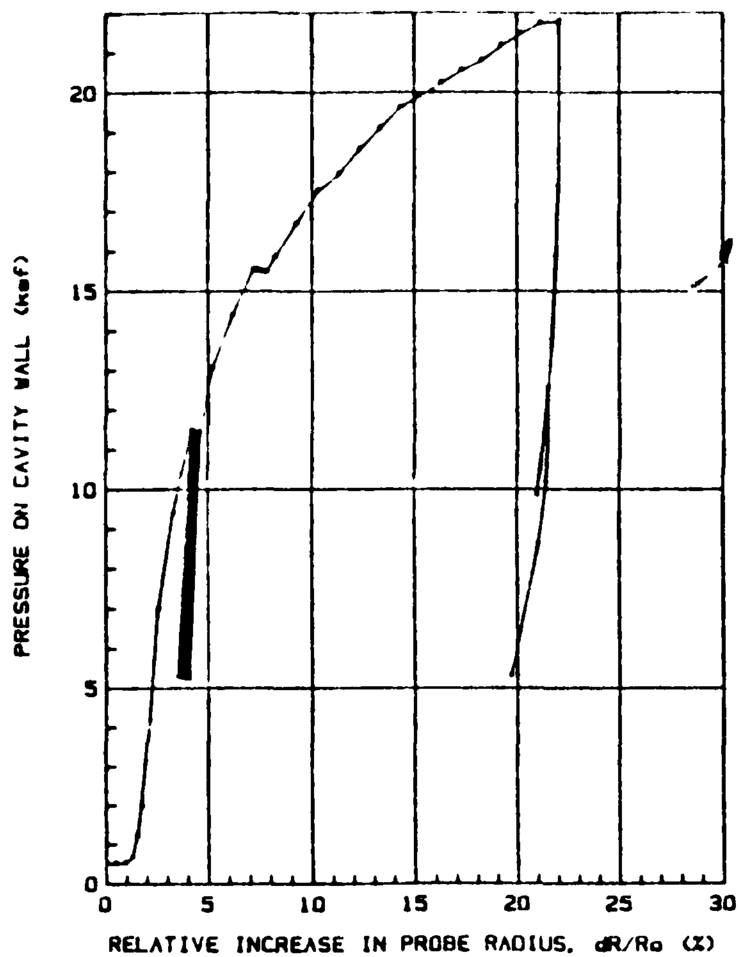

EASTERWOOD AIRPORT (EA-3) 62"-DEPTH PPMT STANDARD AIRPORT TEST

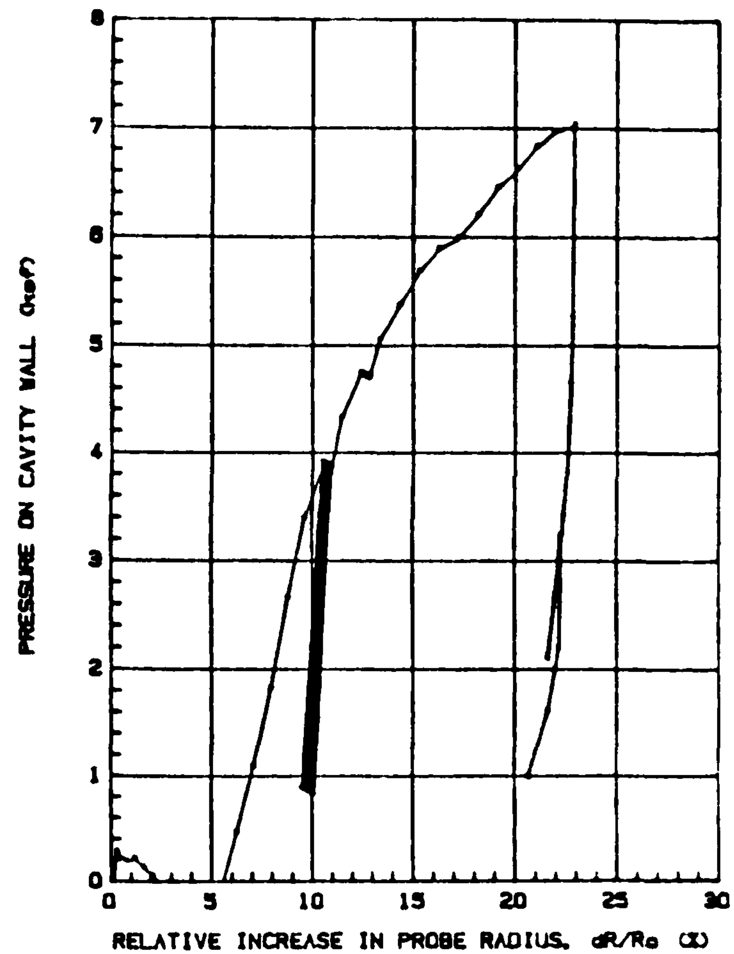

EASTERWOOD AIRPORT (EA-4) 13"-DEPTH CPMT SPECIAL AIRPORT TEST

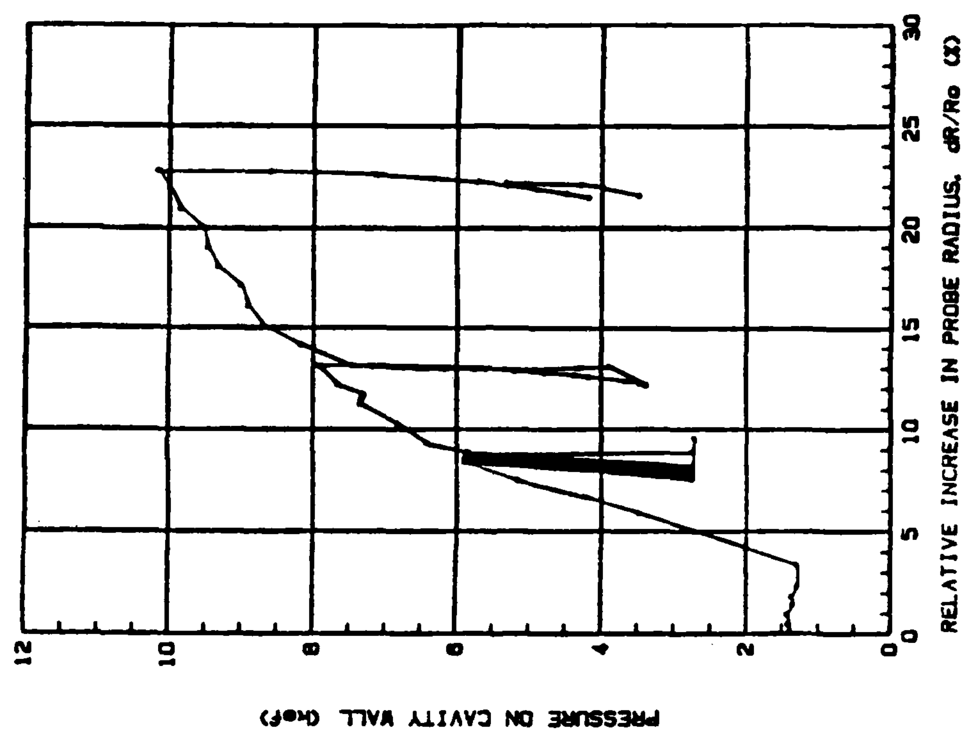

EASTERWOOD AIRPORT (EA-4) 29"-DEPTH CPMT SPECIAL AIRPORT TEST

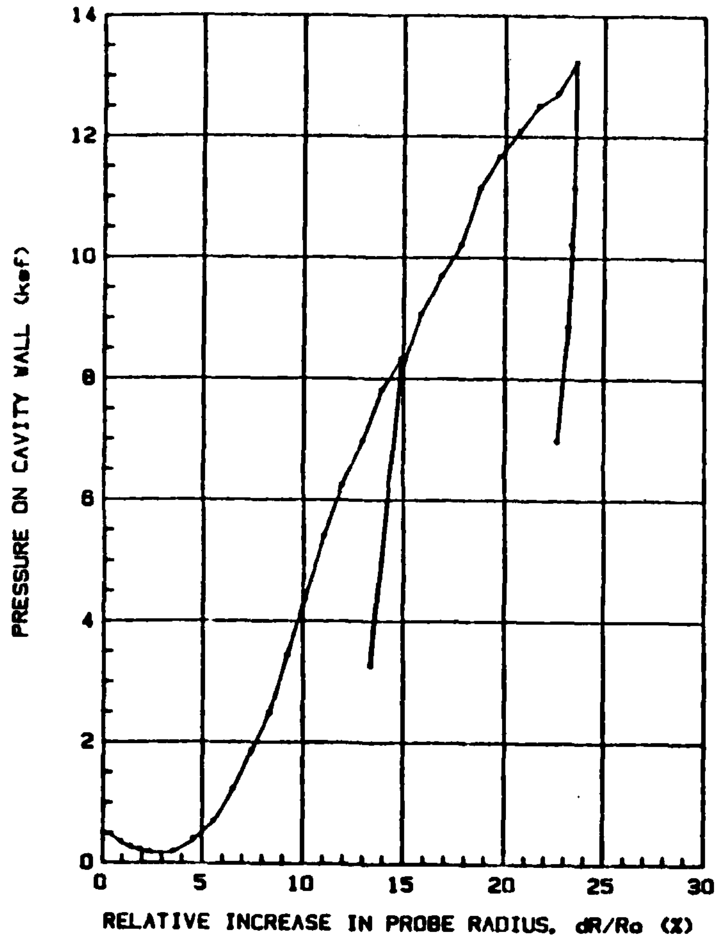

SAN ANTONIO AIRPORT (SA-1) 26"-DEPTH STANDARD PMT TEST

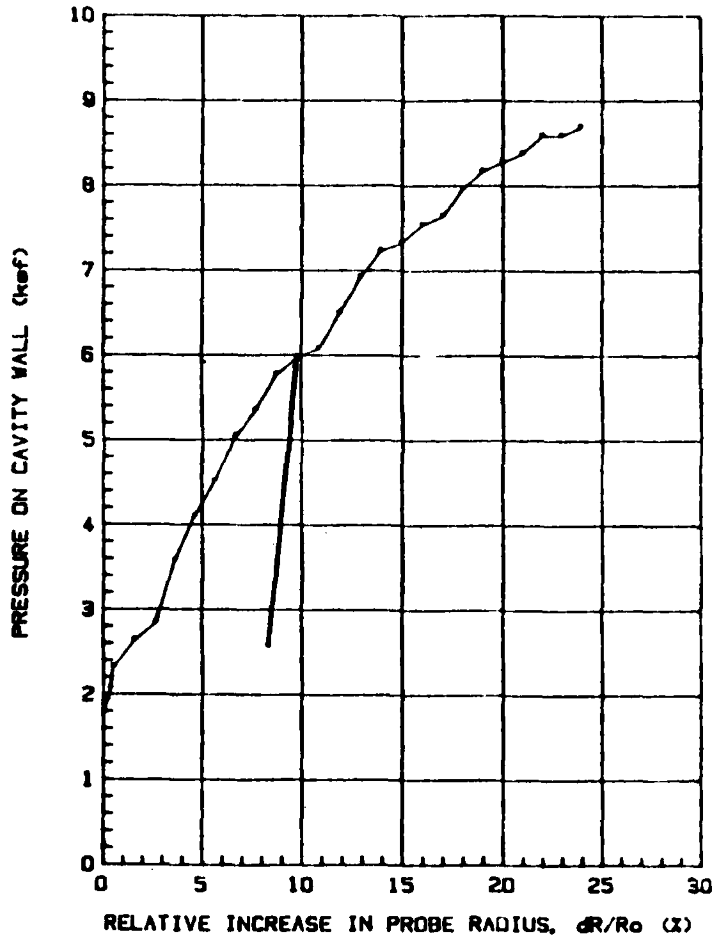

SAN ANTONIO AIRPORT (SA-1) 39"-DEPTH STANDARD PMT TEST

179

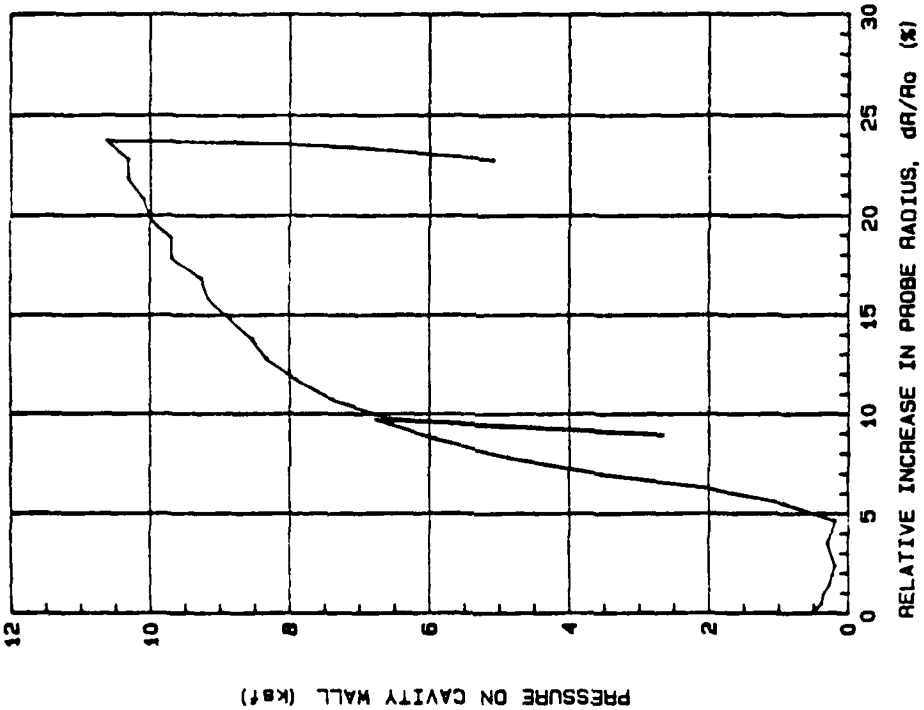

SAN ANTONIO AIRPORT (SA-1) 50'-DEPTH STANDARD TEST

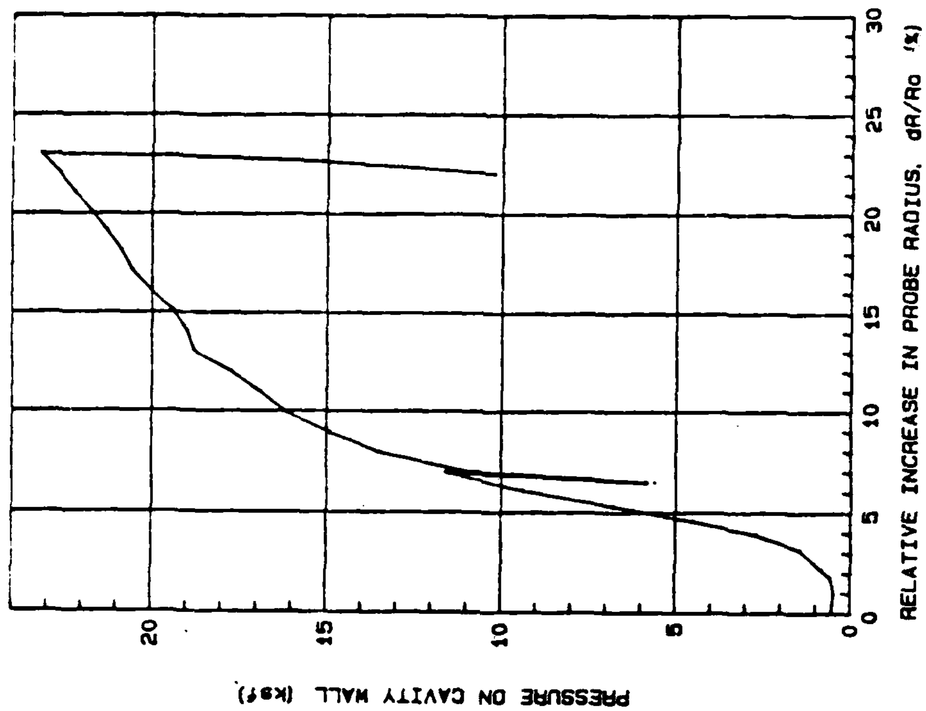

SAN ANTONIO AIRPORT (SA-1) 74'-DEPTH STANDARD TEST

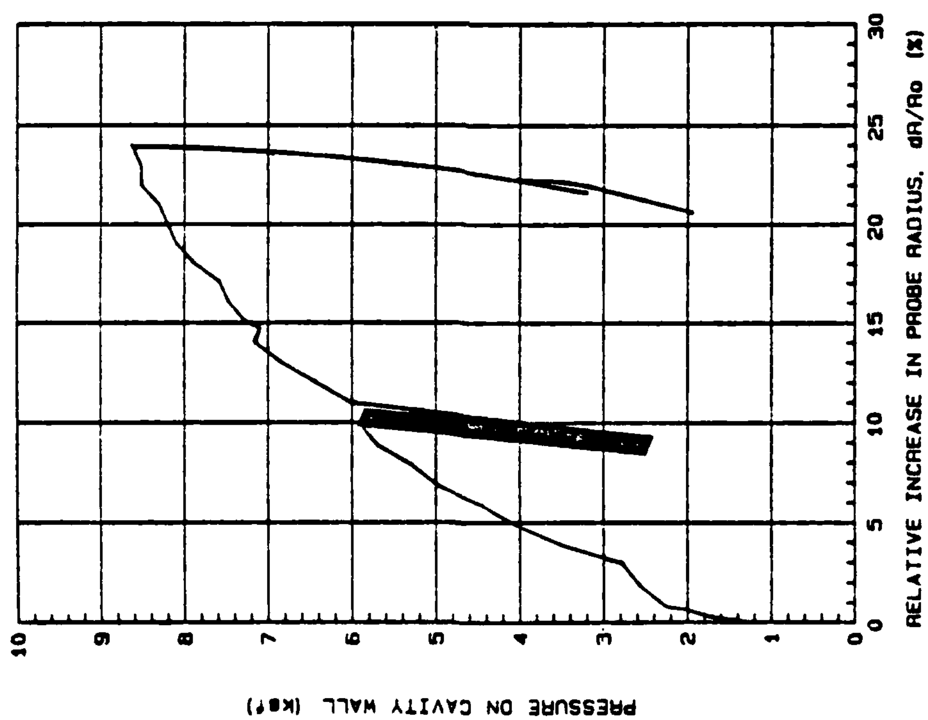

SAN ANTONIO AIRPORT (SA-2) 39°-DEPTH STANDARD AIRPORT TEST

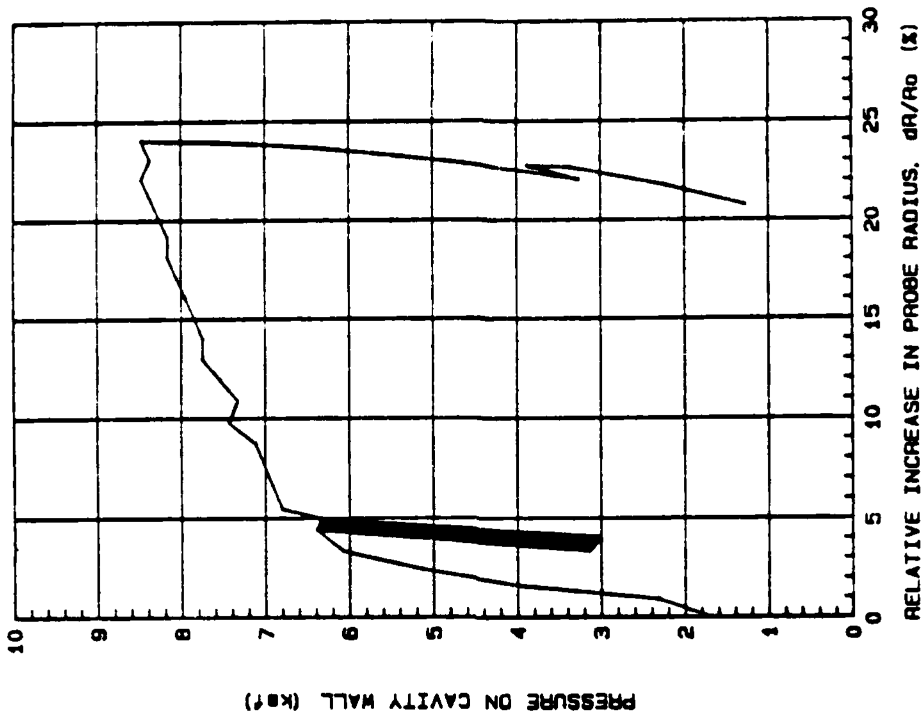

SAN ANTONIO AIRPORT (SA-2) 50°-DEPTH STANDARD AIRPORT TEST

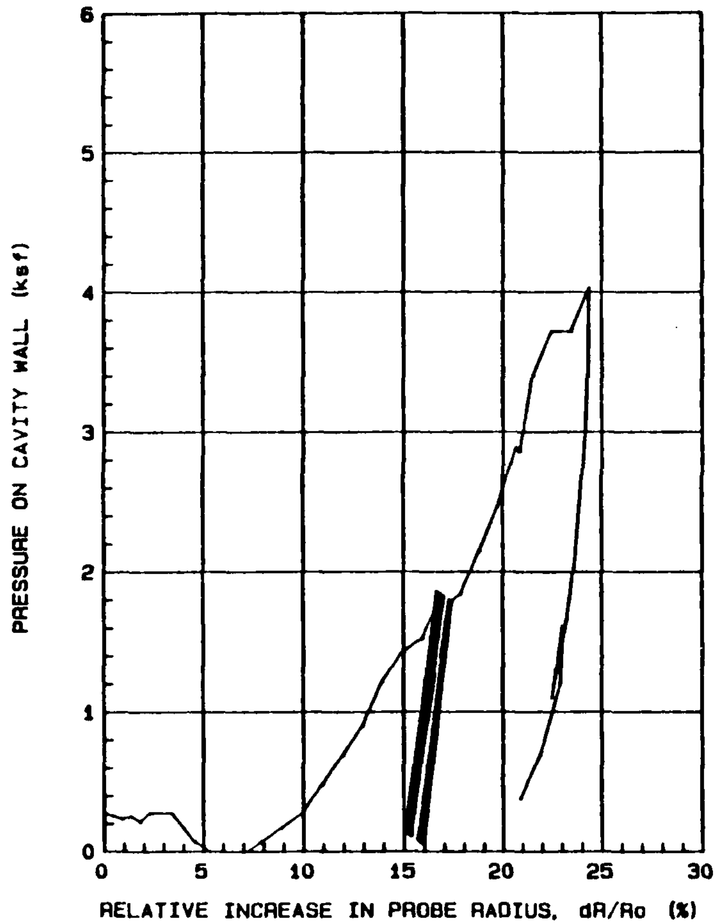

SAN ANTONIO AIRPORT (SA-3) CPMT 26°-DEPTH STANDARD AIRPORT TEST

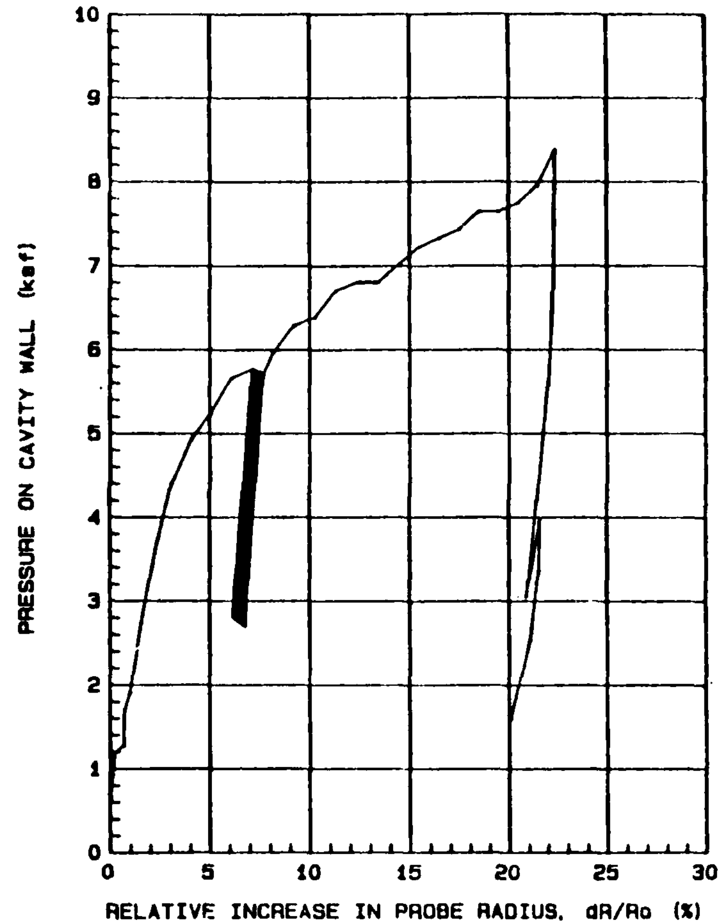

SAN ANTONIO AIRPORT (SA-3) CPMT 39°-DEPTH STANDARD AIRPORT TEST

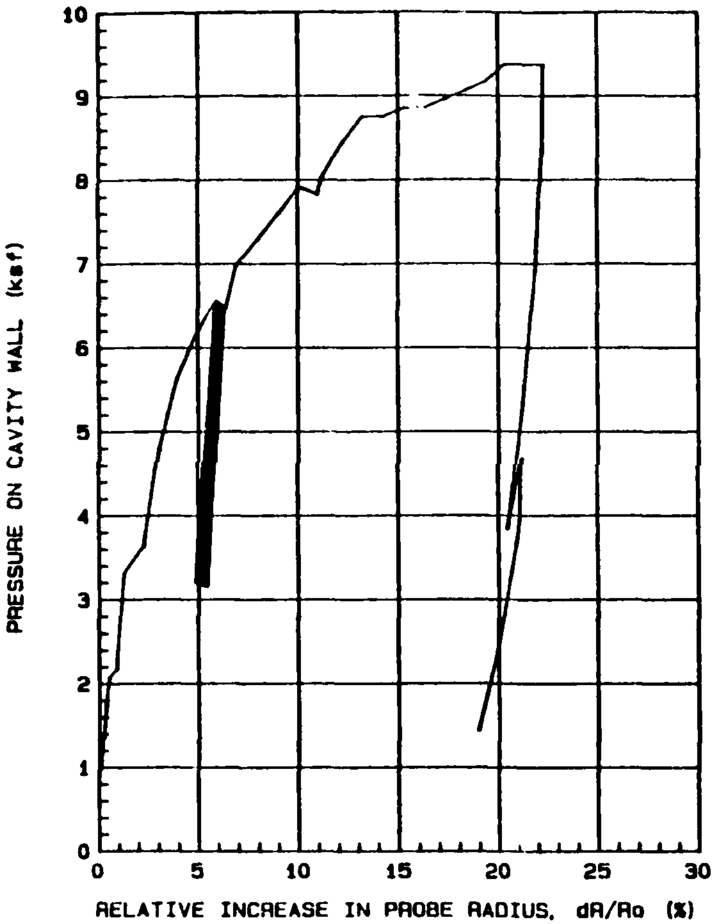

SAN ANTONIO AIRPORT (SA-3) CPMT 50"-DEPTH STANDARD AIRPORT TEST

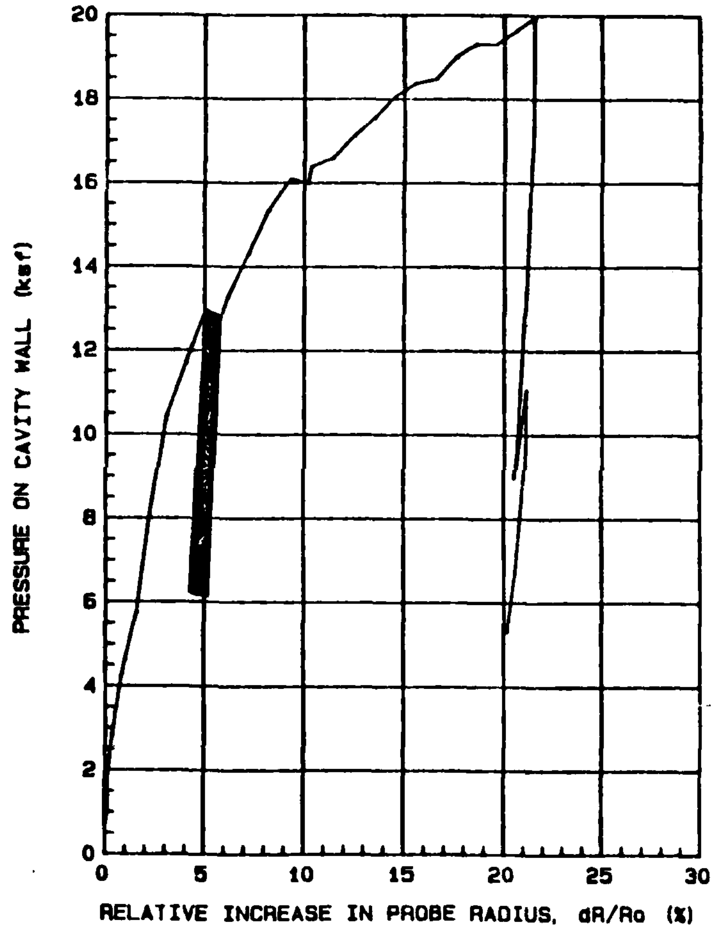

SAN ANTONIO AIRPORT (SA-3) 74"-DEPTH STANDARD AIRPORT TEST

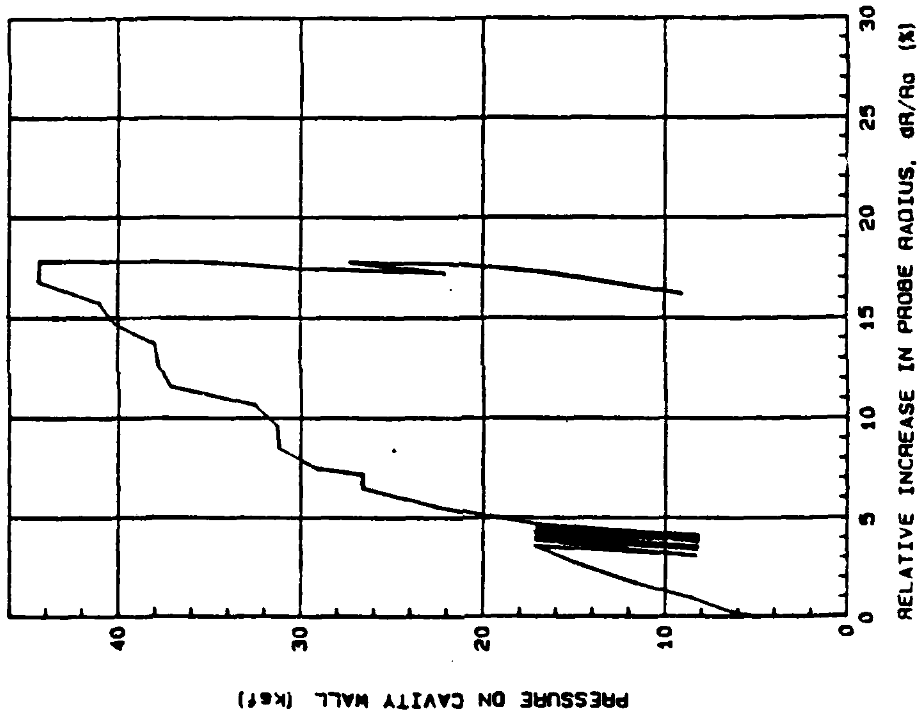

SAN ANTONIO AIRPORT (SA-4) CPMT 28'-DEPTH DRIVEN AIRPORT TEST

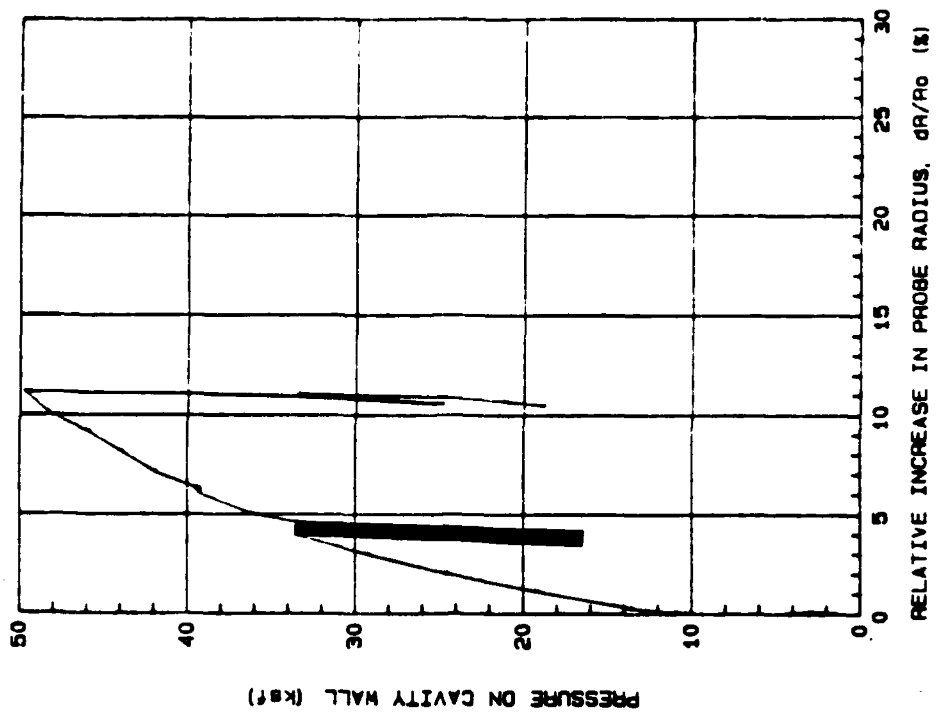

POSSUM KINGDOM AIRPORT (PK-1) 28'-DEPTH DRIVEN AIRPORT TEST

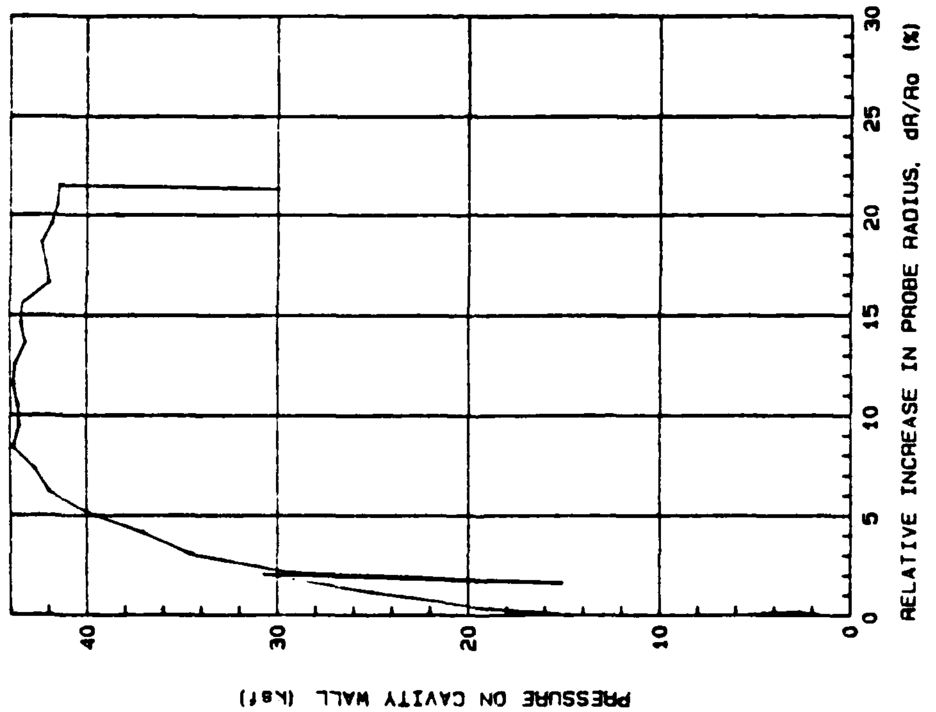

POSSUM KINGDOM AIRPORT (PK-1) 16' STANDARD CPMT TEST

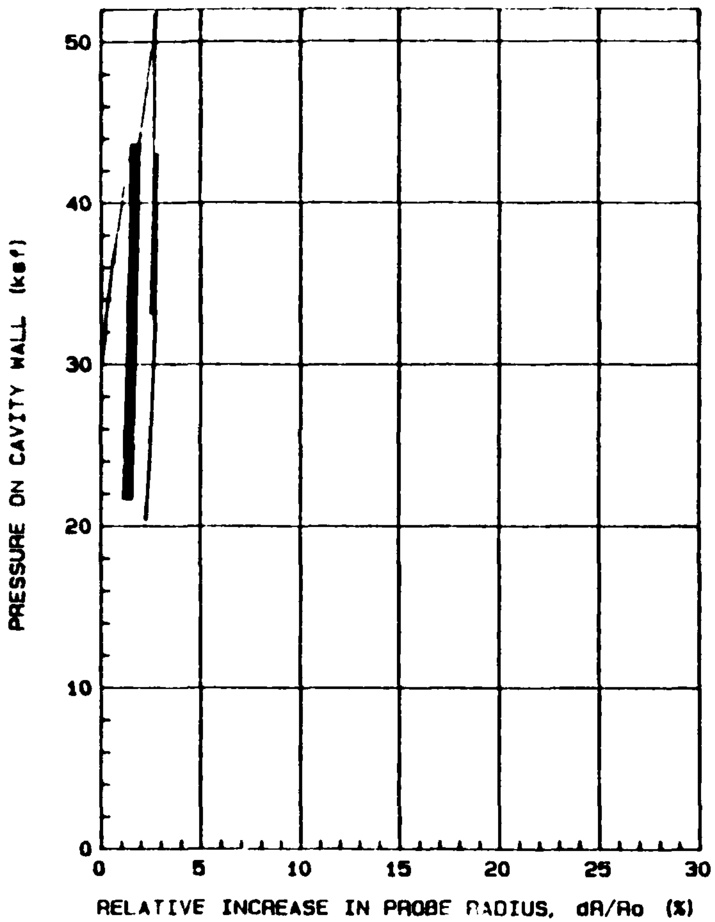

POSSUM KINGDOM AIRPORT (PK-1) 40'-DEPTH DRIVEN AIRPORT TEST

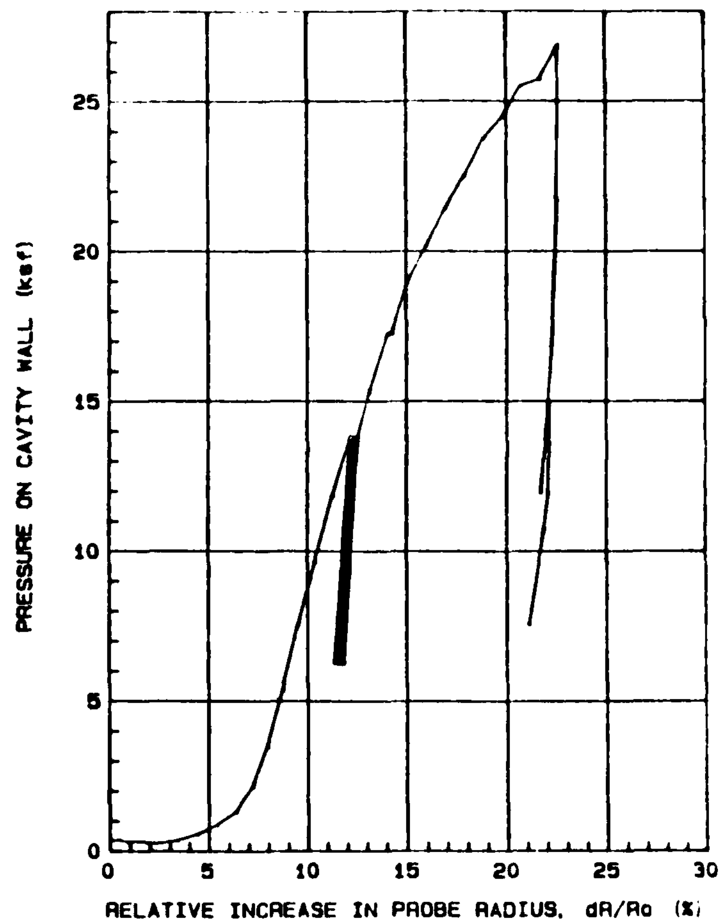

POSSUM KINGDOM AIRPORT (PK-2) 13'-DEPTH STANDARD AIRPORT TEST

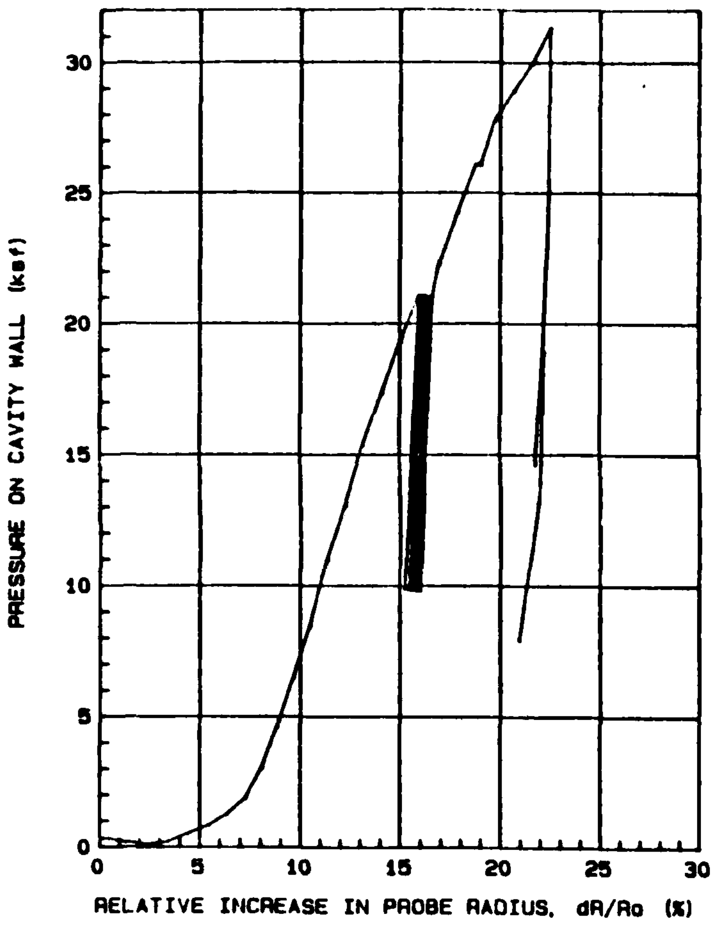

POSSUM KINGDOM AIRPORT (PK-2) 25'-DEPTH STANDARD AIRPORT TEST

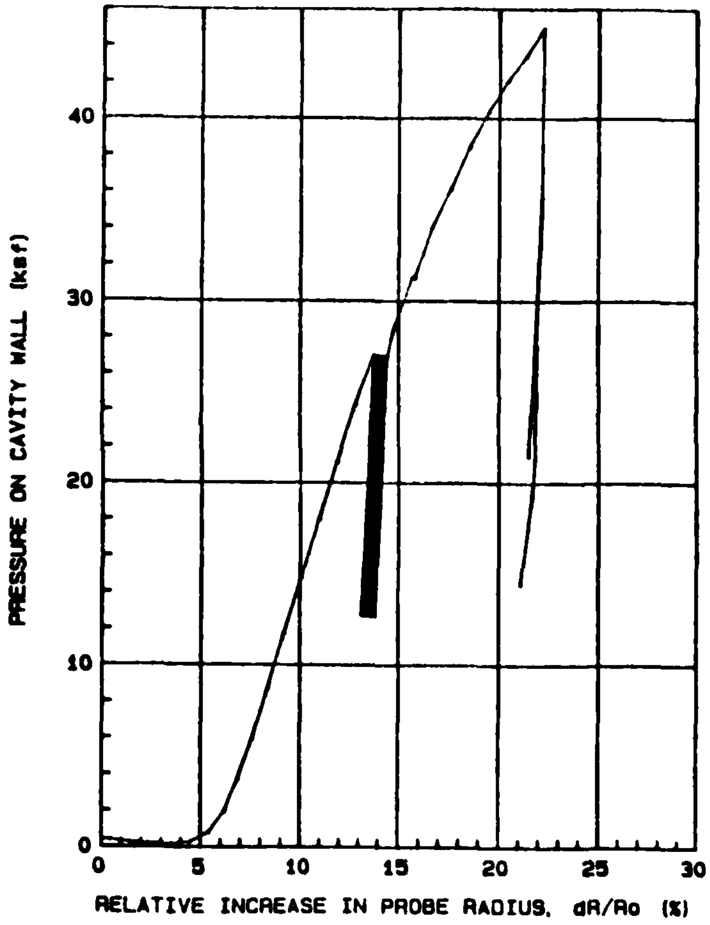

POSSUM KINGDOM AIRPORT (PK-2) 37'-DEPTH STANDARD AIRPORT TEST

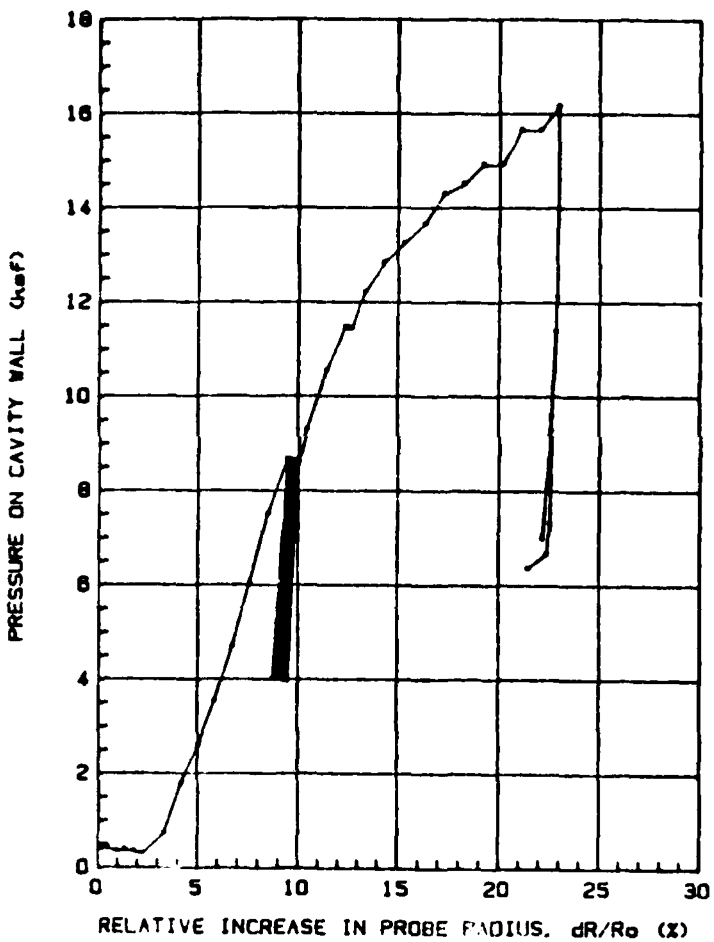

POSSUM KINGDOM AIRPORT (PK-2) 61"-DEPTH STANDARD AIRPORT TEST

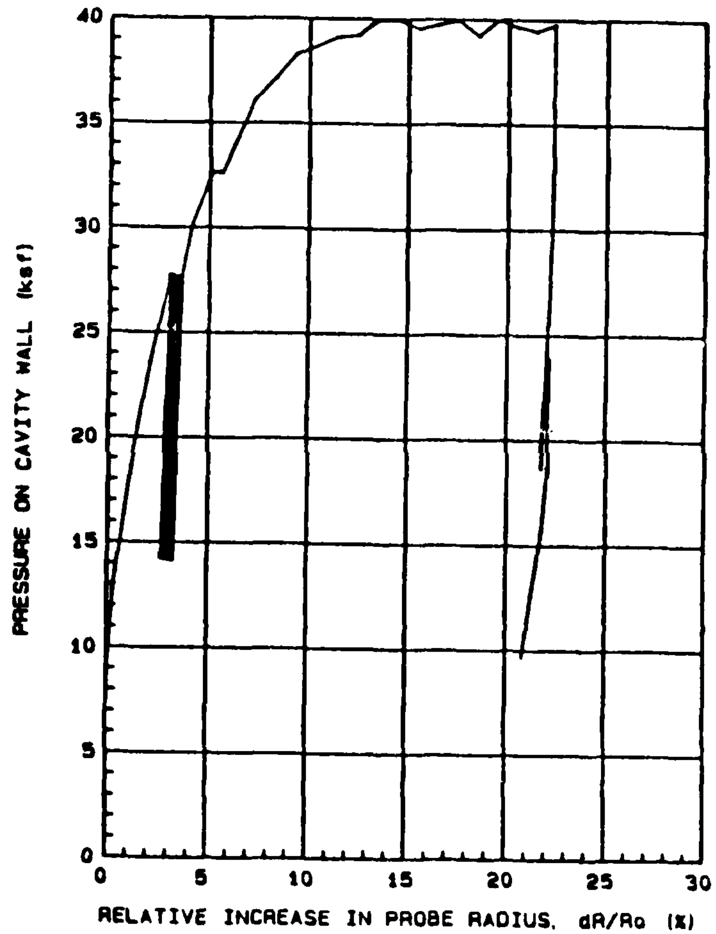

POSSUM KINGDOM AIRPORT (PK-3) 13"-DEPTH DRIVEN AIRPORT TEST

APPENDIX B

Pavement Pressuremeter Test Parameters

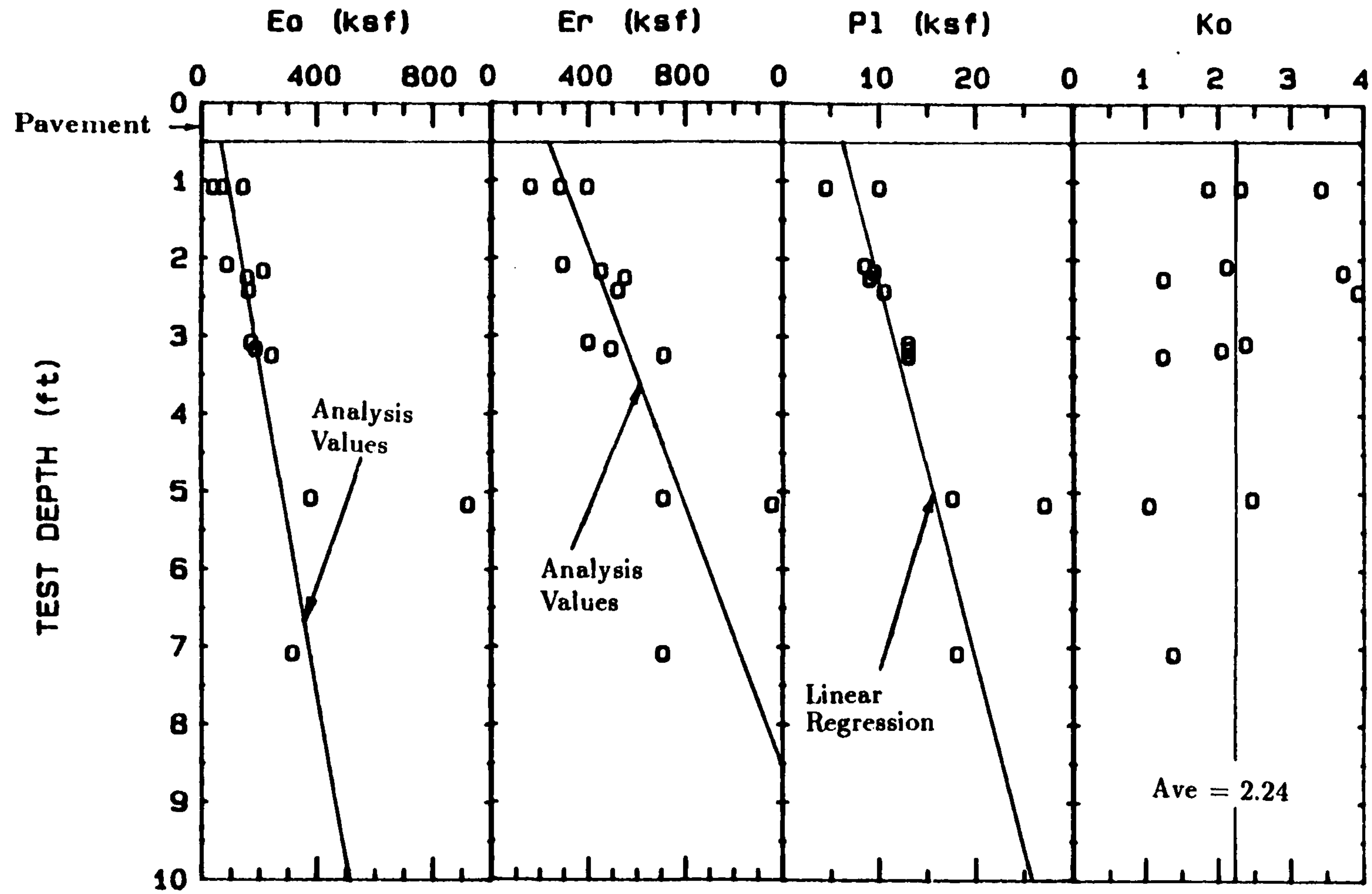

Easterwood Airport PPMT Standard Parameter Summary

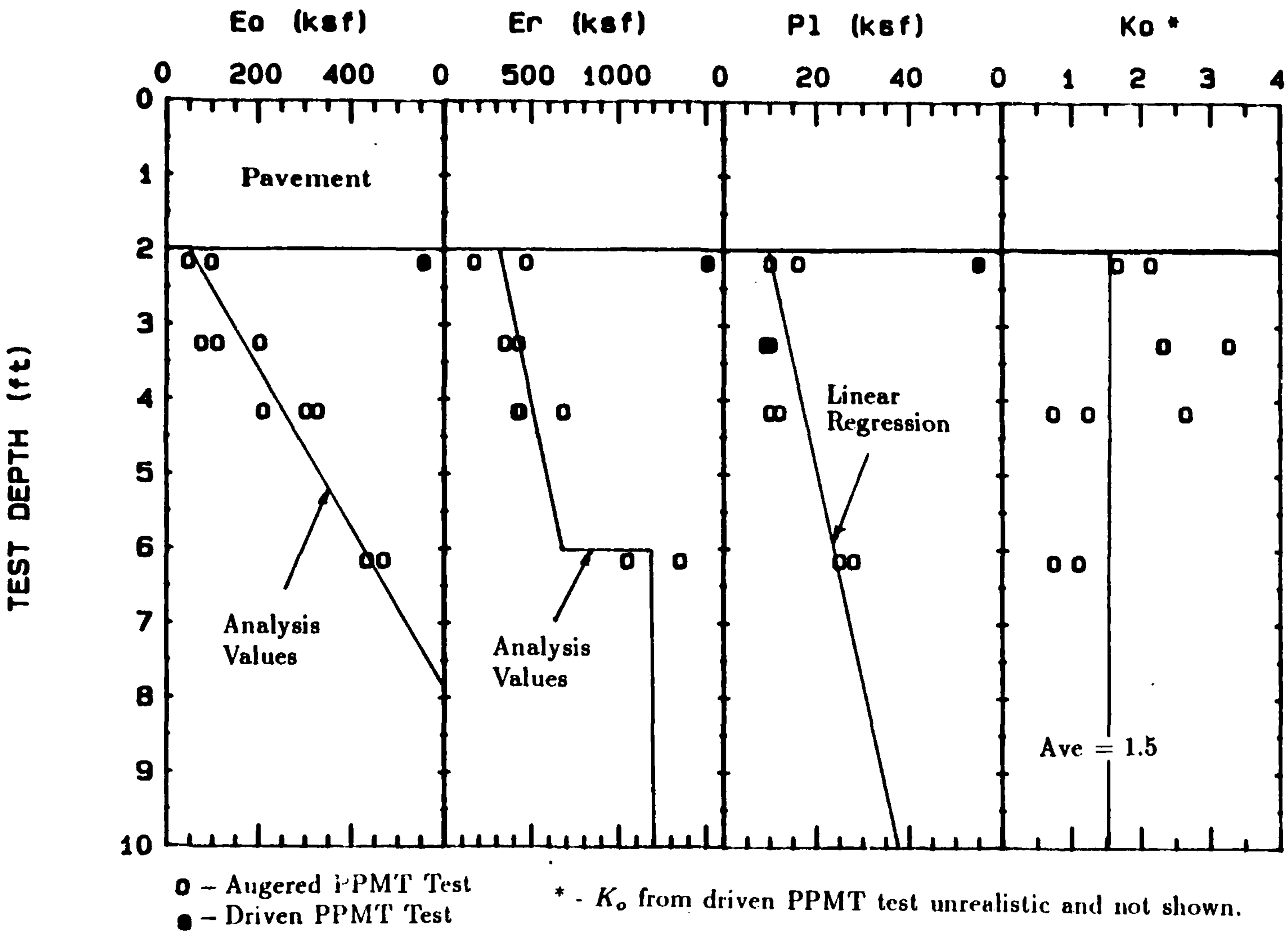

San Antonio Airport PPMT Standard Parameter Summary

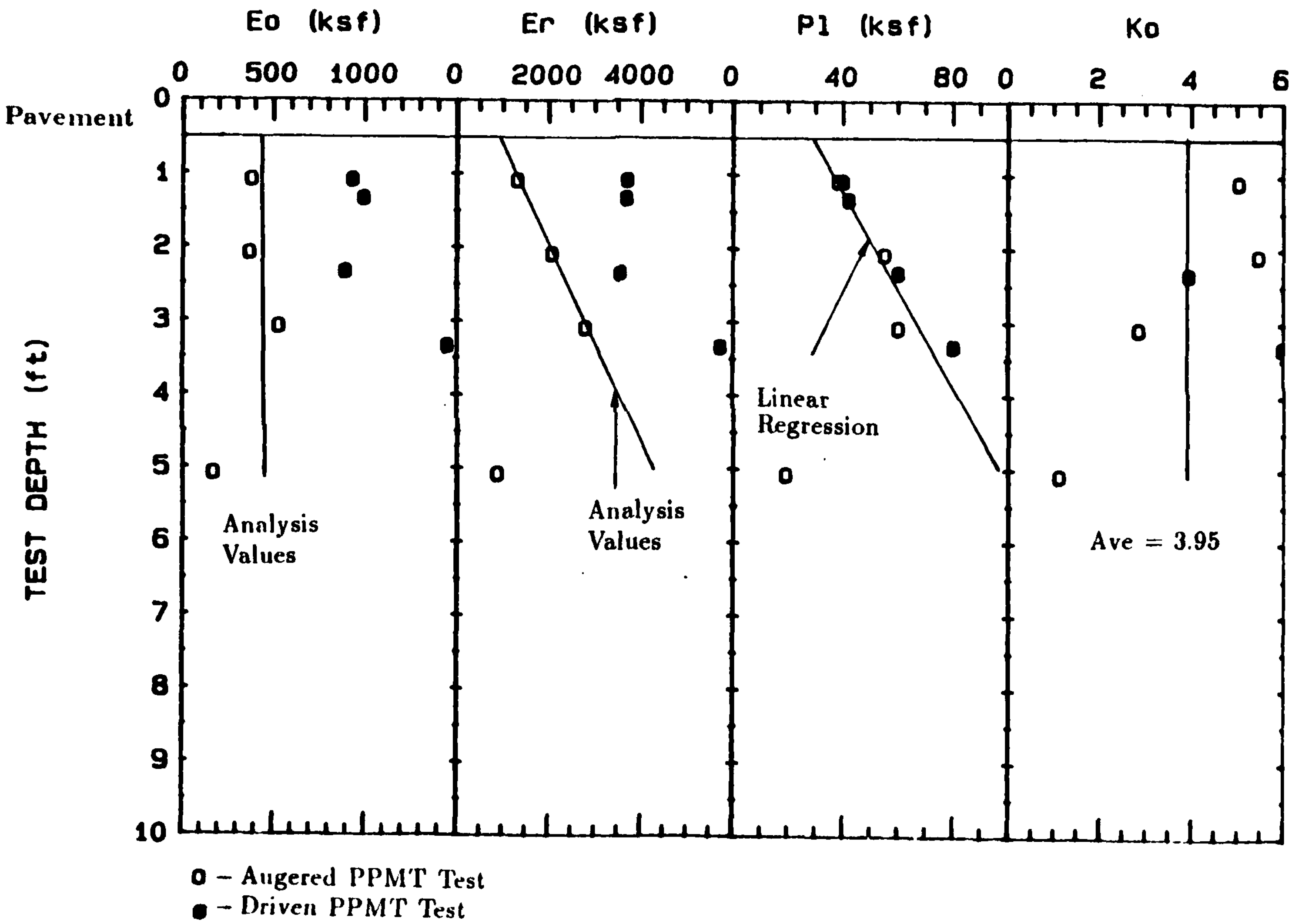

Possum Kingdom Airport PPMT Standard Parameter Summary

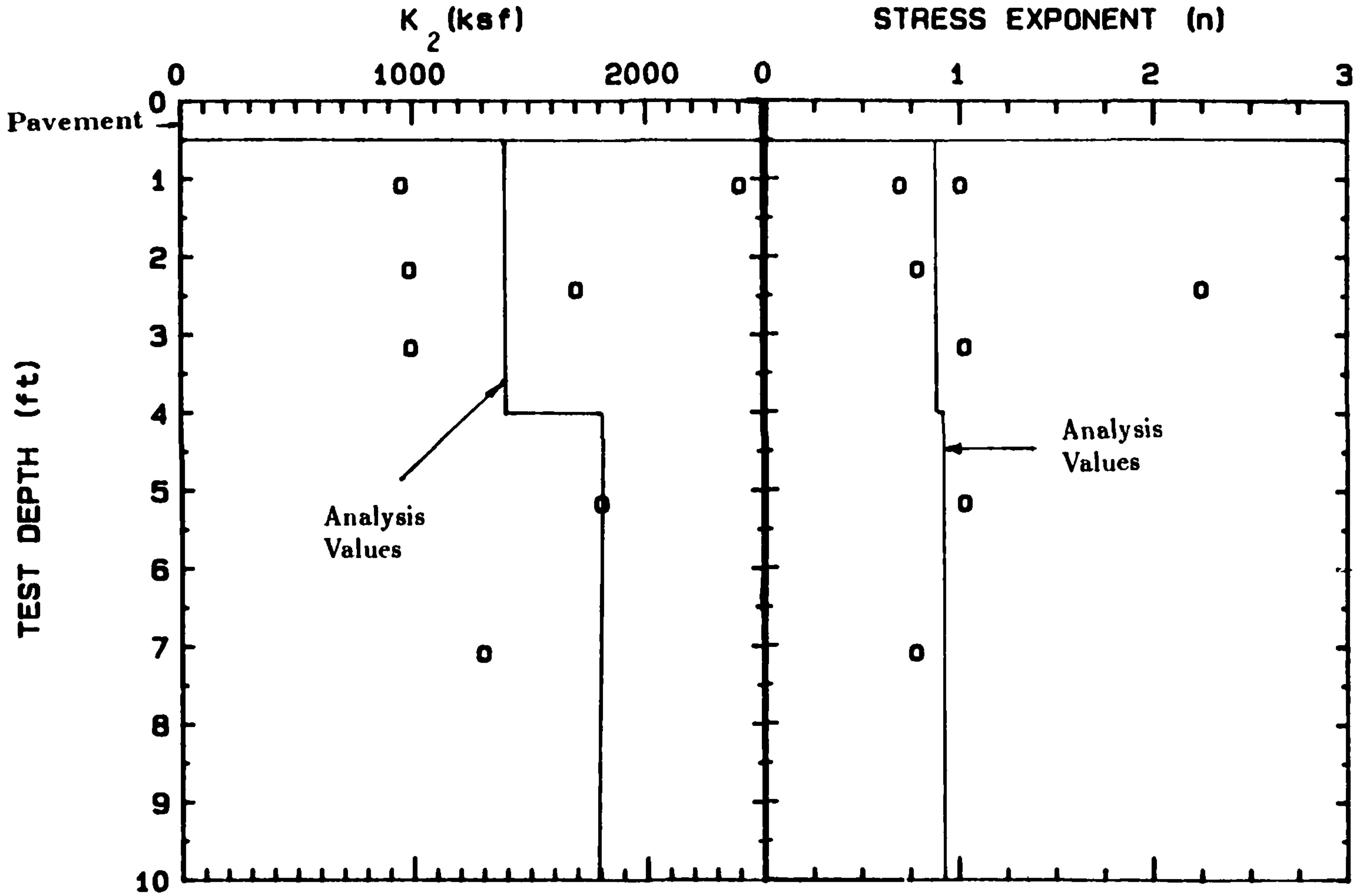

Easterwood Airport PPMT Stress Level Model Parameter Summary

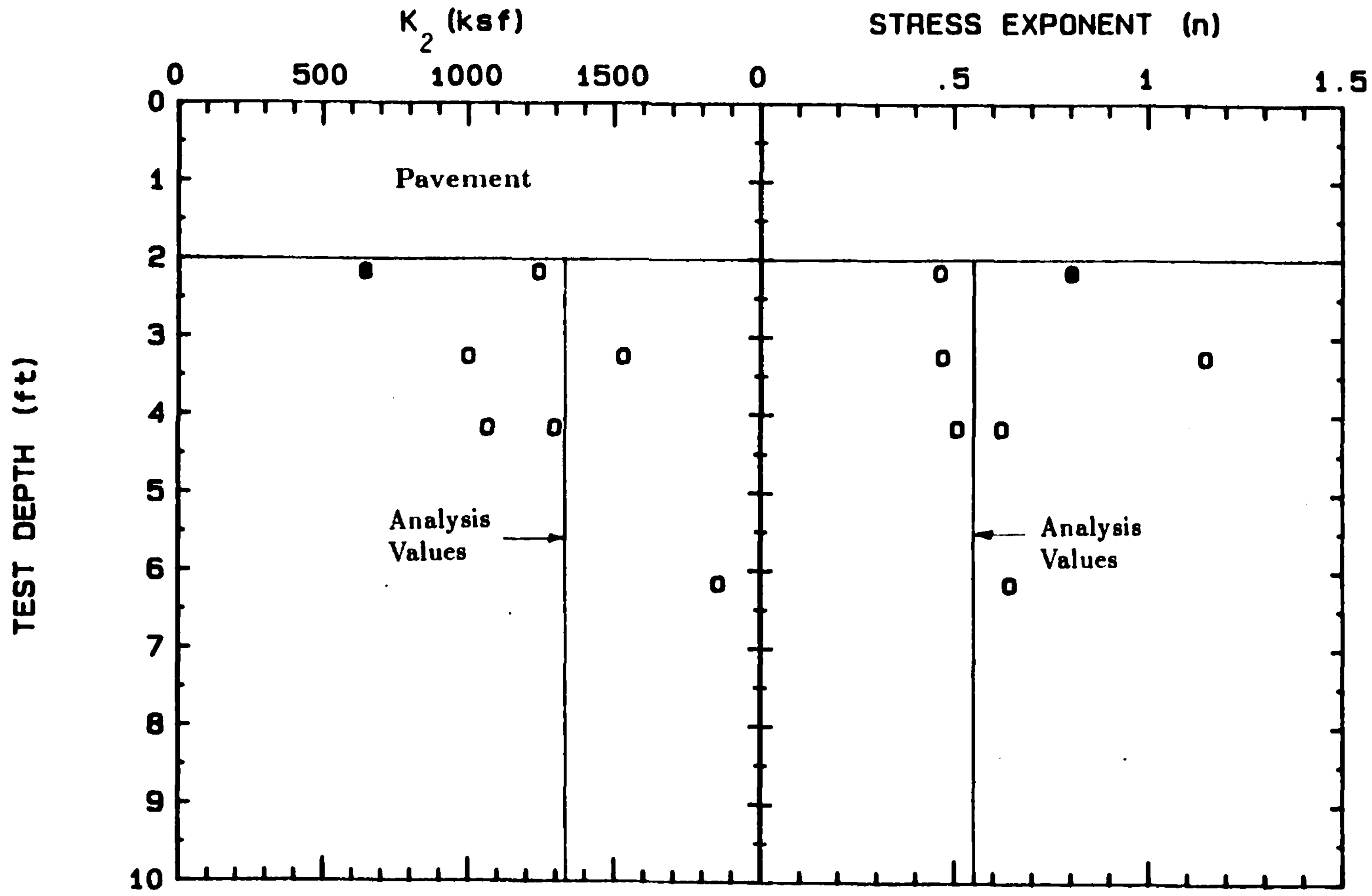

o – Augered PPMT Test
● – Driven PPMT Test

San Antonio Airport PPMT Stress Level Model Parameter Summary

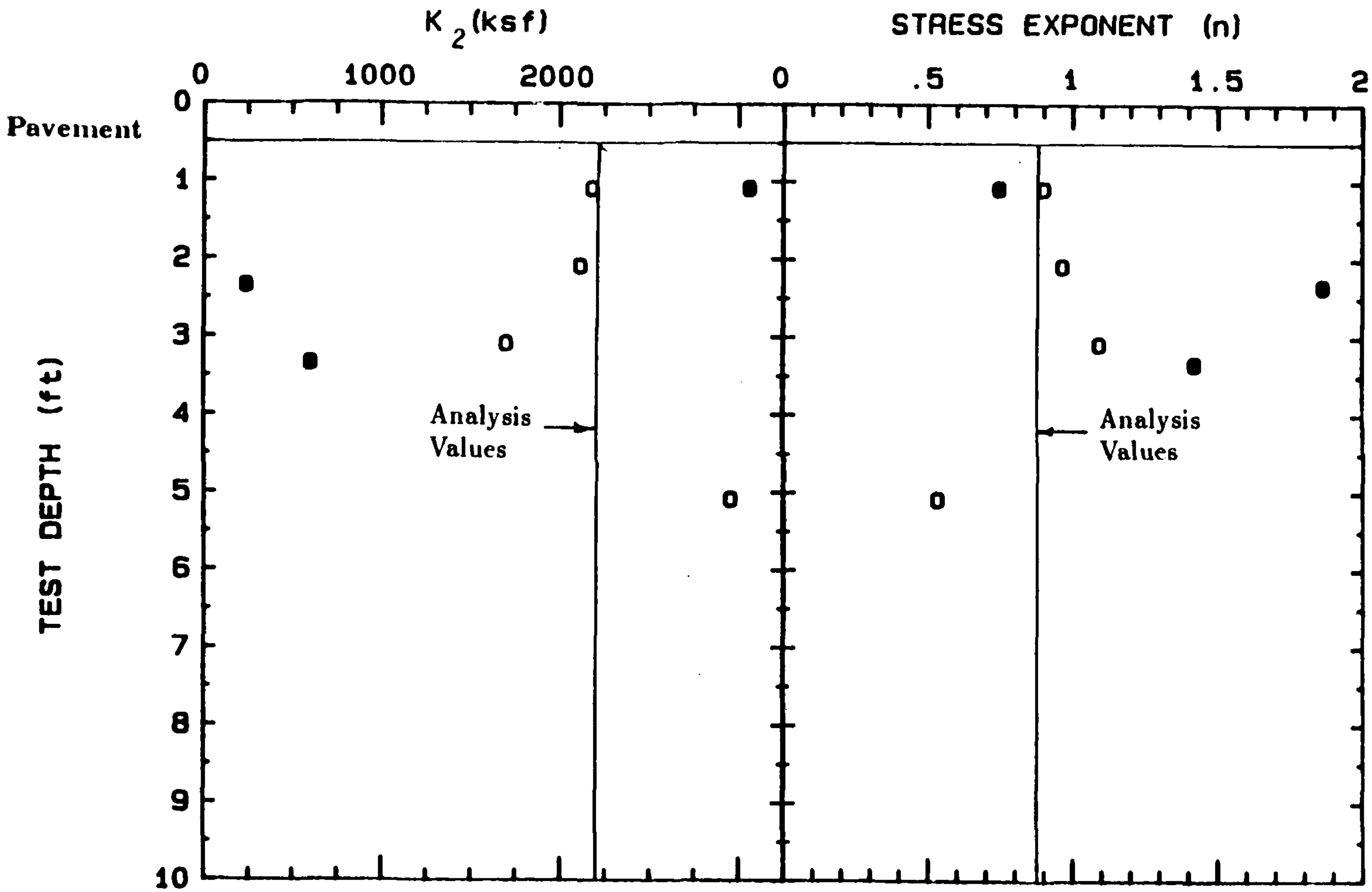

o – Augered PPMT Test
● – Driven PPMT Test

Possum Kingdom Airport PPMT Stress Level Model Parameter Summary

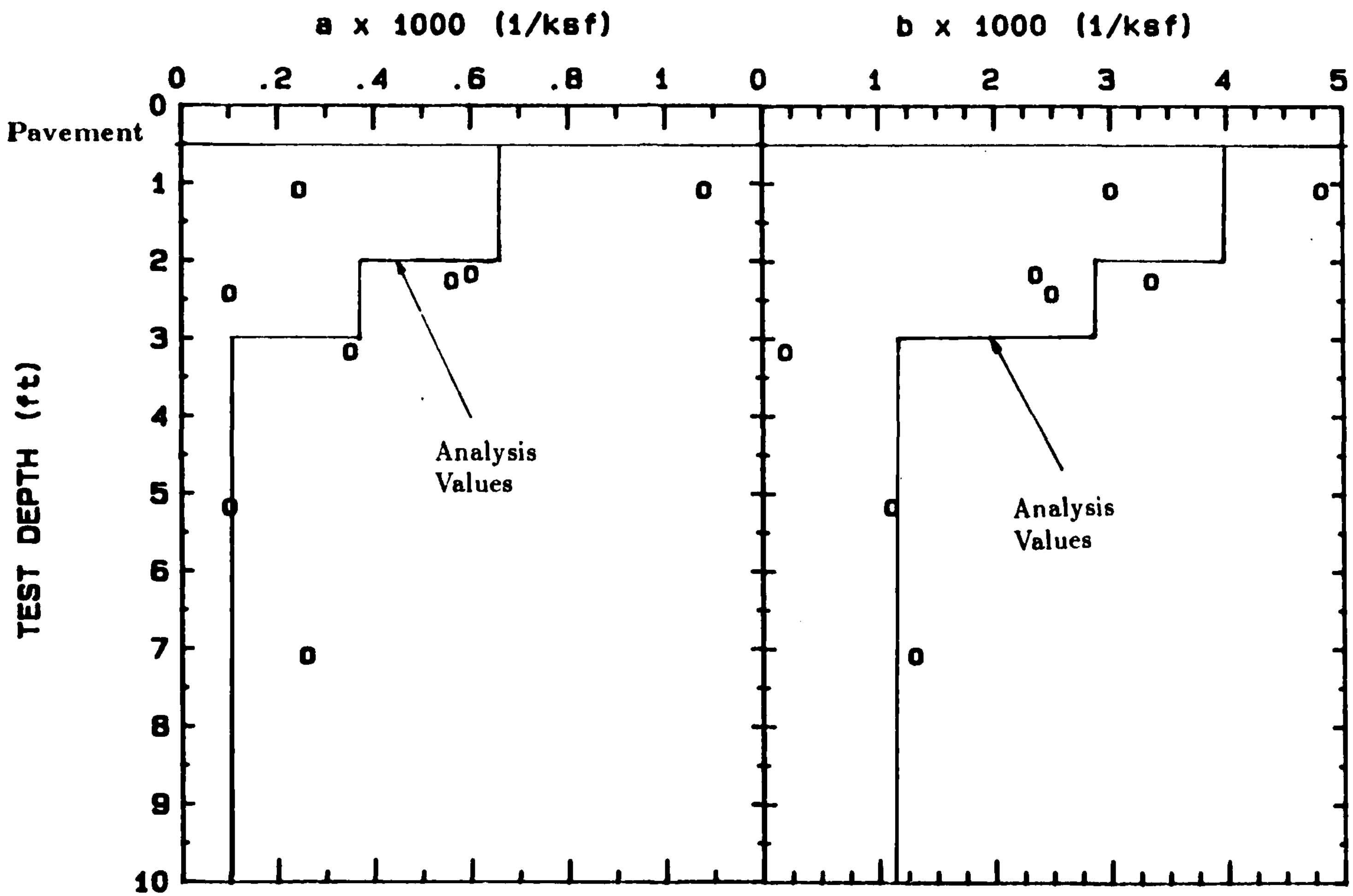

Easterwood Airport PPMT Strain Level Model Parameter Summary

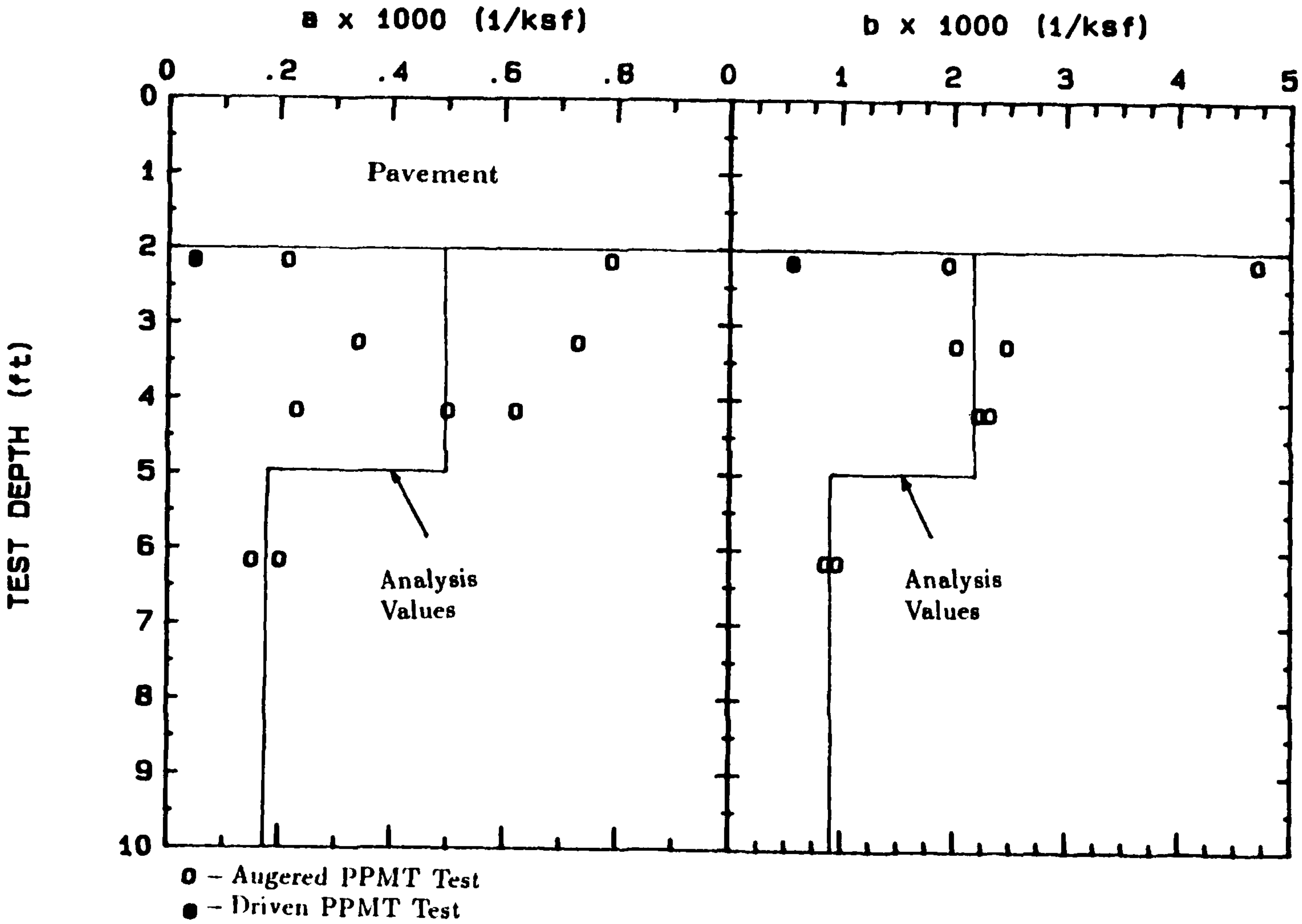

San Antonio Airport PPMT Strain Level Model Parameter Summary

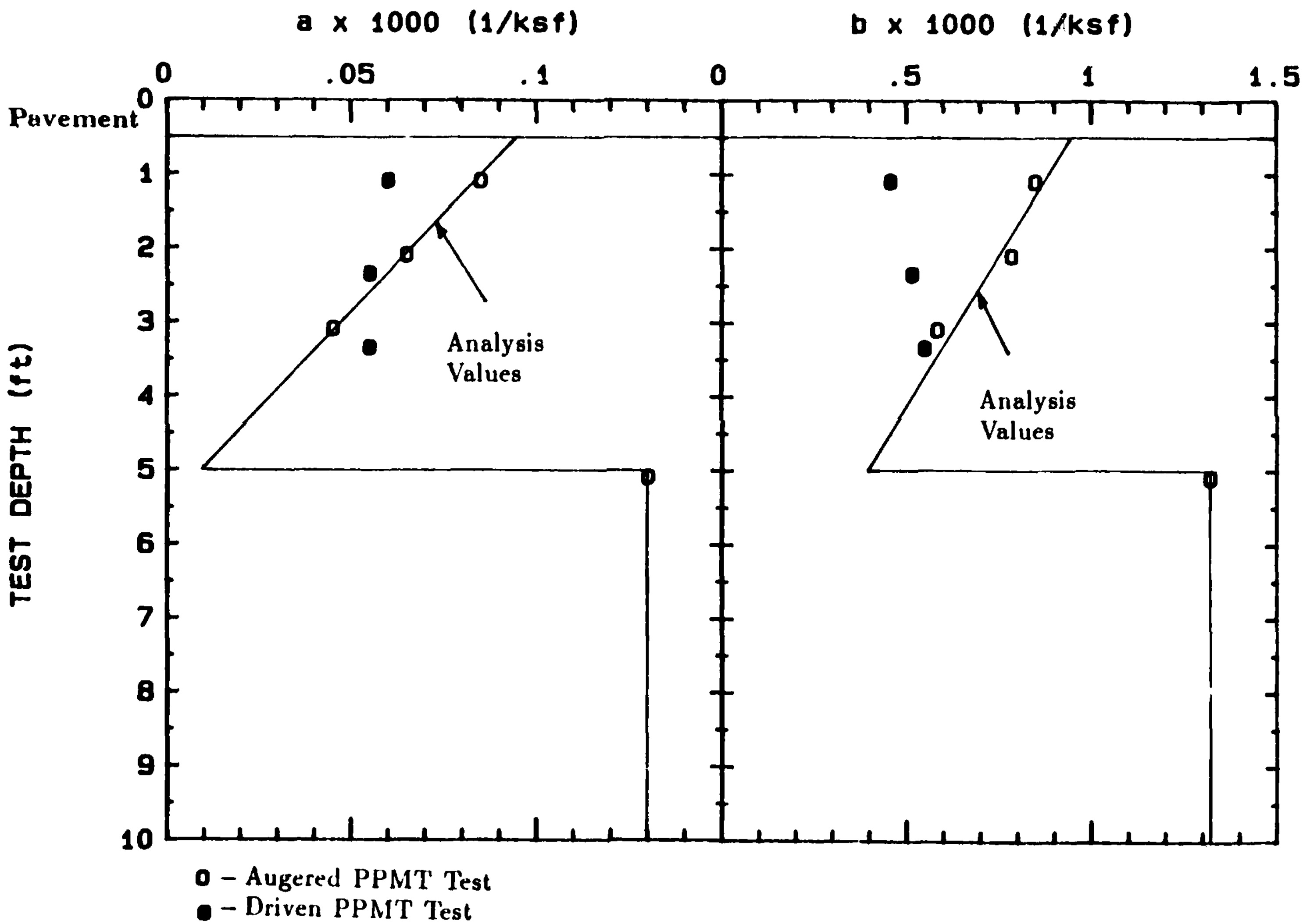

Possum Kingdom Airport PPMT Strain Level Model Parameter Summary

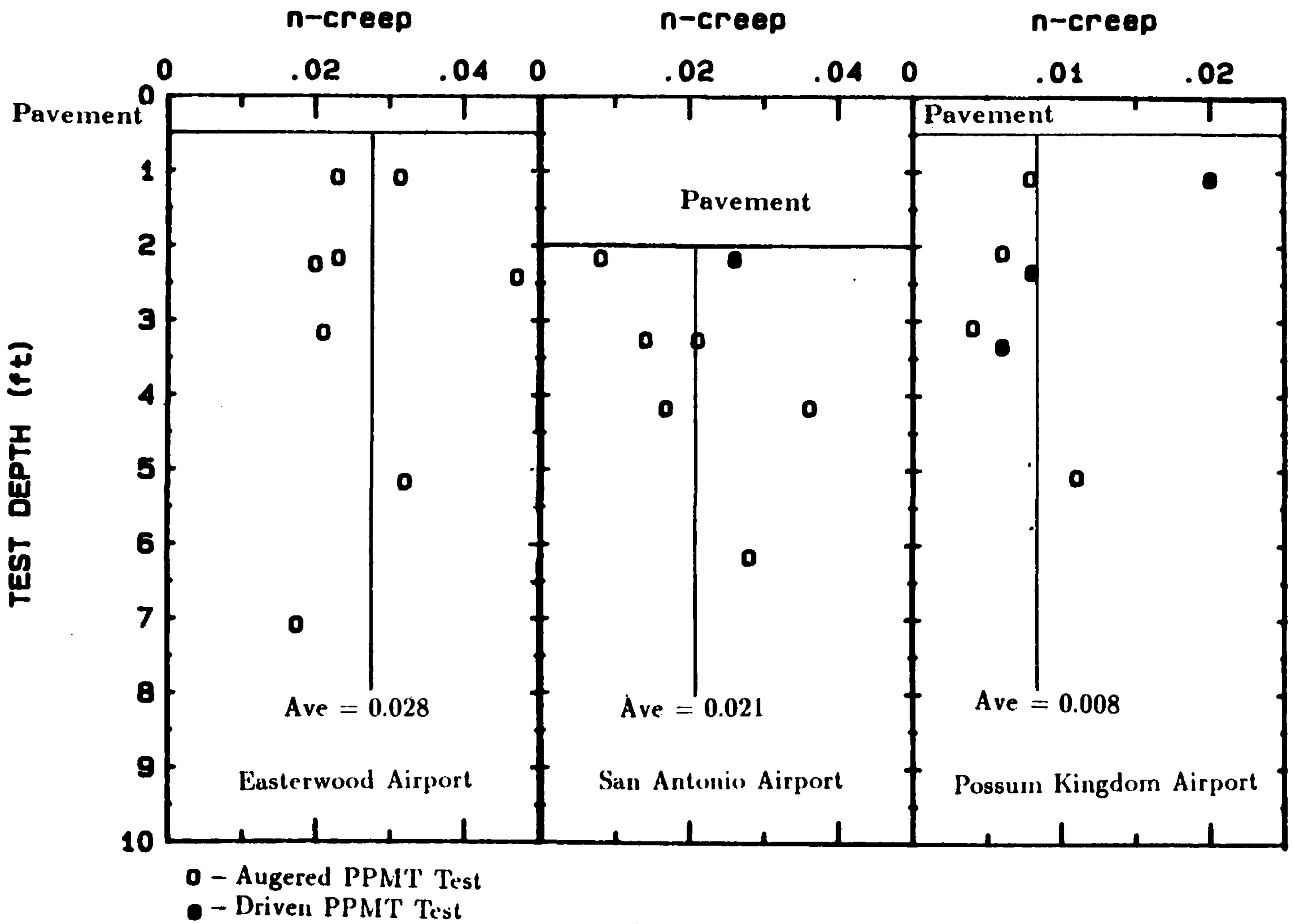

PPMT Creep Model Parameter Summary

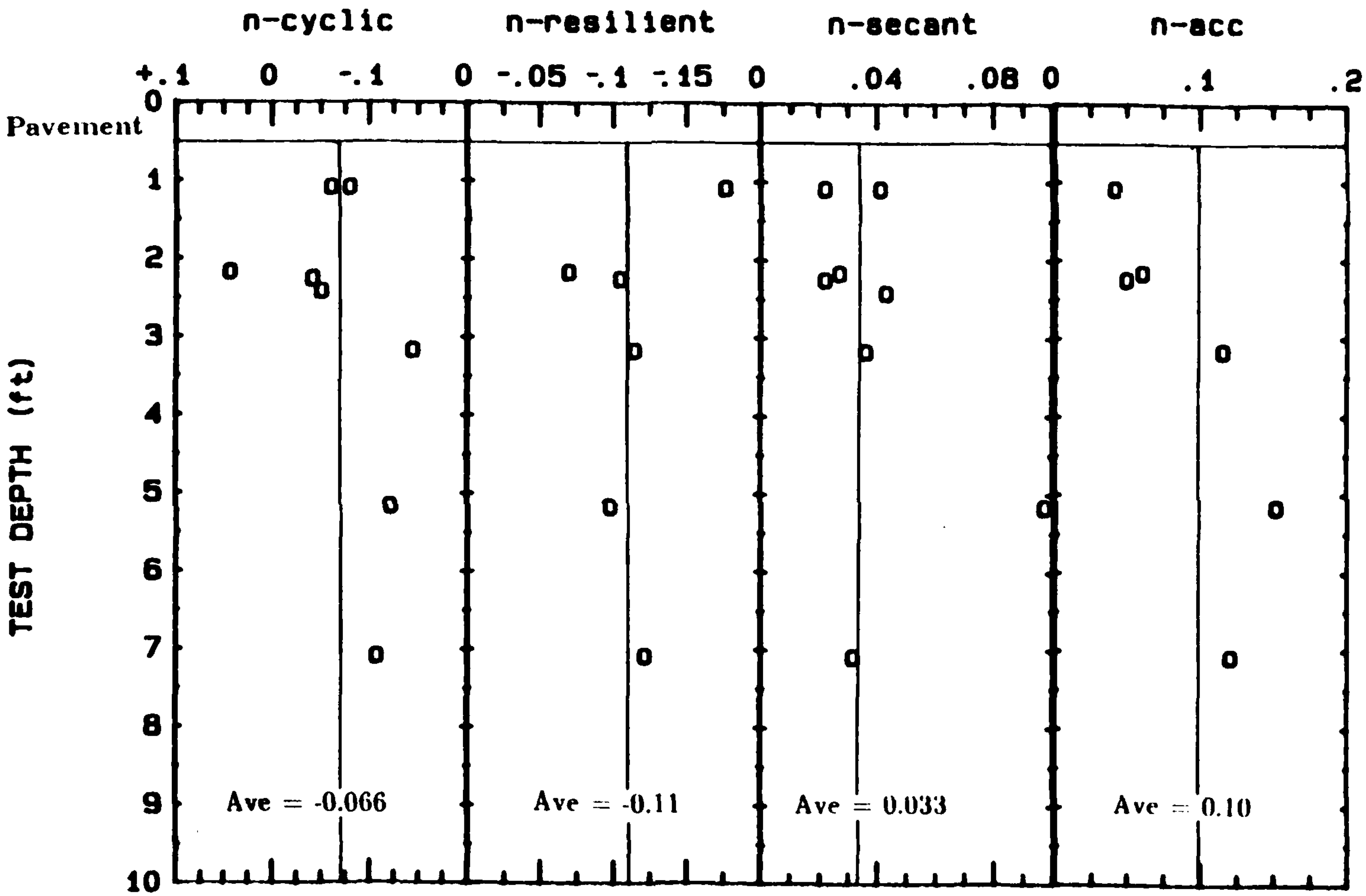

Easterwood Airport PPMT Power Law Exponent Summary

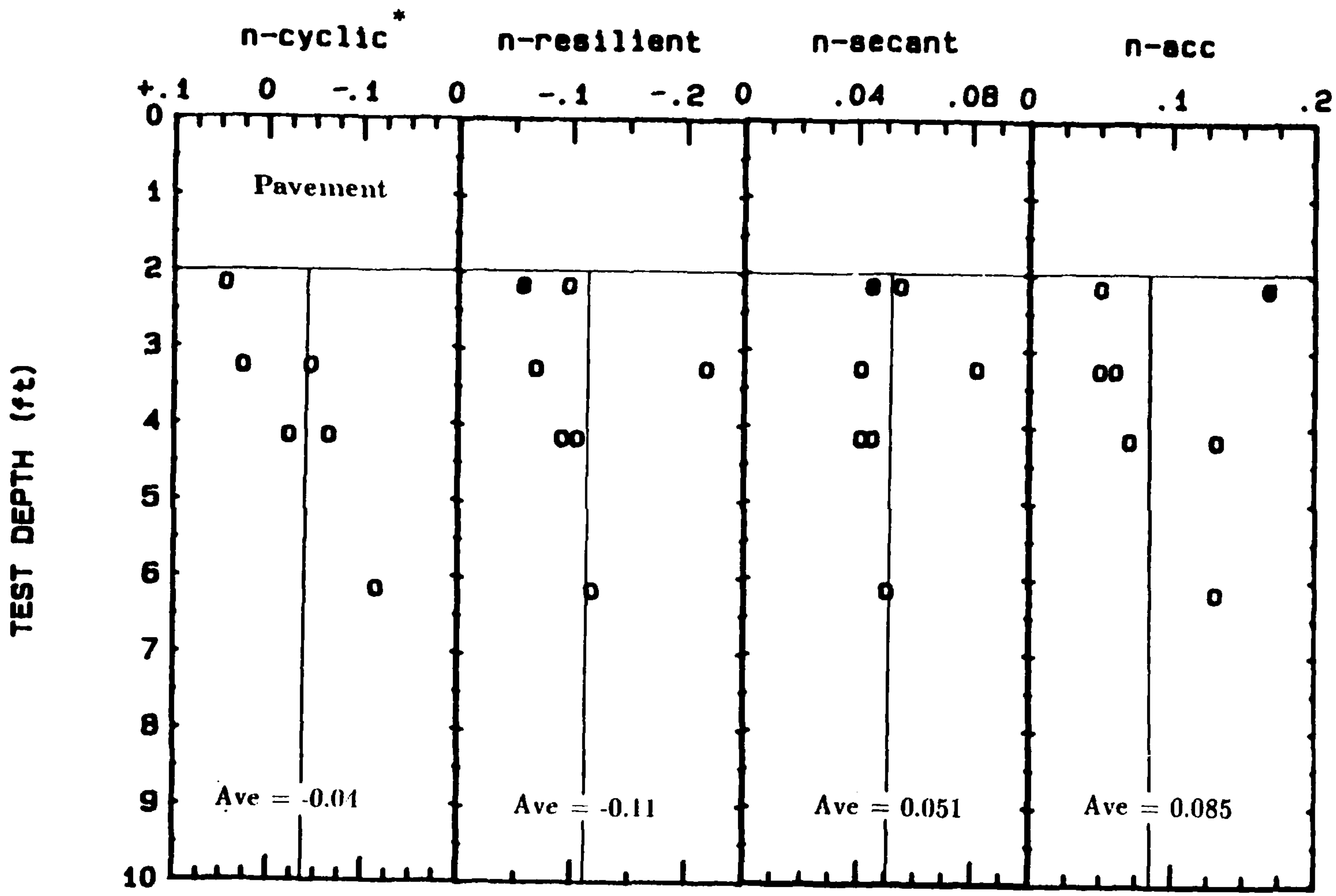

o – Augered PPMT Test
● – Driven PPMT Test

* $-n_{cyc}$ from driven PPMT test unrealistic and not shown.

San Antonio Airport PPMT Power Law Exponent Summary

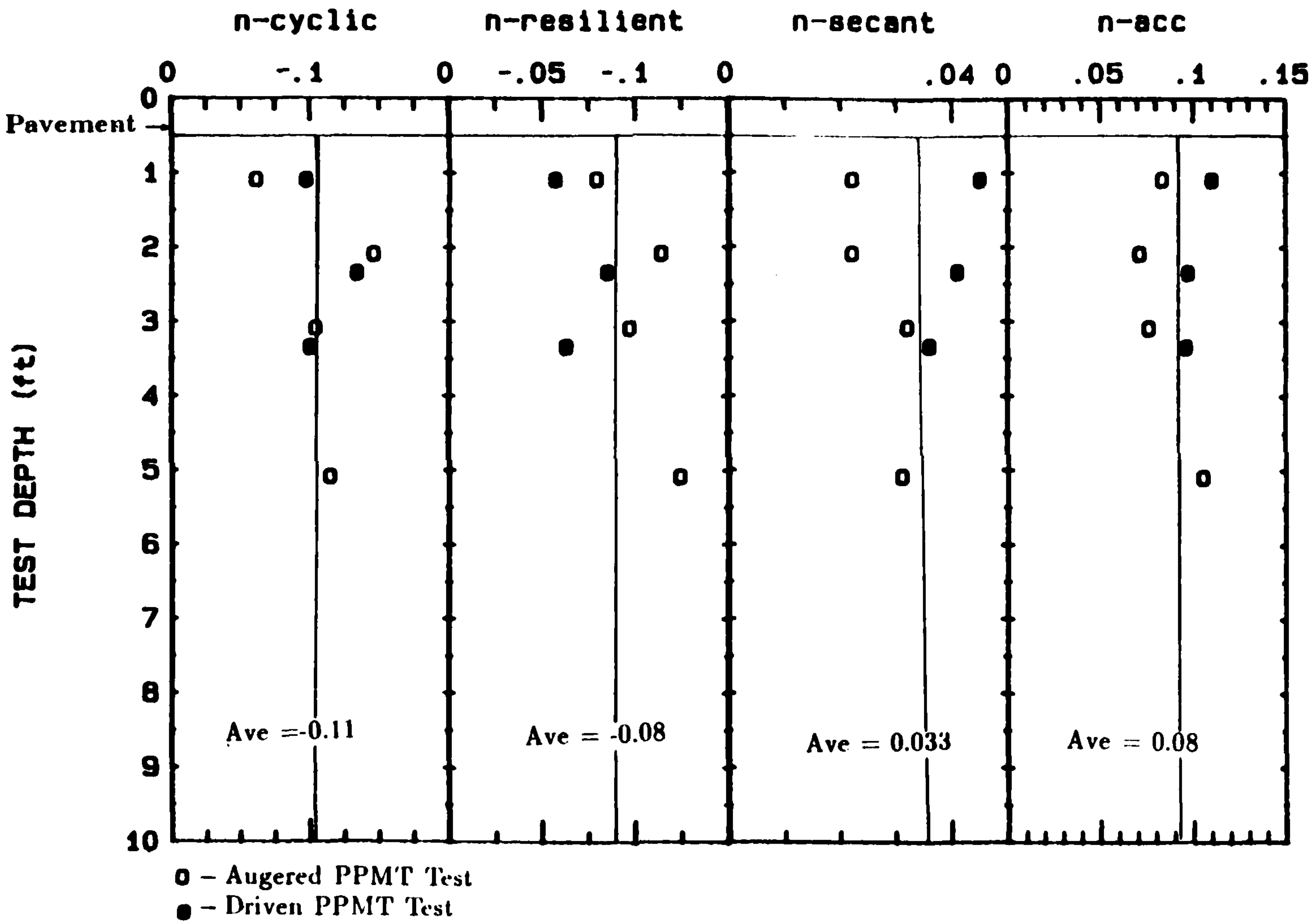

Possum Kingdom Airport PPMT Power Law Exponent Summary

APPENDIX C

AIRPRESS Microcomputer Program User's Manual

Computer System Requirements

The AIRPRESS program requires an IBM PC or compatible computer with at least one floppy disk drive, 256K RAM, DOS 2.0, a graphics card, a printer and an HP7470A pen plotter.

Program Limitations

This program will reduce data from volume-measuring pressuremeters.

Program Structure

After the program has been properly loaded into BASIC there are some initial displays concerning accreditation and basic requirements. The next screen to appear is the main menu from which the following items may be selected.

1. INPUT MEMBRANE CALIBRATION
2. INPUT VOLUME CALIBRATION
3. INPUT PMT TEST
4. USE STORED PMT TEST DATA
5. PLOT TEST ON SCREEN
6. PLOT TEST ON PLOTTER
7. NONE

The two calibration files must be input before a pressuremeter test can be reduced (1 and 2 main menu). The same calibration files may be used to reduce any number of pressuremeter tests. The test data is asked for in terms of displacements and pressures. The displacement may be a volume, such as for the MENARD pressuremeter, or a piston displacement, such as for the TEXAM. Once either a volume or membrane calibration is chosen the program asks for the number of points to be input. All the points are input as indicated on the screen and the program then allows the user to make any necessary corrections. Following the corrections the program asks for a multiplier which changes the probe displacements into injected volume with units of cubic centimeters. The pressures may be input in any units. The program then asks for a multiplier to get the pressures into ksf. These are the units of the remaining calculations.

After the calibrations are input, the raw data is input using the same basic procedure with the exception that the number of cycles must also be input. After the data has been input, the user is given the opportunity to correct the data for incorrect entries.

The following information is also asked for before the data can be reduced.

1. Test Title (used as a heading on printed results)
2. Inflatable length of the probe (cm)
3. Initial radius of the probe (cm)

4. Depth of test (ft)
5. Depth to water table (ft)
6. Unit weight of soil (pcf)
7. K_o to use for P_o calculation
8. Initial pressure reading with probe at gage height
9. Height of gage above ground (ft)
10. File name for volume calibration
11. File name for membrane calibration

The user is also given a chance to review this data for any necessary corrections.

A this point the corrected pressuremeter test is plotted on the screen. The user is first asked for the beginning and end points to calculate an initial pressuremeter modulus, then for the beginning and end points to calculate a reload pressuremeter modulus along the first unloading portion of the test. These moduli are calculated using equation 21 and the two points chosen. It is important to note that the initial modulus is used to set up the starting point for the secant moduli calculations for both the cycles and the creep. Once the user chooses the points for the initial modulus calculation the program extrapolates through these two points to the $\Delta R/R_o$ axis. This establishes a starting point (Point A, Figure 35) which is used as the initial point in the secant moduli calculations associated with the cycles and the creep test. Calculations of the cyclic PMT modulus is done using the top and bottom points of each cycle of the corrected curve. The cyclic correction deserves a special note. This correction is performed using the membrane and volume corrections associated with the top of the cycle, on both the top and bottom points of the cycle. This yields a constant correction for each cycle. The user is then asked for his/her best estimate of the limit pressure. Recall that the limit pressure is defined as the pressure associated with twice the initial volume of the cavity.

The final results are saved on the specified disk and the user is given the option of printing the results in tabular form or plotting the corrected curve on the HP plotter.

EXAMPLE PROGRAM RUN

```
 AAAA     III  RRRRRRR   PPPPPPP  RRRRRRR  EEEEEEE   SSSSSSS   SSSSSSS
A    A     I   R     R   P     P  R     R  E         S         S
A     A    I   R     R   P     P  R     R  E         S         S
AAAAAAAA   I   RRRRRRR   PPPPPPP  RRRRRRR  EEEEE     SSSSSSS   SSSSSSS
A      A   I   R R       P        R R      E               S         S
A      A   I   R  R      P        R  R     E               S         S
A      A   I   R   R     P        R   R    E               S         S
A      A  III  R     R   P        R     R  EEEEEEE   SSSSSSS   SSSSSSS
```

Paul J.Cosentino, Larry M. Tucker and Jean-Louis Briaud
Civil Engineering Department
Texas A&M University

Press any key to continue

This program was developed to reduce pressuremeter test data obtained from hydraulically inflated pressuremeters. See the user's manual for procedures used in correcting the test data, and for proper use of the program.

```
* * * * * * * * * * *  WARNING !  * * * * * * * * * * * *
*                                                        *
*  The program writer assumes no responsibility for      *
*         the answers given by this program.             *
*                                                        *
* * * * * * * * * * * * * * * * * * * * * * * * * * * *
```

Press any key to continue.

YOU MUST HAVE A GRAPHICS CARD TO USE THIS PROGRAM

Press any key to continue.

Note: Membrane and Volume calibrations must be input before the test may be reduced.

```
1. INPUT MEMBRANE CALIBRATION
2. INPUT VOLUME CALIBRATION
3. INPUT PMT TEST
4. USE STORED PMT TEST DATA
5. PLOT TEST ON SCREEN
6. PLOT TEST ON PLOTTER
7. NONE

CHOICE? 1
```

NUMBER OF POINTS= ? 25

```
WHAT MULTIPLIER TO GET VOLUME READINGS IN CM^3:

     1.  MULTIPLIER = 1.0
     2.  MULTIPLIER = 193.05
     3.  OTHER

? 1
```

Note: Option 3 allows input of any multiplier.

```
WHAT UNITS ARE PRESSURE READINGS IN?

  1. bars
  2. kg/cm^2
  3. kPa
  4. other
? 3
```

Note: Option 4 allows input of any multiplier.

```
WHAT DRIVE TO SAVE MEMBRANE CALIBRATION DATA ON (A/B/C)? C

WHAT FILE NAME TO SAVE MEMBRANE CALIBRATION DATA (8 CHARACTERS MAX.)? EXVOL

DATA WILL BE SAVED AS C:EXVOL.CAL

IS THIS CORRECT (Y/N)? Y
```

Note: Calibration files are saved with .CAL extensions unless otherwise specified.

Note: Input ALL displacements, loading pressures and unloading pressures.

```
DISPLACEMENT  1 LOADING PRESSURE  1 UNLOADING PRESSURE 1 ? 0,16,14
DISPLACEMENT  2 LOADING PRESSURE  2 UNLOADING PRESSURE 2 ? 5,26,24
DISPLACEMENT  3 LOADING PRESSURE  3 UNLOADING PRESSURE 3 ? 10,37,33
DISPLACEMENT  4 LOADING PRESSURE  4 UNLOADING PRESSURE 4 ? 15,48,42
DISPLACEMENT  5 LOADING PRESSURE  5 UNLOADING PRESSURE 5 ? 20,55,45
DISPLACEMENT  6 LOADING PRESSURE  6 UNLOADING PRESSURE 6 ? 25,70,60
DISPLACEMENT  7 LOADING PRESSURE  7 UNLOADING PRESSURE 7 ? 30,76,64
DISPLACEMENT  8 LOADING PRESSURE  8 UNLOADING PRESSURE 8 ? 35,86,74
DISPLACEMENT  9 LOADING PRESSURE  9 UNLOADING PRESSURE 9 ? 40,85,75
DISPLACEMENT  10 LOADING PRESSURE  10 UNLOADING PRESSURE 10 ? 45.5,88,72
DISPLACEMENT  11 LOADING PRESSURE  11 UNLOADING PRESSURE 11 ? 50,91,79
DISPLACEMENT  12 LOADING PRESSURE  12 UNLOADING PRESSURE 12 ? 55,97,83
DISPLACEMENT  13 LOADING PRESSURE  13 UNLOADING PRESSURE 13 ? 60,102,88
DISPLACEMENT  14 LOADING PRESSURE  14 UNLOADING PRESSURE 14 ? 65,110,90
DISPLACEMENT  15 LOADING PRESSURE  15 UNLOADING PRESSURE 15 ? 70,110,100
DISPLACEMENT  16 LOADING PRESSURE  16 UNLOADING PRESSURE 16 ? 75,111,99
DISPLACEMENT  17 LOADING PRESSURE  17 UNLOADING PRESSURE 17 ? 80,112,98
DISPLACEMENT  18 LOADING PRESSURE  18 UNLOADING PRESSURE 18 ? 85,114,106
DISPLACEMENT  19 LOADING PRESSURE  19 UNLOADING PRESSURE 19 ? 90,116,114
DISPLACEMENT  20 LOADING PRESSURE  20 UNLOADING PRESSURE 20 ? 95,117,113
DISPLACEMENT  21 LOADING PRESSURE  21 UNLOADING PRESSURE 21 ? 100,120,116
DISPLACEMENT  22 LOADING PRESSURE  22 UNLOADING PRESSURE 22 ? 105,122,118
DISPLACEMENT  23 LOADING PRESSURE  23 UNLOADING PRESSURE 23 ? 110,123,117
DISPLACEMENT  24 LOADING PRESSURE  24 UNLOADING PRESSURE 24 ? 115,124,122
DISPLACEMENT  25 LOADING PRESSURE  25 UNLOADING PRESSURE 25 ? 120,125,125
```

POINT NO.	DISPLACEMENT	LOADING PRESSURE	UNLOADING PRESSURE
1	0.00	16.00	14.00
2	5.00	26.00	24.00
3	10.00	37.00	33.00
4	15.00	48.00	42.00
5	20.00	55.00	45.00
6	25.00	70.00	60.00
7	30.00	76.00	64.00
8	35.00	86.00	74.00
9	40.00	85.00	75.00
10	45.50	88.00	72.00
11	50.00	91.00	79.00
12	55.00	97.00	83.00
13	60.00	102.00	88.00
14	65.00	110.00	90.00
15	70.00	110.00	100.00

Note: Correct any mistakes here.

CORRECTIONS (Y/N)?

16	75.00	111.00	99.00
17	80.00	112.00	98.00
18	85.00	114.00	106.00
19	90.00	116.00	114.50
20	95.00	117.00	113.00
21	100.00	120.00	116.00
22	105.00	122.00	118.00
23	110.00	123.00	117.00
24	115.00	124.00	122.00
25	120.00	125.00	125.00

INPUT: POINT NUMBER , DISPLACEMENT , LOADING PRESSURE ,UNLOADING PRESSURE? 19,90
,116,114

1. **INPUT MEMBRANE CALIBRATION**
2. **INPUT VOLUME CALIBRATION**
3. **INPUT PMT TEST**
4. **USE STORED PMT TEST DATA**
5. **PLOT TEST ON SCREEN**
6. **PLOT TEST ON PLOTTER**
7. NONE

CHOICE? 2

NUMBER OF POINTS= ? 25

```
PRESSURE  1 LOADING DISPLACEMENT 1 UNLOADING DISPLACEMENT 1 ? 30,0,0
PRESSURE  2 LOADING DISPLACEMENT 2 UNLOADING DISPLACEMENT 2 ? 100,5.8,5.4
PRESSURE  3 LOADING DISPLACEMENT 3 UNLOADING DISPLACEMENT 3 ? 150,8.6,8.2
PRESSURE  4 LOADING DISPLACEMENT 4 UNLOADING DISPLACEMENT 4 ? 200,10.8,10.2
PRESSURE  5 LOADING DISPLACEMENT 5 UNLOADING DISPLACEMENT 5 ? 250,12.4,11.4
PRESSURE  6 LOADING DISPLACEMENT 6 UNLOADING DISPLACEMENT 6 ? 300,13.5,12.5
PRESSURE  7 LOADING DISPLACEMENT 7 UNLOADING DISPLACEMENT 7 ? 350,14.6,13.3
PRESSURE  8 LOADING DISPLACEMENT 8 UNLOADING DISPLACEMENT 8 ? 400,15.5,14
PRESSURE  9 LOADING DISPLACEMENT 9 UNLOADING DISPLACEMENT 9 ? 450,15.9,14.7
PRESSURE  10 LOADING DISPLACEMENT 10 UNLOADING DISPLACEMENT 10 ? 500,16.6,15.3
PRESSURE  11 LOADING DISPLACEMENT 11 UNLOADING DISPLACEMENT 11 ? 600,17.5,16
PRESSURE  12 LOADING DISPLACEMENT 12 UNLOADING DISPLACEMENT 12 ? 700,18.2,16.8
PRESSURE  13 LOADING DISPLACEMENT 13 UNLOADING DISPLACEMENT 13 ? 800,18.8,17.6
PRESSURE  14 LOADING DISPLACEMENT 14 UNLOADING DISPLACEMENT 14 ? 900,19.5,18
PRESSURE  15 LOADING DISPLACEMENT 15 UNLOADING DISPLACEMENT 15 ? 1000,20,19.5
PRESSURE  16 LOADING DISPLACEMENT 16 UNLOADING DISPLACEMENT 16 ? 1100,20.5,19
PRESSURE  17 LOADING DISPLACEMENT 17 UNLOADING DISPLACEMENT 17 ? 1200,20.65,19.4
5
PRESSURE  18 LOADING DISPLACEMENT 18 UNLOADING DISPLACEMENT 18 ? 1300,21,19.8
PRESSURE  19 LOADING DISPLACEMENT 19 UNLOADING DISPLACEMENT 19 ? 1400,21.5,20
PRESSURE  20 LOADING DISPLACEMENT 20 UNLOADING DISPLACEMENT 20 ? 1500,22,20.2
PRESSURE  21 LOADING DISPLACEMENT 21 UNLOADING DISPLACEMENT 21 ? 1600,21.9,20.75

PRESSURE  22 LOADING DISPLACEMENT 22 UNLOADING DISPLACEMENT 22 ? 1700,21.9,21.3
PRESSURE  23 LOADING DISPLACEMENT 23 UNLOADING DISPLACEMENT 23 ? 1800,22.4,21.4
PRESSURE  24 LOADING DISPLACEMENT 24 UNLOADING DISPLACEMENT 24 ? 1900,22.3,21.9
PRESSURE  25 LOADING DISPLACEMENT 25 UNLOADING DISPLACEMENT 25 ? 2000,22.3,22.[illegible]
```

POINT NO.	PRESSURE	LOADING DISPLACEMENT	UNLOADING DISPLACEMENT
1	30.00	0.00	0.00
2	100.00	5.80	5.40
3	150.00	8.60	8.20
4	200.00	10.80	10.20
5	250.00	12.40	11.40
6	300.00	13.50	12.50
7	350.00	14.60	13.30
8	400.00	15.50	14.00
9	450.00	15.90	14.70
10	500.00	16.60	15.30
11	600.00	17.50	16.00
12	700.00	18.20	16.80
13	800.00	18.80	17.60
14	900.00	19.50	18.00
15	1000.00	20.00	19.50

CORRECTIONS (Y/N)?

POINT NO.	PRESSURE	LOADING DISPLACEMENT	UNLOADING DISPLACEMENT
16	1100.00	20.50	19.00
17	1200.00	20.65	19.45
18	1300.00	21.00	19.80
19	1400.00	21.50	20.00
20	1500.00	22.00	20.20
21	1600.00	21.90	20.75
22	1700.00	21.90	21.30
23	1800.00	22.40	21.40
24	1900.00	22.30	21.90
25	2000.00	22.30	22.30

CORRECTIONS (Y/N)?

WHAT MULTIPLIER TO GET VOLUME READINGS IN CM^3:

1. MULTIPLIER = 1.0
2. MULTIPLIER = 193.05
3. OTHER

? 1

WHAT UNITS ARE PRESSURE READINGS IN?

1. bars
2. kg/cm^2
3. kPa
4. other

? 3

VOLUME CALIBRATION

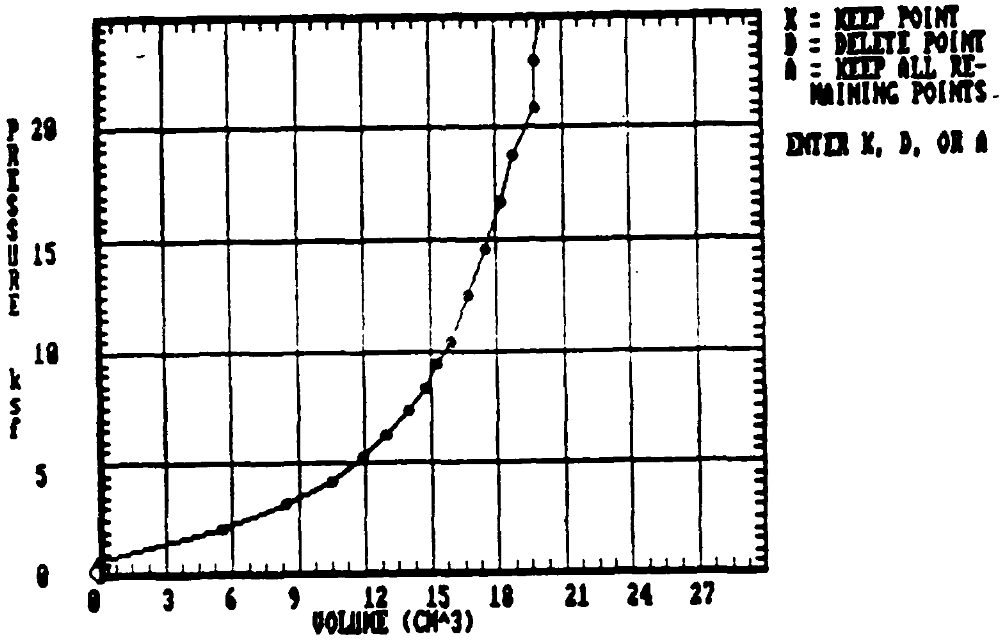

This screen allows for the adjustment of the volume calibration curve to account for the size of the steel calibration tube. A large circle *now located on the first point at the origin* moves along the curve and allows the user to keep the point (K), delete the point (D) or keep all remaining points (A). The program draws a straight line between the first two points that are kept and re-zeroes the calibration curve at the intersection of this line with the volume axis

```
WHAT DRIVE TO SAVE VOLUME CALIBRATION DATA ON (A/B/C)? c

WHAT FILE NAME TO SAVE VOLUME CALIBRATION DATA (8 CHARACTERS MAX.)? volume

DATA WILL BE SAVED AS c:volume.CAL

IS THIS CORRECT (Y/N)? y
```

```
                    1. INPUT MEMBRANE CALIBRATION
                    2. INPUT VOLUME CALIBRATION
                    3. INPUT PMT TEST
                    4. USE STORED PMT TEST DATA
                    5. PLOT TEST ON SCREEN
                    6. PLOT TEST ON PLOTTER
                    7. NONE

          CHOICE? 3
```

```
WHAT DRIVE TO SAVE PMT DATA ON (A/B/C)? c

WHAT FILE NAME TO SAVE PMT DATA IN (8 CHAR. MAX.)? ea375apt

FILES WILL BE SAVED AS: c:ea375apt.RAW
                        c:ea375apt.DAT
                        c:ea375apt.RST

IS THIS CORRECT? y
```

```
NUMBER OF POINTS= ? 70

NUMBER OF CYCLES=? 10

DISPLACEMENT  1 PRESSURE  1 TIME (min)  1 ? 0,-5,
DISPLACEMENT  2 PRESSURE  2 TIME (min)  2 ? 2,0,
DISPLACEMENT  3 PRESSURE  3 TIME (min)  3 ? 4.3,5
?Redo from start
? 4.5,5,
DISPLACEMENT  4 PRESSURE  4 TIME (min)  4 ? 6,15,
DISPLACEMENT  5 PRESSURE  5 TIME (min)  5 ? 8,45,
DISPLACEMENT  6 PRESSURE  6 TIME (min)  6 ? 10,85,
DISPLACEMENT  7 PRESSURE  7 TIME (min)  7 ? 15,200,
DISPLACEMENT  8 PRESSURE  8 TIME (min)  8 ? 20,340,
DISPLACEMENT  9 PRESSURE  9 TIME (min)  9 ? 25,470,
DISPLACEMENT  10 PRESSURE  10 TIME (min)  10 ? 30,575,
DISPLACEMENT  11 PRESSURE  11 TIME (min)  11 ? 27,275,
DISPLACEMENT  12 PRESSURE  12 TIME (min)  12 ? 30.3,575,
DISPLACEMENT  13 PRESSURE  13 TIME (min)  13 ? 27.5,275,
DISPLACEMENT  14 PRESSURE  14 TIME (min)  14 ? 30.6,575,
DISPLACEMENT  15 PRESSURE  15 TIME (min)  15 ? 27.85,275,
DISPLACEMENT  16 PRESSURE  16 TIME (min)  16 ? 30.95,575,
DISPLACEMENT  17 PRESSURE  17 TIME (min)  17 ? 28.25,275,
DISPLACEMENT  18 PRESSURE  18 TIME (min)  18 ? 31.1,575,
DISPLACEMENT  19 PRESSURE  19 TIME (min)  19 ? 28.35,275,
DISPLACEMENT  20 PRESSURE  20 TIME (min)  20 ? 31.3,575,
DISPLACEMENT  21 PRESSURE  21 TIME (min)  21 ? 28.75,275,
DISPLACEMENT  22 PRESSURE  22 TIME (min)  22 ? 31.4,575,
DISPLACEMENT  23 PRESSURE  23 TIME (min)  23 ? 28.9,275,
DISPLACEMENT  24 PRESSURE  24 TIME (min)  24 ? 31.6,575,
DISPLACEMENT  25 PRESSURE  25 TIME (min)  25 ? 29,275,
DISPLACEMENT  26 PRESSURE  26 TIME (min)  26 ? 31.7,575,
DISPLACEMENT  27 PRESSURE  27 TIME (min)  27 ? 29.25,275,
DISPLACEMENT  28 PRESSURE  28 TIME (min)  28 ? 31.8,575,
DISPLACEMENT  29 PRESSURE  29 TIME (min)  29 ? 35,660,
DISPLACEMENT  30 PRESSURE  30 TIME (min)  30 ? 40,725,
DISPLACEMENT  31 PRESSURE  31 TIME (min)  31 ? 45,780,0
DISPLACEMENT  32 PRESSURE  32 TIME (min)  32 ? 45.3,780,.25
DISPLACEMENT  33 PRESSURE  33 TIME (min)  33 ? 45.6,780,.5
DISPLACEMENT  34 PRESSURE  34 TIME (min)  34 ? 45.85,780,.75
DISPLACEMENT  35 PRESSURE  35 TIME (min)  35 ? 46.1,780,1
DISPLACEMENT  36 PRESSURE  36 TIME (min)  36 ? 46.25,780,1.25
DISPLACEMENT  37 PRESSURE  37 TIME (min)  37 ? 46.4,780,1.5
DISPLACEMENT  38 PRESSURE  38 TIME (min)  38 ? 46.5,780,1.75
DISPLACEMENT  39 PRESSURE  39 TIME (min)  39 ? 46.7,780,2
DISPLACEMENT  40 PRESSURE  40 TIME (min)  40 ? 46.8,780,2.25
```

```
DISPLACEMENT  40 PRESSURE  40 TIME (min)  40 ? 46.8,780,2.25
DISPLACEMENT  41 PRESSURE  41 TIME (min)  41 ? 46.95,47.15,2.5
DISPLACEMENT  42 PRESSURE  42 TIME (min)  42 ? 47.15,780,3
DISPLACEMENT  43 PRESSURE  43 TIME (min)  43 ? 47.4,780,3.5
DISPLACEMENT  44 PRESSURE  44 TIME (min)  44 ? 47.6,780,4
DISPLACEMENT  45 PRESSURE  45 TIME (min)  45 ? 47.85,780,4.5
DISPLACEMENT  46 PRESSURE  46 TIME (min)  46 ? 47.95,780,5
DISPLACEMENT  47 PRESSURE  47 TIME (min)  47 ? 50,800,
DISPLACEMENT  48 PRESSURE  48 TIME (min)  48 ? 55,845,
DISPLACEMENT  49 PRESSURE  49 TIME (min)  49 ? 60,890,
DISPLACEMENT  50 PRESSURE  50 TIME (min)  50 ? 65,915,
DISPLACEMENT  51 PRESSURE  51 TIME (min)  51 ? 70,950,
DISPLACEMENT  52 PRESSURE  52 TIME (min)  52 ? 75,975,
DISPLACEMENT  53 PRESSURE  53 TIME (min)  53 ? 80,1000,
DISPLACEMENT  54 PRESSURE  54 TIME (min)  54 ? 85,1020,
DISPLACEMENT  55 PRESSURE  55 TIME (min)  55 ? 90.1,1040,
DISPLACEMENT  56 PRESSURE  56 TIME (min)  56 ? 95,1055,
DISPLACEMENT  57 PRESSURE  57 TIME (min)  57 ? 100,1070,
DISPLACEMENT  58 PRESSURE  58 TIME (min)  58 ? 105,1090,
DISPLACEMENT  59 PRESSURE  59 TIME (min)  59 ? 110,1105,
DISPLACEMENT  60 PRESSURE  60 TIME (min)  60 ? 115,1120,
DISPLACEMENT  61 PRESSURE  61 TIME (min)  61 ? 120,1125,
DISPLACEMENT  62 PRESSURE  62 TIME (min)  62 ? 119.5,925,
DISPLACEMENT  63 PRESSURE  63 TIME (min)  63 ? 119,840,
DISPLACEMENT  64 PRESSURE  64 TIME (min)  64 ? 117.9,740,
DISPLACEMENT  65 PRESSURE  65 TIME (min)  65 ? 115,585,
DISPLACEMENT  66 PRESSURE  66 TIME (min)  66 ? 114.1,550,
DISPLACEMENT  67 PRESSURE  67 TIME (min)  67 ? 114.6,680,
DISPLACEMENT  68 PRESSURE  68 TIME (min)  68 ? 114.1,565,
DISPLACEMENT  69 PRESSURE  69 TIME (min)  69 ? 112,490,
DISPLACEMENT  70 PRESSURE  70 TIME (min)  70 ? 105,330,
```

POINT NO.	DISPLACEMENT	PRESSURE	TIME
1	0.00	-5.00	0.00
2	2.00	0.00	0.00
3	4.30	5.00	0.00
4	6.00	15.00	0.00
5	8.00	45.00	0.00
6	10.00	85.00	0.00
7	15.00	200.00	0.00
8	20.00	340.00	0.00
9	25.00	470.00	0.00
10	30.00	575.00	0.00
11	27.00	275.00	0.00
12	30.30	575.00	0.00
13	27.50	275.00	0.00
14	30.60	575.00	0.00
15	27.85	275.00	0.00

CORRECTIONS (Y/N)?

POINT NO.	DISPLACEMENT	PRESSURE	TIME
16	30.95	575.00	0.00
17	28.25	275.00	0.00
18	31.10	575.00	0.00
19	28.35	275.00	0.00
20	31.30	575.00	0.00
21	28.75	275.00	0.00
22	31.40	575.00	0.00
23	28.90	275.00	0.00
24	31.60	575.00	0.00
25	29.00	275.00	0.00
26	31.70	575.00	0.00
27	29.25	275.00	0.00
28	31.80	575.00	0.00
29	35.00	660.00	0.00
30	40.00	725.00	0.00

CORRECTIONS (Y/N)?

POINT NO.	DISPLACEMENT	PRESSURE	TIME
31	45.00	780.00	0.00
32	45.30	780.00	0.25
33	45.60	780.00	0.50
34	45.85	780.00	0.75
35	46.10	780.00	1.00
36	46.25	780.00	1.25
37	46.40	780.00	1.50
38	46.50	780.00	1.75
39	46.70	780.00	2.00
40	46.80	780.00	2.25
41	46.95	47.15	2.50
42	47.15	780.00	3.00
43	47.40	780.00	3.50
44	47.60	780.00	4.00
45	47.85	780.00	4.50

CORRECTIONS (Y/N)? Y POINT NO.,DISPLACEMENT,PRESSURE,TIME, 41,46.95, 780,2.5

POINT NO.	DISPLACEMENT	PRESSURE	TIME
31	45.00	780.00	0.00
32	45.30	780.00	0.25
33	45.60	780.00	0.50
34	45.85	780.00	0.75
35	46.10	780.00	1.00
36	46.25	780.00	1.25
37	46.40	780.00	1.50
38	46.50	780.00	1.75
39	46.70	780.00	2.00
40	46.80	780.00	2.25
41	46.95	780.00	2.50
42	47.15	780.00	3.00
43	47.40	780.00	3.50
44	47.60	780.00	4.00
45	47.85	780.00	4.50

CORRECTIONS (Y/N)?

POINT NO.	DISPLACEMENT	PRESSURE	TIME
46	47.95	780.00	5.00
47	50.00	800.00	0.00
48	55.00	845.00	0.00
49	60.00	890.00	0.00
50	65.00	915.00	0.00
51	70.00	950.00	0.00
52	75.00	975.00	0.00
53	80.00	1000.00	0.00
54	85.00	1020.00	0.00
55	90.10	1040.00	0.00
56	95.00	1055.00	0.00
57	100.00	1070.00	0.00
58	105.00	1090.00	0.00
59	110.00	1105.00	0.00
60	115.00	1120.00	0.00

CORRECTIONS (Y/N)?

POINT NO.	DISPLACEMENT	PRESSURE	TIME
61	120.00	1125.00	0.00
62	119.50	925.00	0.00
63	119.00	840.00	0.00
64	117.90	740.00	0.00
65	115.00	585.00	0.00
66	114.10	550.00	0.00
67	114.60	680.00	0.00
68	114.10	565.00	0.00
69	112.00	490.00	0.00
70	105.00	330.00	0.00

CORRECTIONS (Y/N)?

```
TEST TITLE ? EASTERWOOD AIRPORT (EA-3) 61" AIRPORT PMT TEST RESULTS

INFLATABLE LENGTH OF PROBE (CM)? 24.6

INITIAL RADIUS OF PROBE (CM)? 1.666

DEPTH OF TEST (FT)? 5.08333

DEPTH TO WATER TABLE (FT)? 15

UNIT WEIGHT OF SOIL (PCF)? 130

Ko TO USE FOR Po CALCULATION? .8

INITIAL PRESSURE READING AT GAGE HEIGHT? 0

HEIGHT OF GAGE ABOVE GROUND (FT)? 3.5

WHAT IS FILE NAME OF VOLUME CALIBRATION (DRIVE:FILENAME.CAL)? A:EAVOL2.CAL

WHAT IS FILE NAME OF MEMBRANE CALIBRATION (DRIVE:FILENAME.CAL)? A:EAMEM2.CAL



                        CHECK INPUT INFORMATION
Press <return> to move to next item.  Retype necessary changes.


TEST TITLE:  EASTERWOOD AIRPORT (EA-3) 61" AIRPORT PMT TEST RESULTS
INFLATABLE LENGTH OF PROBE . . . . . . . . . . .  24.6         CM
INITIAL RADIUS OF PROBE  . . . . . . . . . . . .  1.666        CM
DEPTH OF TEST  . . . . . . . . . . . . . . . . .  5.08333      FT
DEPTH TO WATER TABLE . . . . . . . . . . . . . .  15           FT
UNIT WEIGHT OF SOIL  . . . . . . . . . . . . . .  130          PCF
Ko  . . . . . . . . . . . . . . . . . . . . . .  .8
INITIAL PRESSURE READING AT GAGE HEIGHT  . . . .  0
HEIGHT OF GAGE ABOVE GROUND  . . . . . . . . . .  3.5          FT
VOLUME CALIBRATION FILE . . . . . . . . . . . .  A:EAVOL2.CAL
MEMBRANE CALIBRATION FILE . . . . . . . . . . .  A:EAMEM2.CAL




MORE CORRECTIONS (Y/N) ?
```

```
WHAT MULTIPLIER TO GET VOLUME READINGS IN CM^3:

     1.  MULTIPLIER = 1.0
     2.  MULTIPLIER = 193.05
     3.  OTHER

? 1
```

```
WHAT UNITS ARE PRESSURE READINGS IN?

   1. bars
   2. kg/cm^2
   3. kPa
   4. other
? 3
```

COMMENT : Program pressures operate in kips per square foot.

```
****** REDUCING TEST DATA ******
******     PLEASE WAIT     ******
```

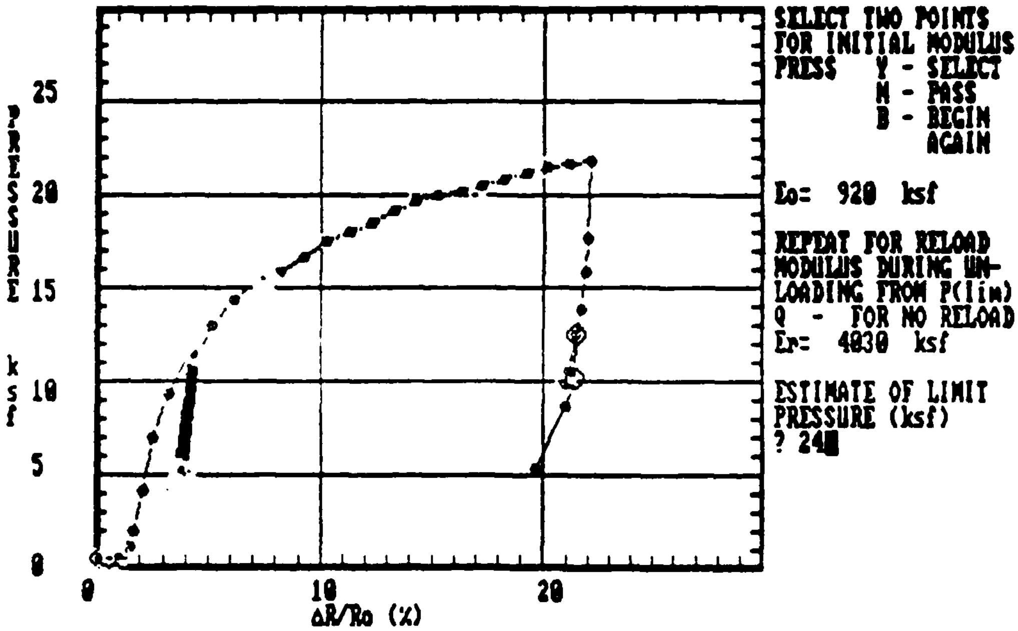

Note: This screen allows the user to specify the two points which will be used first to calculate the initial modulus and then the reload modulus which is along the first unloading portion of the curve. This is done with the large circle moving along the curve and allowing the user to (Y) select the point or (N) pass the point. After the points have been selected the user is asked for an estimate of the limit pressure.

```
        1. PRINT RESULTS
        2. PLOT RESULTS ON PLOTTER
        3. NONE

CHOICE?
```

```
INPUT FILE NAME TO SAVE CYCLIC MODULI (drive:filename.CYC)? C:EA375APT.CYC

FILE WILL BE SAVED AS C:EA375APT.CYC
IS THIS CORRECT? Y
```

```
INPUT FILE NAME TO SAVE CREEP MODULI (drive:filename.CRP)? C:EA375APT.CRP

FILE WILL BE SAVED AS C:EA375APT.CRP
IS THIS CORRECT? Y
```

```
INPUT FILE NAME TO SAVE ACCUMULATED STRAINS(drive:filename.ACC)? C:EA375APT.ACC

FILE WIL BE SAVED AS C:EA375APT.ACC
IS THIS CORRECT (Y/N)? Y
```

TURN PRINTER ON

PRESS ANY KEY TO CONTINUE

EASTERWOOD AIRPORT (EA-3) 61"-DEPTH CPMT STANDARD AIRPORT TEST

POINT NUMBER	MEASURED VOLUME	MEASURED PRESSURE	CORR. VOL. INCREASE (cm^3)	dR/Ro (%)	CORRECTED PRESSURE (ksf)	CYCLE NO. (N)	TIME (min)
1	0.000	-5.0	0.00	0.00	0.43	0	0.00
2	2.000	0.0	1.86	0.43	0.45	0	0.00
3	4.300	5.0	4.02	0.93	0.46	0	0.00
4	6.000	15.0	5.44	1.26	0.60	0	0.00
5	8.000	45.0	6.60	1.53	1.14	0	0.00
6	10.000	85.0	7.48	1.73	1.89	0	0.00
7	15.000	200.0	9.26	2.14	4.08	0	0.00
8	20.000	340.0	11.09	2.55	6.90	0	0.00
9	25.000	470.0	14.30	3.28			

					9.30	0	0.00
10	30.000	575.0	18.32	4.18	11.39	1	0.00
11	27.000	275.0	15.32	3.51	5.19	2	0.00
12	30.300	575.0	18.62	4.25	11.38	2	0.00
13	27.500	275.0	15.82	3.62	5.18	3	0.00
14	30.600	575.0	18.92	4.32	11.37	3	0.00
15	27.850	275.0	16.17	3.70	5.17	4	0.00
16	30.950	575.0	19.27	4.40	11.35	4	0.00
17	28.250	275.0	16.57	3.79	5.16	5	0.00
18	31.100	575.0	19.42	4.43	11.35	5	0.00
19	28.350	275.0	16.67	3.81	5.16	6	0.00
20	31.300	575.0	19.62	4.47	11.34	6	0.00
21	28.750	275.0	17.07	3.90	5.15	7	0.00
22	31.400	575.0	19.72	4.50	11.33	7	0.00
23	28.900	275.0	17.22	3.94	5.15	8	0.00
24	31.600	575.0	19.92	4.54	11.32	8	0.00
25	29.000	275.0	17.32	3.96	5.15	9	0.00
26	31.700	575.0	20.02	4.56	11.32	9	0.00
27	29.250	275.0	17.57	4.02	5.14	10	0.00
28	31.800	575.0	20.12	4.58	11.32	11	0.00
29	35.000	660.0	22.66	5.15	12.96	0	0.00
30	40.000	725.0	27.19	6.15	14.31	0	0.00
31	45.000	780.0	31.81	7.16	15.46	0	0.00
32	45.300	780.0	32.11	7.22	15.46	0	0.25
33	45.600	780.0	32.41	7.29	15.46	0	0.50
34	45.850	780.0	32.66	7.34	15.45	0	0.75
35	46.100	780.0	32.91	7.40	15.45	0	1.00
36	46.250	780.0	33.06	7.43	15.44	0	1.25
37	46.400	780.0	33.21	7.46	15.44	0	1.50
38	46.500	780.0	33.31	7.48	15.44	0	1.75
39	46.700	780.0	33.51	7.53	15.43	0	2.00
40	46.800	780.0	33.61	7.55	15.43	0	2.25
41	46.950	780.0	33.76	7.58	15.43	0	2.50
42	47.150	780.0	33.96	7.62	15.42	0	3.00
43	47.400	780.0	34.21	7.68	15.42	0	3.50
44	47.600	780.0	34.41	7.72	15.41	0	4.00
45	47.850	780.0	34.66	7.78	15.41	0	4.50
46	47.950	780.0	34.76	7.80	15.41	0	5.00
47	50.000	800.0	36.67	8.21	15.78	0	0.00
48	55.000	845.0	41.43	9.23	16.61	0	0.00
49	60.000	890.0	46.18	10.24	17.45	0	0.00
50	65.000	915.0	51.05	11.27	17.86	0	0.00
51	70.000	950.0	55.88	12.27	18.49	0	0.00
52	75.000	975.0	60.75	13.28	19.01	0	0.00
53	80.000	1000.0	65.63	14.28	19.53	0	0.00
54	85.000	1020.0	70.54	15.28	19.85	0	0.00
55	90.100	1040.0	75.55	16.28	20.16	0	0.00
56	95.000	1055.0	80.38	17.25	20.47	0	0.00
57	100.000	1070.0	85.31	18.23	20.72	0	0.00
58	105.000	1090.0	90.22	19.19	21.10	0	0.00
59	110.000	1105.0	95.17	20.15	21.41	0	0.00
60	115.000	1120.0	100.11	21.11	21.66	0	0.00
61	120.000	1125.0	105.10	22.06	21.73	0	0.00
62	119.500	925.0	104.60	21.97	17.55	0	0.00
63	119.000	840.0	104.10	21.87	15.78	0	0.00
64	117.900	740.0	103.00	21.66	13.71	0	0.00
65	115.000	585.0	100.10	21.10	10.49	0	0.00
66	114.100	550.0	99.20	20.93	9.77	0	0.00
67	114.600	680.0	102.11	21.49	12.48	0	0.00
68	114.100	565.0	101.61	21.40	10.09	0	0.00
69	112.000	490.0	99.51	20.99	8.55	0	0.00
70	105.000	330.0	92.51	19.64	5.23	0	0.00

Po = 0.5 ksf   Pl = 24.0 ksf   Pl* = 23.5 ksf
Eo = 920 ksf   E1 = 7086 ksf   E2 = 4030 ksf   Esec = 1706 ksf

EASTERWOOD AIRPORT (EA-3) 61"-DEPTH CPMT STANDARD AIRPORT TEST

TABLE OF CYCLIC AND SECANT MODULI RESULTS

CYCLE NUMBER (N)	CYCLIC MODULUS (ksf)	Ec(N) / Ec(1)	SECANT MODULUS (ksf)	Es(N) / Es(1)
2	1154.53	1.00	572.94	1.00
3	1230.74	1.07	558.71	0.98
4	1231.16	1.07	542.97	0.95
5	1341.17	1.16	536.49	0.94
6	1295.24	1.12	528.08	0.92
7	1444.38	1.25	523.97	0.91
8	1417.51	1.23	515.94	0.90
9	1417.64	1.23	512.01	0.89
10	1502.38	1.30	508.14	0.89

EASTERWOOD AIRPORT (EA-3) 61"-DEPTH CPMT STANDARD AIRPORT TEST

TABLE OF CREEP MODULI

POINT NUMBER (N)	SECANT MODULUS (ksf)	TIME (min)	Es(N) / Es(1)
32	377.45	0.25	1.00
33	373.24	0.50	0.99
34	369.72	0.75	0.98
35	366.26	1.00	0.97
36	364.21	1.25	0.96
37	362.19	1.50	0.96
38	360.86	1.75	0.96
39	358.22	2.00	0.95
40	356.91	2.25	0.95
41	354.98	2.50	0.94
42	352.42	3.00	0.93
43	349.28	3.50	0.93
44	346.81	4.00	0.92
45	343.77	4.50	0.91
46	342.57	5.00	0.91

TABLE OF ACCUMULATED STRAINS

CYCLE NUMBER (N)	ACCUMULATED STRAIN (in/in)	ACCSTR(N) / ACCSTR(1)
2	0.0118	1.0000
3	0.0130	1.0930
4	0.0137	1.1580
5	0.0146	1.2323
6	0.0148	1.2509
7	0.0157	1.3250
8	0.0160	1.3528
9	0.0162	1.3714
10	0.0168	1.4177

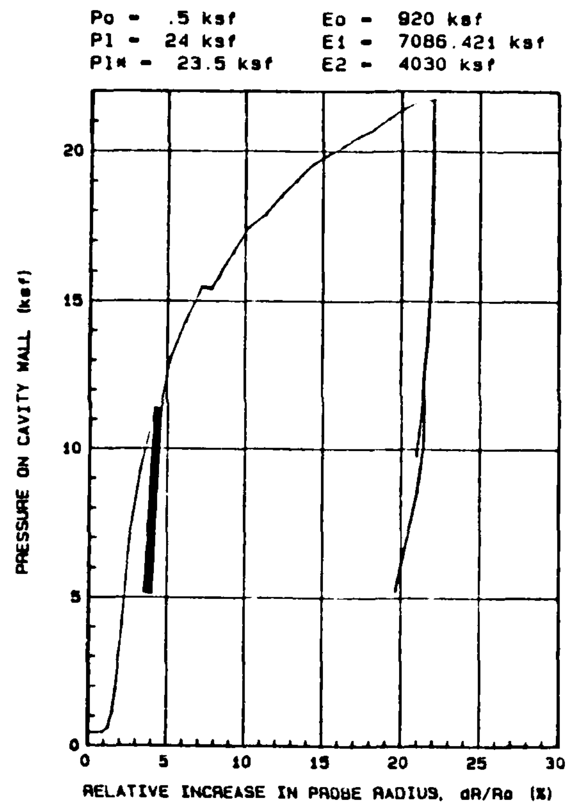

EASTERWOOD AIRPORT (EA-3) 61'-DEPTH PPMT STANDARD AIRPORT TEST

APPENDIX D

Cyclic Triaxial Test Results

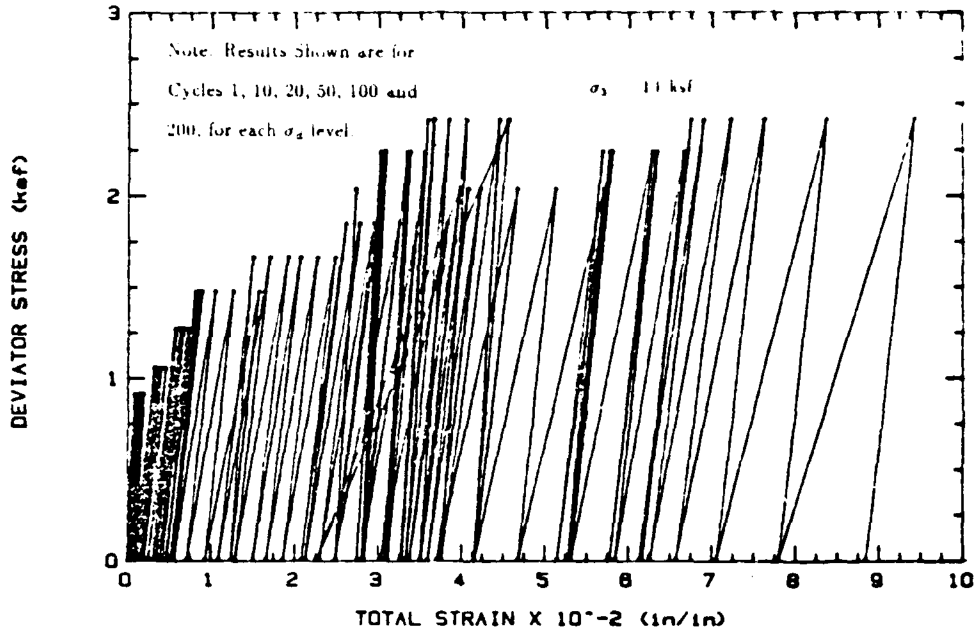

Easterwood Airport 1' Cyclic Triaxial Test Results

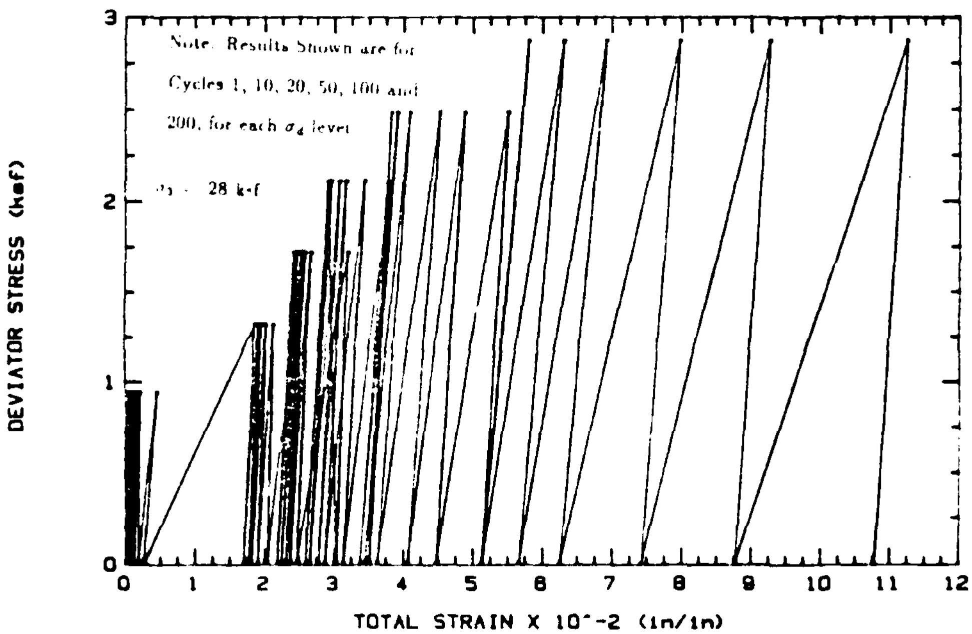

Easterwood Airport 2' Cyclic Triaxial Test Results

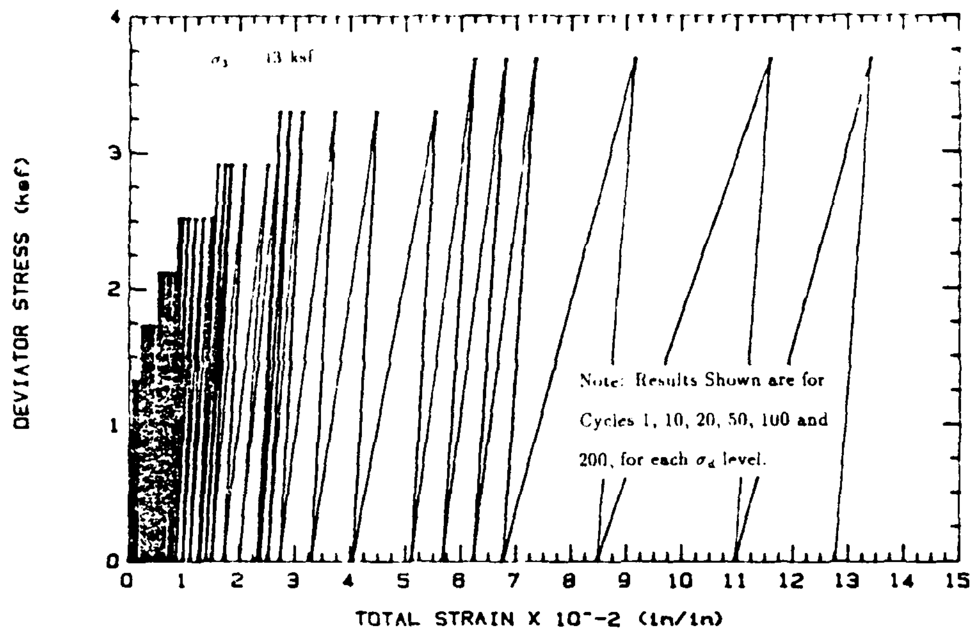

Easterwood Airport 3' Cyclic Triaxial Test Results

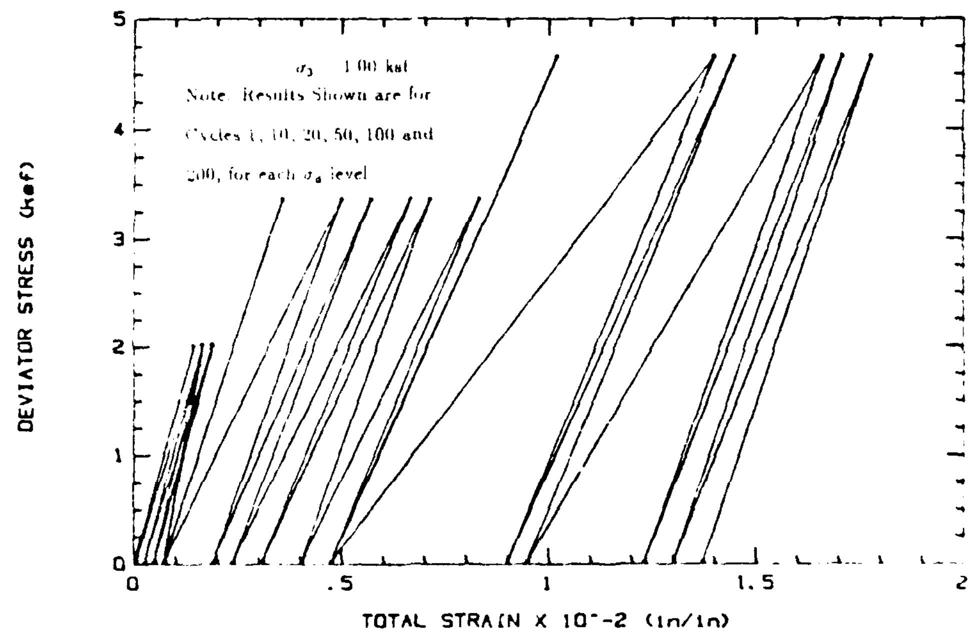

Easterwood Airport 7' Cyclic Triaxial Test Results

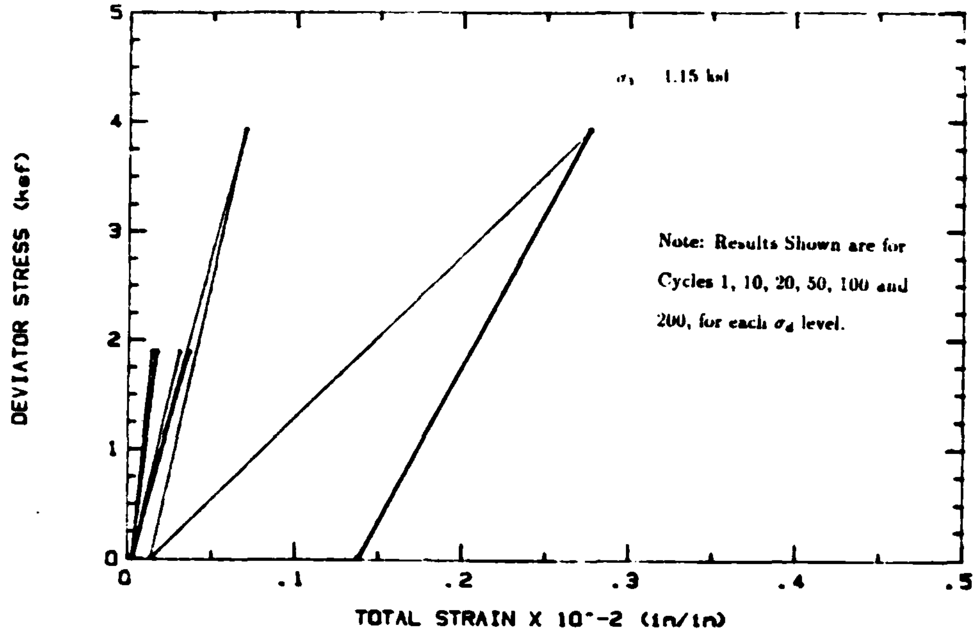

Easterwood Airport 8' Cyclic Triaxial Test Results

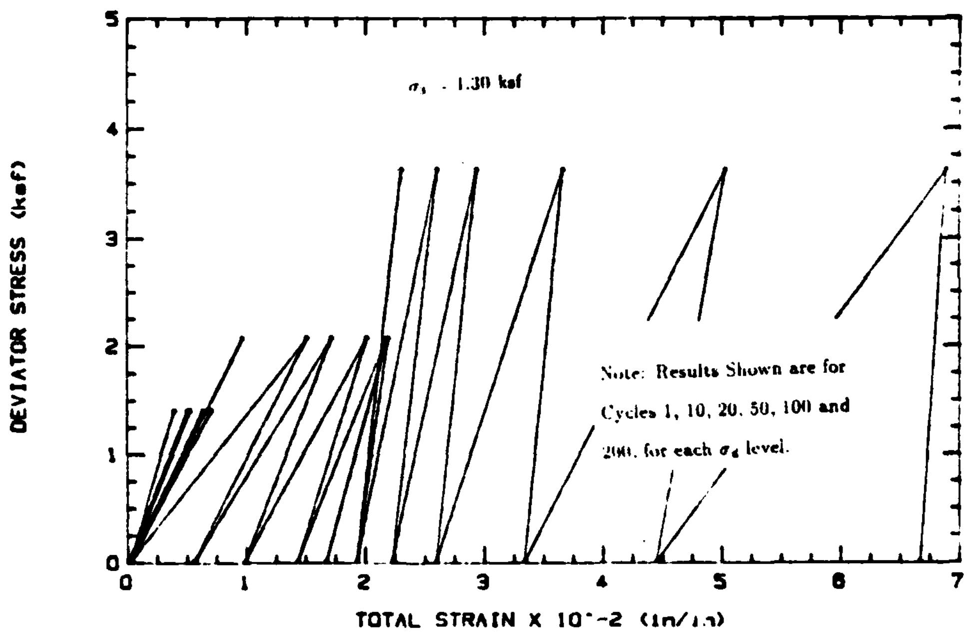

Easterwood Airport 9' Cyclic Triaxial Test Results

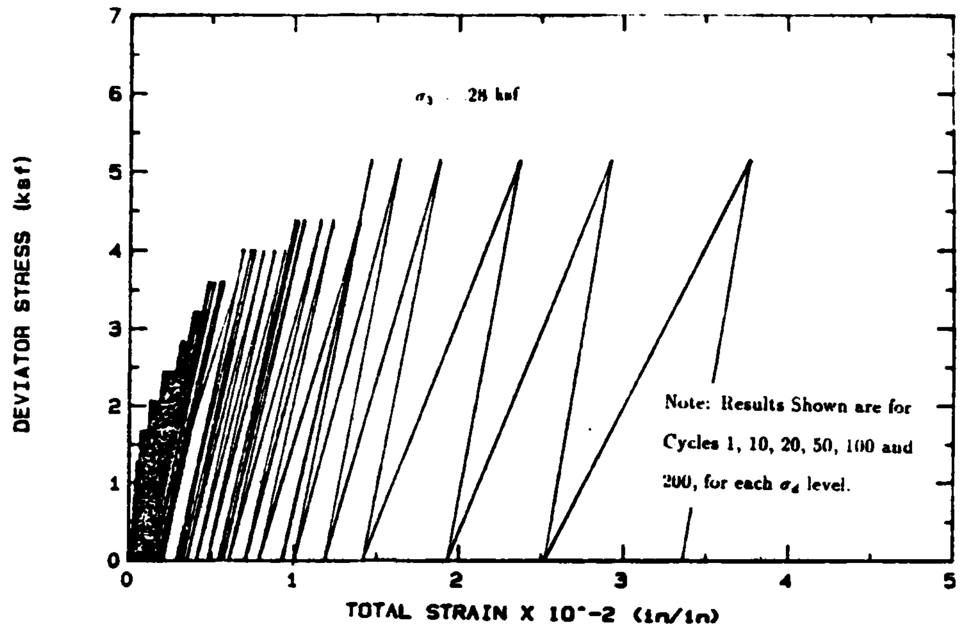

San Antonio Airport 2' Cyclic Triaxial Test Results

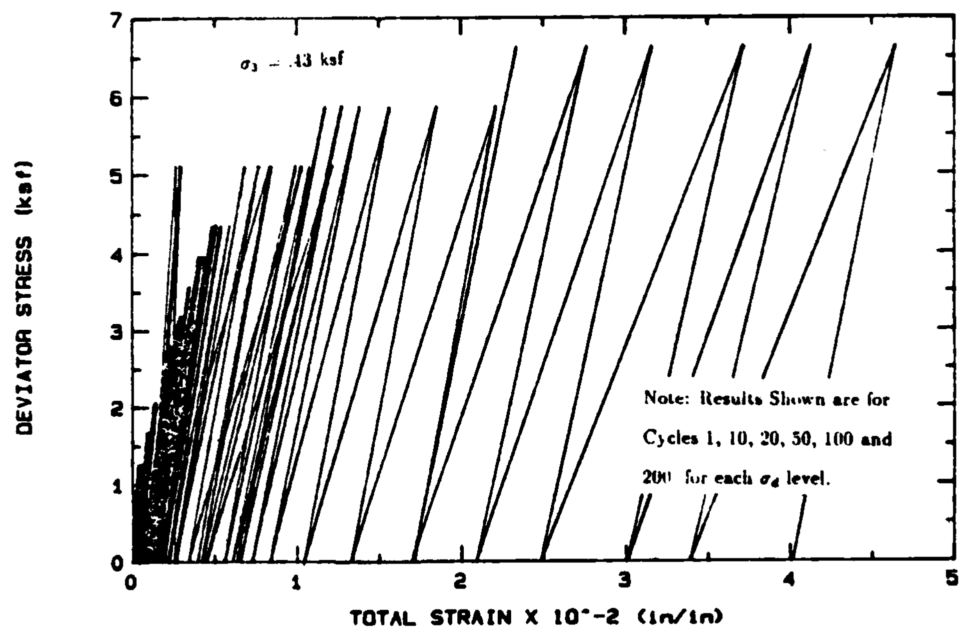

San Antonio Airport 3' Cyclic Triaxial Test Results

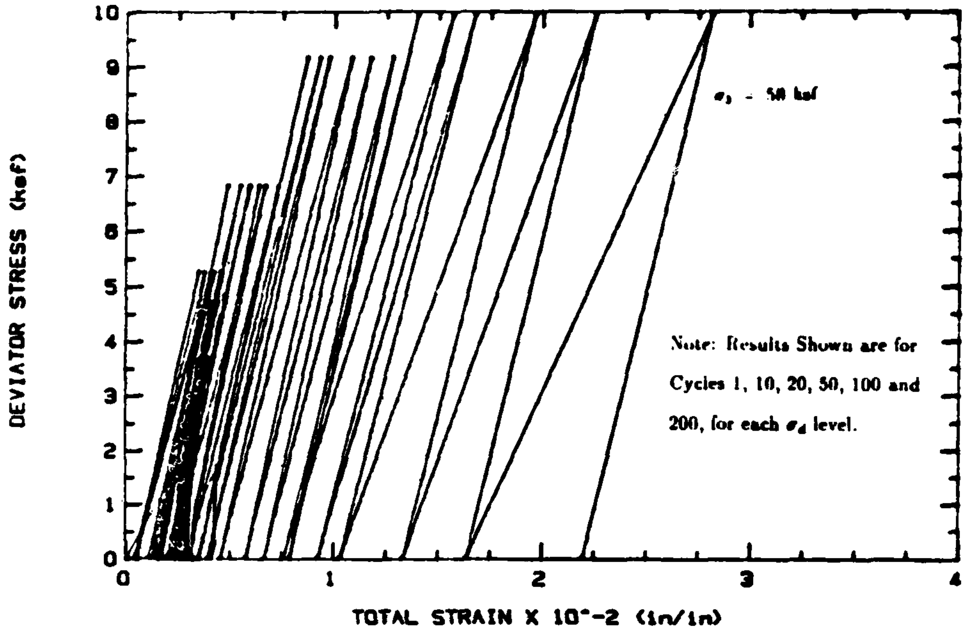

San Antonio Airport 4' Cyclic Triaxial Test Results

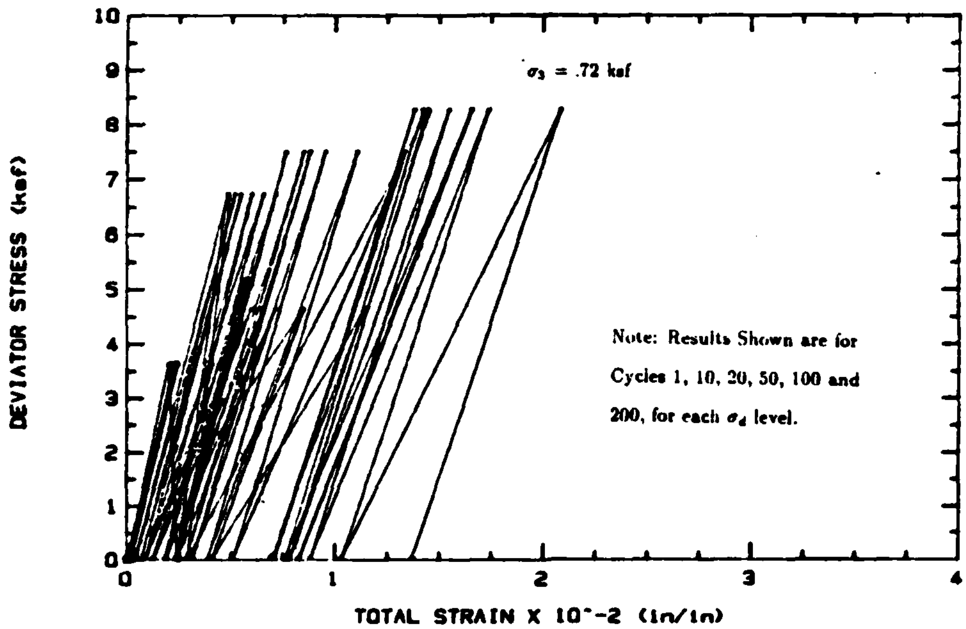

San Antonio Airport 5' Cyclic Triaxial Test Results

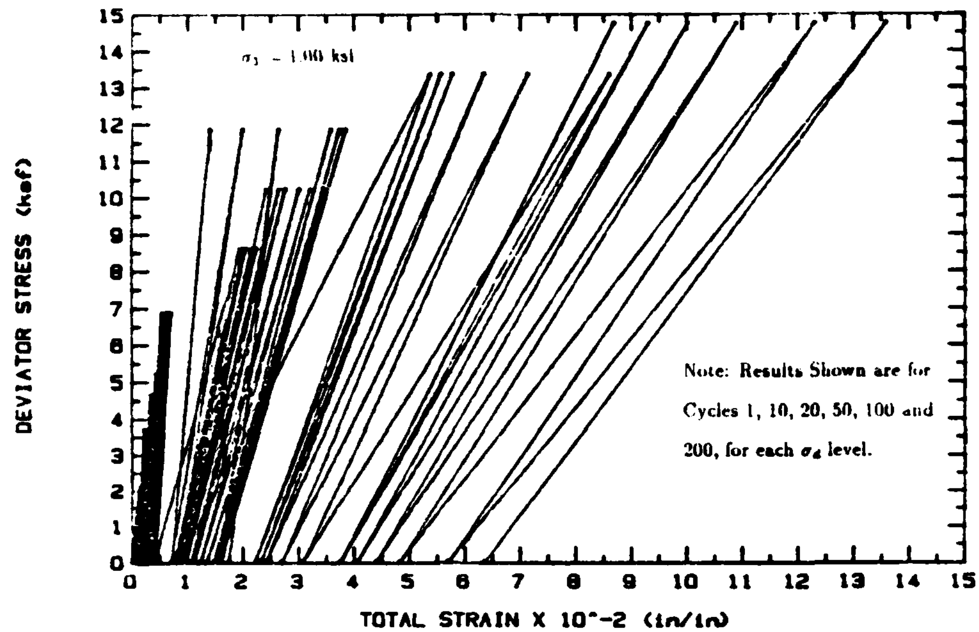

San Antonio Airport 7' Cyclic Triaxial Test Results

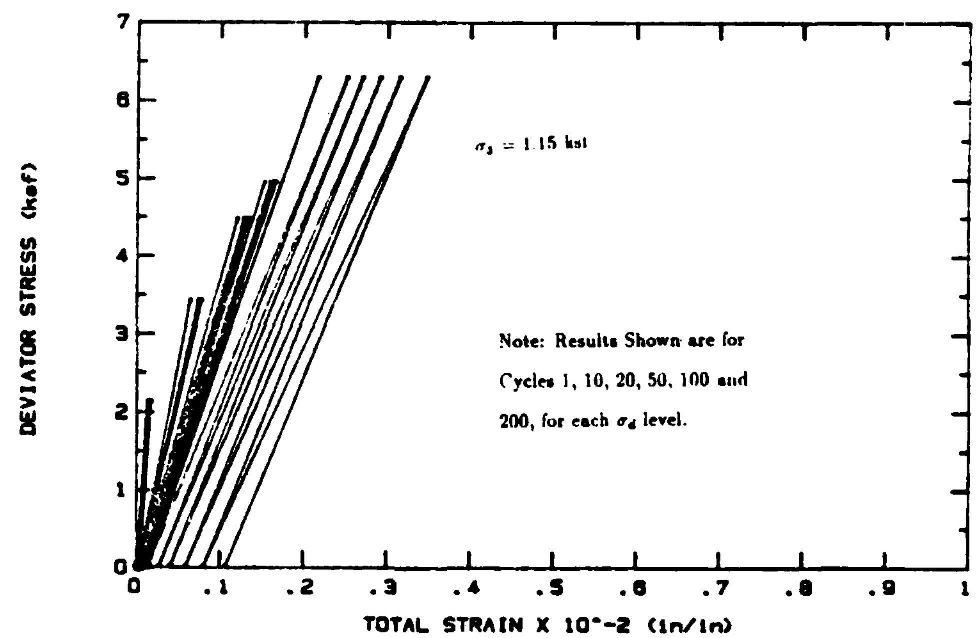

San Antonio Airport 8' Cyclic Triaxial Test Results

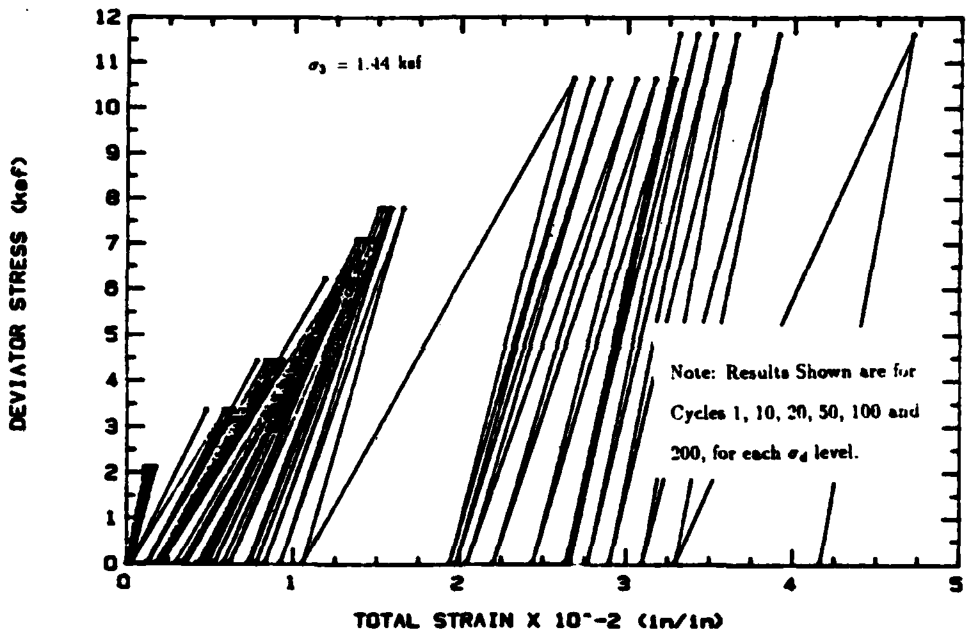

San Antonio Airport 10' Cyclic Triaxial Test Results

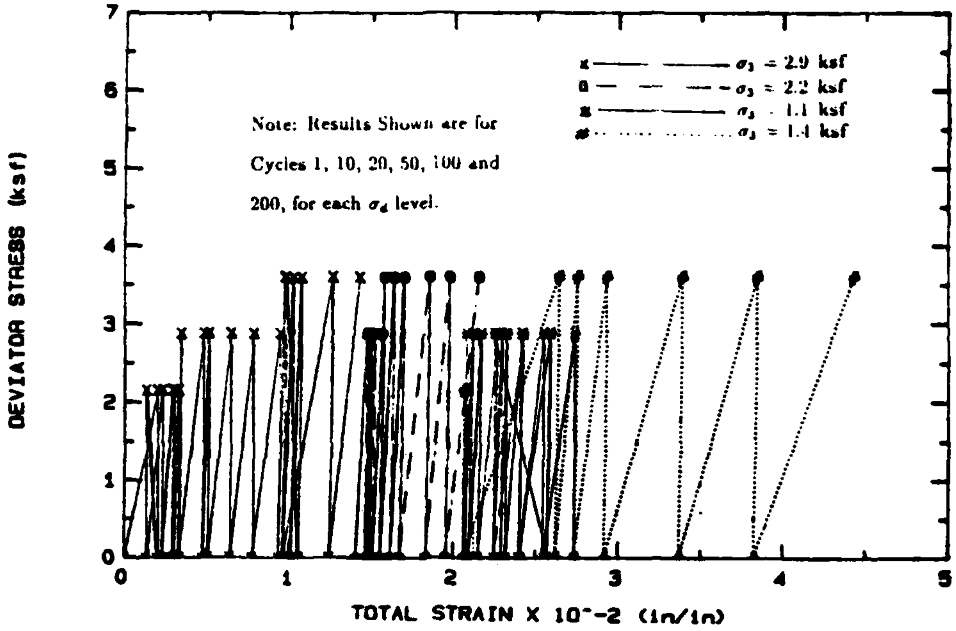

Possum Kingdom Airport 6" Cyclic Triaxial Test Results

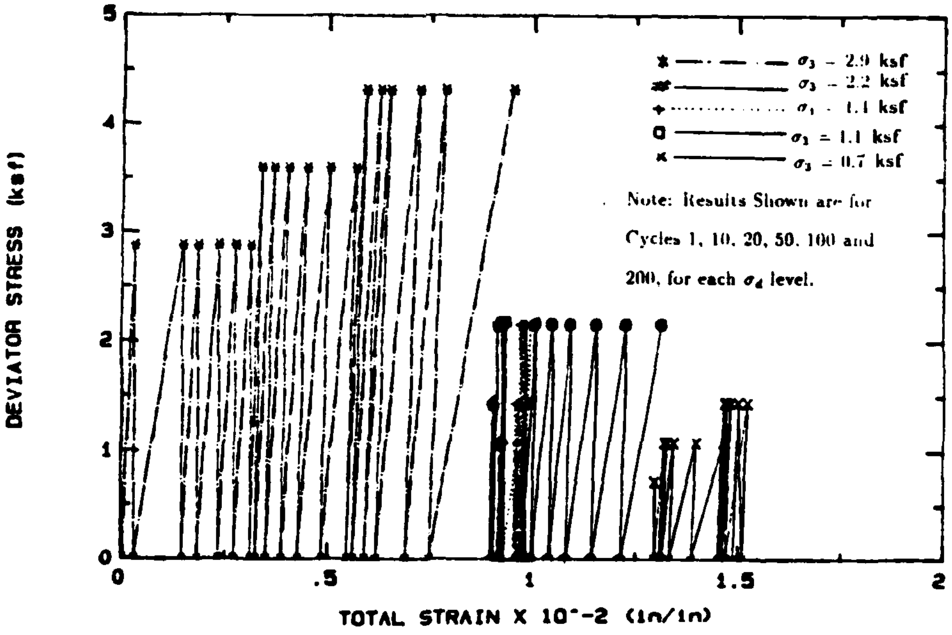

Possum Kingdom Airport 4" Cyclic Triaxial Test Results

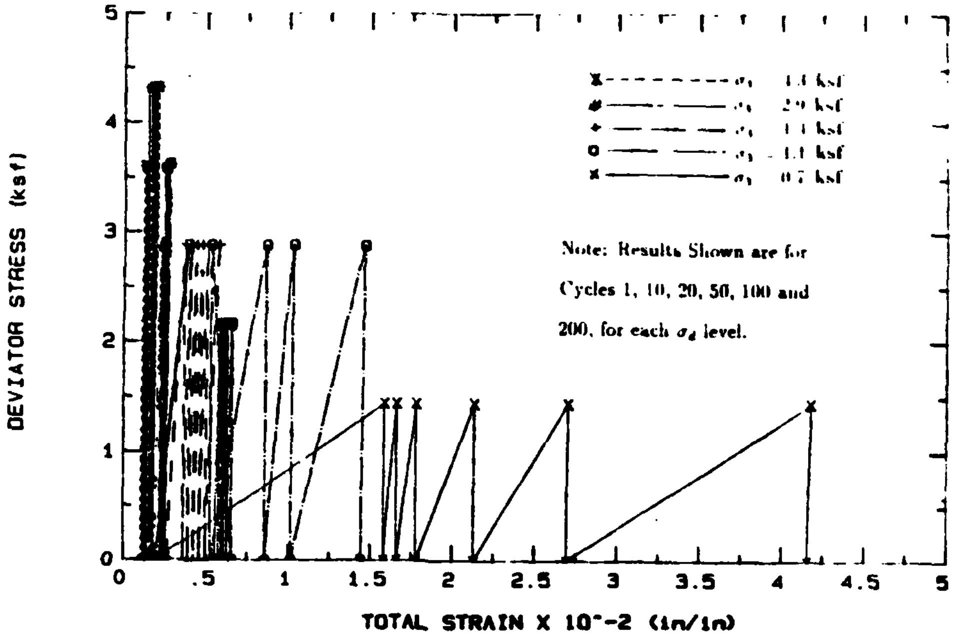

Possum Kingdom Airport 5' Cyclic Triaxial Test Results

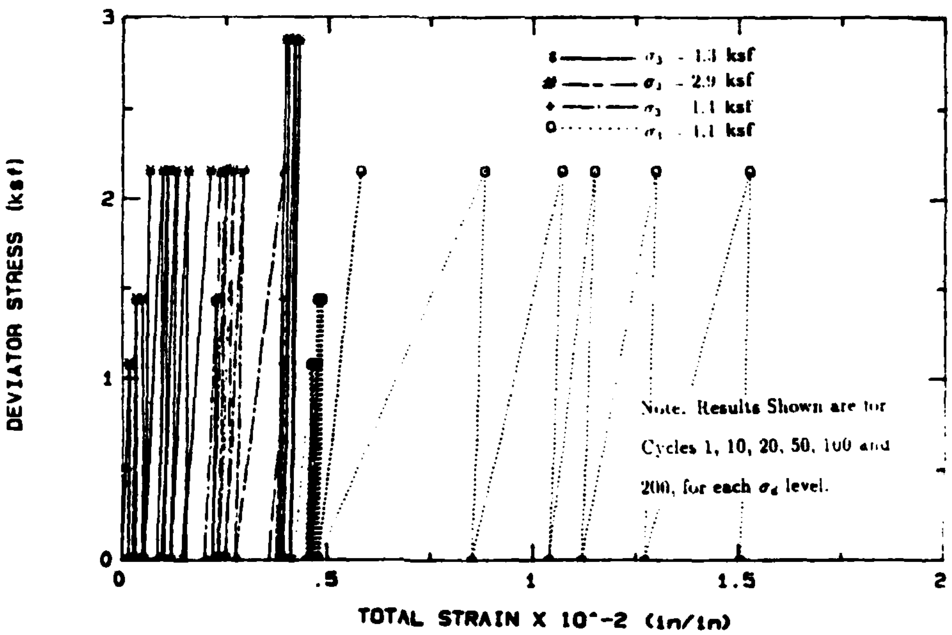

Possum Kingdom Airport 6' Cyclic Triaxial Test Results

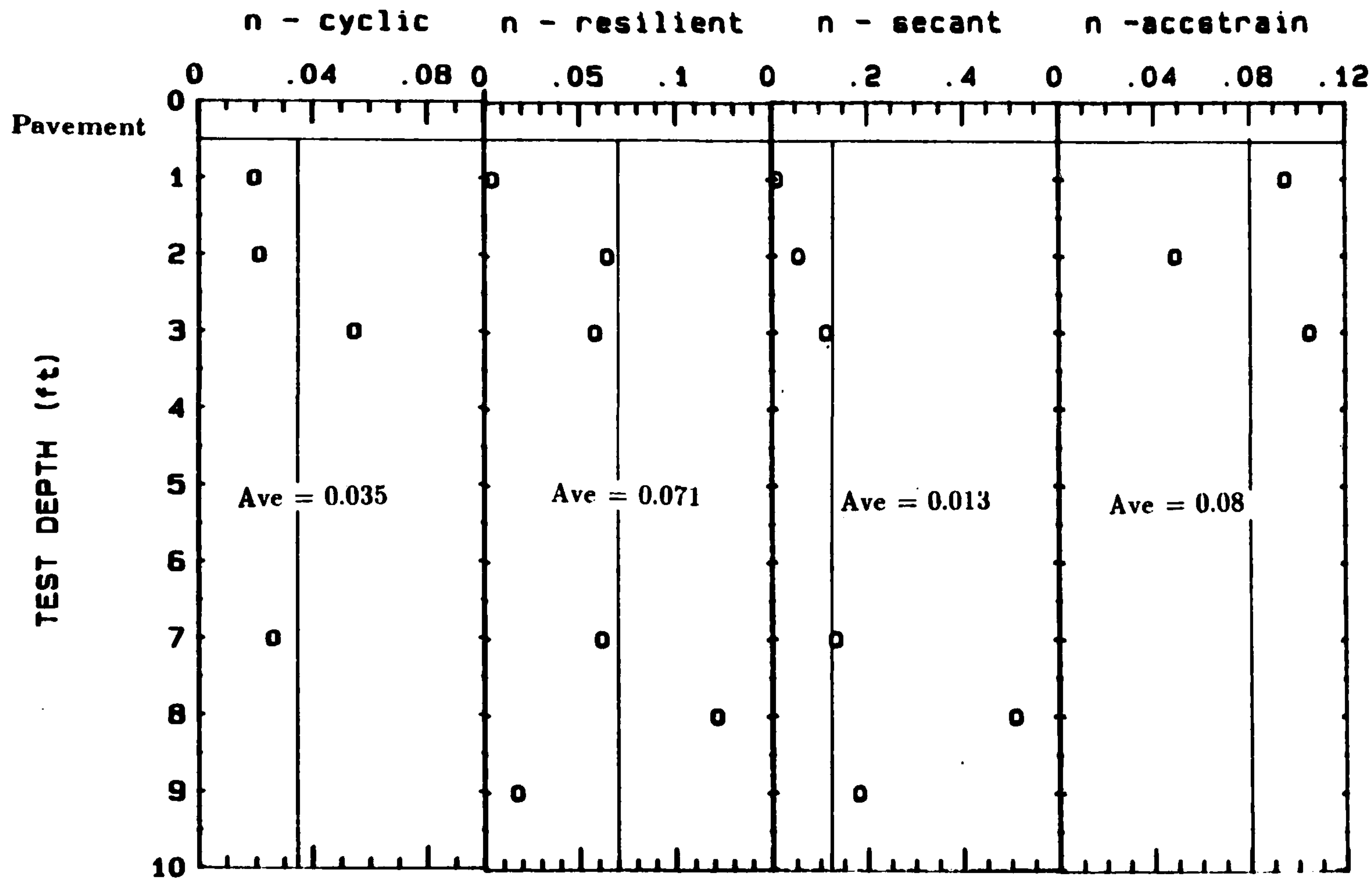

Easterwood Airport CT Power Law Exponent Summary

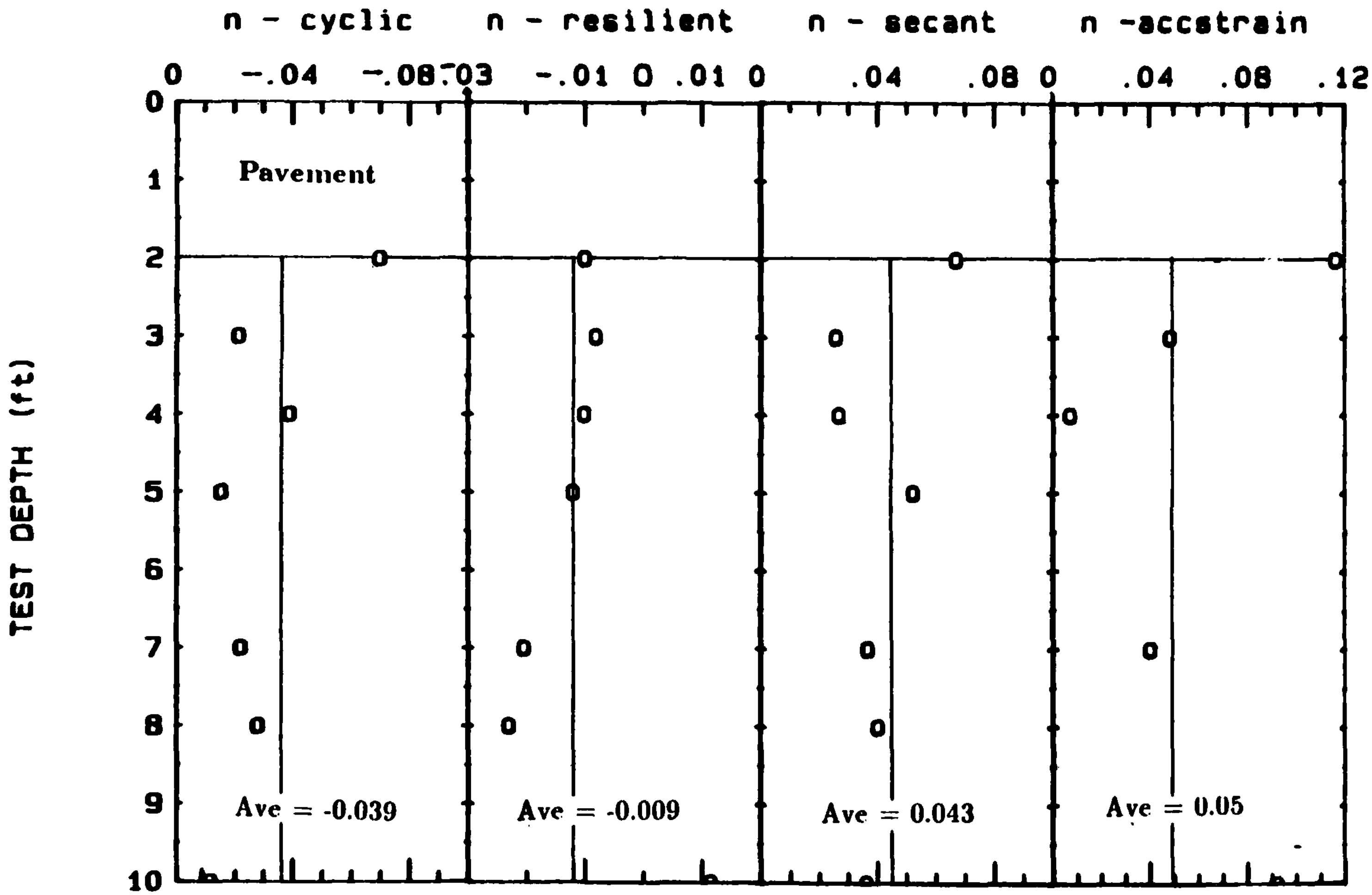

San Antonio Airport CT Power Law Exponent Summary

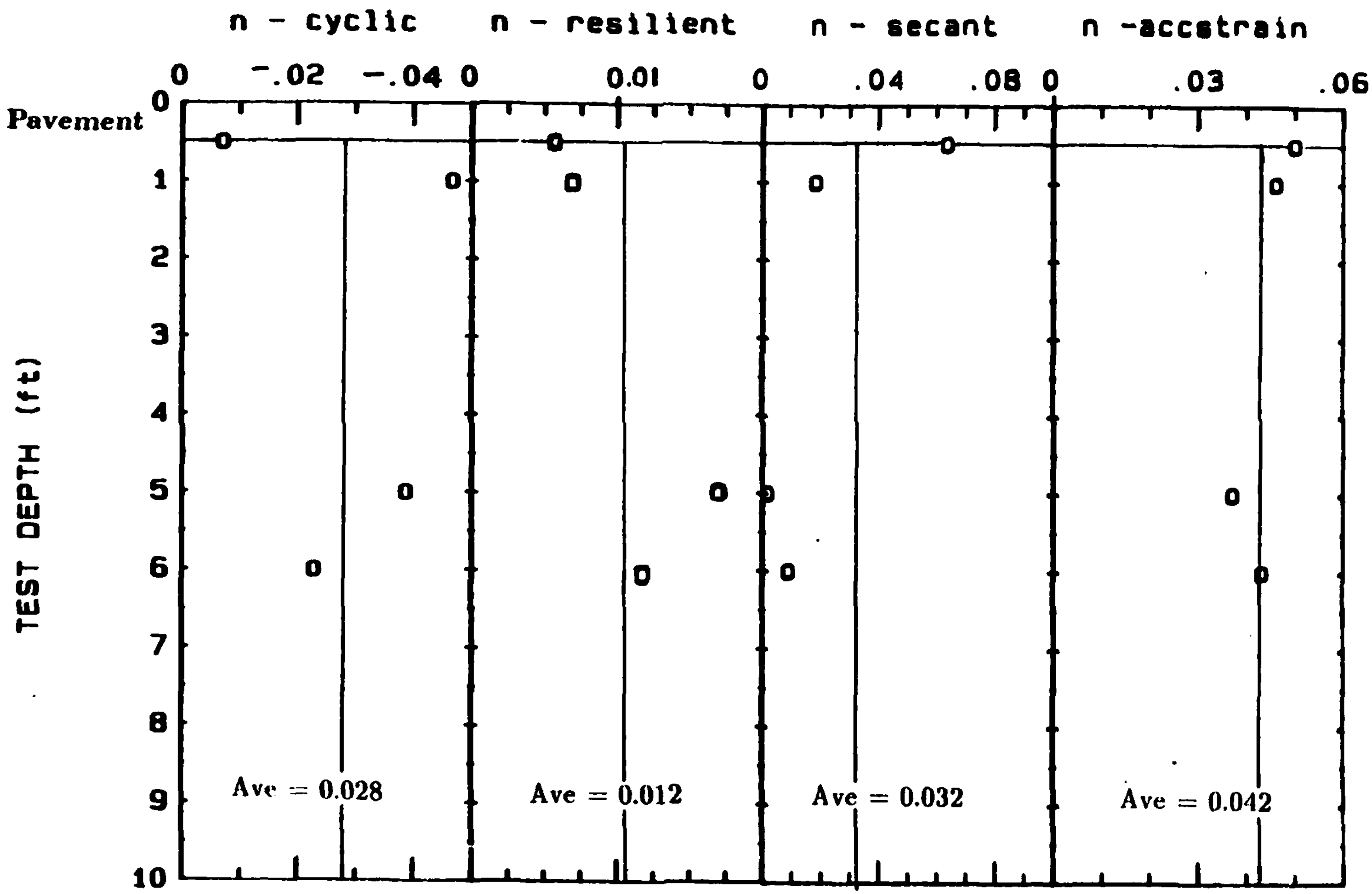

Possum Kingdom Airport CT Power Law Exponent Summary

APPENDIX E

Falling Weight Deflectometer Test Results

NOTE: These tests were performed by ERES International, Inc.

OBJECTIVE OF STUDY

The objective of this study was to determine the foundation support conditions acting at Easterwood, San Antonio International and Possum Kingdom Airports using nondestructive deflection measurements. Deflection testing was conducted on March 25-26, 1986 using the ERES falling weight deflectometer (FWD). Testing was conducted on 12 selected slabs along the apron at Easterwood Airport, on 15 selected slabs along the cargo apron area at San Antonio International Airport and at 20 selected flexible pavement locations along a taxiway at Possum Kingdom Airport.

For each PCC slab tested, loads of approximately 9,000, 13,000, 17,000 and 23,000 pounds-force were applied with surface deflections measured at seven remote locations ranging from 0" to 72" (spaced at 12 inch intervals) from the center of loading. The loading plate was positioned at central slab areas and along transverse and longitudinal joints and cracks. Additionally, repeated loading cycles were conducted on 4 slabs (1 at Easterwood and 3 at San Antonio) using a 23,000 pounds-force load.

At Possum Kingdom Airport, loads of approximately 9,000, 13,000 and 17,000 pounds-force were applied at each location. Two test locations were selected for cyclical testing using a 17,000 and a 23,000 pounds-force load. Surface deflections were measured at remote points identical to those described above.

CONCRETE PAVEMENT ANALYSIS

The initial step of the rigid pavement analysis is the determination of the elastic modulus of the concrete slab. This was done using deflection measurements taken at center slab locations at San Antonio International and Easterwood Airports along with supplied pavement thicknesses. The correct pavement thickness is important in this step of the analysis. The deflection data indicates a large deviation in thicknesses from the new apron to the old apron at Easterwood Airport. The analysis was completed using a 7 inch slab thickness along the old apron, an 11 inch slab thickness at station 1ACEN and a 9 inch pavement thickness at stations 1BCEN and 1CCEN on the new apron. A constant 16 inch slab thickness was for all San Antonio Int'l Airport locations.

The deflection basin "AREA" was computed for each load value using the equation:

$$\text{"AREA"} = (6/D0)*(D0+2D1+2D2+2D3+2D4+2D5+D6)$$

The maximum deflection measured directly beneath the load plate, D0, was used along with the calculated basin "AREA" to determine the slab's modulus using graphical procedures as shown in Figure 1. The lines shown for each E-value were determined using the ILLISLAB finite element computer program. Surface deflections were calculated using ILLISLAB at points coincident with the FWD sensor locations making direct comparisons between measured and computed values possible. Due to the fact that the measured load transfer was quite high, no adjustments for joint effects were necessary.

The resilient modulus of the subgrade was then determined using an iterative process which again compared measured surface deflections to those calculated by the computer. The base course modulus was confined to

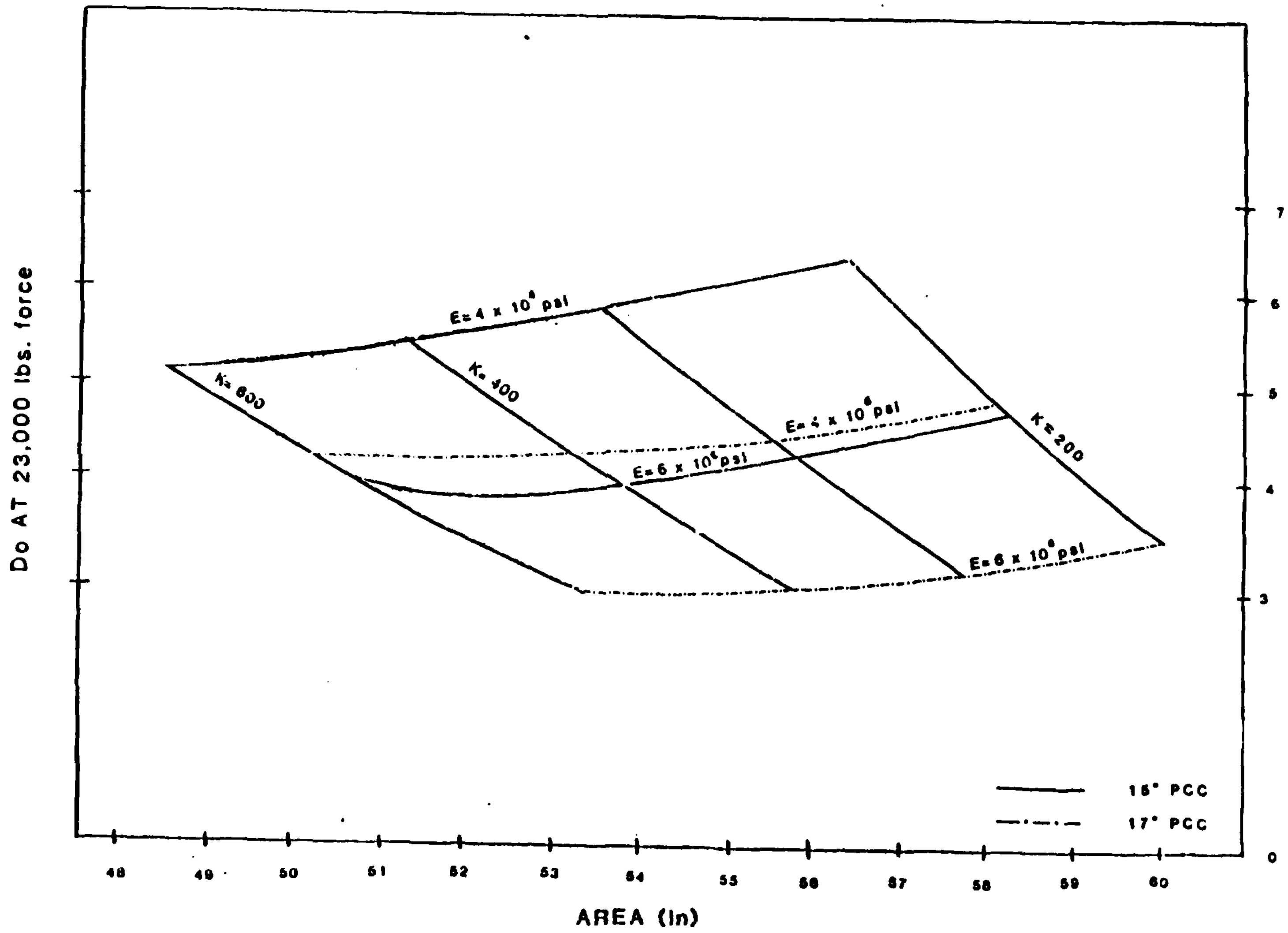

Figure 1: ILLISLAB Grid Used to Determine Elastic Modulus of Concrete Slabs

250,000 psi for asphaltic materials and to 25,000 psi for granular materials during these iterations. These numbers where chosen as representative of the materials present as variations from these values will not significantly influence the final results.

The resilient modulus values determined for each location are presented in units of psi/in. Also supplied for each test location is the FWD dynamic stiffness modulus, DSM, of the pavement calculated using the equation:

$$\text{DSM} = \frac{\text{Maximum Load} - \text{Minimum Load (in pounds)}}{\text{D0 at Max Load} - \text{D0 at Min Load (in mils)}}$$

The DSM is a measure of the overall strength of the pavement with higher values representing stronger pavement systems.

FLEXIBLE PAVEMENT ANALYSIS

The resilient modulus of the subgrade was calculated for each flexible pavement test conducted at Possum Kingdom Airport using a deflection based algorithm developed using the ILLIPAVE stress dependent computer program. This algorithm was developed by R.P Elliot and M.R. Thompson under project IHR-510. This project was undertaken to develop mechanistic design concepts for conventional flexible highway pavements (AC surface + granular base). As the pavement structure at Possum Kingdom closely resembles this type of structure in terms of layer thicknesses and material types, application of these algorithms was deemed appropriate.

The algoritm used for determining the resilient subgrade modulus, Eri, from FWD deflections is as follows:

$$\text{Log Eri} = 1.51 - 0.19\ \text{D3} + 0.27\ \text{Log D3}$$

$$R^2 = 0.99 \quad \text{SEE} = 0.05$$

D3 = Deflection measured 36" from the center of the load plate under a 9000 pound load.

This algorithm was selected as the one with the highest correlation coefficient (R^2) and lowest standard error of estimate (SEE).

The measured deflections were first converted to a standard 9000 pound load and then input into the above equation. The calculated Eri values are presented for each load level used in units of kips/sq.in.

Station	Load	D0	D1	D2	D3	D4	D5	D6	AREA2	%LT	DSM	Eri (ksi)
		Deflection in mils										
1ACEN	9000	5.9	5.4	4.6	3.7	2.8	2.1	1.7	45.6			
	13000	9.4	8.5	7.2	5.8	4.4	3.3	2.6	44.9			
	17000	12.4	11.2	9.5	7.6	5.8	4.3	3.3	44.8			
	23000	17.1	15.4	13.1	10.4	7.8	5.9	4.5	44.5		1250	16.3
1ATRJT	9000	8.5	8.2	5.9	4.3	3.1	2.2	1.6		100		
	13000	13.3	12.8	9.3	6.7	4.8	3.4	2.5		100		
	17000	17.9	17.1	12.4	8.9	6.4	4.5	3.4		100		
	23000	24.9	23.9	17.3	12.5	8.9	6.5	4.7		100	854	
2ACEN	9000	7.4	6.6	5.2	4.1	3.0	2.2	1.7	41.6			
	13000	11.4	10.1	8.1	6.4	4.6	3.4	2.5	41.6			
	17000	15.0	13.2	10.7	8.2	6.1	4.4	3.3	41.4			
	23000	21.1	18.6	14.8	11.3	8.4	6.1	4.5	40.9		1022	15.5
2ATRJT	9000	8.9	8.5	6.1	4.3	3.0	2.2	1.7		100		
	13000	14.2	13.4	9.7	6.7	4.6	3.5	2.6		100		
	17000	18.9	17.8	12.8	8.9	6.3	4.6	3.4		100		
	23000	27.4	25.1	18.2	12.7	8.9	6.5	4.9		100	757	
3ACEN	9000	8.5	7.4	5.7	4.2	3.0	2.3	1.7	39.1			
	13000	13.6	11.8	9.0	6.7	4.9	3.6	2.6	38.9			
	17000	18.4	15.7	11.9	8.8	6.4	4.8	3.5	38.2			
	23000	28.5	22.5	16.9	12.5	9.1	6.7	4.3	35.5		700	13.5
3ATRJT	9000	10.3	8.7	6.3	4.4	3.0	2.2	1.7		100		
	13000	15.7	13.4	9.6	6.7	4.7	3.4	2.6		100		
	17000	21.0	18.2	13.0	9.1	6.3	4.6	3.5		100		
	23000	31.3	25.7	18.2	12.8	8.9	6.5	5.0		100	667	
1BCEN	9000	5.1	4.7	4.0	3.3	2.6	2.0	1.5	46.8			
	13000	8.0	7.3	6.3	5.1	4.1	3.1	2.3	46.6			
	17000	10.5	9.5	8.2	6.8	5.3	4.1	3.1	46.5			
	23000	14.4	13.1	11.0	9.3	7.3	5.5	4.1	46.2		1505	23.3
1BTRJT	9000	7.1	7.0	5.2	3.7	2.7	1.9	1.5		100		
	13000	11.2	11.1	8.1	5.9	4.2	3.1	2.4		100		
	17000	15.0	14.6	10.8	7.8	5.6	4.1	3.1		100		
	23000	21.1	20.6	15.2	11.0	7.8	5.8	4.3		100	1000	
2BCEN	9000	6.4	5.6	4.7	3.7	2.8	2.1	1.5	42.8			
	13000	10.0	8.8	7.1	5.6	4.3	3.2	2.4	42.2			
	17000	13.6	11.8	9.5	7.5	5.8	4.3	3.2	41.7			
	23000	19.4	16.8	13.3	10.6	8.0	6.0	4.4	41.2		1077	16.6

Deflection in mils

Station	Load	D0	D1	D2	D3	D4	D5	D6	AREA2	%LT	DSM	Eri (ksi)
2BTRJT	9000	8.5	7.8	5.8	4.1	2.9	2.1	1.7		100		
	13000	13.2	12.1	8.8	6.3	4.5	3.2	2.5		100		
	17000	17.7	16.1	11.8	8.4	6.0	4.3	3.3		100		
	23000	24.7	22.6	16.6	11.8	8.4	6.1	4.6		100	864	
2ALGJT	9000	11.5	6.3	4.8	3.5	2.5	2.0	1.6		63		
	13000	17.5	9.8	7.4	5.5	4.0	3.1	2.5		65		
	17000	23.0	13.1	9.9	7.3	5.2	4.0	3.3		66		
	23000	31.8	18.6	13.9	10.2	7.4	5.7	4.5		68	690	
2BLGJT	9000	8.0	7.9	5.6	4.0	2.8	2.1	1.7		100		
	13000	12.4	12.3	8.8	6.2	4.4	3.3	2.6		100		
	17000	16.6	16.4	11.7	8.3	5.8	4.3	3.4		100		
	23000	22.9	22.6	16.2	11.4	8.0	6.0	4.8		100	940	
2CLGJT	9000	11.5	6.5	4.9	3.5	2.4	1.9	1.6		65		
	13000	17.4	10.2	7.5	5.4	3.9	3.0	2.4		68		
	17000	23.2	13.7	10.1	7.2	5.1	3.9	3.3		68		
	23000	33.1	19.6	14.3	10.2	7.3	5.6	4.6		68	648	
3BCEN	9000	6.8	6.1	5.0	3.9	3.2	2.2	1.7	43.5			
	13000	10.8	9.7	7.9	6.1	4.7	3.5	2.5	42.8			
	17000	14.6	12.9	10.5	8.2	6.2	4.7	3.5	42.4			
	23000	20.8	18.4	14.7	11.4	9.7	6.5	4.3	41.8		1000	14.8
3BTRJT	9000	8.9	8.1	6.4	4.6	3.2	2.4	1.7		100		
	13000	13.9	12.7	9.7	7.1	4.9	3.6	2.6		100		
	17000	18.6	17.0	12.9	9.3	6.6	4.8	3.5		100		
	23000	26.5	24.0	18.2	13.2	9.3	6.7	4.9		100	795	
1CCEN	9000	6.3	5.6	4.7	3.7	2.8	2.0	1.5	43.2			
	13000	9.7	8.7	7.2	5.7	4.2	3.1	2.3	43.2			
	17000	13.1	11.7	9.7	7.6	5.7	4.1	3.1	43.0			
	23000	18.2	16.1	13.4	10.4	7.7	5.5	4.2	42.4		1176	16.5
1CTRJT	9000	8.3	7.7	5.6	3.9	2.8	2.0	1.6		100		
	13000	13.0	11.9	8.7	6.3	4.5	3.2	2.4		100		
	17000	17.3	15.7	11.6	8.3	5.9	4.2	3.2		100		
	23000	24.2	22.1	15.9	11.7	8.3	6.0	4.4		100	881	
2CCEN	9000	6.4	5.7	4.7	3.7	2.9	2.2	1.6	43.5			
	13000	10.1	9.0	7.3	5.7	4.3	3.3	2.5	42.7			
	17000	13.5	11.9	9.8	7.6	5.8	4.3	3.3	42.5			
	23000	20.1	16.8	13.6	10.7	8.0	6.0	4.6	40.3		1022	16.5

Deflection in mils

Station	Load	D0	D1	D2	D3	D4	D5	D6	AREA2	%LT	DSM	Eri (ksi)
2CTRJT	9000	7.9	7.3	5.6	4.1	3.0	2.1	1.6		100		
	13000	12.4	11.6	8.7	6.4	4.7	3.3	2.4		100		
	17000	16.5	15.5	11.7	8.5	6.2	4.4	3.2		100		
	23000	23.0	21.7	16.4	11.9	8.5	6.1	4.4		100	927	
3CCEN	9000	7.2	6.4	5.1	3.9	3.0	2.3	1.8	42.0			
	13000	11.6	10.0	8.0	6.2	4.8	3.6	2.8	41.2			
	17000	15.6	13.4	10.7	8.2	6.4	4.7	3.7	40.8			
	23000	24.9	19.2	15.1	11.6	9.0	6.7	5.2	36.9		791	14.9
3CTRCK	9000	8.0	7.4	5.7	4.3	3.2	2.3	1.7				
	13000	12.8	11.8	6.8	6.7	5.0	3.6	2.6				
	17000	17.2	15.6	11.8	8.9	6.6	4.7	3.4				
	23000	30.6	21.9	16.4	12.6	9.1	6.7	4.7			619	
3CTRJT	9000	9.5	8.1	6.0	4.3	2.9	2.2	1.6		100		
	13000	13.3	12.6	9.4	6.7	4.8	3.4	2.6		100		
	17000	17.6	16.3	12.4	8.9	6.3	4.5	3.4		100	879	
1ALGJT	9000	9.2	5.6	4.4	3.3	2.5	2.0	1.6		79		
	13000	14.0	8.8	6.9	5.3	3.9	3.1	2.4		82		
	17000	13.7	11.3	9.2	7.0	5.2	4.1	3.3		82		
	23000	26.3	16.6	12.9	9.9	7.4	5.7	4.5		82	819	
1BLGJT	9000	7.5	7.0	5.0	3.6	2.6	1.9	1.6		100		
	13000	11.7	10.9	8.0	5.7	4.1	3.1	2.4		100		
	17000	15.5	14.3	10.7	7.5	5.3	4.0	3.2		100		
	23000	21.6	19.9	14.6	10.4	7.4	5.6	4.3		100	993	
1CLGJT	9000	9.9	5.9	4.4	3.2	2.4	1.8	1.4		77		
	13000	15.2	9.3	7.0	5.1	3.7	2.9	2.3		79		
	17000	20.5	12.3	9.2	6.8	4.9	3.8	3.0		78		
	23000	28.1	17.5	13.2	9.6	7.0	5.3	4.3		81	769	
3ALGJT	9000	13.3	7.2	5.4	3.9	2.8	2.1	1.7		70		
	13000	19.9	10.9	8.2	5.9	4.3	3.2	2.6		71		
	17000	26.4	14.7	11.0	7.9	5.9	4.3	3.5		72		
	23000	36.5	20.9	15.5	11.2	8.1	6.1	4.9		74	603	
3BLGJT	9000	8.6	7.9	5.8	4.0	2.8	2.1	1.7		100		
	13000	13.7	12.5	9.0	6.3	4.4	3.4	2.7		100		
	17000	18.2	16.6	11.9	8.4	5.8	4.4	3.6		100		
	23000	25.7	23.4	16.8	11.7	8.2	6.2	5.1		100	819	

		Deflection in mils									
Station	Load	D0	D1	D2	D3	D4	D5	D6	AREA2	%LT	DSM
3CLGJT	9000	10.7	7.9	5.7	4.0	2.9	2.2	1.8		95	
	13000	16.4	12.1	8.8	6.1	4.3	3.3	2.6		96	
	17000	22.1	16.2	11.8	8.2	5.8	4.4	3.6		95	
	23000	30.8	23.1	16.7	11.7	8.3	6.2	5.0		97	597

Station	Load	D0	D1	D2	D3	D4	D5	D6	AREA2	Eri (ksi)
		Deflection in mils								
2CCEN	23000	19.7	17.1	13.8	10.8	8.2	6.1	4.5	41.5	15.7
	23000	19.9	17.2	13.7	10.9	8.2	6.2	4.6	41.4	15.8
	23000	19.7	17.2	13.9	10.9	8.2	6.2	4.5	41.8	15.9
	23000	19.7	17.2	13.8	10.8	8.2	6.1	4.5	41.5	15.9
2CCEN	23000	19.7	17.2	13.9	10.9	8.2	6.1	4.6	41.7	15.8
	23000	19.8	17.2	13.8	10.9	8.2	6.1	4.5	41.4	15.9
	23000	19.8	17.3	13.9	10.9	8.2	6.1	4.5	41.5	15.5
	23000	19.7	17.2	13.8	10.9	8.2	6.1	4.6	41.6	15.8
2CCEN	23000	20.0	17.3	13.9	10.9	8.2	6.1	4.6	41.2	16.0
	23000	20.2	17.2	13.9	10.9	8.2	6.1	4.5	40.8	15.7
	23000	19.8	17.3	13.9	10.9	8.2	6.1	4.5	41.5	15.9
	23000	19.8	17.4	13.9	11.0	8.2	6.1	4.6	41.7	15.6
2CCEN	23000	19.7	17.3	13.9	10.9	8.2	6.1	4.5	41.7	15.7
	23000	19.8	17.4	13.9	10.9	8.2	6.1	4.5	41.6	15.7
	23000	19.9	17.6	14.0	11.2	8.4	6.2	4.6	42.0	15.2
	23000	19.8	17.3	13.9	10.9	8.2	6.1	4.5	41.5	15.6
2CCEN	23000	20.2	17.5	14.1	11.0	8.2	6.2	4.6	41.2	15.5
	23000	19.9	17.4	13.9	10.9	8.1	6.1	4.5	41.4	15.6
	23000	20.2	17.4	14.0	10.9	8.2	6.1	4.5	41.0	16.0
	23000	20.0	17.4	13.9	10.9	8.2	6.1	4.5	41.3	15.8
2CCEN	23000	21.1	17.3	14.0	10.9	8.3	6.2	4.6	39.6	15.4
	23000	20.0	17.3	13.9	10.9	8.3	6.2	4.6	41.3	15.8
	23000	20.0	17.4	14.0	11.0	8.2	6.1	4.6	41.4	15.6
	23000	20.2	17.5	14.1	11.1	8.4	6.2	4.7	41.4	15.9

		Deflection in mils										
Station	Load	D0	D1	D2	D3	D4	D5	D6	AREA2	%LT	DSM	Eri (ksi)
1ACEN	9000	2.7	2.5	2.3	1.9	1.6	1.4	1.1	51.6			
	13000	4.4	4.0	3.5	3.0	2.5	2.1	1.7	49.5			
	17000	5.7	5.2	4.6	3.9	3.3	2.7	2.2	49.8			
	23000	7.7	7.0	6.3	5.4	4.4	3.7	3.0	50.1		2890	30.0
1ATRJT	9000	3.3	3.0	2.6	2.1	1.7	1.4	1.1		100		
	13000	5.2	4.8	4.0	3.2	2.6	2.1	1.7		100		
	17000	6.8	6.3	5.2	4.2	3.4	2.7	2.2		100		
	23000	9.6	8.7	7.1	5.8	4.6	3.7	3.0		100	2222	
1BCEN	9000	3.7	3.2	2.7	2.3	1.8	1.5	1.2	45.2			
	13000	5.8	5.1	4.4	3.6	2.9	2.4	2.0	46.1			
	17000	7.6	6.6	5.6	4.6	3.8	3.0	2.4	45.2			
	23000	10.5	9.2	7.7	6.3	5.1	4.1	3.4	45.0		2059	26.6
1BTRCK	9000	3.4	3.2	2.7	2.3	1.8	1.5	1.2				
	13000	5.4	4.9	4.2	3.5	2.8	2.3	1.8				
	17000	7.1	6.5	5.5	4.6	3.7	3.0	2.4				
	23000	9.9	8.9	7.6	6.2	5.0	4.0	3.3			2154	
1BTRJT	9000	3.3	3.2	2.8	2.3	1.7	1.4	1.2		100		
	13000	5.3	5.1	4.2	3.5	2.7	2.1	1.8		100		
	17000	7.1	6.7	5.5	4.4	3.5	2.8	2.2		100		
	23000	9.7	9.3	7.6	6.1	4.8	3.7	3.0		100	2188	
1CCEN	9000	3.4	3.0	2.6	2.2	1.7	1.5	1.2	46.9			
	13000	5.4	4.8	4.0	3.3	2.7	2.3	1.9	46.1			
	17000	7.1	6.2	5.3	4.4	3.6	2.9	2.5	46.0			
	23000	9.7	8.4	7.1	5.9	4.8	3.9	3.2	45.2		2222	28.4
1CTRJT	9000	3.4	3.2	2.6	2.2	1.7	1.2	1.0		100		
	13000	5.5	5.1	4.2	3.4	2.7	2.1	1.6		100		
	17000	7.1	6.6	5.4	4.4	3.4	2.7	2.2		100		
	23000	9.9	9.1	7.5	6.0	4.7	3.6	2.9		100	2154	
1ALGJT	9000	4.9	2.2	1.9	1.6	1.3	1.2	1.0		52		
	13000	7.7	3.4	2.9	2.4	2.1	1.8	1.6		51		
	17000	10.2	4.4	3.8	3.3	2.8	2.4	2.1		50		
	23000	14.1	6.2	5.3	4.4	3.7	3.2	2.2		51	1522	
1BLGJT	9000	4.6	2.9	2.4	2.1	1.6	1.4	1.1		73		
	13000	6.9	5.8	4.0	3.3	2.7	2.2	1.8		97		
	17000	8.9	6.7	5.4	4.4	3.5	2.8	2.4		87		
	23000	12.0	10.4	7.5	6.0	4.8	3.9	3.2		100	1892	

Deflection in mils

Station	Load	D0	D1	D2	D3	D4	D5	D6	AREA2	%LT	DSM
1CLGJT	9000	4.6	2.4	2.1	1.8	1.5	1.3	1.1		60	
	13000	7.3	3.8	3.3	2.8	2.4	2.1	1.8		60	
	17000	9.5	5.0	4.3	3.7	3.1	2.7	2.3		61	
	23000	13.2	6.9	5.9	5.0	4.2	3.6	3.1		60	1628

Deflection in mils

Station	Load	D0	D1	D2	D3	D4	D5	D6	AREA2	DSM
1	9000	3.6	3.1	2.8	2.4	2.0	1.6	1.3	47.8	
	13000	5.6	4.8	4.3	3.7	3.1	2.6	2.0	47.8	
	17000	7.6	6.4	5.8	4.9	4.0	3.4	2.7	46.8	
	23000	10.5	8.7	7.8	6.3	5.5	4.5	3.6	46.1	2029
2	9000	3.8	3.1	2.7	2.3	1.8	1.5	1.2	43.9	
	13000	5.9	4.8	4.1	3.5	2.8	2.3	1.8	43.4	
	17000	7.9	6.3	5.4	4.6	3.7	3.0	2.4	42.8	
	23000	10.9	8.7	7.5	6.2	5.0	4.1	3.3	42.5	1972
3	9000	4.0	3.2	2.9	2.6	2.1	1.7	1.4	45.6	
	13000	6.1	4.9	4.4	3.8	3.2	2.6	2.2	45.3	
	17000	7.7	6.4	5.7	4.9	4.1	3.3	2.7	45.1	
	23000	10.8	8.6	7.7	6.6	5.4	4.5	3.7	44.5	2059

Deflection in mils

Station	Load	D0	D1	D2	D3	D4	D5	D6	AREA2	%LT	DSM	Eri (ksi)
1ACEN	9000	1.8	1.8	1.6	1.5	1.3	1.1	1.0	58.0			
	13000	2.7	2.6	2.4	2.2	1.9	1.7	1.5	57.3			
	17000	3.6	3.3	3.1	2.8	2.5	2.2	1.9	55.5			
	23000	5.1	4.7	4.3	3.9	3.5	3.1	2.6	54.9		4242	30.5
1ATRJT	9000	2.7	2.3	2.0	1.7	1.4	1.2	1.1		92		
	13000	4.0	3.4	2.9	2.5	2.1	1.7	1.5		92		
	17000	5.3	4.5	3.8	3.3	2.8	2.3	2.0		92		
	23000	7.4	6.1	5.3	4.5	3.8	3.2	2.7		89	2979	
2ACENA	9000	2.0	1.8	1.7	1.5	1.3	1.1	1.0	53.4			
	13000	3.2	2.7	2.6	2.3	2.0	1.8	1.6	51.8			
	17000	4.1	3.6	3.3	3.0	2.7	2.3	2.0	52.5			
	23000	5.5	4.7	4.4	4.0	3.6	3.1	2.7	52.1		4000	34.4
2ATRCK	9000	2.2	2.0	1.8	1.6	1.4	1.2	1.0				
	13000	3.2	3.1	2.6	2.3	2.1	1.8	1.5				
	17000	4.3	3.9	3.6	3.1	2.7	2.3	2.0				
	23000	5.8	5.3	4.8	4.2	3.7	3.1	2.7			3629	
2ACENB	9000	1.8	1.7	1.6	1.5	1.3	1.1	1.0	57.3			
	13000	2.7	2.5	2.3	2.1	1.9	1.6	1.5	55.6			
	17000	3.5	3.3	3.1	2.8	2.5	2.2	2.0	57.1			
	23000	5.0	4.7	4.3	4.0	3.5	3.1	2.7	56.3		4375	29.3
2ATRJT	9000	2.8	2.4	2.0	1.7	1.4	1.2	1.0		91		
	13000	4.0	3.3	2.9	2.5	2.1	1.8	1.5		88		
	17000	5.2	4.4	3.8	3.2	2.8	2.3	2.0		90		
	23000	7.1	5.9	5.1	4.4	3.7	3.1	2.7		88	3256	
3ACEN	9000	1.9	1.8	1.7	1.5	1.4	1.2	1.0	57.2			
	13000	3.0	2.7	2.5	2.3	2.0	1.8	1.6	54.4			
	17000	3.9	3.5	3.3	3.0	2.7	2.3	2.0	54.6			
	23000	5.1	4.6	4.3	3.9	3.5	3.0	2.7	54.6		4375	33.0
3ATRJT	9000	2.5	2.3	2.1	1.8	1.5	1.3	1.1		100		
	13000	3.9	3.5	3.1	2.7	2.3	2.0	1.7		99		
	17000	5.1	4.5	4.0	3.5	3.1	2.5	2.2		93		
	23000	7.0	6.1	5.5	4.8	4.3	3.5	2.9		97	3111	
4ACEN	9000	2.1	1.9	1.8	1.6	1.4	1.2	1.1	54.3			
	13000	3.1	2.7	2.5	2.4	2.1	1.8	1.6	53.6			
	17000	4.1	3.5	3.3	3.1	2.7	2.4	2.1	53.0			
	23000	5.5	4.8	4.4	4.1	3.6	3.2	2.3	52.9		4118	33.3

		Deflection in mils										
Station	Load	D0	D1	D2	D3	D4	D5	D6	AREA2	%LT	DSM	Eri (ksi)
4ATRJT	9000	3.0	2.6	2.2	1.9	1.6	1.3	1.1		99		
	13000	4.6	3.8	3.3	2.9	2.4	2.0	1.7		95		
	17000	6.2	5.1	4.4	3.7	3.2	2.6	2.2		94		
	23000	8.5	6.9	6.0	5.2	4.4	3.6	3.0		93	2545	
1BCEN	9000	2.2	2.1	1.9	1.8	1.6	1.4	1.2	57.3			
	13000	3.2	3.0	2.8	2.5	2.2	2.0	1.7	56.1			
	17000	4.3	4.0	3.7	3.4	3.0	2.7	2.3	56.1			
	23000	5.9	5.4	5.1	4.6	4.1	3.6	3.2	55.6		3734	26.0
1BTRJT	9000	2.4	2.1	1.7	1.6	1.3	1.1	1.0		96		
	13000	3.6	3.1	2.8	2.3	1.9	1.6	1.3		94		
	17000	4.8	4.1	3.6	3.1	2.6	2.2	1.8		93		
	23000	6.6	5.7	5.1	4.2	3.6	3.0	2.5		94	3333	
2BCEN	9000	1.8	1.8	1.7	1.5	1.3	1.1	1.0	58.7			
	13000	2.9	2.5	2.4	2.2	1.9	1.6	1.4	52.8			
	17000	3.7	3.4	3.3	2.9	2.5	2.3	1.7	55.8			
	23000	5.1	4.6	4.3	3.9	3.4	3.0	2.6	54.2		4242	32.7
2BTRJA	9000	2.5	2.2	1.9	1.6	1.3	1.1	0.9				
	13000	3.8	3.2	2.8	2.3	1.9	1.6	1.3				
	17000	5.1	4.2	3.6	3.1	2.6	2.1	1.8				
	23000	7.0	5.9	5.1	4.3	3.6	3.0	2.5			3111	
2BTRJB	9000	2.8	2.4	2.0	1.7	1.4	1.1	0.9				
	13000	4.2	3.5	3.1	2.5	2.1	1.7	1.4				
	17000	5.5	4.6	4.0	3.4	2.8	2.3	1.9				
	23000	7.7	6.3	5.4	4.6	3.8	3.1	2.6			2857	
3BCEN	9000	1.8	1.7	1.7	1.6	1.3	1.1	1.0	58.7			
	13000	2.8	2.5	2.5	2.3	2.0	1.7	1.5	56.4			
	17000	3.6	3.3	3.2	2.9	2.5	2.2	1.9	56.2			
	23000	5.1	4.6	4.4	4.1	3.5	3.1	2.6	55.4		4242	30.5
3BTRJT	9000	2.5	2.2	1.9	1.8	1.4	1.2	1.1		93		
	13000	3.7	3.1	2.8	2.4	2.1	1.7	1.5		93		
	17000	4.8	4.1	3.6	3.2	2.7	2.3	2.0		95		
	23000	6.6	5.6	5.0	4.4	3.7	3.2	2.7		94	3415	
4BCEN	9000	1.9	1.9	1.7	1.6	1.4	1.2	1.0	58.4			
	13000	2.9	2.8	2.6	2.3	2.0	1.8	1.5	56.7			
	17000	3.9	3.7	3.4	3.1	2.7	2.4	2.1	56.3			
	23000	5.4	5.1	4.7	4.2	3.7	3.3	2.8	55.3		4000	28.1

Deflection in mils

Station	Load	D0	D1	D2	D3	D4	D5	D6	AREA2	%LT	DSM	Eri (ksi)
4BTRJT	9000	3.0	2.4	2.0	1.8	1.5	1.2	1.1		85		
	13000	4.5	3.5	3.1	2.6	2.2	1.8	1.6		82		
	17000	6.0	4.6	4.0	3.4	2.9	2.4	2.1		81		
	23000	8.2	6.2	5.4	4.6	3.9	3.2	2.8		80	2692	
1CCEN	9000	1.6	1.5	1.4	1.3	1.1	1.0	0.9	56.6			
	13000	2.4	2.2	2.1	1.9	1.7	1.5	1.3	56.2			
	17000	3.1	2.9	2.7	2.5	2.2	1.9	1.7	56.5			
	23000	4.3	4.1	3.7	3.5	3.1	2.7	2.4	57.1		5185	34.3
1CTRJT	9000	3.2	2.6	2.5	2.1	1.7	1.4	1.2		85		
	13000	5.0	4.0	3.5	3.1	2.5	2.2	1.9		84		
	17000	6.5	5.2	4.6	4.0	3.4	2.9	2.4		84		
	23000	8.6	6.9	6.1	5.3	4.5	3.7	3.2		84	2593	
2CCEN	9000	2.0	1.9	1.9	1.6	1.4	1.2	1.1	57.3			
	13000	3.1	2.9	2.7	2.4	2.1	1.9	1.7	55.7			
	17000	4.1	3.8	3.6	3.3	2.9	2.5	2.2	56.3			
	23000	5.6	5.1	4.9	4.4	3.9	3.4	3.0	55.7		3869	27.7
2CTRJT	9000	2.4	1.9	1.7	1.5	1.3	1.1	0.9		87		
	13000	3.7	2.8	2.5	2.2	1.9	1.6	1.4		83		
	17000	4.3	3.7	3.3	3.0	2.5	2.1	1.3		85		
	23000	6.6	5.2	4.6	4.1	3.5	3.0	2.6		87	3333	
3CCEN	9000	1.8	1.7	1.6	1.5	1.3	1.1	1.0	57.3			
	13000	2.8	2.6	2.5	2.3	2.0	1.8	1.6	57.4			
	17000	3.6	3.4	3.2	2.9	2.6	2.2	2.0	57.0			
	23000	5.1	4.7	4.4	4.0	3.6	3.2	2.8	56.1		4242	29.8
3CTRJT	9000	2.8	2.2	1.9	1.7	1.4	1.2	1.1		85		
	13000	4.4	3.2	2.9	2.5	2.1	1.8	1.5		79		
	17000	6.0	4.5	4.0	3.5	2.9	2.4	2.1		81		
	23000	7.9	5.7	5.0	4.3	3.7	3.1	2.6		76	2745	
4CCEN	9000	1.9	1.8	1.7	1.6	1.4	1.2	1.1	58.1			
	13000	2.8	2.6	2.5	2.3	2.0	1.8	1.6	57.4			
	17000	3.7	3.5	3.3	3.0	2.7	2.4	2.1	57.7			
	23000	5.2	4.8	4.5	4.1	3.7	3.3	2.9	56.4		4242	28.9
4CTRJT	9000	2.7	2.3	1.9	1.7	1.3	1.1	1.0		92		
	13000	4.2	3.3	2.9	2.4	2.1	1.7	1.5		85		
	17000	5.5	4.4	3.8	3.3	2.8	2.3	2.0		87		
	23000	7.5	5.9	5.1	4.4	3.7	3.1	2.6		85	2917	

		Deflection in mils									
Station	Load	D0	D1	D2	D3	D4	D5	D6	AREA2	SLT	CSM
1ALGJT	9000	2.4	2.0	1.8	1.5	1.3	1.1	0.9		90	
	13000	3.4	2.8	2.5	2.2	1.8	1.5	1.3		89	
	17000	4.5	3.8	3.4	3.0	2.4	2.0	1.7		91	
	23000	6.4	5.2	4.7	4.1	3.4	2.9	2.4		88	3500
1BLGJT	9000	3.0	2.7	2.4	2.1	1.7	1.4	1.2		98	
	13000	4.5	4.0	3.5	3.0	2.4	2.0	1.7		96	
	17000	6.0	5.3	4.6	4.0	3.3	2.7	2.3		96	
	23000	8.2	7.2	6.2	5.2	4.4	3.7	3.0		95	2692
1CLGJT	9000	2.0	1.5	1.5	1.3	1.1	0.9	0.7		81	
	13000	3.0	2.4	2.3	2.0	1.6	1.4	1.2		87	
	17000	4.0	3.2	3.0	2.5	2.1	1.8	1.5		87	
	23000	5.6	4.6	4.1	3.5	2.9	2.5	2.1		89	3839
2ALGJA	9000	2.4	2.3	2.0	1.7	1.4	1.2	1.0			
	13000	3.6	3.3	2.9	2.5	2.1	1.7	1.4			
	17000	4.7	4.4	3.8	3.2	2.7	2.2	1.8			
	23000	6.5	6.0	5.2	4.5	3.8	3.1	2.5			3415
2ALGJB	9000	2.3	2.2	1.9	1.7	1.3	1.1	0.9			
	13000	3.5	3.2	2.3	2.4	2.0	1.7	1.4			
	17000	4.6	4.2	3.6	3.1	2.7	2.2	1.9			
	23000	6.4	5.7	5.0	4.3	3.6	3.0	2.5			3415
2BLGJT	9000	2.5	2.4	2.2	1.2	1.5	1.3	1.1		100	
	13000	3.7	3.4	3.0	2.6	2.2	1.8	1.6		100	
	17000	5.0	4.5	3.9	3.3	2.9	2.4	2.0		97	
	23000	6.9	6.1	5.4	4.7	4.0	3.3	2.8		96	3182
2CLGJT	9000	3.5	3.1	2.8	2.4	1.9	1.6	1.2		96	
	13000	5.2	4.6	4.0	3.4	2.8	2.2	1.9		96	
	17000	6.8	6.0	5.3	4.4	3.6	3.0	2.4		96	
	23000	9.5	8.3	7.2	6.0	5.0	4.1	3.4		95	2333
3ALGJT	9000	2.4	2.3	2.0	1.7	1.4	1.2	1.1		100	
	13000	3.7	3.3	2.8	2.5	2.1	1.3	1.5		97	
	17000	4.8	4.3	3.7	3.2	2.8	2.3	2.0		97	
	23000	6.8	6.0	5.2	4.6	3.9	3.2	2.7		96	3132
3BLGJT	9000	2.9	2.6	2.2	1.9	1.6	1.3	1.1		97	
	13000	4.3	3.9	3.3	2.8	2.3	2.0	1.6		96	
	17000	5.6	5.2	4.4	3.8	3.2	2.6	2.2		100	
	23000	7.7	6.9	5.9	5.0	4.2	3.4	2.9		97	2917

Normalized Deflection data from file --> **SAN ANTONIO INT'L AIRPORT: CARGO APRON**

Deflection in mils

Station	Load	D0	D1	D2	D3	D4	D5	D6	AREA2	%LT	DSM
3CLGJT	9000	2.5	2.3	2.0	1.7	1.4	1.1	0.9		100	
	13000	4.0	3.5	3.1	2.6	2.1	1.8	1.5		95	
	17000	5.3	4.5	3.9	3.3	2.8	2.3	1.9		92	
	23000	7.1	6.0	5.2	4.5	3.7	3.1	2.5		92	3043
4ALGJT	9000	2.5	2.3	2.0	1.7	1.5	1.2	1.1		100	
	13000	3.7	3.3	3.0	2.5	2.2	1.8	1.6		97	
	17000	4.8	4.4	3.8	3.3	2.9	2.4	2.0		99	
	23000	6.5	5.7	5.0	4.4	3.8	3.1	2.7		95	3500
4ELGJT	9000	3.0	2.8	2.4	2.1	1.7	1.4	1.2		100	
	13000	4.5	4.1	3.5	3.1	2.5	2.1	1.8		99	
	17000	6.0	5.4	4.6	4.0	3.3	2.7	2.3		98	
	23000	8.3	7.4	6.4	5.5	4.5	3.8	3.2		97	2642
4CLGJT	9000	2.7	2.3	2.0	1.7	1.4	1.2	1.0		92	
	13000	4.0	3.4	2.9	2.5	2.1	1.7	1.5		92	
	17000	5.4	4.6	3.9	3.4	2.9	2.4	2.0		92	
	23000	7.5	6.3	5.4	4.7	3.9	3.3	2.7		91	2917

		Deflection in mils								
Station	Load	D0	D1	D2	D3	D4	D5	D6	AREA2	Eri
2ACENY	23000	5.1	4.7	4.4	4.0	3.5	3.0	2.6	55.2	30.7
	23000	5.2	4.8	4.5	4.0	3.6	3.1	2.6	55.2	30.0
	23000	5.0	4.7	4.4	4.0	3.5	3.0	2.6	56.2	29.4
	23000	5.1	4.7	4.4	4.0	3.5	3.0	2.6	55.2	30.7
2ACENX	23000	5.1	4.7	4.4	3.9	3.5	3.0	2.6	54.9	30.3
	23000	5.1	4.7	4.3	3.9	3.5	3.0	2.6	54.7	31.7
	23000	5.1	4.8	4.4	4.0	3.6	3.1	2.6	55.9	29.4
	23000	5.1	4.7	4.4	4.0	3.5	3.1	2.6	55.4	30.7
2ACENX	23000	5.1	4.7	4.4	4.0	3.5	3.0	2.6	55.2	30.7
	23000	5.1	4.7	4.4	4.0	3.5	3.0	2.6	55.2	30.7
	23000	5.1	4.7	4.4	4.0	3.5	3.0	2.6	55.2	30.7
	23000	5.1	4.7	4.5	4.0	3.6	3.1	2.6	55.9	29.6
2ACENX	23000	5.1	4.7	4.4	4.0	3.5	3.0	2.6	55.2	30.7
	23000	5.1	4.7	4.4	4.0	3.5	3.0	2.6	55.2	30.7
	23000	5.1	4.7	4.4	4.0	3.5	3.0	2.6	55.2	30.7
	23000	5.1	4.7	4.4	4.0	3.5	3.0	2.6	55.2	30.7
2ACENX	23000	5.1	4.7	4.5	4.0	3.4	3.0	2.6	55.2	30.8
	23000	5.1	4.8	4.5	4.0	3.5	3.0	2.6	55.6	30.1
	23000	5.1	4.7	4.4	4.0	3.4	3.0	2.6	54.9	30.8
	23000	5.1	4.7	4.4	4.0	3.4	3.0	2.6	54.9	30.8
2ACENX	23000	5.1	4.8	4.4	4.0	3.5	3.0	2.6	55.4	30.7
	23000	5.1	4.7	4.4	4.0	3.5	3.0	2.6	55.2	30.7
	23000	5.1	4.7	4.4	4.0	3.4	3.0	2.6	54.9	30.3
	23000	5.0	4.7	4.4	4.0	3.4	3.0	2.6	55.9	30.5
2ACENY	23000	5.1	4.7	4.5	4.1	3.5	3.0	2.7	55.8	29.9
	23000	5.1	4.7	4.5	4.0	3.6	3.1	2.7	56.0	29.4
	23000	5.1	4.7	4.4	4.0	3.5	3.1	2.6	55.4	30.7
	23000	5.1	4.7	4.4	4.0	3.4	3.0	2.6	54.9	30.8
2ACENY	23000	5.1	4.7	4.4	4.0	3.5	3.0	2.6	55.2	30.7
	23000	5.0	4.6	4.4	4.0	3.4	3.0	2.6	55.7	30.7
	23000	5.0	4.6	4.4	4.0	3.4	3.0	2.6	55.7	30.7
	23000	5.1	4.7	4.4	4.0	3.4	3.0	2.6	54.9	30.8
2ACENY	23000	5.2	4.5	4.3	3.9	3.4	2.9	2.6	52.3	34.5
	23000	5.1	4.5	4.2	3.8	3.4	3.0	2.6	53.5	33.9
	23000	5.1	4.5	4.2	3.8	3.4	3.0	2.5	53.4	33.9
	23000	5.1	4.5	4.2	3.8	3.4	2.9	2.6	53.3	33.9

Deflection in mils

Station	Load	D0	D1	D2	D3	D4	D5	D6	AREA2	Eri
2ACENY	23000	5.1	4.5	4.2	3.9	3.4	2.9	2.6	53.5	33.7
	23000	5.1	4.5	4.3	3.9	3.4	2.9	2.6	53.8	33.7
	23000	5.1	4.5	4.3	3.9	3.4	2.9	2.6	53.8	33.7
	23000	5.1	4.5	4.2	3.9	3.4	2.9	2.6	53.5	33.7
2ACENY	23000	5.1	4.5	4.3	3.9	3.4	3.0	2.5	53.9	33.7
	23000	5.2	4.6	4.3	3.9	3.4	3.0	2.6	53.3	34.2
	23000	5.2	4.6	4.3	3.9	3.4	3.0	2.5	53.2	34.2
	23000	5.1	4.5	4.2	3.8	3.4	2.9	2.5	53.2	33.9
2ACENY	23000	5.1	4.5	4.2	3.8	3.4	2.9	2.5	53.2	33.9
	23000	5.1	4.5	4.2	3.9	3.4	3.0	2.5	53.6	33.7
	23000	5.1	4.6	4.2	3.9	3.4	3.0	2.6	54.0	33.7
	23000	5.2	4.6	4.3	3.9	3.4	2.9	2.6	53.1	34.2
2ACENY	23000	5.1	4.6	4.3	3.9	3.4	3.0	2.6	54.2	33.7
	23000	5.2	4.6	4.3	3.9	3.5	3.0	2.6	53.5	33.6
	23000	5.1	4.6	4.2	3.8	3.5	3.0	2.6	54.0	33.6
	23000	5.2	4.6	4.3	3.9	3.5	3.0	2.6	53.5	33.4
2ACENY	23000	5.1	4.6	4.3	3.9	3.5	3.0	2.6	54.5	33.5
	23000	5.2	4.6	4.3	3.9	3.5	3.0	2.6	53.5	33.4
	23000	5.1	4.6	4.3	3.9	3.5	3.0	2.6	54.5	33.5
	23000	5.1	4.6	4.3	3.9	3.5	3.0	2.6	54.5	33.5
2ACENY	23000	5.1	4.6	4.4	3.9	3.5	3.0	2.6	54.7	33.5
	23000	5.2	4.6	4.3	3.9	3.5	3.0	2.6	53.5	33.4
	23000	5.2	4.6	4.4	4.0	3.5	3.0	2.6	54.0	33.3
	23000	5.2	4.6	4.3	3.9	3.5	3.0	2.6	53.5	33.4
2ACENY	23000	5.1	4.6	4.2	3.9	3.4	3.0	2.6	54.0	33.7
	23000	5.1	4.6	4.3	3.9	3.5	3.0	2.6	54.5	33.5
	23000	5.1	4.6	4.3	3.9	3.4	3.0	2.6	54.2	33.3
	23000	5.2	4.7	4.3	4.0	3.5	3.1	2.7	54.3	32.1
2ACENY	23000	5.2	4.5	4.3	3.7	3.5	3.0	2.6	53.3	34.3
	23000	5.2	4.6	4.3	3.9	3.5	3.0	2.6	53.5	33.4
	23000	5.1	4.6	4.3	3.8	3.5	3.0	2.5	54.1	33.5
	23000	5.2	4.6	4.3	3.9	3.5	3.0	2.6	53.5	33.4
2ACENY	23000	5.2	4.6	4.3	3.9	3.5	3.0	2.6	53.5	33.4
	23000	5.2	4.6	4.3	3.9	3.6	3.0	2.6	53.8	33.3
	23000	5.1	4.6	4.3	3.9	3.5	3.0	2.6	54.5	33.5
	23000	5.1	4.6	4.3	3.9	3.6	3.0	2.6	54.7	33.3

		Deflection in mils								
Station	Load	D0	D1	D2	D3	D4	D5	D6	AREA2	Eri
2ACENY	23000	5.1	4.5	4.3	3.9	3.5	3.0	2.6	54.2	33.5
	23000	5.2	4.6	4.4	4.0	3.5	3.0	2.6	54.0	33.3
	23000	5.2	4.6	4.4	4.0	3.5	3.0	2.6	54.0	33.3
	23000	5.2	4.5	4.4	4.0	3.5	3.0	2.6	53.8	32.9
2ACENY	23000	5.2	4.6	4.4	4.0	3.5	3.0	2.6	54.0	33.3
	23000	5.1	4.5	4.4	4.0	3.5	3.0	2.6	54.7	33.0
	23000	5.2	4.5	4.3	4.0	3.5	3.0	2.6	53.5	33.0
	23000	5.1	4.5	4.4	4.0	3.5	3.0	2.6	54.7	33.0
18CENA	23000	5.9	5.4	5.1	4.7	4.1	3.7	3.2	56.0	25.5
	23000	5.8	5.4	5.1	4.6	4.1	3.6	3.2	56.5	25.2
	23000	5.9	5.4	5.1	4.6	4.1	3.6	3.2	55.6	26.4
	23000	5.9	5.4	5.0	4.6	4.1	3.7	3.3	55.7	26.2
18CENA	23000	5.8	5.3	5.0	4.6	4.1	3.6	3.2	56.1	25.7
	23000	5.8	5.3	5.0	4.6	4.1	3.6	3.2	56.1	25.7
	23000	5.3	5.4	5.0	4.6	4.1	3.7	3.2	56.5	25.2
	23000	5.3	5.4	5.0	4.6	4.1	3.6	3.2	56.3	25.5
18CENA	23000	5.9	5.4	5.1	4.6	4.2	3.7	3.2	56.0	25.7
	23000	5.9	5.4	5.1	4.7	4.1	3.7	3.3	56.1	25.5
	23000	5.9	5.4	5.1	4.6	4.1	3.6	3.2	55.6	26.2
	23000	5.9	5.4	5.0	4.6	4.1	3.6	3.2	55.4	26.6
18CENA	23000	5.9	5.4	5.1	4.6	4.1	3.6	3.2	55.6	26.0
	23000	5.9	5.4	5.0	4.6	4.1	3.6	3.2	55.4	26.4
	23000	6.0	5.4	5.1	4.7	4.2	3.7	3.2	55.4	26.4
	23000	5.9	5.4	5.1	4.7	4.2	3.6	3.3	56.1	25.5
18CENA	23000	5.9	5.4	5.0	4.7	4.2	3.7	3.2	56.0	25.5
	23000	5.9	5.3	5.0	4.6	4.1	3.6	3.2	55.2	22.1
	23000	5.9	5.3	5.0	4.6	4.1	3.6	3.2	55.2	27.1
	23000	5.9	5.4	5.0	4.6	4.1	3.6	3.2	55.4	26.6
18CENA	23000	5.3	5.3	5.1	4.6	4.1	3.7	3.2	56.5	25.2
	23000	5.9	5.4	5.1	4.6	4.1	3.7	3.2	55.8	25.7
	23000	5.9	5.3	5.1	4.6	4.1	3.6	3.2	55.4	26.6
	23000	5.9	5.4	5.1	4.6	4.1	3.6	3.2	55.6	26.2
18CENA	23000	5.9	5.4	5.1	4.7	4.2	3.7	3.2	56.2	25.2
	23000	5.9	5.4	5.1	4.7	4.1	3.7	3.2	56.0	25.5
	23000	5.9	5.4	5.0	4.6	4.1	3.7	3.2	55.6	26.6
	23000	5.9	5.4	5.0	4.6	4.1	3.6	3.2	55.4	26.6

Deflection in mils

Station	Load	D0	D1	D2	D3	D4	D5	D6	AREA2	Eri
1BCENA	23000	5.8	5.3	5.1	4.6	4.1	3.6	3.2	56.3	25.5
	23000	5.9	5.4	5.1	4.7	4.1	3.6	3.3	55.9	25.7
	23000	5.8	5.3	5.0	4.6	4.1	3.6	3.2	56.1	25.7
	23000	5.9	5.4	5.1	4.7	4.1	3.7	3.2	56.0	25.5

Deflection in mils

Station	Load	D0	D1	D2	D3	D4	D5	D6	AREA2	DSM	Eri
10A	9000	17.9	8.1	4.0	2.6	2.1	1.7	1.4	19.0		12.66
	13000	25.4	11.8	5.9	4.1	3.1	2.5	2.0	19.4		12.5
	17000	33.4	15.7	7.3	5.4	4.1	3.3	2.7	19.5	516	12.32
9A	9000	13.2	8.2	4.1	2.8	2.1	1.6	1.4	18.9		12.66
	13000	29.2	12.3	6.0	4.0	3.0	2.3	1.9	17.7		12.81
	17000	36.6	16.1	7.9	5.3	4.0	3.2	2.6	18.4	435	12.78
8A	9000	17.1	8.2	4.1	2.7	2.0	1.6	1.3	19.5		13.14
	13000	26.5	12.5	6.1	4.0	3.0	2.3	1.9	19.1		12.82
	17000	35.8	16.6	8.2	5.4	4.0	3.1	2.5	18.9	428	12.53
7A	9000	17.7	7.8	3.9	2.6	1.9	1.5	1.3	18.4		13.56
	13000	26.4	11.9	5.8	3.8	2.9	2.2	1.9	18.5		13.38
	17000	34.9	15.9	7.9	5.1	3.8	3.0	2.5	18.7	465	12.94
6A	9000	17.0	8.4	4.3	2.8	2.1	1.6	1.3	20.0		12.64
	13000	25.6	12.5	6.2	4.1	3.0	2.4	1.9	19.7		12.51
	17000	35.1	16.6	8.3	5.4	4.0	3.1	2.6	19.2	442	12.52
5A	9000	16.5	8.3	4.3	2.8	2.1	1.6	1.3	20.4		12.73
	13000	24.5	12.4	6.2	4.1	3.1	2.4	2.0	20.3		12.22
	17000	31.9	16.5	8.3	5.5	4.1	3.2	2.7	20.7	519	12.27
4A	9000	18.0	8.7	4.4	3.0	2.1	1.8	1.5	19.8		11.75
	13000	26.8	12.9	6.5	4.4	3.2	2.7	2.2	19.8		11.60
	17000	34.2	16.9	8.5	5.8	4.2	3.6	2.9	20.2	494	11.55
3A	9000	18.7	8.8	4.5	3.1	2.2	1.7	1.4	19.5		11.66
	13000	28.0	13.1	6.6	4.3	3.2	2.5	2.1	19.2		11.88
	17000	36.2	17.2	8.7	5.7	4.2	3.3	2.7	19.4	457	11.80
2A	9000	18.7	8.2	4.4	2.9	2.1	1.7	1.4	18.8		12.14
	13000	27.9	12.5	6.5	4.2	3.1	2.4	2.0	18.8		12.16
	17000	36.4	16.4	8.5	5.6	4.2	3.2	2.7	18.9	452	11.99
1A	9000	17.5	8.3	4.3	2.7	2.0	1.5	1.3	19.7		13.17
	13000	27.2	13.2	6.4	4.1	3.0	2.3	2.0	19.2		12.48
	17000	36.9	17.4	8.4	5.4	4.0	3.1	2.6	18.9	412	12.21
10B	9000	19.1	8.5	4.3	3.0	2.3	1.8	1.4	18.9		11.72
	13000	27.6	12.6	6.3	4.3	3.3	2.6	2.1	19.1		11.90
	17000	34.9	16.5	8.1	5.6	4.2	3.4	2.8	19.5	506	12.02

Normalized Deflection data from file --> **POSSUM KINGDOM AIRPORT: TAXIWAY**

		Deflection in mils									
Station	Load	00	01	02	03	04	05	06	AREA2	OSM	Cri
98	9000	20.3	8.2	4.2	2.8	2.1	1.7	1.4	17.6		12.55
	13000	30.1	12.4	6.2	4.2	3.1	2.5	2.1	17.7		12.14
	17000	40.5	16.3	8.0	5.5	4.1	3.3	2.7	17.4	396	12.21
88	9000	22.9	8.2	4.2	2.8	2.1	1.6	1.3	16.2		12.50
	13000	33.3	12.5	6.2	4.1	3.1	2.4	2.0	16.6		12.34
	17000	42.7	16.7	8.2	5.5	4.1	3.2	2.7	17.0	404	12.13
78	9000	18.8	8.5	4.0	2.7	1.9	1.5	1.2	18.3		13.06
	13000	28.6	12.9	6.0	3.9	2.9	2.2	1.8	18.1		13.06
	17000	38.4	17.3	8.1	5.3	4.0	3.1	2.5	18.2	408	12.67
68	9000	20.7	8.9	4.1	2.7	1.9	1.6	1.2	17.5		13.08
	13000	32.6	13.3	6.1	3.9	2.9	2.2	1.8	16.8		13.05
	17000	48.4	17.8	8.2	5.3	3.9	3.0	2.5	15.8	289	12.68
58	9000	23.3	8.9	4.1	2.7	2.0	1.5	1.2	16.2		12.93
	13000	33.8	13.5	6.1	4.0	2.9	2.3	1.9	16.6		12.69
	17000	42.3	17.9	8.2	5.3	3.9	3.1	2.6	17.3	421	12.61
48	9000	22.2	8.6	4.2	2.7	2.1	1.6	1.4	16.8		12.91
	13000	33.4	13.0	6.1	4.0	3.0	2.3	2.0	16.6		12.70
	17000	44.4	17.2	8.1	5.3	3.9	3.1	2.5	16.5	360	12.60
38	9000	23.1	8.1	4.2	2.8	2.0	1.6	1.3	16.1		12.79
	13000	36.7	12.2	6.1	4.0	2.9	2.3	1.9	15.3		12.65
	17000	45.0	16.3	8.1	5.3	3.9	3.1	2.5	16.1	365	12.61
28	9000	19.1	8.4	4.4	2.9	2.0	1.6	1.3	19.2		12.04
	13000	28.5	12.7	6.6	4.3	3.1	2.4	2.0	18.7		12.14
	17000	38.7	16.9	8.7	5.7	4.1	3.2	2.6	18.4	368	11.72
18	9000	18.4	8.3	4.3	2.8	1.9	1.6	1.3	18.7		12.57
	13000	27.8	12.6	6.2	4.0	2.9	2.3	1.9	18.5		12.71
	17000	36.7	16.5	8.2	5.3	3.8	3.0	2.5	18.4	437	12.70

Deflection in mils

Station	Load	D0	D1	D2	D3	D4	D5	D6	AREA2	Eri
3AA	17000	43.1	17.0	3.3	5.4	4.0	3.2	2.6	16.9	12.18
	17000	38.5	15.7	7.9	5.4	4.0	3.2	2.6	17.7	12.25
	17000	36.6	15.5	7.9	5.5	4.1	3.2	2.7	18.3	12.22
	17000	35.8	15.4	7.9	5.5	4.1	3.2	2.7	18.6	12.14
3AA	17000	35.3	15.3	7.9	5.4	4.0	3.2	2.6	18.6	12.21
	17000	35.2	15.2	7.9	5.5	4.1	3.2	2.7	18.7	12.24
	17000	35.5	15.2	7.9	5.4	4.1	3.2	2.6	18.5	12.21
	17000	35.3	15.2	7.9	5.5	4.1	3.2	2.6	18.6	12.16
3AA	17000	34.9	15.2	7.9	5.4	4.0	3.2	2.6	18.7	12.44
	17000	34.7	15.2	7.9	5.4	4.1	3.2	2.7	18.8	12.26
	17000	34.4	15.2	7.9	5.5	4.1	3.2	2.7	19.0	12.24
	17000	34.4	15.2	7.9	5.5	4.1	3.2	2.7	19.0	12.23
3AA	17000	34.0	15.2	7.9	5.5	4.1	3.2	2.7	19.1	12.23
	17000	34.1	15.1	7.8	5.4	4.0	3.2	2.6	19.0	12.20
	17000	34.3	15.2	7.9	5.5	4.1	3.2	2.7	19.0	12.18
	17000	[illegible]	[illegible]	7.9	5.5	4.1	3.2	2.7	19.1	12.22
3AA	17000	33.3	16.5	3.3	5.4	4.0	3.2	2.7	13.1	12.14
	17000	37.6	16.0	8.1	5.5	4.1	3.3	2.7	18.2	12.16
	17000	35.7	15.8	8.1	5.4	4.1	3.2	2.7	18.8	12.15
	17000	35.1	15.8	8.1	5.4	4.1	3.2	2.7	19.0	12.16
3AA	17000	34.9	15.9	8.1	5.5	4.1	3.2	2.7	19.1	12.10
	17000	34.4	15.7	8.1	5.5	4.1	3.3	2.7	19.3	12.15
	17000	34.8	15.9	8.1	5.5	4.1	3.3	2.3	19.2	12.14
	17000	34.3	15.7	8.1	5.5	4.2	3.3	2.7	19.2	12.14
2AA	17000	39.0	17.6	8.5	5.6	4.0	3.2	2.7	18.4	11.93
	17000	36.9	15.9	8.0	5.4	3.9	3.2	2.7	18.3	12.32
	17000	35.0	15.7	8.0	5.4	4.0	3.2	2.7	18.9	12.29
	17000	34.6	15.5	7.9	5.4	4.0	3.2	2.7	19.0	12.33
2AA	17000	34.3	15.4	7.9	5.4	4.0	3.2	2.7	18.8	12.29
	17000	34.4	15.3	7.9	5.4	4.0	3.2	2.7	19.0	12.34
	17000	34.2	15.3	7.9	5.4	4.0	3.2	2.7	17.0	12.45
	17000	34.0	15.3	7.9	5.4	4.0	3.2	2.7	19.1	12.30
2AA	17000	35.9	15.5	7.9	5.4	4.0	3.2	2.7	18.1	12.32
	17000	35.1	15.4	7.9	5.4	4.0	3.3	2.7	18.3	12.32
	17000	34.1	15.3	7.9	5.5	4.0	3.3	2.7	19.1	12.15
	17000	34.4	15.3	7.9	5.4	4.0	3.3	2.7	19.0	12.15

		Deflection in mils								
Station	Load	D0	D1	D2	D3	D4	D5	D6	AREA2	Eri
2AA	17000	34.7	15.2	7.9	5.4	4.0	3.3	2.7	18.8	12.30
	17000	34.5	15.2	7.9	5.4	4.0	3.3	2.7	18.9	12.32
	17000	34.1	15.2	7.9	5.4	4.0	3.3	2.7	19.1	12.31
	17000	33.9	15.2	7.9	5.4	4.0	3.3	2.7	19.2	12.28
2AA	17000	35.6	15.2	7.9	5.4	4.1	3.2	2.7	18.5	12.30
	17000	34.6	15.2	7.9	5.4	4.0	3.2	2.7	18.8	12.35
	17000	34.0	15.1	7.9	5.5	4.0	3.2	2.7	19.1	12.13
	17000	34.1	15.0	7.8	5.4	4.0	3.2	2.7	18.9	12.32
2AA	17000	34.4	15.0	7.8	5.4	4.0	3.2	2.7	18.8	12.29
	17000	34.5	15.0	7.9	5.4	4.0	3.2	2.7	18.8	12.31
	17000	34.8	15.1	7.9	5.4	4.0	3.2	2.7	18.7	12.25
	[illegible]	33.8	15.0	7.9	5.4	4.0	3.2	2.7	19.1	12.26

APPENDIX F

Derivation of the Average Strain and Average Stress in the Soil Mass During a Pressuremeter Unload-Reload Cycle

As mentioned in section 5.2, the pressuremeter modulus E is calculated based on the average stress and strain developed in the zone surrounding the pressuremeter (Eq. 21). It was suggested that the average hoop strain in the soil mass surrounding the pressuremeter $\bar{\varepsilon}_{\theta\theta} = (u/\Delta r)_{ave} = (\Delta R_c/R_c)_{ave}$ be defined as:

$$\bar{\varepsilon}_{\theta\theta} = 0.32\, \varepsilon_{\theta\theta} \tag{F1}$$

It was also suggested that the average radial stress in the soil mass be defined as:

$$\bar{\sigma}_{rr} = 0.40\ \ \sigma_{rr} \tag{F2}$$

Equation F.2 comes from the theory of plasticity and the assumption that $\bar{\sigma}_{rr}$ is best represented by the average stress within the plastic zone during a pressuremeter expansion since the stress gradient is larger in the plastic zone in the immediate vicinity of the pressuremeter.

The derivation of equations F.1 and F.2 follows.

From the theory of elasticity and the expansion of a cylindrical cavity the following relationship for the strain in the soil surrounding the pressuremeter can be derived (Baguelin et al. 1978):

$$\varepsilon = \frac{\varepsilon_o r_c^2}{r^2} \tag{F3}$$

where: ε is the radial strain at any point in the soil medium
r_c is the radius of the pressuremeter cavity,
ε_o is the radial strain at the cavity wall (associated with r_c), and
r is the distance from the axis of the cylindrical cavity to the point where ε is calculated.

A plot of equation F.3 for radial strain is shown in Figure F1. If the radius of influence r_e is used as a limit over which an average hoop strain or radial strain is to be calculated then from the theory of elasticity we find:

$$\bar{\varepsilon}_{\theta\theta} = \frac{1}{r_e - r_c} \int_{r_c}^{r_e} \frac{\varepsilon_o r_c^2}{r^2}\, dr \tag{F4}$$

which can be written as:

$$\bar{\varepsilon}_{\theta\theta} = \frac{\varepsilon_o r_c^2}{r_e - r_c} \int_{r_c}^{r_e} \frac{1}{r^2}\, dr \tag{F5}$$

performing the integration and evaluating the integral leads to:

$$\bar{\varepsilon}_{\theta\theta} = \varepsilon_o \frac{r_c}{r_e} \tag{F6}$$

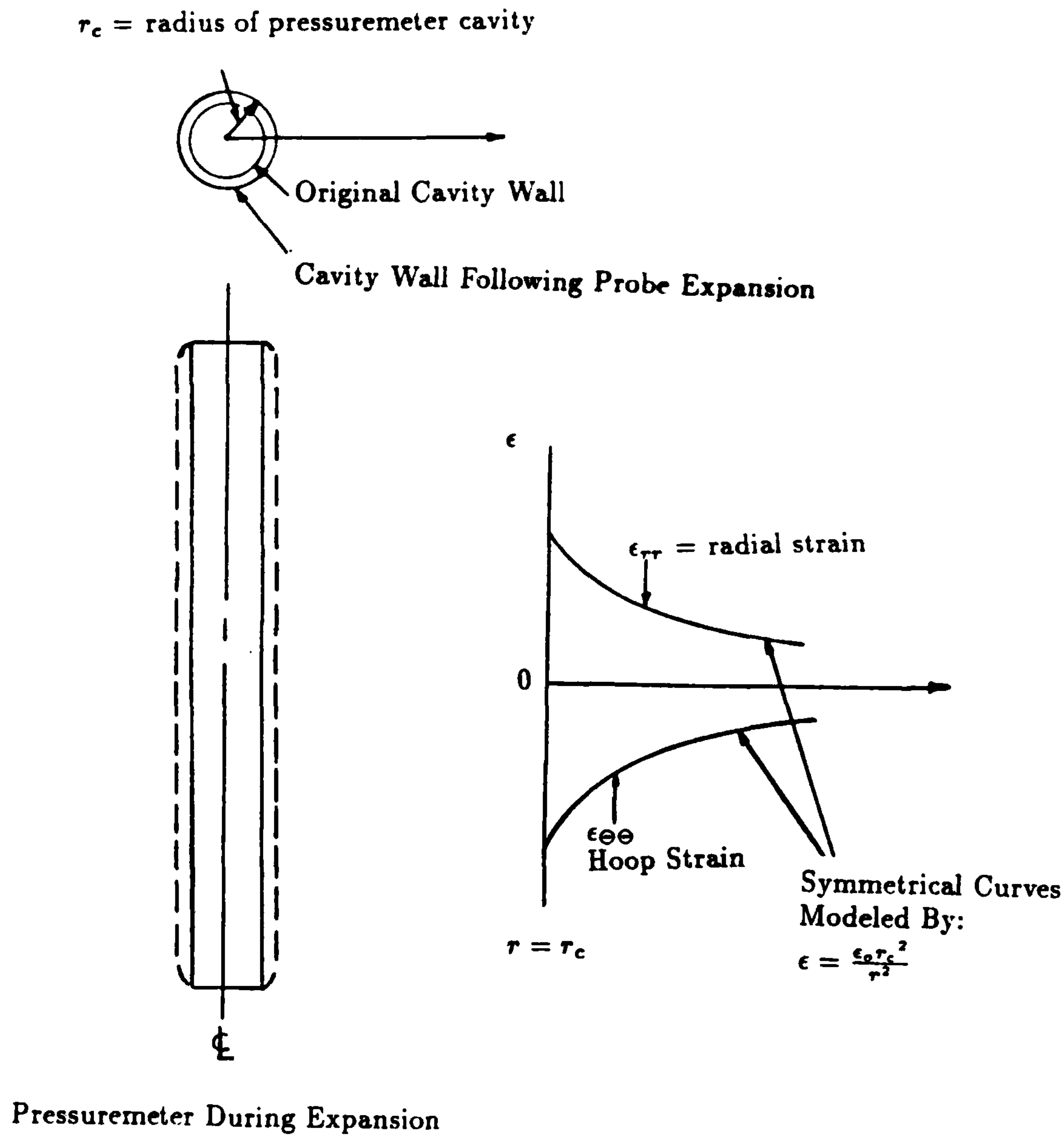

Fig. F1 Pressuremeter Strains versus Radial Distances from Cavity Centerline

In elasticity the change in radial stress $\Delta\sigma_{rr}$ throughout the radius of influence is (Baguelin et al. 1978):

$$\Delta\sigma_{rr} = 2G\,\varepsilon_{\theta\theta} \tag{F7}$$

where G is the shear modulus at the cavity wall:

$$\Delta\sigma_{rr_c} = 2G\,\varepsilon_o \tag{F8}$$

At the radius of influence r_e:

$$\Delta\sigma_{rr_e} = 2G\,\frac{\varepsilon_o r_c^2}{r_e^2} \tag{F9}$$

If it is assumed that the zone of influence of the pressuremeter extends to the radial distance at which only 10% of the radial stress at the cavity wall remains, the following relationship exists:

$$\Delta\sigma_{rr_e} = 0.1\ \Delta\sigma_{rr_c} \tag{F10}$$

Then it comes, by substituting equations F.8 and F.9 into equation F.10 that:

$$\frac{1}{r_e^2} = 0.1\,\frac{1}{r_c^2} \tag{F11}$$

Solving for r_e yields:

$$r_e = 3.16\ r_c \tag{F12}$$

which when substituted into equation E.6 yields:

$$\overline{\varepsilon}_{\theta\theta} = \varepsilon_o\,\frac{r_c}{3.16\ r_c} \tag{F13}$$

Recall from equation F.3 that ε_o was the strain associated with r_c therefore it may also be written as $\varepsilon_{\theta\theta}$ and equation F.13 becomes:

$$\overline{\varepsilon}_{\theta\theta} = 0.32\,\varepsilon_{\theta\theta} \tag{F14}$$

This proves equation F.1; the average hoop strain within the plastic zone surrounding the pressuremeter cavity is 32% of the hoop strain at the cavity wall. The derivation of equation F.2 follows.

The problem is to calculate the average stress $\overline{\sigma}_m$ in the plastic zone of the soil surrounding the pressuremeter. A sketch of the problem is shown in Figure F2. During this study only two types of subgrade soils were encountered. At two airports the subgrade was a clay and at the third airport the subgrade was a sand.

The derivation for the expressions of the stresses σ_{rr} and $\sigma_{\theta\theta}$ in the plastic zone around a pressuremeter probe is explained in detail in "The Pressuremeter and Foundation Engineering" by Baguelin, Jezequel and

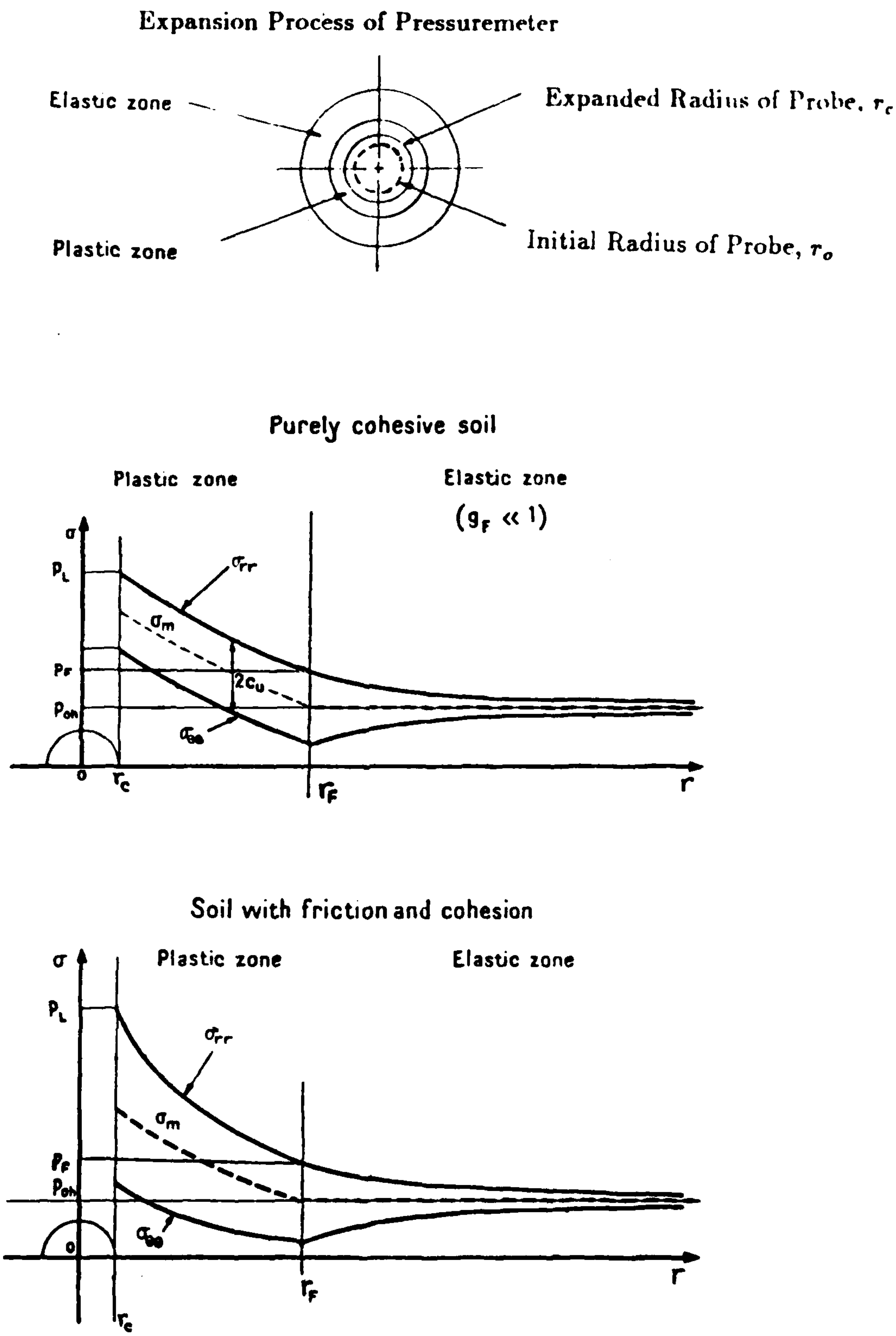

Fig. F2 Stresses in Elastic-Plastic Soil (from Baguelin et al. 1978)

Shields (1978). This procedure will be summarized in order to clearly present the problem. The pressuremeter measures the radial stress σ_{rr} at the cavity wall, which is equal to:

$$\sigma_{rr} = p_{oh} + \Delta\sigma_{rr} \tag{F15}$$

where: p_{oh} is the at rest horizontal stress and
$\Delta\sigma_{rr}$ is the additional stress applied to the soil by the pressuremeter.

The hoop strain $\sigma_{\theta\theta}$ can be expressed as:

$$\sigma_{\theta\theta} = p_{oh} + \Delta\sigma_{\theta\theta} \tag{F16}$$

For cohesionless soils in the plastic zone the radial stress σ_{rr} is related to the hoop stress $\sigma_{\theta\theta}$ by the active earth pressure coefficient K_a (yield criterion) as follows:

$$\sigma_{\theta\theta} = K_a \sigma_{rr} \tag{F17}$$

Assume K_a is 0.4. Therefore, at the interface between the plastic and elastic zones (r_F, Fig. F2) σ_m is equal to the at rest horizontal stress p_{oh}, that is:

$$\sigma_m = p_{oh} \quad \text{for } r = r_F \tag{F18}$$

Now the average stress σ_m at the wall of the cavity is:

$$\sigma_m = \frac{1}{2}(\sigma_{rr} + K_a\sigma_{rr}) = \frac{\sigma_{rr}}{2}(1 + 0.4) \tag{F19a}$$

or

$$\sigma_m = 0.7\,\sigma_{rr} \quad \text{for } r = r_c \tag{F19b}$$

Baguelin, Jezequel and Shields (1978) developed the following equations giving the variation of σ_{rr} and $\sigma_{\theta\theta}$ in the plastic zone of soils with both friction and cohesion:

$$\sigma_{rr} + \frac{c}{\tan\phi} = \left(p_F + \frac{c}{\tan\phi}\right)\left(\frac{r_F^2}{r^2}\right)^{\frac{1-K_a}{2}} \tag{F20}$$

and

$$\sigma_{\theta\theta} + \frac{c}{\tan\phi} = K_a\left(p_F + \frac{c}{\tan}\right)\left(\frac{r_F^2}{r^2}\right)^{\frac{1-K_a}{2}} \tag{F21}$$

where: c is the cohesion,
ϕ is the angle of internal friction,
p_F is the radial stress at the boundary between the plastic zone

and the elastic zone. It is the pressure at which the soil begins to fail (Fig. F2) and is given by: $p_F = p_{oh}(1 + \sin\phi) + c\cos\phi$ for c, ϕ soils.

For purely cohesive soils they developed the following equations for σ_{rr} and $\sigma_{\theta\theta}$:

$$\sigma_{rr} = p_F + C_u \ln\left(\frac{r_F^2}{r^2}\right) \quad \text{(F22)}$$

$$\sigma_{\theta\theta} = \sigma_{rr} - 2C_u = p_F - 2C_u + C_u \ln\left(\frac{r_F^2}{r^2}\right) \quad \text{(F23)}$$

For purely cohesive soils p_F is given by: $p_F = p_{oh} + C_u$. In this study, the subgrade soils encountered were a sand with zero cohesion and two clays for which undrained behavior was assumed. For the sand equations F.20 and F.21 reduce to:

$$\sigma_{rr} = p_F\left(\frac{r_F^2}{r^2}\right)^{\frac{1-K_a}{2}} \quad \text{(F24)}$$

$$\sigma_{\theta\theta} = K_a\,(p_F)\left(\frac{r_F^2}{r^2}\right)^{\frac{1-K_a}{2}} \quad \text{(F25)}$$

If the average stress σ_m at any radial distance r in the elastic zone of a purely cohesive soil is required then equations F.22 and F.23 can be averaged to yield:

$$\sigma_m = \frac{\sigma_{rr} + \sigma_{\theta\theta}}{2} = p_F + C_u\left(\ln\left(\frac{r_F^2}{r^2}\right) - 1\right) \quad \text{(F26)}$$

substituting for p_F yields:

$$\sigma_m = p_{oh} + C_u\left(\ln\left(\frac{r_F^2}{r^2}\right)\right) \quad \text{(F27)}$$

If the average stress σ_m in a purely cohesionless soil is required, then equations F.24 and F.25 can be averaged to yield:

$$\sigma_m = (1 - K_a)\,\frac{p_F}{2}\left[\frac{r_F^2}{r^2}\right]^{\frac{1-K_a}{2}} \quad \text{(F28)}$$

substituting for p_F yields:

$$\sigma_m = (1 - K_a)\,\frac{p_{oh}}{2}\,(1 + \sin\phi)\left[\frac{r_F^2}{r^2}\right]^{\frac{1-K_a}{2}} \quad \text{(F29)}$$

Baguelin, Jezequel and Shields (1978) also give the expression for r_f:

$$r_f^2 = r_c^2 \frac{G}{p_{oh} \sin\phi} \quad \text{for purely cohesionless soils (F30)}$$

$$r_f^2 = r_c^2 \frac{G}{C_u} \quad \text{for undrained behavior of clays (F31)}$$

In order to arrive at an approximate relationship between r_c and r_F for sand, typical properties will be chosen and substituted into equation F.30. These properties are:

γ_t = 120 pcf = total unit weight
z = 3 feet = depth of test
K_o = 0.8 = at rest earth pressure coefficient
ϕ = 32° = angle of internal friction
G = 200,000 psf = shear modulus

Making the proper substitutions yield:

$$r_F = 36.5\ r_c$$

In order to obtain a similar relation in clay, the following properties were chosen:

γ_t = 120 pcf = total unit weight
z = 3 feet = depth of test
K_o = 0.8 = at rest earth pressure coefficient
c_u = 2000 psf
G = 200,000 psf

For these values the parameter r_F is (Eq. F.31):

$$r_f = 10\ r_c$$

For the two subgrade soils encountered at the airports, values of the average stress σ_m will be calculated at several distances from the center of the pressuremeter. Calculations will be made at the following radial distances: $r_c = r_c$, $r_F = r_F$ and $r_c = (r_F - r_c)/2$. For the clay subgrade if a value of c_u is assumed as 2000 psf and p_{oh} is calculated from the previously assumed parameters for the clay substitution into equation F.27 yields:

$$\sigma_m\ (r = r_c) = 4.75 \text{ tsf}$$

$$\sigma_m\ (r = r_F) = 0.14 \text{ tsf}$$

$$\sigma_m\ (r = \frac{r_F - r_c}{2}) = 1.74 \text{ tsf}$$

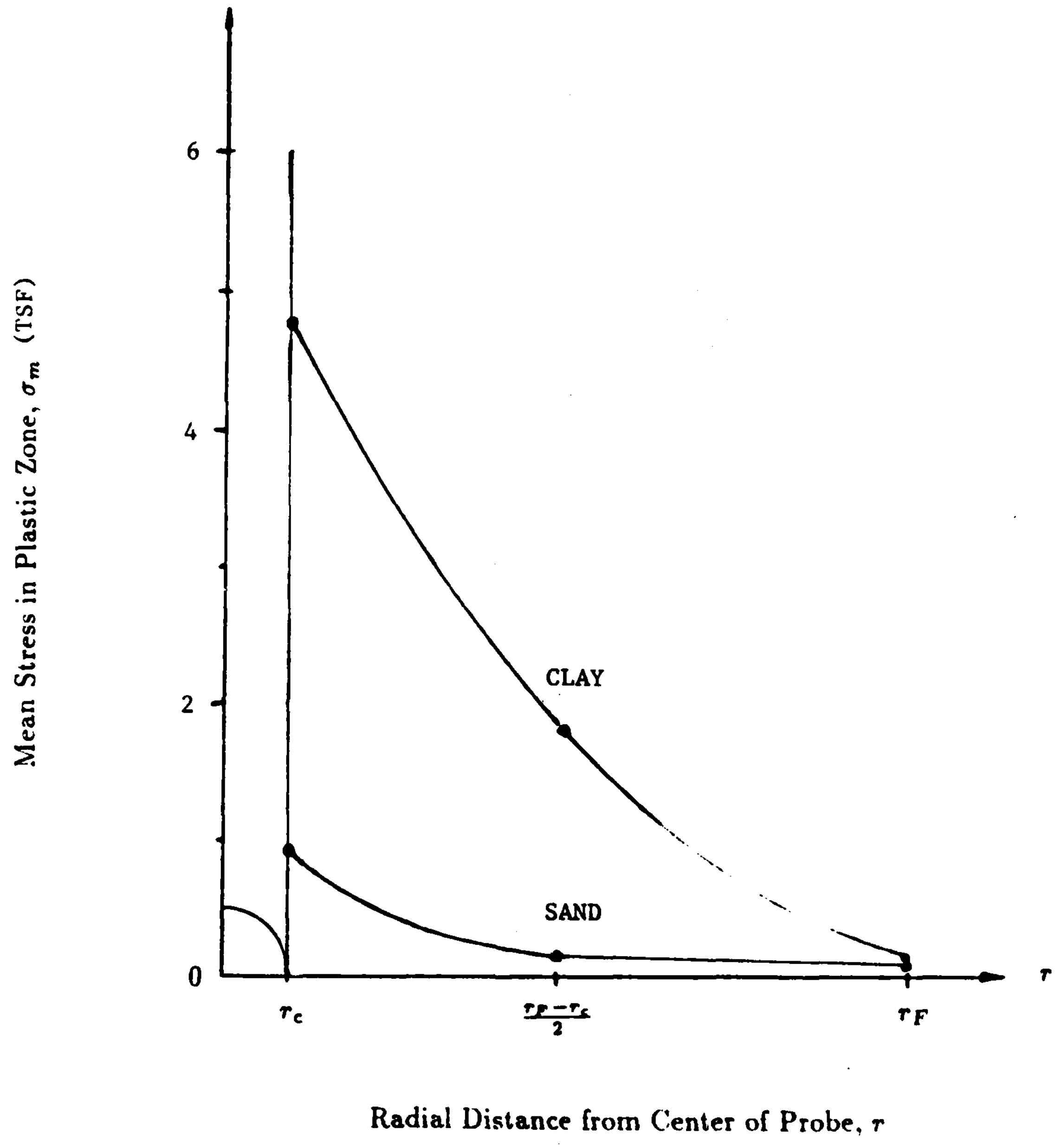

Fig. F3 Average Stresses in Pastic Zone of Soil

For the sand subgrade using the previously assumed parameters for the sand and substituting into equation F.29 yields the following:

$$\sigma_m \; (r = r_c) = 0.92 \text{ tsf}$$

$$\sigma_m \; (r = r_F) = 0.076 \text{ tsf}$$

$$\sigma_m \; (r = \frac{r_F - r_c}{2}) = 0.125 \text{ tsf}$$

The following table summarizes the previous calculations:

Soil Type	Radial Distance	m
Clay	r_c	4.75 tsf
	4.5 r_c	1.74 tsf
	10 r_c	0.14 tsf
Sand	r_c	0.92 tsf
	17.7 r_c	0.12 tsf
	36.5 r_c	0.076 tsf

The summary data from this table is plotted in Figure F3. In order to find the average stress in the plastic zone for both subgrade types the areas under the curves depicted for each soil is calculated using the trapezoidal rule.

For the clay subgrade:

$$A_{clay} = 16.53 \; r_c$$

For the sand subgrade:

$$A_{sand} = 10.53 \; r_c$$

To calculate the mean stress for each type of soil divide the area by the radius of influence of the plastic zone (i.e. $r_F = r_c$). For the clay subgrades:

$$\sigma_m = \frac{16.53 \; r_c}{10 \; r_c - r_c} = 1.84 \text{ tsf}$$

and for the sand subgrade:

$$\sigma_m = \frac{10.53 \; r_c}{36.5 \; r_c - r_c} = 0.297 \text{ tsf}$$

In order to calculate the ratio between the pressure at the cavity wall and the average stress σ_m in the plastic zone of the surrounding soil mass the average stress is divided by the maximum radial stress at the cavity wall ($r = r_c$). For the clay subgrades this yields:

$$\frac{\overline{\sigma}_m}{\sigma_{rr}} = \frac{1.84}{4.75} = 0.39$$

and for the sand subgrade this yields:

$$\frac{\bar{\sigma}_m}{\sigma_{rr}} = \frac{0.247}{0.92} = 0.32$$

After several calculations with other assumed soil properties the following relationship was selected for this study:

$$\bar{\sigma}_m = 0.40 \; \sigma_{rr}$$

which is equation F2.